TITLE: **A novel method for detecting and recording movement and functional performance of cardiac valve prostheses exposed to the static magnetic field associated with magnetic resonance imaging**

AUTHOR: **Maria-Benedicta Edwards**

DEGREE: **PhD**

YEAR: **2013**

DEPARTMENT: **Bioengineering**

UNIVERSITY: **University of Strathclyde**

DECLARATION OF AUTHENTICITY AND AUTHOR'S RIGHTS

The thesis, dissertation, design or report shall include, on the page immediately subsequent to the title-page, the following declarations of authenticity and author's rights:

‘This thesis is the result of the author’s original research. It has been composed by the author and has not been previously submitted for examination which has led to the award of a degree.’

Signed: Maria-Benedicta Edwards

Date: 22nd March, 2013

ABSTRACT

Aging and disease processes are known to compromise tissue strength and consequently increase the risk of harmful movement or detachment of a heart valve prosthesis *in vivo* when exposed to strong magnetic forces associated with magnetic resonance imaging (MRI). Research however, has failed to fully assess prosthetic valve movement or functional valve impedance in the MR environment. This study seeks to design and evaluate an MR compatible device which aims to detect and measure *ex vivo*, frequency, direction and magnitude of movements and leaflet function *in vitro* of nine prosthetic heart valves in the static magnetic field (B_0) of a 1.5 Tesla (T) and a 3.0 T MR system. A valve holder incorporating strain gauges connected to a strain gauge recorder and laptop computer were used to detect and record displacement and rotational valve movements and, a hydro-pneumatic system recorded pressure changes across the valve indicative of any MR induced alteration in leaflet performance *in vitro*.

The data confirms the compatibility of the test apparatus in the MR environment and its capacity to detect and record valve movement and changes in functional valve performance in field strengths $\leq$3.0 T. Real-time three-dimensional movements were detected in both B_0 fields in all valves, differences in entry and return profiles and static and dynamic measurements were recorded. Furthermore, applied magnetic forces leading to prosthesis movement were greater than previously reported. Functional valve impedance was detected in three valves but no commonality between valve types or sub-groups regarding this, type, frequency, magnitude or patterns of valve movements were noted. These data suggests magnetism is induced and retained in valve prostheses during exposure to the MR environment and patients with friable valvular tissue are at significantly increased risk of prosthetic valve movement and/or dehiscence. Furthermore, current uses of static measurements to assess risk are inadequate.

CONTENTS

ACKNOWLEDGEMENTS

I would like to thank Stefan Solomonidis and John McClean of the Department of Bioengineering, University of Strathclyde who very generously gave their time and expertise in helping with the design and fabrication of the test apparatus.

My eternal gratitude and thanks to Dr John Mclean of Department of Neurosciences, Southern General, Glasgow who so generously gave up his weekends and evenings to help with the execution of my experiments and ensured my safety in the MR environment. I cannot thank him enough.

My thanks also to Professor Barrie Condon, Greater Glasgow and Clyde Health Board and Glasgow University who listened to my ideas, reviewed my manuscript and offered helpful input.

A special thanks to Simon Ambury who so eloquently explained the mysteries and the magic of quadratic equations.

To Professor Kenneth M Taylor, Professor of Cardiothoracic Surgery, Hammersmith Hospital, London (retired) and Professor Ian Young, Senior Research Fellow, Department of Electrical and Electronic Engineering Imperial College, London my thanks for their early support and encouragement.

To Professor Terry Gourlay, Professor of Bioengineering at the University of Strathclyde, I offer my thanks for his support and unstinting belief in the investigation and my abilities to complete the task.

Lastly, to my husband David and my daughter Pippa, my deepest thanks for your unending patience, emotional support and for giving me a happy balance in life.

LIST OF TABLES

LIST OF FIGURES

ABBREVIATIONS & ACRONYMS

Abbreviation/Acronym	Expansion of abbreviation
APS	antiphospholipid syndrome
AR	aortic regurgitation
aS	aortic stenosis
AV	atrio-ventricular
AVR	aortic valve replacement
B	gradient magnetic field
B_0	static magnetic field
B_1	RF magnetic field
BAV	balloon aortic valuloplasty
bpm	beats per minute
BSCC	Björk-Shiley Convexo-Concave valve
cm	centimetres
CPB	cardiopulmonary-bypass
CT	computer tomography
dB/dt	time varying gradient field
dB/dx	static gradient magnetic field

E	East
FID	free induction decay
g	grams
G	Gauss
GHz	gigahertz
G/cm	Gauss per centimetre
HIV/AIDS	human immunodeficiency virus/acquired immune deficiency syndrome
HVMAS	Heart Valve Motion Analysis System
HP	Haemodynamic Plus (reference: St Jude mechanical valve)
Hz	hertz
IE	infective endocarditis
INR	international normalized ratio
IV	intravenous
IVF	intrinsic valve failure
kHz	kilohertz
l/min	litres per minute
LV	left ventricle
M	magnetization vector
m	metres

MHz	megahertz
ml	millilitres
mm	millimetres
MPa	megapascal
mR	mitral regurgitation
MR	magnetic resonance
mS	mitral stenosis
m/s^2	meters/second ^{2}
MVP	mitral valve prolapse
MRI	magnetic resonance imaging
MVR	mitral valve replacement
M_z	magnetization vector parallel to the applied magnetic field
M_{xy}	magnetization vector perpendicular to the applied magnetic field
N	North
Nwt	Newton(s)
NBTE	non-bacterial thrombotic endocarditis
N-E	north-east
N-E-W	north-east-west
N-S-E	north-south-east

NMR	nuclear magnetic resonance imaging
NMV	nuclear magnetization vector
N-S	north-south
N-W	north-west
PAVR	percutaneous aortic valve replacement
PHV	percutaneous heart valve
PNS	peripheral nerve stimulation
PPL	para-valvular leak
PPM	prosthetic patient-mismatch
pS	pulmonary stenosis
PVC	polyvinyl chloride
PVe	prosthetic valve embolization
PVE	prosthetic valve endocarditis
PVR	pulmonary valve replacement
PVS	pulmonary valve stenosis
PVT	prosthetic valve thrombosis
RF	radiofrequency
rpm	revolutions per minute
SAR	Specific Absorption Rate
S	south

secs	seconds
S-E	south-east
S-E-N	south-east-north
SVD	structural valve deterioration
S-W	south-west
t	time
T/cm	Tesla per centimetre
T	Tesla
TVR	tricuspid valve replacement
UK	United Kingdom
VHD	valvular heart disease
W	west
W-E	west-east
W/kg	watts per kilogram
χ	magnetic susceptibility

INTRODUCTION

What is this thesis about ?

This study assesses a novel device designed specifically to detect and quantitatively measure prosthetic heart valve movement *ex vivo* [1] and functional valve performance *in vitro* during exposure to the static magnetic field (B_0) associated with magnetic resonance imaging (MRI).

Background to this investigation

My interest in identifying ways in which movement of prosthetic heart valves within the B_0 field and its associated magnetic gradient field (dB/dx) associated with MRI stems from my work managing the United Kingdom (UK) Heart Valve Registry for a number of years. This Registry was a national patient database which prospectively collected pre- and post-operative implant data of all patients who underwent heart valve replacement and repair with a prosthetic heart valve or annuloplasty ring between 1986 and 2007. The data collected included valve and ring specific information such as the make, model, site, size, type and serial number as well as patient and centre data. Patients were followed up post implantation until their death thus any and all valve-related reoperations and deaths were captured and data on long-term valve performance collected and recorded. As the Registry's existence and reputation grew other clinical communities outside cardiac surgery, such as the radiological community, began to contact the Registry and request specific information with regards to the safe exposure of valve implant patients to MRI. When the Registry received its first request for safety information from the hospital's own MRI unit in 1999 the average monthly number of such requests over the next 18 months approximated 1-2 per month. However, by the

[1] The term *ex vivo* in this document refers to all non-fluid investigations and measurements of the interaction of the B_0 field and heart valve prostheses. In contrast, the term *in vitro* refers to all fluid investigations and measurements of the prostheses' leaflets with the B_0 field.

time of its closure in 2007 it received an average of 7 requests per day from centres nationally, prosthetic valve manufacturers and other agencies.

As part of the process for gathering information pertaining to MRI safety and heart valve prostheses to include in a reference booklet containing information on the different makes, models and materials used in each manufacturer's heart valves and annuloplasty rings (Edwards 2000; Edwards 2006), I noted the major concerns expressed by MR operators, clinicians and physicists related to the interaction of these passive implants with magnetically induced translation and rotational forces, the potential to cause harmful prosthesis movement or detachment from the surrounding tissue and, functional valve failure as a result of an interaction of the valve's leaflets with the MR environment. This process also highlighted the paucity of published data and few, if any investigations being conducted. Furthermore, I also noted there was substantial confusion amongst many who worked daily in the MR environment about exposing patients with bioprostheses to MRI. From the numerous conversations I had with MR operators I found many were advised bioprostheses were not contraindicated for MRI because of the use of human and animal tissue neither of which is ferromagnetic. However, little or no consideration was given to the valves' other non-tissue materials and their potential to interact with the magnetic environment. Thus, I had identified a genuine need for accurate and reliable information on the interaction of all types of heart valve prostheses with MR associated magnetically induced forces and safe exposure of these patients to MRI. Furthermore, as my knowledge of the causes and effects of valvular disease leading to valve repair and replacement grew I became interested in the possible consequences of the interaction of applied magnetic forces on valvular implants *in vivo* in tissue which had become severely weakened by the aging and disease processes.

A review of the literature suggested the aging and disease processes can severely compromise tissue strength but, there was a dearth of empirical data about the reduction in cardiac valvular tissue strength. This led me to design and conduct a study to

determine the required forces to cause partial or total detachment of cardiac valve prostheses in patients with age-related degenerative diseases and those with known infective endocarditis exposed to MRI (Edwards 2005). This investigation examined 18 tissue samples excised during routine heart valve replacement surgery which were then subjected to a suture pull-out test using a tensile materials testing machine. The resultant forces were compared with applied magnetic forces associated with 4.7 T. Although tissue samples excised from patients with calcific and stenotic tissue required a significantly greater force to yield or rupture than those demonstrated by the applied magnetic force, tissue taken from patients with infective endocarditis yielded and fully ruptured at significantly lower forces in comparison. The results of this investigation are highly significant because elderly patients, those with multiple valve prostheses and intravenous drug users are at increased risk of developing prosthetic valve endocarditis and, as Chapters 1 & 4 of this thesis note, the extremely invasive nature of this type of infection makes it more destructive than endocarditis of the native valve. Therefore, patients with highly friable tissue resulting from prosthetic valve endocarditis are, for example, already at significantly greater risk of tissue rupture than patients with healthy valvular tissue, stenotic and calcific tissue. Thus, if strong magnetic forces such as those present in the MR environment interact with an implanted valve prosthesis causing prosthesis movement, it may be these forces are strong enough to cause catastrophic partial or total detachment of the valve from the surrounding tissue. Moreover, these risks may be further amplified with exposure to higher field strength MR systems which, as Chapter 5 describes, are becoming more and more commonplace in clinical practice today.

My approach to this investigation

Having proven the potential for prosthetic valvular movement leading to valve dehiscence in highly friable tissue a comprehensive assessment of this risk in relation to the MR associated B_0 field needed to be conducted. To this end I designed the study presented in this thesis to detect and record movement of a number of different heart

valves in response to translation and rotational forces associated with the B_0 field. As part of the preliminary investigations I evaluated and adapted the current standard apparatus and methodology, first introduced by New et al (1983), to assess its capacity to accurately detect and record applied displacement and rotational forces on 102 different prosthetic heart valves exposed to 1.5 T and 4.7 T *ex vivo* and, to see what additional modifications might be required. This rudimentary apparatus was able to detect displacement and rotational movements in more than three-quarters of the heart valves tested. However, a number of limitations in the test apparatus and methodology were identified. Firstly, the apparatus was only capable of measuring single, separate and static measurements. Measurements were one-dimensional, assessment of torque force was subjective, the magnitude of applied force had to be calculated later and could not be quantitatively measured at the time valve movement occurred, frequency of prosthesis movements could not be assessed, nor could the effects of constraint by retentive structures or counteractive forces acting on the prosthesis be evaluated. Furthermore, each measurement was time consuming and reading the angle of displacement was subject to human error. In addition, the absence of any form of hydro-pneumatic flow prevented assessment of the valve's functional performance and hence, potential interaction of its leaflets with the B_0 field. Consequently, the *in vivo* behavior of the prosthesis under the normal clinical settings, including movement of the patient through the B_0 field, could not be properly assessed nor the risk of harmful prosthesis movement. Thus, revision of the test apparatus culminated in a device in which the *ex vivo* component incorporated a specially designed valve holder encompassing strain gauges connected to a strain gauge recorder and laptop computer to detect and record: three-dimensional valvular movement as the prosthesis continuously advanced through the B_0 field, frequency, magnitude and location of valvular movement(s) within magnetic field environment. In addition, the *in vitro* component was fitted with manometer lines connected to electro-dynaphramatic pressure transducers to capture any changes in the fluid profile indicative of MR induced alteration in leaflet performance so that any changes *in vitro* in the dynamic profile as a measure of functional valve performance could be captured.

Thus, the focus of this thesis is to describe this apparatus and the methodology adopted to detect and record prosthetic valvular movement within the B_0 field environment as well as functional valve performance and, to determine whether the study's aims and objectives were met and the null hypothesis (H_0) which states: "this novel device will lack the sensitivity and capacity to detect and record the occurrence, frequency, direction and magnitude of prosthetic valve movement and, valve function as the valve moves through the dB/dx and B_0 field associated with an MR environment" disproved. In addition, this thesis presents a unique set of dynamic results showing the *ex vivo* valvular movements and *in vitro* leaflet function of prostheses moving through the B_0 field.

Chapter 1 examines some of the most common types of valve pathologies which impede cardiac function and require surgical intervention with a valve prosthesis and discusses how, over the last fifty years classification of cardiovascular disease has continued to change to reflect changing aetiology of diseases, clinical comprehension and technological advances. **Chapter 2** charts the evolution of cardiac surgery following the first successful repair of the human heart in 1896 and outlines the innovations which have contributed to the development of surgical techniques and procedures for the repair and replacement of diseased native valves. **Chapter 3** presents a review of the historical milestones in the development of artificial heart valves from the early 'bottle-stopper' valve to the mechanical caged-occluder and leaflet valves, human and tissue prostheses to the newer percutaneous, polymeric and tissue engineered valves of the 21st Century. **Chapter 4** describes the basic principles of magnetic resonance imaging and its relevance to this study namely, the potential interaction of heart valve prostheses with associated magnetically induced forces. The chapter looks at the relationship between magnetism, materials and biological systems and presents a review of the potential physiological effects and the hazards associated with the interaction of the magnetic field with an implant. **Chapter 5** primarily describes the test apparatus designed and fabricated for this investigation. The chapter is divided into three sections with Part I describing the materials and methods adopted for the

preliminary investigations and how the limitations of this methodology contributed to the design of the new experimental apparatus and methodology. Part II presents a detailed description of the apparatus and additional components essential to this investigation, the problems encountered with the functional design and how these were overcome. Part III describes the methodology employed for calibrating the equipment, plotting the magnetic fields of the two MR environments and conducting the baseline and experimental measurements. **Chapter 6** reports the results of both the preliminary and main investigations with the results from the introductory investigations in which magnetic field interactions were recorded by 77% of the valve prostheses in field strengths ≤4.7 T presented in Part I. The greater part of the chapter presents the results relating to the test apparatus and the experimental methodology. Part II focuses on the results from the calibration of the *ex vivo* component of the apparatus including the baseline measurements and Part III reports on the magnetic field interactions of the individual heart valve prostheses as a measure of the sensitivity and capacity of the test apparatus. Finally, Part IV of the Results chapter presents the results from the *in vitro* dynamic fluid flow investigations. **Chapter 7** reviews the results of this investigation to determine whether the study's aims and objectives were met and also whether the hypothesis was proven. In addition, the discussion examines the results of the individual heart valve prostheses and evaluates their responses to the B_0 field in light of current knowledge of the implants' materials and magnetic properties and thus, the potential for harmful valvular or leaflet movement. The chapter also reviews the results in relation to others' methodologies and findings in an effort to determine what if anything, this novel device can add to our knowledge of prosthetic valvular behavior during exposure to the MR environment and, provide clinicians with a clearer picture of the potential *in vivo* behavior of the prosthesis within B_0 fields ≤3.0 T. Finally, **Chapter 8** summarizes the study and its findings and discusses the limitations identified during the course of this investigation. Improvements to the test apparatus and methodology are also outlined and suggestions for future work presented.

CHAPTER 1

The human heart and valvular heart disease ♥

1. Introduction

There are many expressions which refer to the heart: "the *heart* of the matter", "*heart* and soul....", "change of *heart*", "sweet*heart*", "*heart*hrob", "take *heart*", "lose *heart*", "brave*heart*" etc. For centuries philosophers, poets and scientists have described the heart as the dominant force controlling *all* human feelings ranging from the emotional, moral, spiritual and intellectual. Our romantic images of the heart are thought to derive from illustrations based on the seed or fruit of the now extinct silphium plant depicted on coins from the ancient city of Cyrene (Figure 1.1). Later illustrations are thought to stem from the anatomy of the cow's heart although, despite its likeness to the iconic heart shape the bovine heart bears only a slight resemblance to the human heart. 21st Century symbolism has added the emoticon <3 as a representation of the heart and, for the less romantic the heart can now even be represented mathematically by plotting a graph of either $(x^2 + y^2 - 1)^3 = x^2y^3$ (i.e. the Cartesian equation) or, in polar form, r =a (1 − cos (φ)) (Figure 1.2). Despite centuries' long history romantic depiction the heart is in fact shaped more like an upside-down pear. Moreover, its purpose is more intrinsic to human well-being; the maintenance of blood flow and thus life.

Figure 1.1

A silver Attic drachm 510-470 BC depicting the seed or fruit of the silphium plant.

Printed with the permission of TV Buttrey author of "The Coins from the Sanctuary of Demeter and Persephone" published in Expedition Magazine 1992;34(1-2):62). This coin was found in the excavation of the Sanctuary of Demeter and Persephone at Cyrene).

Figure 1.2

Mathematical representation of the cardioid (polar form)

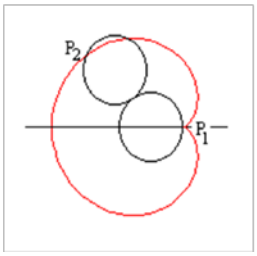

$r = a\,(1 - \cos(\varphi))$

where a is the common radius of the two circles and φ is the polar angle.

The heart is essentially a large muscular pump and like any pump is designed and built for endurance and longevity. Its purpose is to maintain a sufficient circulation of blood supplying oxygen and other nutrients to, and removing waste products from, every organ, cell and tissue within the body. It functions properly only if it can maintain an adequate blood flow and pressure in response to the body's needs. However, like any pump it may suffer from inherent defects as well as the aging process making it susceptible to structural and mechanical failure. Such failures may involve the heart's valves requiring clinical intervention to either repair or replace them.

This chapter looks at the different types of valve pathology commonly seen by clinicians today which impede cardiac function. The chapter begins with a summary description of the basic anatomy of the human heart and regulation of blood flow as a precursor to a discussion on types of valvular heart disease ranging from congenital to acquired diseases and how changing age and disease profiles have led to increases in the number of people undergoing heart valve repair and/or replacement surgery with a cardiac valve prosthesis. The Chapter ends with a brief discussion on the emerging immunological, inflammatory and environmental causes of cardiac valve disease.

1.1 Basic anatomy and function of the human heart

The heart is essentially a large muscular pump. It is formed from the primitive vascular tube between the second and sixth weeks of gestation and, as Figure 1.3 shows, when fully developed has four chambers; the thin walled collecting chambers known as the atria and the thick muscular walled ventricles which act as the heart's pump. The developed human heart typically measures approximately 12.5 cm from base to apex and is normally positioned near the anterior chest walls of the thorax directly posterior to the sternum and covered on its anterior surface by the overlapping lungs. The long axis is orientated from the hypogastrium towards the right shoulder so the lower border (apex) is anchored to the diaphragm. The upper border (base) sits posterior to the sternum and is tethered to adjacent structures by the body's main blood vessels; the aorta which is responsible for carrying nutrient-rich blood away from the heart to the rest of the body and, the pulmonary artery which connects the heart with the lungs where blood is re-oxygenated.

The continuous expansion and contraction of the heart's chambers and coordinated opening and closing of a series of valves (see below) allows blood to enter and exit the four chambers. Each heart beat (i.e. cardiac cycle) is distinguished by alternating periods of relaxation (diastole) and contraction (systole) followed by a brief resting phase during which time the chambers prepare for the next cycle. The start of the cardiac cycle is marked by atrial systole when all four chambers are relaxed and blood flows passively from the atria to the ventricles until they are approximately three-quarters full (ie. 70%). As atrial contraction progresses atrial pressure increases and forces blood through the open valves connecting the atria and ventricles known as the atrio-ventricular (AV) valves (see below), into the ventricles resulting in ventricular capacity reaching maximum by the end of this phase. Atrial systole lasts approximately 100 msecs and is followed by atrial diastole which begins at the same time and continues until the start of the next cardiac cycle and ventricular systole. In all, this continuous

pumping of the heart forces approximately 5 litres of blood around the body via the circulatory system.

Figure 1.3 Anatomy of the human heart

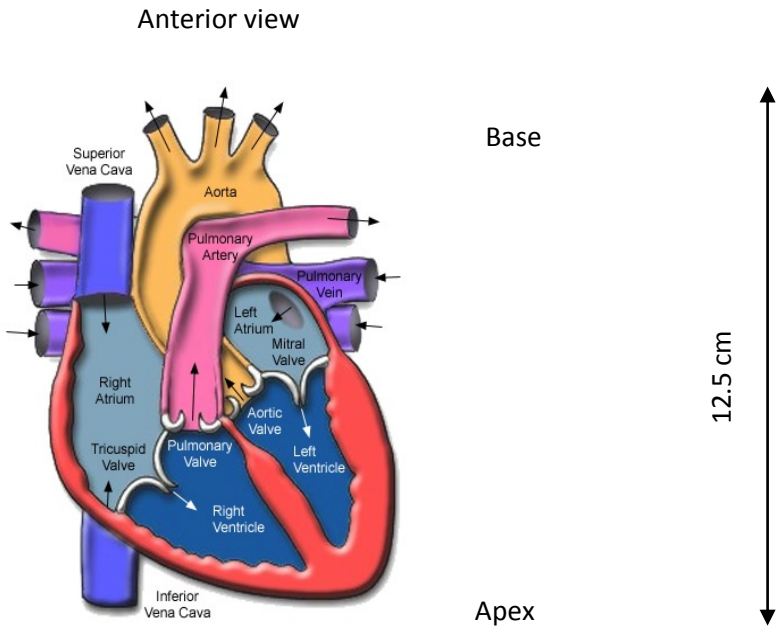

De-oxygenated (venous) blood from the systemic circuit for transport to the lungs and subsequent re-oxygenation is received by the right side of the heart which is also responsible for initiating the electrical impulses which spread through the atria causing atrial contraction. Blood flows into the right atrium via the superior (upper body) and inferior (lower body) vena cavae and into the right ventricle and is regulated by a set of rudimentary valves in addition to one of two AV valves (i.e. tricuspid valve). Subsequent blood flow from the right ventricle into the pulmonary trunk at the start of the pulmonary circuit is controlled by the pulmonary valve, one of two semi-lunar valves (see below). The left side of the heart is responsible for pumping oxygenated blood (i.e. arterial) to the rest of the body. Blood collects in the left atrium from the left and right pulmonary veins and flow between these two chambers is regulated by the left

AV valve (i.e. mitral valve; Figure 1.3). Blood flow from the left ventricle into the ascending aorta is via the remaining major valve, the aortic valve. During ventricular diastole the aorta swells into three sinuses immediately above this valve and one opposite each leaflet. Subsequent ventricular ejection causes pressure increases in the aorta above that of the ventricle as blood flows through the aortic arch and into the descending aorta causing closure of the aortic valve and preventing regurgitation or backflow.

1.2 Regulation of blood flow

As previously mentioned four main valves regulate blood flow through the heart, the mitral and tricuspid valves, known as the atrio-ventricular valves and, the aortic and pulmonary valves known as the semi-lunar valves. These one-way valves prevent blood flowing back into the chambers during contraction.

1.2.1 Atrio-ventricular valves

The AV valves consist of leaflets and a fibrous tissue core known as the fibrosa and continuous distally with the dense fibrous collagen strands known as chordae tendinae. During diastole the chordae tendinae and papillary muscles, which anchor the leaflets of the AV valves to the ventricular myocardium, are loose and offer little or no resistance to the blood flow from atria to ventricles. However, during ventricular systole inter-ventricular pressure and contraction of the papillary muscles causes tension of the chordae tendinae forcing the leaflets to coapt. Moreover, these fibrous strands prevent the leaflets from collapsing and entering the atria thus preventing ballooning and regurgitation. The first of the two AV valves, the mitral valve, regulates blood flow between the left atrium and left ventricle. This valve has only two leaflets an anterior leaflet and a posterior leaflet which resemble a Bishop's mitre thus giving the valve its name. Although bicuspid, the leaflets differ in size. The anterior leaflet is larger and

rises higher than the left and protects approximately two-thirds of the valve. However, the posterior leaflet has a larger surface area. In addition, the valve's opening is surrounded by a fibrous ring known as the mitral valve annulus. The three leaflet tricuspid valve guards the right atrium from the right ventricle. Each of the valve's leaflets is named according to its position i.e. anterior (in the coronal plane), posterior (parallel to the diaphragm) and septal (parallel to the septum) and the base of each leaflet is attached to the fibrous ring of the valve. As previously mentioned, a series of delicate fibrous strands (i.e. chordae tendinaea) tether the edges of the leaflets to three conical muscular projections (i.e.papillary muscles) of the ventricular wall preventing the leaflets from blowing back into the atrium during ventricular systole.

1.2.2 Semi-lunar valves

The positioning of leaflets in the semi-lunar valves coupled with the fact the walls of the atria do not contract make these valves more stable than their AV counterparts and as a consequence, do not require muscular anchors. The leaflets are prevented from attaching to the wall of the aorta and sticking open by the aortic sinuses and when these valves close the symmetrical leaflets support each other like the legs of a tripod. The aortic valve regulates blood flow from the left ventricle to the aorta and a normal aortic valve has three leaflets arranged in the posterior, right and left positions. During ventricular systole pressure increases in the left ventricle above aortic pressure causes the valve to open and blood to flow from the left ventricle into the aorta. At the end of ventricular systole, left ventricular pressure drops rapidly and aortic pressure forces the aortic valve to close. Blood flow from the right ventricle to the pulmonary trunk is regulated by the pulmonary valve. As Figure 1.4 shows the pulmonary valve, like the aortic valve is tri-leaflet. The leaflets are orientated in a convex direction towards the ventricle and concave towards the trunk and each has a fibrous nodule at its centre and is named according to the positions it occupies i.e. anterior, right and left. As with the aortic valve, the pulmonary valve opens during ventricular systole as right ventricular pressure rises above pressure in the pulmonary artery. Closure of the valve occurs in

response to a rapid decrease in right ventricular pressure and corresponding increase in pulmonic pressure.

Figure 1.4 Valves of the heart

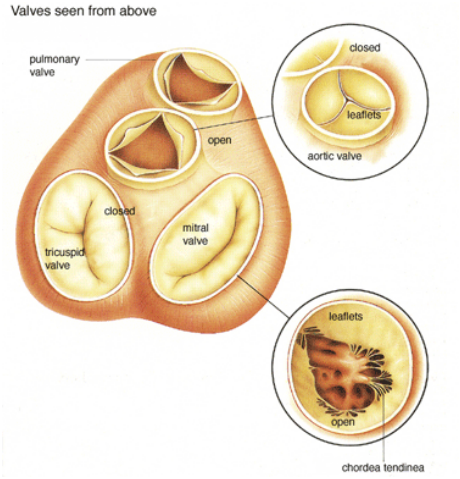

The first part of this chapter briefly described the basic anatomy of the human heart and how blood flow through the heart is controlled by a series of four main valves. However, during its lifetime the heart may experience some mode of failure as a result of some form of cardiovascular disease [2]. This may be either congenital or acquired. The next section looks at how changing trends in the age profile of the population has had an impact on the types of cardiac disease pathology with particular reference to cardiac valvular diseases presented in modern clinical practice and, the emergence of new immunological, inflammatory and environmental causes of valve disease.

1.3 Changing trends patient profiles and valvular disease pathology

Over the years the classification of cardiovascular disease has continued to change to reflect the changing aetiology of diseases, clinical comprehension and technological advances. One of the most noticeable modifications has been the change in the

[2] Cardiovascular disease is an umbrella term for a number of different diseases affecting the heart including valvular disease.

classification of valvular heart disease because, despite a significant reduction in the incidence of rheumatic fever and its sequelae valvular surgery continues to rise in many modern industrialized communities. In the United Kingdom (UK) for example, between 1986 and 2005 the number of first-time valve replacement operations performed nearly doubled from 4,728 to 9,022 (UK Heart Valve Registry 2007). Thus, such a significant increase in the rate of valvular surgery lends support to the suggestion of the influence of other mirco-organisms and prevalence of new types of valve disease.

The most significant change in cardiac valvular disease pathology has been the reduction in rheumatic fever and increase in age-related degenerative (ie. atherosclerosis) valve disease. Improved and easier access to medical care, better housing and standard of living in many modern societies has led to an increased lifespan and consequently, an increase in the numbers of elderly (i.e. ≥60 years) within populations. Worldwide it is estimated 10% of the world's population is now aged ≥60 years (Christ 2008; Office for National Statistics (ONS) 2010) and in the UK alone by the end of 2008 16% of the UK population were aged ≥60 years. Furthermore, predictions suggest in the next quarter century this sector will have increased nearly threefold to 16.4 million and represent nearly one-quarter of the total population (ONS 2010). In addition, the growth in the numbers of very elderly (i.e. ≥85 years) has been significant and between 1983 and 2008 these numbers more than doubled from 0.6 million to 1.3 million people (ie. 1% to 2%) with projected estimates suggesting a doubling again to 3.3 million by 2033 representing 5% of the total population (ONS 2010). As a consequence of changing age profiles, disease profiles have also changed.

Deaths due to infectious diseases and acute illnesses have declined whilst mortality resulting from chronic and degenerative diseases such as cardiovascular disease has increased (National Centre for Chronic Diseases and Health Promotion 2002; Allender 2008; World Health Organization (WHO) 2011). Morbidity due to progressive diseases continues to increase and approximately 20 million people annually worldwide survive heart attacks and strokes with many requiring long-term clinical care (WHO 2011).

Reflecting these changes, data from the UK Heart Valve Registry (2007) reveals the average age of patients undergoing first-time valve replacement increased from 58.6 years in 1986 to 67.1 years in 2005. Furthermore, the proportion of ≥70 year olds undergoing first-time valve replacement surgery more than quadrupled from 12.4% to 50.6% for the same period. In addition, reflecting changes in associated disease profiles mitral valve replacements (MVR) accounted for 45% of all valve replacements in 1986 compared with 55% in the aortic position (AVR). In contrast, by 2005 MVR had fallen to just 18% whilst AVR had increased to more than three-quarters of all replacements (ie. 81%). Tricuspid and pulmonary valve replacement (TVR; PVR) surgery accounted for the remainder of adult valve surgeries. Not all cardiac valvular diseases however, are the result of the degenerative process and some diseases are caused by congenital or inherited abnormalities.

1.3.1 Congenital valvular disease

Congenital defects can affect any part of the heart and it is estimated between 8 and 14 babies born per 1,000 have some form of congenital heart defect making this the most common type of birth defect (Hoffman 2002; Marelli 2007; Giannoglou 2009). Progress made in the diagnosis and treatment of congenital heart disease has resulted in more than 95% of children with congenital heart disease surviving into adulthood and, as a consequence, there is a substantial growth in adult congenital heart disease (Warnes 2005). Congenital valvular disease is one form of congenital heart disease and commonly affects the aortic or pulmonary valves. Congenital abnormalities may take the form of wrong size valve, malformed leaflets or leaflets not properly attached to the annulus. The aortic valve is more commonly affected by such abnormalities and reports suggest it occurs in approximately 1-2% of the population (Warnes 2003; Verheugt 2008). Others however, report a higher incidence of pulmonary valve disease and suggest a realistic estimate is 11% (Giannoglou 2009). However, as with the mitral and tricuspid valves in which defects occur only rarely, any abnormalities of the pulmonary valve are often treated in childhood.

Malformation of the aortic valve leaflets tends to present as uni- or bi-cuspid leaflets (Figures 1.5a-b) instead of the normal tricuspid valve and research has shown the congenitally bicuspid valve is responsible for the majority of older patients suffering with isolated aortic stenosis (Figure 1.5c; Rapaport 1975; Hoffman 2002). Unequal leaflet sizes coupled with commissural fusion result in an inability of the valve to open fully causing turbulent blood flow and subjecting the leaflets to undergo constant trauma. Consequently, the leaflets become thickened, fibrosed and fused until they eventually become rigid predisposing them to calcium deposits which cause stenosis of the valve. Congenital aortic stenosis in younger individuals i.e. aged ≤15 years tends to result from uni-cuspid aortic valve formation and tends to be stenotic from birth (Roberts 2008). However, the congenitally bicuspid aortic valve is more commonplace in adults and, although these are infrequently stenotic at birth the condition develops with increasing age as a result of calcific deposits on the aortic aspects of the cusps (Roberts 1970). As previously mentioned, bicuspid aortic valves have been reported as more common than any other congenital cardiac anomaly and in many cases the condition does not cause any problems in later life. However, as the aging process progresses a bicuspid aortic valve is more likely than a normal valve to undergo stenosis and calcification resulting in the cusps being unable to close fully causing aortic regurgitation as well as, making the valve more prone to infective endocarditis. Studies have reported ≥5% incidence of bicuspid aortic valve stenosis in an adult population (lung 2003) and between 1.5% and 22% incidence of aortic regurgitation (aR) secondary to a bicuspid valve (Yener 2002; Roberts 2006).

Sadee et al (1992) reported three distinct groups of congenital valves associated with aR (a) purely bicuspid valves (b), bicuspid valves with a conjoined leaflet containing a raphe and (c), valves with a conjoined leaflet and distinct central indentation of the free edge. The authors suggested conjoined leaflets, as described in the latter description were more likely to interfere with coaptation of the leaflets, particularly once degenerative age related changes occurred making the leaflets less mobile and likely to

cause aR. aR however, does not exclusively occur in bicuspid aortic valves but can occur in normal tricuspid valves arising primarily because of the prolapse of one or more leaflets, usually with elongation of the free edge. In addition, aR may also result from dilation of the aortic root and annulus which causes the aortic valve leaflets between the commissures to stretch leading to central leakage due to inadequate leaflet apposition (Sadee 1992; Roberts 2006). aR can also be caused by the post-inflammatory processes of infective endocarditis and rheumatic fever which causes the leaflets to retract thus allowing highly invasive organisms in the bloodstream to lodge on a normal valve causing leaflet deformation and destruction. Reports suggest the estimated incidence of bicuspid related infective endocarditis ranges from between 10-16% (Lamas 2000; Yener 2002).

Congenital abnormalities of the pulmonary valve affects blood flow between the right ventricle and pulmonary artery and therefore blood supply from the heart to the lungs. Abnormal development of this valve occurs during the first eight weeks of pregnancy when the fetal heart is developing and deformation of the valve can lead to difficulty in leaflet opening and allowing forward blood flow. The unicuspid or bicuspid pulmonary valve, a general feature of tetralogy of Fallot the most common cyanotic heart defect and cause of 'baby blue syndrome', can cause partial fusion and/or thickening of the leaflets causing valvular stenosis such that the valve is unable to fully open. Although stenosis of the valve occurs in approximately 7-12% of patients with congenital heart disease it accounts for 80% of right ventricular outflow tract obstruction (Bashore 2007; Giannoglou 2009). Pulmonary valve stenosis (PVS) increases the workload of the right ventricle as it attempts to move blood through the pulmonary valve until eventually the ventricle becomes hyperplastic causing peripheral oedema.

Figure 1.5 Congenital abnormal aortic valve

(a) Unicuspid aortic valve with visible stenosis **(b) Bicuspid aortic valve**

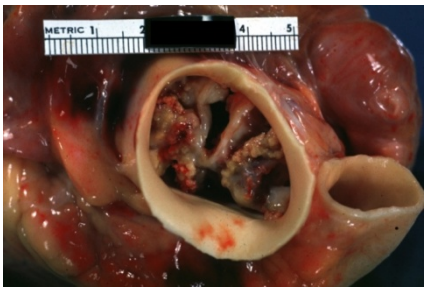

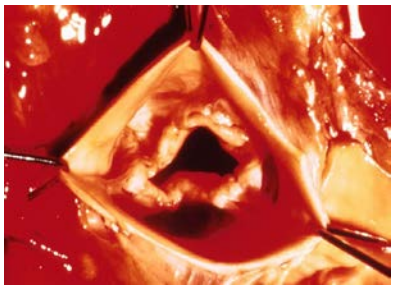

(c) Gross image of a stenotic bicuspid aortic valve

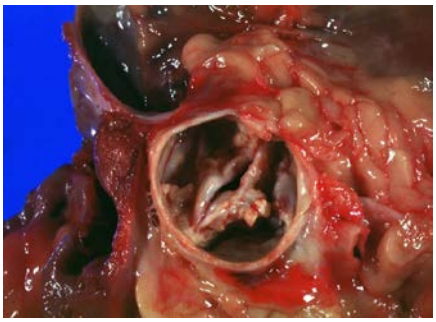

Congenital mitral and tricuspid valve diseases are relatively rare in adults. Stenosis of the mitral valve orifice to ≤ 1 cm^2 increases left atrial pressure as it attempts to push blood through the valve. However, this constant pressure overload in the atrium also increases its size and makes it prone to developing atrial fibrillation and loss of atrial kick which in turn, causes pressure transfer into the pulmonary vasculature and rapid decrease in cardiac output causing pulmonary hypertension and sudden congestive heart failure. Abnormalities of the tricuspid valve include Ebstein's anomaly which, during fetal development is displaced downwards towards the apex of the right ventricle although the valve annulus develops in the normal position. Normally, the tricuspid

valve has three leaflets. However, as Figure 1.6 shows in Ebstein's anomaly one or two of the leaflets adhere to the right ventricular wall and septum causing the anterior leaflet to become typically enlarged as well as the right atrium to the detriment of the right ventricle. Malformation of this valve causes regurgitation and in extreme cases, because the right ventricle is undersized, insufficient blood flow is carried to the lungs causing the individual to become cyanotic. In most adult cases of Ebstein's anomaly symptoms tend to be relative mild. However, if regurgitation becomes moderate to severe individuals may experience arrhythmia, decreased stamina, fluid retention and heart failure (Mulder 2003). Under such circumstances, the individual may require either valve repair or valve replacement with a prosthetic valve (see Chapter 2).

Figure 1.6 Common abnormality of the tricuspid valve - Ebstein's Anomaly

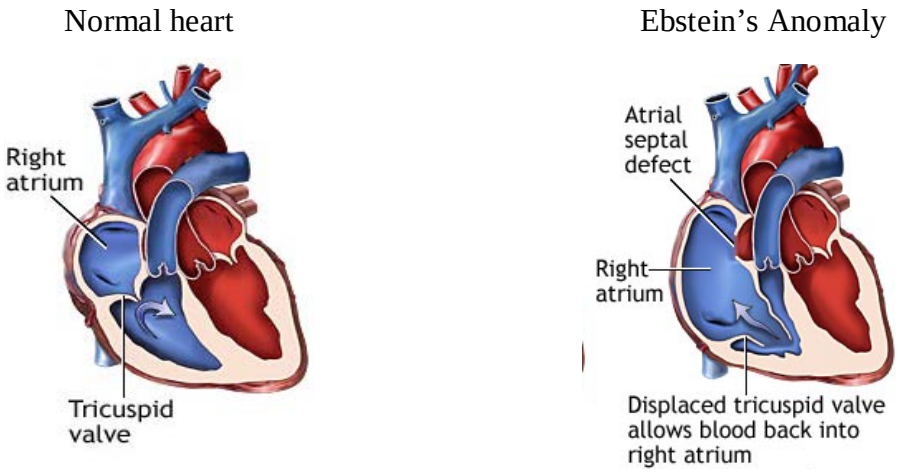

1.4.2 Acquired valvular disease

Acquired valvular disease develops in valves that were once normal and can change them in a number of ways. The chordae tendinea or papillary muscles for example, may become stretched or rupture, the valve annulus can dilate or the valve's leaflets may become fibrotic and calcified. The mitral and aortic valves are more commonly affected and although diseases of the tricuspid and pulmonary valves do occur these tend to be relatively rare. Native heart valves may be subjected to inflammatory diseases, stenotic

or regurgitant lesions or, infective or non-infective vegetations and, depending upon which of these states is present the valve will have either structural abnormalities or an abnormal function. Stenotic valves almost always have some form of anatomical abnormality, usually fibrosis or calcification, which often take years to develop. In contrast, regurgitant valves tend not display any anatomical defect although any defects may be valve-related or related to the surrounding supporting structures and, unlike stenotic valves the lesions may be chronic or acute. The next part of the chapter looks at the impact of the differently acquired valvular diseases, such as rheumatic fever and degenerative valve disease, which can lead to valvular stenosis and regurgitation/insufficiency causing pulmonary congestion, oedema, contractile dysfunction and heart failure. In addition, micro-organisms in the bloodstream are known to cause infections of the heart's valves and surrounding tissues and so this next section of the chapter looks at the effects of infective endocarditis on the functionality of the heart valve as well as the impact of the infection on the structure and strength of the valve and surrounding tissues and the potential for abscess formation, thrombo-embolic complications and heart failure.

1.4.3 Rheumatic Fever

Rheumatic fever is an important acquired cardiovascular disease in which the initial infection occurs in children and adolescents although the associated heart problems may not be seen until 20-40 years later. Despite the dramatic decline of acute rheumatic fever in developed countries its prevalence is still significant in some indigenous populations and countries with low socioeconomic status, malnutrition, poor hygiene and poor access to health care (Cilliers 2006; Madden 2009). Carapetis (2005) reported 16-20 million people worldwide are affected by rheumatic fever of which 79% come from less developed countries. Overall, it is estimated the prevalence rates in less developed countries ranges from 2.5 to 3.2 cases per 100,000 compared with $\leq$1 per 100,000 population in higher income populations (Carapetis 2005; Cilliers 2006). However, due to changes in the world's migratory system some of the more developed

countries such as Spain for example, are witnessing increases in cases of rheumatic fever because of an influx of immigrants from countries where rheumatic fever is still prevalent (Bernal 2008). Furthermore it is estimated 10-35% of all cardiac admissions are for patients with rheumatic fever or chronic rheumatic heart disease (Soler-Soler 2000).

Rheumatic fever is a multi-system inflammatory disease characterized by involvement of the heart, joints, central nervous system, subcutaneous tissues and skin. It is an inflammatory non-supprative complication of phyaryngitis caused by Group A beta-haemolytic Streptococcus and can be sub-acute or chronic, self-limiting or be slowly progressive. The acute phase causes inflammation of all three layers of the heart, the myocardium, pericardium and endocardium (ie. pancarditis) and approximately 53% of patients suffering an attack of rheumatic fever will suffer from carditis which may result in valvular heart disease, heart failure and death (Tubridy-Clark 2007). All four valves may be affected but the most commonly affected is the mitral valve (75-80% cases) followed by the aortic (30% cases) and tricuspid and pulmonary (≤5% respectively) (Cheitlin 1993). The most common chronic valvular abnormality resulting from rheumatic fever is mitral stenosis (mS) followed by aortic valve insufficiency, also known as aR (Roberts 2008). At an acute level small thrombi develop along the lines of closure of the valve on the atrial sides of the atrioventricular valves (mitral and tricuspid valves) and ventricular side of the semilunar valves (aortic and pulmonary valves) although they are not complicit in the destruction of the valve. In addition, there may be associated oedema and cellular infiltration of the leaflets. Chronic rheumatic fever can cause inflammation of the valvular tissue and thickening of the leaflet due to fibroses and deposition of calcium causing valvular stenosis, obstruction of blood flow, incomplete closure and regurgitation (Leong 2006; Roberts 2008). The chordae often become thickened and shortened and the presence of short thick chords attached almost directly to the papillary muscles give the appearance the sub-valvular chordal space has disappeared. In addition, commissural fusion and erosion of the surface endothelium in

the mitral position can often occur in addition to overlying of thrombus material giving the typical 'fish mouth' appearance of the rheumatic stenotic mitral valve.

Mitral regurgitation (mR) [3] may also result from the long-term effects of rheumatic fever or post-inflammatory diseases in which, as described above, the leaflets become opaque and thickened and the chordae tendineae become thinned and stretched. Although, in some cases these can appear slightly thickened by fibrous tissue or even mildly fused causing elongation of the ostium which in turn becomes funnel shaped. As consequence of the leaflets being unable to fully coapt when the valve is closed it prolapses into the left atrium causing mR and rapid volume overload in the left-side of the heart. Left atrial volume and pressure overload restricts drainage from the lungs via the pulmonary veins and in acute mR causes pulmonary congestion and oedema. Patients suffering from chronic mR may be asymptomatic for many years during which time the gradual increase in size of the left atrium allows it to compensate such that there is no noticeable increase in atrial and pulmonary venous pressures until late in the course of the disease when progressive left ventricular dilation leads to eventual increase in afterload, contractile dysfunction, and heart failure. mR is, in fact, the second most common valvular disease and it is estimated it occurs in as many as 57% of patient populations (lung 2003; Leong 2006; Roberts 2008).

1.4.4 Degenerative valve disease

Aortic stenosis (aS) is now the most common valve abnormality and is associated primarily with degenerative calcification in the majority of patients compared with post-inflammatory involvement and congenital lesions (Stewart 1997; Otto 1999; lung 2003; Faggiano 2006; Roberts 2008). Despite a significant reduction in rheumatic fever and thus, rheumatic valve disease in most modern industrialized countries this has not been matched by a reduction in the numbers of valvular surgeries performed. lung (2003) reported 47% of patients in the Euro Heart Survey surgical sub-group had a diagnosis of

[3] Mitral regurgitation is also known as mitral insufficiency or mitral incompetence.

aS and, as previously mentioned data from the UK show mitral valve replacement (MVR) fell from 54% to just 18% of all valve replacements performed between 1986 and 2005 compared with an increase from 54% to 81% in aortic valve replacement (AVR) (UK Heart Valve Registry 2007). Although data was not collected in the UK on valve pathology for the whole period it was suggested shifts in trends in valve replacement surgery reflect both changes in the age profile and associated disease pathology.

Degenerative aortic valve disease is characterized by increased leaflet thickness, stiffening and calcification without commissural fusion and results in aortic valve stenosis. As a result the volume of blood able to flow through the valve is severely restricted and a reservoir accumulates in the chamber. By age ≥65 years the tricuspid aortic valve displays a grossly deformed rigid structure with dense nodular calcifications causing some degree of immobility. As age progresses the diameter of the aortic root and valve annulus increases and by aged 80 years the aortic valve annulus is similar to that of the mitral valve. Furthermore, there may be calcification of the aortic valve ring which spreads to the anterior (aortic) leaflet of the mitral valve and the membranous part of the inter-ventricular septum where it interferes with the atrio-ventricular conduction system causing ventricular arrhythmias. Heavily stenosed valves can cause haemolytic anaemia and left ventricular hypertrophy may result due to the difficulty in pumping blood through the stenosed valve. Moreover, approximately 10% of patients with aS develop infective endocarditis (Vahanian 2007; see below). Calcification of the mitral valve and ensuing stenosis causes rigidity of the left atrium and restricted atrial dilation resulting in increased pulmonary venous pressure and vascular resistance (Cheitlin 1993). It has however been suggested the aging process is not the only contributory factor in the development of valvular disease. Soler-Soler (2000) for example reported 25-45% of octogenarians do not have aortic calcification thereby suggesting valve disease is not universally present in the elderly. Although it is accepted there is a positive relationship between degenerative valve disease and increasing age studies suggest this is an active yet reversible process, similar to atherosclerosis, including lipid

deposition, macrophage infiltration and the production of osteopontin and other proteins which play an increasingly significant role in the development of degenerative valve disease (Stewart 1997; Faggiano 2006; Veinot 2006; Roberts 2008; Rajamannan 2009).

Degenerative diseases of the mitral valve are more commonly seen as regurgitant. Although degenerative mitral regurgitation is the most common aetiology in Europe ischaemic and functional mitral regurgitation are gaining prominence (lung 2003). mR may result from degenerative diseases such as myxomatous degeneration which is a primary cause of mitral valve prolapse (MVP), now identified as the most common cause of mR and occurring in approximately 5% of the population overall (Cheitlin 1993). mR caused by myxomatous degeneration is characterized by atrophy of connective and valve tissue such that the valve becomes thickened though soft and pliable. Chordal rupture is uncommon but if it occurs the ruptured chords may fuse in a random and irregular fashion on the underside of the valve leaflets yet leaving the commissures unfused.

1.4.5 Native valve infective endocarditis

Infective endocarditis (IE) of the native valve is an infection of the endocardium which arises as micro-organisms in the bloodstream become enmeshed in fibrin and platelet deposits on the valvular endothelium of damaged, roughened valve leaflets with congenital or acquired lesions (e.g. bicuspid aortic valve, rheumatic valvular disease, MVP, tissue surrounding a prosthetic valve) and form irregular vegetations. These micro-organisms multiply within the fibrin-platelet matrix and products from their metabolism cause disruption to the connective tissue of the valve causing constant haemodynamic stresses acting on the valve to weaken the collagen structure and tear, the result being valvular incompetence. These vegetations vary in size and can also become friable making them susceptible to small fragments breaking off and increasing the risk of systemic or pulmonary thrombo-embolic potential (McConnell 1967; Mylonakis 2001; Vilacosta 2002; Habib 2006). In addition, other complications such as heart

failure and valvular or myocardial abscesses may occur. IE of the aortic valve can spread to the ventricular septum or, it may cause abscesses to develop which may rupture into the right heart or, interfere with conduction of the cardiac impulse and cause atrioventricular block. Septic abscesses of the mitral valve can affect the papillary muscles or cause destruction of the valve annulus resulting in flail mitral valves that require prompt surgical correction (Weale 1992).

IE can also arise on functionally normal valves particularly in cases of intravenous drug misuse. Current estimates suggest the incidence of IE amongst this sector ranges from 1-5% a year and appears to be increasing steadily in part because treatment of this group is made more difficult by their drug behaviour and poor compliance with treatment (McConnell 1967; Benyon 2006). Moreover, research has shown the use of intra-cardiac and intravascular devices, especially those left in place for long periods, are also promoters of infective endocarditis (Perlman 1971; Mylonakis 2001; Johnston 2004; Cabell 2004; Anguera 2004; Fong 2009). Also at risk are immuno-suppressed patients with intravenous catheters and those undergoing haemodialysis (MacGregor 1989). The incidence of IE has remained relatively unchanged over the past two decades at approximately 1.7-6.2 cases/100,000 years (Hoen 2002; Prendergast 2006) and is low in the young, excluding intravenous drug users, but increases with age. Mylonakis (2001) for example, reports an increase in median age from 30-40 years during the pre-antibiotic era to 47-69 years post introduction of antibiotics whilst Hoen (2002) reporting on the results of two studies conducted in France identified a peak incidence of 14.5 episodes per 100,000 patients years in patients aged 70-80 years. The bicuspid aortic valve, which is the most common congenital valvular abnormality (see above) and already predisposed to aS, is also highly susceptible to developing IE and evidence suggests it occurs in 7-25% of autopsy cases and between 12% and 45% of surgical cases (Lamas 2000; Yener 2002). IE is thought to predominate in the mitral valve and reports suggest an incidence of between 24% and 86% of autopsied patients (MacGregor 1989; Weale 1992; Boudoulas 2002) compared with 5-36% for aortic valves alone and between 5% and 42% for combined aortic and mitral valves (Weale 1992; Boudoulas

2002). However, contrary to these findings, others have reported a predominance of IE in the aortic valve (Schulz 1996). Tricuspid and pulmonic valve IE is less prevalent although is more common amongst intravenous drug abusers (MacGregor 1989).

Historically IE has been clinically divided into acute and sub-acute presentations which classify the rate of progression and severity of the disease. Acute infection tends to be culminant, developing over a period of days or weeks rather than weeks or months as seen in the sub-acute phase. The acute disease, which is more commonly found in normal hearts of intravenous drug abusers, may cause destruction of valves or dislodgment of valve cusps, rupture or aneurysms and abscesses of the myocardium which infiltrate into other cardiac chambers with fistula formation (Leong 2006). Although cured of the infection patients may continue to be at risk from the acute phase of the disease long after completion of the antibiotic therapy because the weakened valve and surrounding tissue is highly susceptible to tearing and rupture which may not occur until later, and is certainly so with prosthetic valves (Weale 1992; Saxena 2009; see below). Sub-acute endocarditis presents as a low virulence and mild to moderate illness in patients with an underlying cardiac abnormality. The disease progresses slowly over weeks and months and has a less traumatic clinical course than the acute disease.

1.5 Common complications of replacement heart valves

The majority of heart valve replacements function without problem. However, some replacement valves develop complications as a result of changes in normal physiological processes (eg. immunology, inflammation, blood coagulation) or, because of mechanical valve failure and require replacement. Estimates from the UK suggest on average $\leq 3\%$ of replacement heart valves are explanted and re-replaced annually with another type of heart valve, half of which are due to valve-related causes (Weerasinghe 1999; UK Heart Valve Registry 2007). The next section of this chapter therefore looks at some of the

complications associated with prosthetic heart valves starting with infections of the valve prosthesis.

1.5.1 Prosthetic valve endocarditis

Prosthetic valve endocarditis (PVE) remains an infrequent but serious complication following native valve replacement. Research suggests an overall incidence ranging from between 0.3% to 6% of the population (Sett 1993; Edwards 1998; Mylonakis 2001; Habib 2005; Relic 2009) with an annual incidence in the first year post-operative of 3% reducing to 1% per year thereafter (Lytle 1996; Prendergast 2006). PVE is classified according to time of onset after valve implantation with early onset of the disease occurring ≤60 days post-operative and late onset occurring anytime thereafter, the spectrum of which mirroring that of native valve IE. Despite a relatively broad range of potential candidates responsible for the development of PVE most cases result from a small number of organisms with a distinction between early and late onset PVE. Research has identified staphylococcus aureus as the primary culprit of early-onset PVE originating from intra-operative contamination and post-operative wound infection. Furthermore, the majority of cases occur within the first year post-operative (Fong 2009). In contrast, late-onset PVE results from streptococci infection, the course of which is similar to native valve IE (MacGregor 1989; Schulz 1996; Habib 2005; Fong 2009). Complications associated with PVE are common and include heart failure, ventricular obstructive outflow, stroke, intra-cardiac abscesses and abnormalities of cardiac conduction and high risk of in-hospital mortality (Cavarocchi 1983; Habib 2005; Hassoulas 2009; Fong 2009). Antibiotic therapy can effectively treat PVE particularly when the infection is limited to the prosthetic valve leaflets. However, in patients with infection of the valve annulus a combination of prosthetic valve replacement and antibiotic therapy is required. Moreover, in patients with ‘cured’ prosthetic valve endocarditis re-operation is often eventually required (Lytle 1996).

Reports on the prominence of aortic versus mitral valve in the development of PVE are conflicting and although Weale (1992) and Rekik (2009) in their respective studies identified the mitral valve as being more susceptible to PVE many others have found to the contrary (Sett 1993; David 1995; Schulz 1996; Edwards 1998; Hassoulas 2009). Aortic PVE is considered the most destructive because the infection usually spreads to the aortic root causing abscess formation often necessitating major reconstructive procedures for the repair of the root or repair of the mitral valve annulus. In addition, the infection often spreads through the aortic wall to other structures and cavities (Cavarocchi 1983; Saxena 2009). Bioprosthetic valves have been reported as being more susceptible to PVE than mechanical valves (Schulz 1996; Lytle 1996; Habib 2005; UK Heart Valve Registry 2007). However, Habib et al (2005) noted when onset of PVE is considered mechanical prostheses demonstrate a greater susceptibility to developing early onset PVE than either bioprostheses or homografts but, the reverse is true with late onset PVE.

Early onset PVE in bioprosthetic and homograft valves is very destructive and occurs mainly in the fibrin layer covering the valve leaflets and is liable to cause obstruction or perforation of the leaflets and subsequent valvular insufficiency. Progression of the infection into the annulus and surrounding host tissue promotes paravalvular abscess formation and as David (1995) reported this ranges from between 16% and 42% of cases. Paravalvular abscess formation may however, also occasionally form without leaflet involvement if the loci of infection begin at the site of the valve annulus. Vegetation growth may also occur on the leaflet surface causing leaflet destruction, stenosis or valvular insufficiency particularly in bioprostheses. In contrast, mechanical valve PVE often begins at the sewing ring as a result of the synthetic materials in the valves acting as a barrier against the growth of micro-organisms. Abscess formation at the ring site is a common feature (Lytle 1996) and annular inflammation and extreme tissue friability make it difficult to seat and anchor the prosthesis thereby increasing the risk of prosthetic valve dehiscence, severe paravalvular and post-operative valve regurgitation and paravalvular leak (PVL) (Cavarocchi 1983; Masri 1990; van der Vorm

2000; Hassoulas 2009; Saxena 2009). The incidence of PVL has been reported as being as high as 48% in the aortic site early post-implantation in the absence of infection (Rallidis 1999). Others however, such as Jindani et al (1991) and Gudbajartsson and colleagues (2008) have reported considerably lower incidences of 2.5% and 1-1.5% per patient year respectively suggestive of improved surgical techniques and valve design over the last thirty years. It should be noted however, PVL may occasionally result from improper implantation of the valve. PVE of the composite aortic valve and ascending aorta is often localized in the junction between the sewing ring of the valve and the aortic annulus. Development of large post-operative pseudo-aneurysms resulting from this infection is a recognized complication and the potential additional stresses exerted at the suture line and aortic wall may increase the risks of rupture, thrombo-embolic complications (thrombotic and/or septic), metastatic abscesses, and cerebrovascular events (Kouchoukos 1991; Oechslin 1995).

1.5.2 Thrombo-embolism

One of the most common complications associated with prosthetic heart valves, and in particular mechanical valves is the formation of thrombi and associated emboli causing transient or fatal events. Blood exposed to an artificial surface may induce thrombo-embolization and according to Virchow's triad, thrombus formation is largely dependent on three predisposing factors. Firstly, endothelial factors which include the surface characteristics (ie. material and design) of the prosthesis and therefore represent the valve's biocompatibility and its interaction with the suture zone. Secondly, haemodynamic factors which involve haemodynamic characteristics which may induce variations in local rheology leading to turbulence, reduced blood flow velocity and subsequently, reduction in cardiac output and a stagnation of blood. Finally, haemostatic factors (ie hypercoagulability) which, during the early post-operative period are particularly challenging due to the need to balance the risks of over anticoagulation and associated haemorrhagic complications with those of under anticoagulation and thrombus formation.

Prosthetic valve thrombosis (PVT), as defined by Edmunds et al (1996), is a thrombus which in the absence of infection is attached to or near an operated valve and occludes blood flow or interferes with valvular function. Mechanical valves are more susceptible to PVT than bioprostheses and reports suggest an incidence of 0.7-10% per patient years (Vongpatanasin 1996; Crawley 2000; Dűrrleman 2004; Laplace 2004; Roudaut 2007). Moreover, mitral valve prostheses show a greater susceptibility to developing PVT and estimates suggest they may be as much as four times more likely to do so (Dűrrleman 2004). Vongpatanasin and colleagues (1996) on the other hand, suggest there is a similar incidence of PVT in patients with mechanical prostheses who receive adequate anticoagulant therapy compared with those with bioprosthetic valves (Bettadapur 2002). PVT may manifest clinically as pulmonary congestion, poor peripheral perfusion or systemic embolization the latter usually involving the central nervous system and often causing transient or fatal events. The incidence of prosthetic valve embolization (PVe) has been reported as 2% per year in patients on warfarin although this increases fourfold in patients not anticoagulated (Cannegieter 1994). Mitral valve prostheses and mechanical valves carry a greater risk of PVe than aortic valve prostheses and bioprostheses (Vongpatanasin 1996; Bettadapur 2002) and researchers have suggested the risk of PVe in patients with mechanical prostheses without any antithrombotic therapy is 4% per patient-year, decreasing to 2% for those on antiplatelet therapy and 1% for those on warfarin (Vongpatanasin 1996; Crawley 2000; Bettadapur 2002). In comparison, the prevalence of embolization of bioprosthetic valves is estimated at $\leq$1% per year (Bonow 1998), similar to mechanical valves which are adequately anticoagulated. Type of prosthesis, older age (ie. $\geq$70 years), atrial fibrillation and poor left ventricular function have also been identified as significant contributory risk factors leading to embolization (Vongpatanasin 1996; Bettadapur 2002).

1.5.3 Haemorrhagic complications

Anticoagulant therapy is not without risk and by attempting to reduce the risk of thrombo-embolic events the risk of bleeding complications is increased (Crawley 2000; Oxenham 2003). A review of the literature by Vongpatanasin et al (1996) of thrombo-embolic complications in prosthetic heart valve patients receiving anticoagulant therapy reported a reduced incidence of thrombo-embolic and haemorrhagic events when INR (international normalized ratio) is maintained between 2.5 and 4.9 overall. When individual valve types are considered the authors found patients with caged-ball valves or those with multiple mechanical valves benefitted when their INR was maintained between 4.0 and 4.9. However, patients with bileaflet valves suffered fewer adverse events when their INR was maintained at half this level (ie. 2.0-2.9) with those with single-tilting disk valves suffering fewer events with an INR level mid-way between the other two (ie. 3.0-3.9). Although the authors suggest age is not a pre-determining factor and that the overall risk for any bleeding event is no higher in elderly patients compared with younger ones, a review by Fihn (1996) found younger aged patients are generally more tolerant of anticoagulant therapy. Efforts to reduce the incidence of thrombo-embolic events without increasing the risk of bleeding using anti-platelet therapy with warfarin found the annual rate of major thrombo-embolic events was significantly reduced but was matched by a rise in the incidence of bleeding complications (Turpie 1993). Criticism of Turpie's study however, relates to the inclusion of all minor bleeding events such as bruising, epistaxes and haematuria which may have contributed to the reported higher incidence rates not found by others. When only the risk of major haemorrhagic events was assessed no significant differences between groups (ie. aspirin versus placebo) were found. Furthermore, a meta-analysis conducted by Massel and colleagues (2001) found the net beneficial effect gave a favourable risk-to-benefit profile.

1.5.4 Intrinsic valve failure

Intrinsic valve failure (IVF), also referred to as structural valve failure, is a relatively rare complication of heart valve replacement with a replacement valve accounting for approximately 2% of all valve replacements in the UK between 1986 and 2007 (UK Heart Valve Registry 2007). IVF affects all types of prosthetic heart valves and presents as material degeneration leading to premature failure of the mechanical components and may present as tearing of the leaflet(s), strut or leaflet fracture and leaflet escape. In addition, valve failure may occur as the result of non-structural dysfunction associated with abnormal tissue-prosthesis reactions leading to calcification of the leaflets, suture line disruption leading to paravalvular leakage, suture failure and suture line (Masri 1990; Hammermeister 2000; Bloomfield 2002; UK Heart Valve Registry 2007). Malfunction of mechanical valves is often abrupt and catastrophic and can result from degeneration of the occluder (Peterman 2006), strut fracture (Ringel 1983; Omar 2001) and impaired mechanical failure due to thrombus and pannus formation (Cleland 1973; Shiono 2005) or, infection (see above for PVE). The most well documented failure of a mechanical heart valve is the Björk Shiley 60º convexo-concave tilting disc valve which was withdrawn from the market in 1986. Research found the risk of strut fracture in this valve was 0.5% to 2% per patient year and was likely to cause disc embolization, acute valvular regurgitation and/or sudden fatality particularly in young patients (ie. ≤50 years at implantation), those with an opening angle of 70º and those with a diameter of ≥29mm (van der Graaf 1992; see below).

Bioprosthetic valves have a higher freedom from thrombus formation usually without the need for anticoagulation therapy but nonetheless, because of their altered biological materials still undergo the degenerative process. Structural valve deterioration of bioprosthetic valves has been shown to begin at 3 years post-implantation (Bloch 1984) though average estimates suggest 8 years post-implantation reaching ≥60% at 15 years (Gudbjartsson 2008). Furthermore, structural valve deterioration has been reported to be inversely related to a patient's age at implantation. Hoffman et al (2008) reported a rate

of degeneration exceeding 40% in younger patients (ie. ≤40 years) with porcine bioprostheses at 10 years post-implantation compared with 15% in the 60 – 70 year old age group and 10% in the ≥70 year olds. At 15 years post-implantation, pericardial valve degeneration was similar to porcine valves and fewer than 10% of patients aged ≥65 years required a re-replacement of their prosthetic valve. Calcification has also been shown to be a primary contributor to valve failure of bioprosthetic valves which, like native valves, can restrict leaflet motion and produce leaflet tears. In a study by Farivar (2003) which investigated the causes of valve failure at one institution the authors found sterile degeneration accounted for 74% of all bioprosthetic valve failures and it was frequently associated with calcification of the leaflets and leaflet tears.

1.5.5 Prosthetic patient mismatch

Valve dysfunction can also result from inappropriate sizing of the prosthesis which may sometimes be misdiagnosed as IVF. The reported prevalence of prosthetic patient-mismatch (PPM) varies and reports suggest it may range from between 20-70% in moderate cases and 2-11% in severe cases (Pibarot 2006). PPM occurs when the effective orifice area of the prosthetic valve is less than the patient's normal native valve orifice area and associated body size (Rahimtoola 2003). As a consequence of the discrepancy between native and prosthetic effective orifice area, transvalvular gradient increases. Research has shown patients with PPM do not generally improve clinically post valve implantation and may even worsen irrespective of implant site. In a study by Pibarot et al (2006) the authors found PPM in the aortic site caused deteriorating haemodynamic function, reduced regression of LV hypertrophy, congestive heart failure as well as other additional cardiac events. Li et al (2005) reported no change post implantation of PPM in the mitral position (ie. 69% versus 68%) and a persistence of arterial hypertension compared with a significant reduction in the prevalence of pulmonary hypertension (ie. 69% pre-operative to 19%) post-operative in patients with no PPM. Furthermore, patients with PPM of both the aortic and mitral sites have also been shown to demonstrate a lower survival rate than those without PPM unless the

mismatched valve is not replaced with a larger one or one of a different type and enlarging the annulus (Pibarot 2006; Li 2005).

1.6 Emerging valve disease

This chapter has so far discussed the traditional causes of valvular heart disease. However, over recent decades a number of emerging causes of heart valve disease have become more prevalent such as inflammatory-immunological diseases associated with acquired immune deficiency syndrome (ie. HIV/AIDS) and the antiphospholipid syndrome, drug-related diseases caused by agents with a common chemical structure as the neuro-hormone serotonin [4] for example, anorexogenic and ergotamine products for the treatment of migraines, Parkinson's Disease and restless legs syndrome (Wilke 1997; Schade 2007; Connolly 1997). The final part of this chapter takes a brief look at some of these emerging causes of valvular heart disease starting with non-bacterial thrombotic endocarditis, a complication of HIV/AIDS and other inflammatory-immunological causes.

1.6.1 Non-bacterial thrombotic endocarditis (NBTE)

The most common valvular involvement associated with HIV/AIDS is marantic endocarditis, also referred to as non-bacterial thrombotic endocarditis (NBTE), which causes friable, fibrinous clumps of platelets and red cells similar to sterile verrucae attached to coaptation points of the valves. Reviews by Currie (1995) and Soler-Soler (2000) reported an incidence of NBTE of 3-7% in necropsy series although, both reviewers suggested, based on their experiences, these figures may be an overestimation. Although any valve can be involved NBTE usually involves the low pressure side of the mitral and aortic valve in HIV negative patients (ie. 92%; (Moss 2003)). An estimated 8-14% of NTBE occurs in tricuspid valves and occurs more commonly in AIDS-positive patients who are intravenous drug users (Currie 1995; Moss 2003). Pulmonary valve

[4] Serotinin is a neuro-hormone and plays a significant role in the development of cardiac valve disease.

involvement is rare (Moss 2003). Complications associated with right-sided NBTE are either cardiac or pulmonary with both resulting in tricuspid regurgitation with volume overload, right-sided chamber dilatation and heart failure.

1.6.2 Auto-immune diseases and valvular heart disease

Antiphospholipid syndrome (APS) is a recognised systemic auto-immune disease associated with a hypercoagulable state, vascular thrombosis and fetal loss (Cervera 1991). Cardiac valvular involvement has however, also been gaining recognition as a serious complication of the disease and heart valve lesions are the most common cardiac manifestation described in patients with primary [5] and secondary [6]APS. Doppler echocardiography of patients with APS has shown chordal fusion and retraction as well as valves deformed by vegetations, fibroses, scarring and calcification causing stenosis and regurgitation (Cervera 1991; Nesher 1997). Although in many cases individuals may be asymptomatic severe valvular dysfunction may result in cardiac failure requiring heart valve replacement (Nesher 1997). The prevalence of valvular involvement in patients with primary APS ranges from between 18% and 38% and is predominant in patients aged ≥40 years (Cervera 1991; Nesher 1997; Krause 2005). Mitral and aortic valve regurgitation are the most common haemodynamic dysfunctions and reports suggest the occurrence ranges from between 4% and 31% of patients half of whom it has been suggested, will require valve replacement surgery (Bulckaen 2003; Krause 2005). Twenty-two percent of individuals with primary APS develop mR which occurs more commonly than aR (ie. 6-10%) (Nesher 1997). In addition, studies have reported patients with APS, antiphospholipid antibodies and severe valvular heart diseases are at increased risk of developing thrombosis (Cervera 1991; Bulckaen 2003). Moreover, this is dramatically increased if there is a history of thrombo-embolic events. Cervera (1991) reported that 52% of APS patients with valvulopathy suffered a stroke or transient

[55] Primary antiphospholipid syndrome (APS) is used when APS occurs in the absence of any other related illness.

[6] Secondary APS is referred to when seen in conjunction with other auto-immune diseases such as systemic lupus erthymatosus (SLE).

ischaemic attack compared with only 15% of patients without valvuloplathy ($p<0.01$) and in a study by Bulckaen et al (2003) 50% of patients who had a history of thrombo-embolic events experienced a new thrombo-embolic event during the follow-up period. However, the research also noted that in patients receiving anticoagulation therapy this risk appeared to be reduced.

1.6.3 Medication-related valvular disease

Medications used for the treatment of migraines (eg. ergotamine and methysergide), Parkinson's Disease and restless legs syndrome (eg. pergolide mesylate) as well as appetite suppressants (eg. fenfluramine-phentermine) have been linked to the development of valvular heart disease (Connolly 1997; Loke 2002; Hopkins 2003; Schade 2007). Ergotamine and methysergide are ergot alkaloid derivatives which share a common chemical structure to the neuro-hormone serotonin, an agent responsible for valve disease involving endocardial fibrosis. Soler-Soler's (2000) reports ergot alkaloid cardiac valve lesions can only occur after prolonged use and in a review of research investigating the effects of these two drugs noted that patients in one study by Redfield (1992) had received treatment for a minimum of six years and more usually 20 years. However, in a study which looked at the dopamine antagonists, pergolide and cabergoline used in the treatment for Parkinson's disease, shorter exposure times were found to be significant in the development of valvular disease. Schade (2007) reported daily doses of pergolide or cabergoline ≥ 3 mg for a period of ≥ 6 months produced endocardial thickening resulting from a fibrotic reaction that coats valves, chordae, papillary muscles and the endomycoardial surface. Valve and chordae retraction caused by this fibrosis lead to valvular stenosis or regurgitation.

Two appetite suppressants, fenfluaramine and phentermine, popular and successful treatments in the 1990s for obesity have, when given in combination, been found to be high risk for the development of cardiac valvular regurgitation (Connolly (1997). Like

ergot alkaloid drugs, these appetite suppressants cause valvular thickening with plaque development, chordal thickening and retraction. The original study by Connolly (1997) highlighted the high risk of valvulopathy associated fenfluaramine-phentermine combination which has subsequently been confirmed by others (Loke 2002; Hopkins 2003; Dahl 2008). However, strong debate relating to the incidence of valvulopathy associated with these anorexogenic drugs persists with some reporting incidences of 20% whilst other report it is as high as 33% (Loke 2002; Hopkins 2003). Appetite suppressants have demonstrated an increasing prevalence of progressive valvular regurgitation with increasing exposure to the drugs (Dahl 2008) and continue long after cessation. Indeed, Prasad (1999) reported a case of valvulopathy requiring surgery seven years after cessation of the drug. However, unlike ergot alkaloid drugs (see above), appetite suppressants cause damage after only a few months of treatment.

1.7 Chapter summary

In summary, cardiac valvular disease is a corollary of congenital, inherited or acquired abnormalities. This chapter focuses on some of the most common valve pathologies which affect valve function and compromise the heart's ability to pump blood through the circulatory system, ultimately causing cardiac and/or systemic failure. The heart is designed to last a life-time however, during its lifespan it is subjected to intrinsic defects and the aging process making it susceptible to structural and mechanical failure. Over the last few decades we have seen a reduction in communicable diseases that affect the heart and in particular, the heart's valves and an increase in age-related degenerative diseases and environmental factors. Furthermore, diagnostic and treatment advances have given rise to an increase in the proportion of individuals born with congenital abnormalities surviving into adulthood. Complications associated with cardiac valvular diseases are not only confined to native heart valves but also affect replacement valves and, although the majority function without problems complications can prove highly destructive and in some cases, fatal. The last few decades have also witnessed an emergence of some new causes of heart valve disease associated with the inflammatory

and auto-immune response as well as those associated with IV drug use and reactions to medications used in the treatment of some common conditions. All these complications can require some form of surgical intervention, whether it is valve repair and/or valve replacement with a prosthesis or homograft. However, before looking at the types of prostheses used in these procedures the thesis presents a glimpse of the evolution of valvular surgery from the first successful closed valve repair in the late 1800s to open heart surgery in the 20th Century and a reversal of preferences towards closed procedures in the 21st Century.

CHAPTER 2

Evolution of valvular surgery

2. Introduction

Valvular heart disease (VHD), as noted in Chapter 1, is an important cause of cardiovascular morbidity and mortality worldwide. Changing age and disease profiles of populations, improved standards of living, better access to vaccinations, antibiotics and healthcare as well as medical and surgical advances have led to increased longevity for many individuals suffering from VHD who may not otherwise have survived. One of the primary aims of any treatment for VHD is to lessen symptoms and protect the valve from further damage. However, although medical treatments such as angiotensin-converting enzymes (ACE) inhibitors, anti-arrhythmic drugs, anticoagulants, antibiotics, anti-hypertensives, calcium channel blockers and diuretics can effectively alleviate complications they do not correct the mechanical problems resulting from fusion of the leaflets or stenosis of the valve. Failure of these medical treatments, worsening symptoms and/or continued valve deterioration often results in the need for valve(s) repair or replacement. Valve repair is, in many cases, seen as preferable because of the significantly lower risk of post-operative infective endocarditis developing, low rates of thrombo-embolism, no requirement for life-long anticoagulation and good late durability (de Oliviera 2006). The UK for example has witnessed a steady decline in the numbers of mitral valve replacements over the last two decades from 45% of all valve replacements in 1986 to just under 18% in 2005 (UK Heart Valve Registry 2007) and in Germany, one in two operations on the mitral valve is a reconstruction (Hoffman 2008). Whilst these figures reflect changes in patient demographics and disease pathologies they also reflect changes in approaches to the treatments for VHD and the desire to retain whenever possible, the patient's native valve.

William Harvey, a 17th Century English physician, was the first person to comprehensively describe the systematic circulation and properties of blood being pumped to the body by the heart. As Figure 2.1 shows modern cardiac surgery is relative new beginning with early attempts to repair stab wounds in the late 19th Century before antibiotics, blood transfusions, specifically designed instrumentation, in-depth

knowledge of anatomy and physiology and the ability to visualize the heart were available. Not until the 1950s were surgeons able to visualize the heart during open heart surgery through thoracotomy and median sternotomy. Prior to this cardiac surgery was performed 'blind' during closed procedures and surgeons strived to find ways to operate with the chest open, the heart stopped and exposed and within a bloodless environment. However, just 60 years later surgeons desire to perform cardiac surgery under closed conditions has come full circle as they strive to perform minimally invasive procedures through partial sternotomy, parasternal incision, mini- thoracotomy or sternotomy but this time with the advantage of being able to visualize the heart using video-assist or video-directed devices which transmit real time images of the heart. Chapter 2 charts the evolution of cardiac surgery following the first successful repair of the human heart by Rehn in 1896 and outlines the innovations which have contributed to the development of surgical techniques and procedures for the repair of diseased native valves.

Figure 2.1 Evolution of cardiac reparative valve surgery

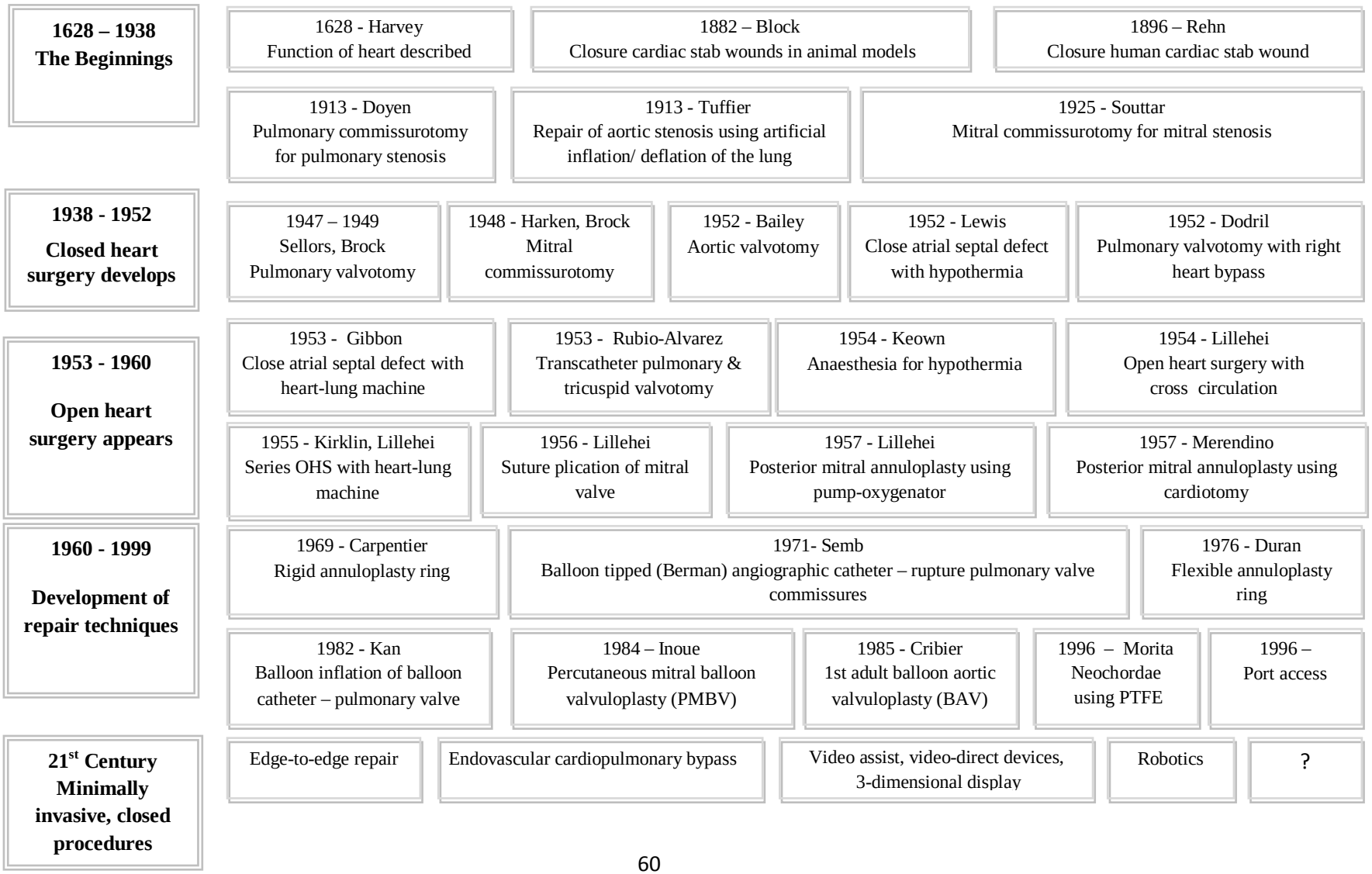

2.1 Operating 'blind'. The development of early surgical techniques

Modern cardiac surgery is considered to have been launched by Ludwig Rehn in 1896 who performed the first successful repair of a stab wound to a human heart although, experimental work had started a decade or so earlier when, in 1882 Block had successfully closed heart wounds in rabbits. However, despite these successes which encouraged others to consider the possibility the heart could be surgically repaired for any number of conditions, progress in developing procedures for relieving the symptoms of cardiac disease was initially very slow. Furthermore, opposition to performing surgery on the human heart from the surgical establishment itself was very strong and Brunton's article daring to suggest others might be encouraged to hope such results could soon be applied to cases of mitral stenosis evoked fierce condemnation from the Lancet which helped to retard the development of cardiac surgery for many years (Brunton 1902; Lancet 1902; Weisse 2009). It wasn't until 1913 the first operations on cardiac valves were preformed. The first of two operations performd by French surgeon Eugène Doyen attempted to relieve symptoms of congenital pulmonary stenosis using a tenotome knife [7]. In the second operation he used the different technique of digital compression to relieve calcific stenosis in a patient. Although the procedures were successful both patients died post-operatively. In that same year Tuffier performed the first successful operation to relieve aortic stenosis using a technique to artificially inflate and deflate the lungs with a tracheal catheter. However, a further decade passed before the first successful surgical procedure to alleviate the symptoms of mitral stenosis was performed by Elliot Cutler (1923). Cutler carried out a valvotomy, also referred to as commissurotomy [8], on a severely symptomatic patient who suffered frequent attacks of

[7] A tenotome is a knife used in tenotomy which refers to the cutting of a tendon. The blade, which is curved slightly forward, has a blunt rounded tip. The shape of the knife means it can be inserted under the tendon without damage to local nerves and blood vessels and can cut outwards without the tendon slipping off the knife.

[8] Commissurotomy is the surgical or digital division of the commissures and is often performed for stenosis of the mitral valve in which the thickened adherent leaflets are separated in order to increase the valve orifice.

haemoptysis. The valve was accessed via the left ventricle using a valvulotome [9] and the patient survived for four and a half years with improved health. Two years later Henry Souttar operated on a teenage patient suffering from combined mitral stenosis and mitral regurgitation by accessing the valve via the left atrium and, after palpating the opening digitally enlarged the valve rather than using a valvulotome. Although the patient suffered a tear to the atrial appendage it was easily repaired and the patient lived for several years. Despite Souttar's success he never performed the procedure again bowing instead to the establishment's opinion it could not be justified (Khan 1996). Years later however, Souttar's procedure became the standard procedure for closed repair of mitral stenosis (see below).

During the next two decades cardiac surgery remained in the doldrums although other significant advances in medicine were made such as, the appearance of antibiotics, maturation of blood-banking methods and advances in surgical techniques and anaesthesia (Keown 1982; Moore 1999; Ramsey 2009). Interest in treating cardiac valvular disease was revived by Dwight Harken who, during the 2nd World War successfully removed shell fragments from within the hearts of wounded soldiers without leaving any permanent damage thus demonstrating the heart's recuperative powers (Harken 1946). In the late 1940s attempts to relieve symptoms of stenosis changed from an atrial to a transventricular approach which made finding the leaflets and commissures easier and also prevented entanglement with chordae tendineae. T Holmes Sellors was one of the first to successfully perform a closed valvotomy for pulmonic valvular stenosis via the right ventricle using a tenotomy knife in 1946 however, unaware of Sellor's work Russell Brock also reported three successful transventricular pulmonary valvotomies for pulmonary stenosis. This method was eventually adopted as the standard procedure for pulmonic stenosis until the development of open heart surgery after which the valve was approached directly through the pulmonary artery. In 1948 Harken and Bailey, also working independently of each other, reported on their successes in relieving mitral

[9] A valvulotome is an instrument used in valvulotomy.

stenosis. However, the reliance of touch in digital fracture of the fused commissures with the index finger still remained a less than perfect technique. Lack of surgeon experience, variable anatomy of the rheumatic valve which was resistant to digital fracture led to the development of a variety of instruments (ie. valvulotomes, valve dilator [10]) to assist in the procedure. The instruments were introduced alongside the finger and used to dilate the valve up to a measured diameter so the commissures were under tension and could then be fractured digitally or, the tough fibrous tissue of the commissures could be incised. Consequently, the success rate of valvotomy [11] significantly improved and reported operative mortality ranged from 1-7% of elective cases (Ellis 1959; Merendino 1959; Boyle 1961). The technique is still widely used in less developed countries because it is both safe and quick and, considerably cheaper then alternative procedures (see below) (Iyer 1998; Attman 1999).

2.2 The move to a bloodless operation and the development of direct vision techniques

The 1950s heralded the beginning of experimentation into the possibilities of hypothermia and extracorporeal circulation. Research had shown a reduction in body temprature to 20ºC could render the brain anoxic for up to ten minutes thus providing sufficient time for a rapid intracardiac procedure to be performed (Bigelow 1950). However, surgeons aknowledged intracardiac repairs required an extended window than that offered by hypothermic methods furthermore, the body and in particular the brain still needed oxygen to be delivered via blood flow. In other words, cardiac and respiratory function would need to be provided by artificial methods (ie. cardiopulmonary bypass). In 1953 Gibbon reported the first open heart surgical procedures using extracorporeal circulation by means of an oxygenator (ie. stationary vertical screen oxygenator). Although oxygenator-related problems resulted in a high patient mortality rate (Fou 1997) Gibbon's techniques proved mechanical oxygenation was possible and

[10] The valve dilator is a two-bladed instrument which is introduced into the stenotic valve with the aid of the examining finger in the left atrium via a small stab-ventriculotomy in the apex of the left ventricle.
[11] Valvotomy (valvulotomy) is also referred to as commissurotomy.

provided the stimulus for others to modify his designs to incorporate a greater uptake of oxygen as blood flowed (Kirklin 1956; Mulder 1957). In 1954 Lillehei performed the first open heart surgery under direct vision to repair a ventricular septal defect in a young patient using a technique known as cross-circulation in which the patient's father was used as an oxygenator [12] (Lillehei 1955). The success of this procedure led Lillehei to conduct a further 45 open heart surgical procedures on patients with otherwise irreparable complex intra-ventricular defects using controlled cross circulation thus making corrective surgery possible. However, despite being a major advancement and demonstrable success proving biological oxygenation provided a bloodless field it was not widely adopted because it was considered too high risk for both patient and donor carrying a 200% risk of mortality (Lillehei 1955) and was only suitable for children with a parent with a compatible blood group. As a result of these risks together with the technical challenges it presented controlled cross circulation became redundant but it nevertheless paved the way for open heart surgery and in the following year Lillehei and his colleagues introduced the first clinically successful bubble oxygenator which remained the standard for extracorporeal circulation until the late 1970s (Lillehei 1956). After cardiopulmonary bypass became available in the 1950s and hypothermia and extracorporeal techniques continued to be refined during the remainder of the 1950s, 1960s surgeons were given the opportunity to visualize and to safely stop and restart the heart raising the possibility defective parts, such as heart valves, could be replaced rather than repaired. As a result surgeons began to shift their focus from repair techniques to developing artificial heart valves made from artificial materials that would mimick the function of native heart valves (see Chapter 3).

[12] Blood flow was routed from the patient's caval system to the father's femoral vein and lungs for oxygenation before it was returned to the patient via the carotid artery. Thus, the donor acted as a 'heart-lung' machine.

2.3 Development of repair techniques

Development of repair techniques to preserve the native valve apparatus continued despite a new interest in developing techniques to replace rather than repair diseased or defective valves using direct vision and artificial oxygenation. Procedures to treat mR resulting from 'billowing' and/or prolapsing leaflets focused on reducing the size of the valve by folding, tucking and shortening parts of the valve structure such as the commissures, annulus (ie. plication/suture annuloplasty/valuloplasty) and papillary muscles in an effort to force the leaflets to contact with each other (Lillehei 1958; Kay 1962; Belcher 1964; Gillinov 1998; David 2005; Tuladhar 2006). Of the various techniques for shortening chordae for example, neo-chordae repair using a synthetic material, polytetrafluoethylene (PTFE) has fast gained popularity because of its similar viscoelastic and biological properties as well as its long-term durability (Kobayashi 2000). This repair procedure replaces unnaturally elongated native chordae and by creating new chordae between the coapting edge of the leaflet and the associated papillary muscle sucessfully resuspends the leaflets (David 1995; Tesler 2009; Bizzarri 2010). Redundant and/or loose segments of the leaflets were removed in a procedure known as quandrangle resection often in conjunction with a sliding plasty, to reduce the height of the posterior leaflet and avoid left ventricular outflow obstruction (Gillinov 1998; Gatti 2003; David 2005). More recently the edge-to-edge repair or Alfieri procedure to improve leaflet coaptation by suturing or clipping the anterior and posterior leaflets together at a single point mid-way between the circumference of the leaflets to create a double orifice valve with reduced leaflet excursion and therefore less regurgitation has been gaining prominence (Alfieri 2001; St Goet 2003; Fann 2004; Fedak 2008; Feldman 2009; Maisano 2009).

In addition, methods of supporting the valve annulus using a synthetic implant were developed and in the early/mid 1970s the first synthetic annuloplasty ring was introduced. Designed by Alain Carpentier this rigid ring was intended to reduce and reshape the valve

annulus whilst maintaining its formation and avoiding further dilation (Carpentier 1995). However, critics argued the design was too restrictive and impeded the annulus' natural movement during the cardiac cycle and suggested a flexible ring would be more likely to provide greater freedom of movement and preserve left ventricular function (Duran 1976). In light of such criticism Carpentier introduced a modified version of his classic rigid ring, the Carpentier Physio Annuloplasty Ring, (Figure 2.2) which demonstrated selective flexibility in its anterior portion with a slight three-dimensional shape which conformed better to the normal annulus movement and shape (Carpentier 1995). Subsequent designs of annuloplasty rings and annuloplasty bands [13] have sought to address the non-uniform nature of deformation of the mitral valve annulus during the cardiac cycle and, accommodate the underlying valve pathology rather than replicate the 'normal' mitral annulus. As Figure 2.2 shows there is a large variety of geometrically shaped rings available today which coupled with their good long-term results has led to a significant increase in repair with an annuloplasty ring at the expense of suture annuloplasty (Braunberger 2001; Fundarò 2007).

[13] An annuloplasty band is a full or partial annuloplasty ring. The band can be sutured around the mitral valve annulus in order to provide stability to the annulus and minimise stress on the valve.

Figure 2.2: Examples of annuloplasty rings and bands for repair of mitral and/or tricuspid valves

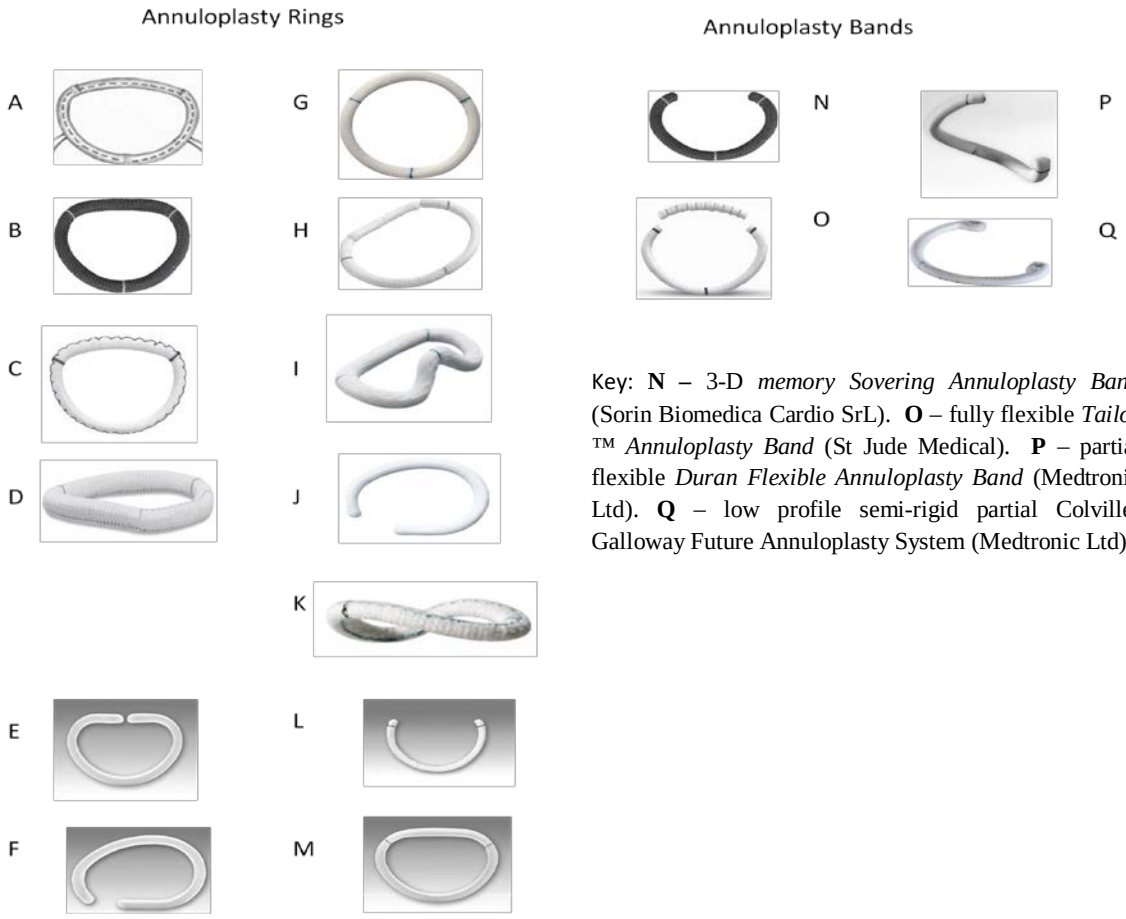

Key: **N –** 3-D *memory Sovering Annuloplasty Band* (Sorin Biomedica Cardio SrL). **O** – fully flexible *Tailor ™ Annuloplasty Band* (St Jude Medical). **P** – partial flexible *Duran Flexible Annuloplasty Band* (Medtronic Ltd). **Q** – low profile semi-rigid partial Colville-Galloway Future Annuloplasty System (Medtronic Ltd).

Key: Annuloplasty Rings

A - semi-flexible adjustable annular *Sculptor Annuloplasty Ring* (Medtronic Ltd). **B** – flexible 3-D memory *Sovering Annuloplasty Ring* (Sorin Biomedica Cardio SrL). **C** – flexible *Seguin Annulplasty Ring* (St Jude Medical Ltd). **D –** asymmetrical *Carpentier-McCarthy-Adams IMR ETtlogix Ring* (Edwards Lifesciences Ltd). **E** (mitral) **& F** (tricuspid) – kidney-shaped *Carpentier Edwards Rigid Ring* – (mitral) and oval-shape *Carpentier Edwards Rigid Ring* (tricuspid) (Edwards Lifesciences Ltd). **G** – *Duran Flexible Annuloplasty Ring* (Medtronic Ltd). **H** – flexible 3-D *AnnuloFlex Ring* for partial or complete annuloplasty (Sorin Biomedica Cardio SrL). **I –** geometrically designed *GeoForm Annuloplasty Ring* (Edwards Lifesciences Ltd). **J –** 3-D flexible Edwards MC^3 Annuloplasty Ring (Edwards Lifesciences Ltd). **K** – 3-D saddle-shaped *St Jude Rigid Saddle Annuloplasty Ring* (St Jude Medical Inc.). **L -** 3-D C-shape flexible *Cosgrove-Edwards Annuloplasty Ring* (Edwards Lifesciences Ltd). **M –** kidney-shaped *Carpentier Edwards Physio Annuloplasty Ring* (Edwards Lifesciences Ltd.

2.4 Percutaneous approaches

Despite development of open heart procedures for valvular repair interest in less invasive approaches continued and in the early 1950s the first attempts to repair a stenotic valve employing balloon valvotomy via percutaneous transcatheter delivery was performed using a wire to cut open the stenotic valve (Kan 1982). Use of percutaneous balloon intervention continued to develop throughout the 1970s and 1980s spawing techniques which used over the wire single and multi-cylindrical balloon catheters as well as the very popular Inoue percutaneous balloon catheter to enlarge the aortic valve orifice (i.e. balloon aortic valuloplasty (BAV)). The Inoue balloon catheter was unique because the degree of inflation could be varied according to individual patient's pathophysiology and, unlike other balloon catheters it demonstrated greater positioning and stability as a result of its use of curved stylet rather than a guide wire (Inoue 1991; Shaw 1994). However, reports suggest these techniques met with only limited success and demonstrated a high complication rate of between ≥5% and 10% of all patients with an incidence of restenosis ≤6 – 12 months (Kuntz 1991). Furthermore, medium and long-term results were similar to closed valvotomy and medical therapy (Ray 1993; Lieberman 1995; Iyer 1998, Palacios 1998).

During the last 15-20 years new techniques aimed at minimizing exposure of the heart during cardiac surgery have been developed and have, despite early scepticism (Baldwin 1998; Cooley 2000) rapidly gained popularity (Mohr 1998; Loulmet 1998; Reichenspurner 2000). Traditional open cardiac surgical procedures require sizeable median sternotomy and are associated with post-operative bleeding, wound infection, back pain, sternal dehiscence and visible scaring. Minimally invasive procedures however, are appealing to clinicians because they need only small incision thoracotomy or sternotomy through which the heart can be accessed, cannulated, given myocardial protection and visualized using thorascopes and stereoscopes. Furthermore, they are considered a way of reducing open procedure complications and reducing recovery time

and cost (Cosgrove 1996; Arom 1999). However, valve repair performed via minimally invasive procedures is not without difficulties. Loulmet (1998) noted variability in the quality of exposure of the mitral valve following mini-incisions as well as patient variability in the spatial relationship between different structures of the heart and chest wall. Reduced illumination of the operative field restricted visualisation of the heart. Furthermore, as a result of the direct contact between the ventricle and surrounding structures which had a tendency to re-warm faster after cooling, it was found myocardial protection could potentially be jeopardized and de-airing and defibrillation were also made difficult because of limited access to the ventricles. However, improvements in procedural techniques and in particular, instrumentation such as endovascular cardiopulmonary bypass assisted by three-dimensional thorascope attached to a robotic arm, have significantly increased the level of visualisation as well as the ability to operate via a very small and confined incision (Reichenspurner 2000). Surgical assisted robotic procedures have demonstrated a distinct advantage over surgeon only procedures which require incisions large enough to allow the surgeons hands plus instrumentation. Incisions made by the robotic arm in comparison are considerably smaller and may only be millimetres thick. In addition, a three-dimensional camera can project the whole valve apparatus onto a screen whilst the robotic arm holds the camera in a stable position or, both surgeon and assistant helmets project a three-dimensional display of the endoscopic image of the operative site into their eyes or on the endoscopic picture inside the helmet without them having to move their heads. Thus, some parts of the operation can be performed using direct vision and others using the endoscope. Problems of de-airing and those associated with cardiopulmonary-bypass (CPB) have also been resolved by retrograde de-airing using a venting catheter and by conventional cannulation for mini-sternotomy or parasternal incisions. However, as Reichenspurner notes the Port-Access System uses transthoracic aortic clamps for femoral cannulation together with endovascular balloon occlusion of the ascending aorta in procedures using mini-sternotomy thereby lengthening total operation time, CPB time and duration of cross clamping compared with conventional mitral valve surgery. Patient recovery time was

nonetheless found to be quicker resulting in earlier discharge (Reichenspurner 2000; Raanani 2010).

2.5 Chapter summary

Despite its relatively brief history beginning in an era when the very idea of operating on the heart was taboo and fierce opposition to violating the sanctity of the human heart effectively delayed its development, cardiac surgery and in particular cardiac valvular surgery, is now able to treat the majority of cardiac defects and diseases. The emergence of a new generation of post World War II surgeons who were not only prepared to operate on the heart but also began to rack up one success after another resulted in cardiac surgery becoming more readily and widely adopted. Although initial procedures were performed in a 'blind' field surgeons nonetheless, successfully reduced mortality rates to single figures. This was achieved by the use of a different access route to the heart, developing specially designed instrumentation and broadening their experience and thus confidence. The development of cardiac surgery however owes much of its existence to other developments in medicine and life support during surgery. One of the most crucial developments was the discovery of the relationship between body temperature and oxygen requirements which paved the way for establishing hypothermia as a prophylactic against infarction. However, despite being able to maintain the body's temperature at 28-30ºC for 8-10 minutes surgeons recognized longer procedures would require more time than that offered by hypothermia alone. The answer lay in mechanical oxygenation which banished time constraints and afforded surgeons the time, space and ability to directly visualize the heart within a bloodless field and therefore treat all manner of congenital and acquired cardiac lesions. Added to this armamentarium more recent techniques for repair and reconstruction have rapidly gained prominence as their successes have been reported. The development of the synthetic annuloplasty ring and introduction of the balloon-tipped catheter heralded the era of interventional cardiology

and led to the first percutaneous balloon mitral valvuloplasty for patients with symptomatic mitral stenosis.

The end of the 20th and beginning of the 21st Centuries have witnessed a change in attitudes towards open heart surgery and a move once again towards closed cardiac procedures in an effort to reduce morbidity and mortality associated with open cardiac procedures and, extend treatment to those currently excluded from surgery. Much of the current excitement is focused on the possibilities offered by minimally invasive procedures although these have not been without challenges. Advances in procedural techniques and instrumentation have however, led to significant improvements in the level of visualisation of the heart and surrounding structures as well as problems associated with CPB and of physically operating via a very small and confined incision. Nonetheless, although significant advances in repair techniques have been achieved many valves are considered too damaged and are thus required to be totally replaced. The next chapter therefore looks at the development of the replacement heart valve from the early valves implanted during open heart procedures to the newer tissue valves implanted via percutaneous delivery systems.

CHAPTER 3

The development of prosthetic heart valves

3. Introduction

The development and introduction of the heart-lung machine in the early 1950s was fundamental in changing how cardiac surgery was performed. For the first time surgeons had direct vision of the heart during surgery and were able to safely stop and restart it. Consequently, in the following years the notion of replacing diseased and defective heart valves went from possibility to reality and since the 1950s ≥100 models of replacement heart valves have been developed and implanted. Current estimates suggest nearly 300,000 heart valves are implanted annually worldwide and this figure is expected to triple to ≥850,000 by 2050 (Dasi 2009). Initial attempts to replicate the natural heart valve using silicone and urethane-coated fabrics (e.g. Bahnson Flexible Cusp Valve (1960) proved unsatisfactory. Fibrin desposition and tissue-ingrowth quickly led to leaflet stiffness, tearing, thrombus formation and valve failure. Thus, it became apparent materials would have to be chemically inert, compatible with human tissue, atraumatic to blood and non-thrombogenic. In addition, they had to be durable, susceptible to changes in pressure gradients, able to open and close rapidly, maintain flow direction (i.e. forward), prevent regurgitation in the closed position and not have areas where blood can collect and stagnate. Finally, they have to be easy to implant and remain securely in place. Chapter 3 presents a review of the historical milestones in the development of replacement cardiac valves from the early 'bottle stopper' valve to the mechanical caged-occluder and leaflet valves, human and animal tissue prostheses to the newer percutaneous valves and discusses emerging technologies, such as polymeric heart valves and tissue engineered valves, which are currently being investigated.

3.1 Types of heart valves

As Figure 3.1 shows there are two distint categories of replacement heart valves, the mechanical valve and the biological tissue, referred to as bioprosthetic valves. Within the mechanical group there are four different types, the caged-ball, caged-disc, single

disc/leaflet and bileaflet valves, and all are made from synthetic materials such as metal, polymers (e.g. Pyrolyte) [14] and ceramics. Although very durable these valves are highly thrombogenic and require life-long anticoagulation. In contrast, bioprotheses have low thrombogenicity, do not require life-long anticoagulation but are less durable and, as Chapter 1 mentioned are more susceptible to age-related structural deterioration. Made from either animal or human tissue ± additional synthetic materials these valves are classfied as xenografts (also referred to as heterografts) or homografts (also referred to as allografts). Xenografts use porcine or bovine tissue (pericardial or valvular) treated with a sterilising solution (ie. glutaraldehye) and are either stented or stentless [15]. Homograft valves are preserved human aortic or pulmonary valves harvested from cadavers, patients who have suffered brain death and have agreed to organ donation or, explanted from the hearts of patients underoing heart transplant. These valves are treated in antibiotic solution before being stored in either fixative or cryopreserved. In addition, a patient's own valve, usually the pulmonary valve, may be havested and transplanted into another site (referred to as an autograft) and a homograft from another donor is then implanted into the harvested site.

[14] Pyrolyte (ie. pyrolitic carbon) is the most commonly used compound and was originally developed for the encapsulation of nuclear fuel rods. It's use came about as a result of a chance rading by Jack Bokros, a materials engineer, of a paper reporting the biocompatibility of blood with certain materials. Experiments found highly polished pyrolitic carbon did not bond with heparin and was highly thromboresistant.

[15] Stented valves are reinforced with a cloth-covered polymer scaffolding, known as a stent, attached to a sewing ring which secures and supports the valvular material in its natural anatomically-functional position and makes implantation easier because it allows the surgeon to attach the valve to the patient's annulus using a single row of sutures. Stentless valves do not have any supporting structure, are technically more difficult to implant and are sewn 'hand-free'.

Figure 3.1 Classification of heart valves

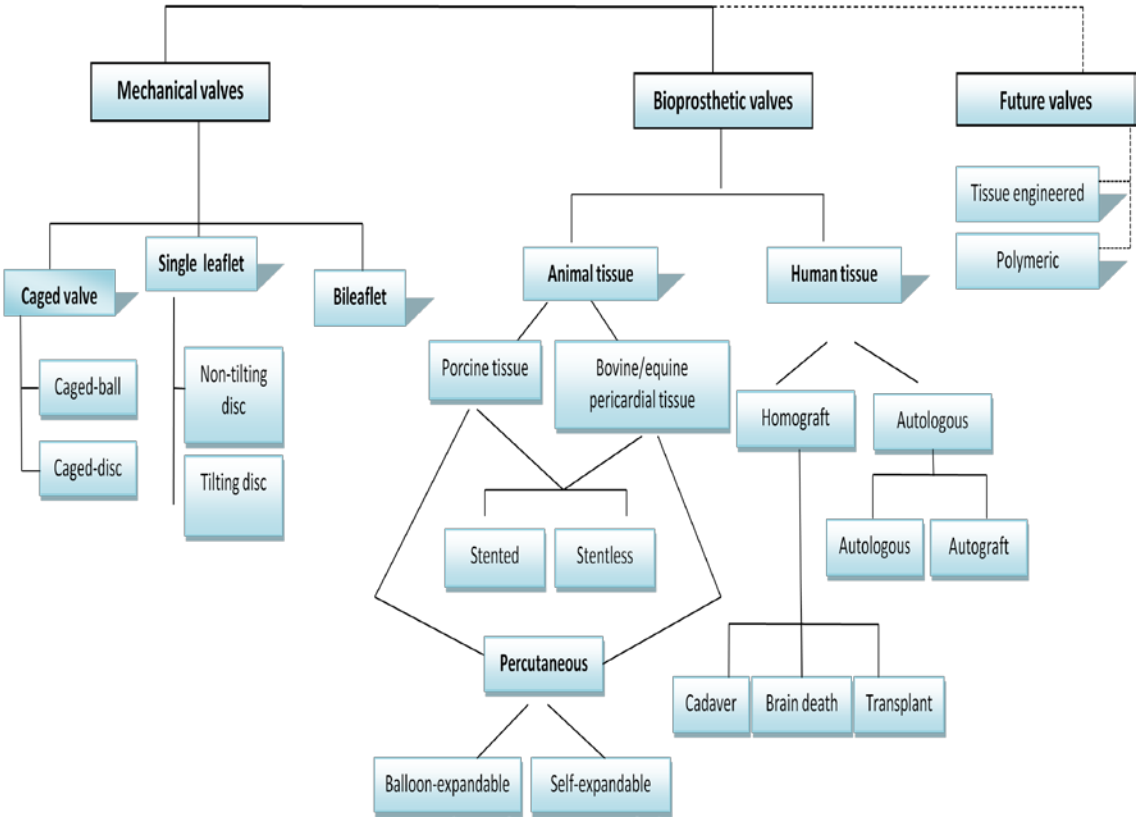

3.1.1 Mechanical Heart Valves

(a) *Caged-ball and caged-disc valves*

Early designs of the artificial heart valve stem from the Hufnagel design of a chambered ball valve based on an 19th Century wine bottle-stopper patented by John Williams in 1858. Although this valve was originally designed for use in the proximal descending thoracic aorta it demonstrated certain foreign materials could be implanted in the bloodstream without causing harm. The Hufnagel valve, as seen in Figure 3.2, initially

used a small hollow plexiglass ball [16] inside a chambered plastic tube (i.e. highly polished methyl methacrylate) which allowed free vertical movement of the ball. The first clinical implantations were performed prior to the introduction of the heart-lung machine and therefore under closed conditions (1952) assisted by the use of serrated plastic rings (ie. multipoint fixations) for quick fixation. However, because the valve only prevented regurgitation from the lower body cardiac output and coronary flow were only marginally improved. Furthermore, the valve was highly thrombogenic, noisy and unsuitable for patients with aortic stenosis (French 1961; Kaufman 1982). Nonetheless, Hufnagel's pioneering efforts marked the beginning of the era of artificial heart valve development.

1960 marked the watershed in the history of artificial heart valves with the introduction of the first mechanical valves. Dwight Harken who, as previously mentioned in Chapter 2 demonstrated the recuperative powers of the heart (Harken 1946), introduced the first clinical caged-ball valve in which the ball, retained within a metal cage was forced downstream and held distal to the open orifice during high pressure but occluded the orifice passively preventing backflow during systole. Also introduced in 1960 was the Braunwald-Cutter valve which used a flexible polyurethane-Dacron fabric with attached Teflon tape chordae tendineae (Figure 3.2). However, the valve was susceptible to infiltration of fibrous connective tissue and subsequent thrombus formation and, despite modifications such as covering the housing with fabric to eliminate infiltration, problems persisted and in 1979 production of the valve ceased (Blackstone 1977). In 1962 Magovern and Cromie developed a closed cage design using a rapid sutureless mechanical fixation which initially consisted of a single row of horizontally curved pins which emerged from the sewing ring when the valve holder was rotated. Modifications incorporated two plates (upper and lower) of vertically curved pins, perfect for implantation in high risk patients where speed of implantation was paramount. Nonetheless, the valve which is also shown in Figure 3.2 demonstrated susceptibility to streamer clot formation at the junction of the two struts as well as ball variance.

[16] This plexiglass ball was later replaced by a polyethylene ball.

In 1964 the Smellof-Cutter open-cage ball valve was clinically introduced. It was the first prosthetic valve to employ the 'full-flow' orifice concept achieved by using a double cage with open apex and bare orifice machined from a single bar of titanium [17] which eliminated the potential for weld fractures. Free movement of the ball from one cage to the other was achieved because the diameter of the valve orifice was larger than the ball. As a result minimal backflow occurred and was effective in 'washing' away adherent formed elements from the ball's surface. As Figure 3.2 shows, one of the striking features of the Smelloff-Cutter valve was that, unlike other valves the struts were shorter and therefore projected less into the left ventricle. Initially, as with other silicone rubber poppet valves ball variance was a problem but was remedied by the change in the curing method of the silicone in the mid 1960s. Nevertheless, concerns about ball variance persisted and in 1967 DeBakey and Cromie introduced their closed cage valve, which again as Figure 3.2 shows, was similar to the Starr-Edwards valve. Addressing the problems of ball variance the 1969 model of the DeBakey-Cromie valve used a high molecular weight polyethylene poppet. However, this poppet could only be gas-sterilised and therefore proved impractical; it was subsequently replaced with pyrolyte which limited ball variance but its relative hardness constantly contacting the soft titanium cage caused excessive wear on the struts and caused strut fracture and it was therefore discontinued.

The Starr-Edwards valves, arguably the most widely known of all the caged ball valves and still implanted in the 21st Century (UK Heart Valve Registry 2007) used a single rather than double cage and, despite a number of modifications to improve performance and reduce thrombo-embolic potential, the overall design of the valve has not changed since 1962 only the materials and construction techniques. Figure 3.2 shows the range of models of Starr Edwards caged ball valves with modifications which include:

[17] Titanium has favourable qualities for use in biomedical implants. It is light-weight, has a resistance to corrosion, is durable and biocompatible and is easily machinability producing intricate, weldless designs.

- substituting the original Lucite cage (Models pre-1000) with Stellite metal (Model 1200),

- replacing the silicone rubber occluder, which was prone to lipid absorption leading to ball variance and deterioration, with Stellite-21 (Model 1250) which however, proved noisy and distressing for patients,

- re-substituting the Stellite-21 poppet with a silicone rubber post modifications to the heat curing process of silicone [18] which served to eliminate ball variance and deterioration (Model 1260; equivalent mitral valve Model 6120 [19]),

- increasing the clearance and seating the occluder on raised studs rather than the orifice cloth (Model 2320),

- limiting the amount of exposed metal by covering the struts with cloth (Models 2300) to prevent wear and,

- covering the orifice with siliconized and multi-filament Dacron knitted in a lock stitch to prevent runs and promote neo-intimal growth (Model 2400).

[18] Ball variance and deterioration was eliminated by heating the silicone occluder post moulding at relatively high temperatures for several hours (1966).

[19] The mitral version (Model 6000) Starr Edwards valves evolved in a similar manner to the aortic valves and in 1966 the Model 6120 was introduced.

Figure 3.2 Caged-ball valves

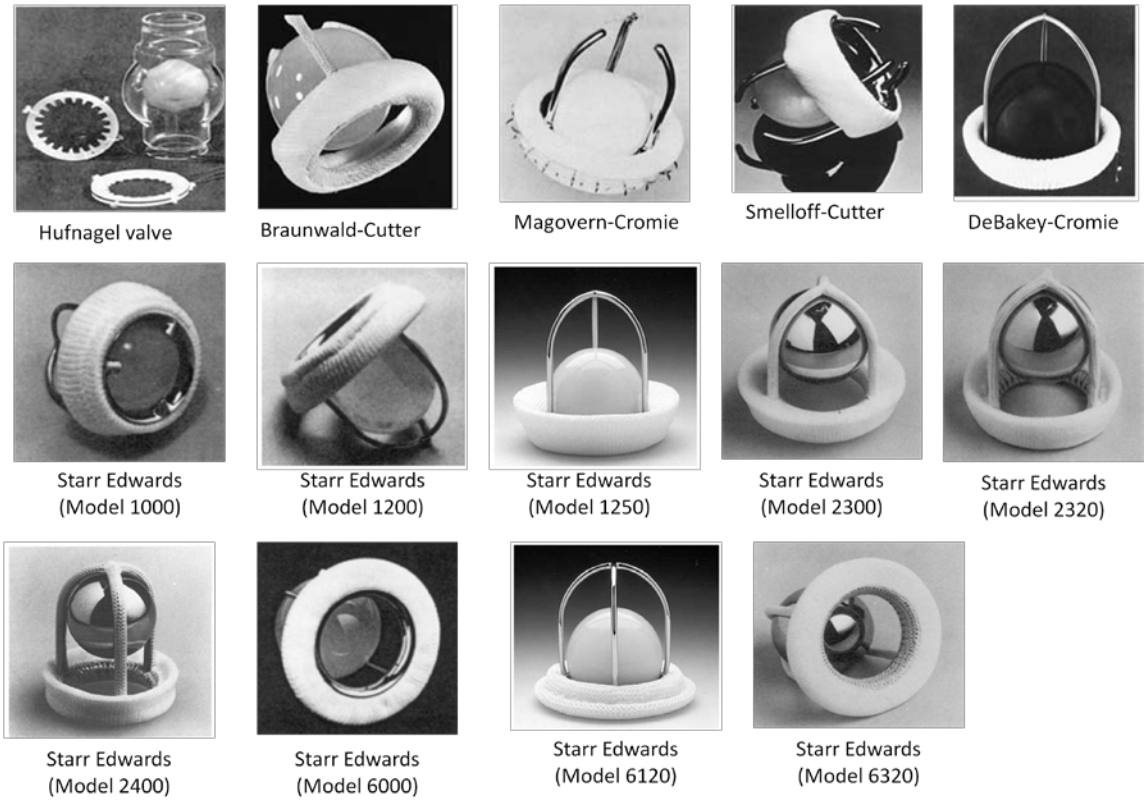

Braunwald-Cutter, Magovern-Cromie valves (Gott 2003) permission granted July 2012 by RightsLink/Elsevier transaction to reproduce these images. Smelloff-Cutter, Starr Edwards valves (Edwards 2007).

(b) Caged-disc (non-tilting) valves

The large profile design of the caged-ball valve gave rise to a potential for interference of the valve with anatomical structures after implantation. Furthermore, the large pressure drops across the valve and higher turbulent stresses distal to the valve as a result of the central occluder led to the development of low-profile caged-disc valves in the mid-1960s which used a flat lens-like disc in place of the ball. As Figure 3.3 shows the caged disc

valve [20] was designed like the caged-ball valve so that the occluder moved vertically. However, this design had a number of advantages over its caged-ball competitor. Firstly, the lens allowed a larger orifice size than was possible with a ball valve and this was critical for patients with a small left ventricle who required mitral valve replacement. Secondly, the lighter-weight disc meant less force was required to overcome the valve's inertia and as a result, the regurgitive potential was reduced. Lastly, valve function was quieter. However, non-tilting disc valves demonstrated a tendency for excessive wear because, unlike the spherical ball which turned randomly in the stream of blood the uneven closure of disc subjected it to constant notching by the struts. In fact, poppet wear became an all too common problem with both caged-ball and caged-disc valves and getting the right combination of materials for the poppet and housing proved difficult. Too soft a poppet led to erosion resulting from constant contact with the harder strut material and too hard a poppet often lead to erosion of the softer struts. Although the lower profile caged-disc valves had definite advantages over their bulkier caged-ball associates the occluder nonetheless remained relatively obstuctive in the open position. Thus, the idea of a free-floating disc which could tilt within the valve ring and not obstruct blood flow in the open position was an exciting concept and led to the development of the tilting disc valve.

Figure 3.3 Caged-disc valves

Kay-Shiley, Beall-Surgitool, Cooley-Cutter valves: Gott (2003) permission granted July 2012 by ~~RightsLink/Elsevier transaction to r~~eproduce these images.

(c) Tilting disc valves

The next significant development in the evolution of heart valves was the introduction of the tilting disc which acted like an aerofoil when the valve was open allowing the blood to flow over and around it minimising flow disturbance and improving haemodynamics. As Figure 3.4 shows early models of the valves, such as the Lillehei-Kaster disc valve, had a hinged disc along a straight segment of ring, similar to the way a toilet seat is attached. Blood flowed along the inflow surface of the disc but areas between the open disc and aortic wall allowed blood to collect and stasis to occur leading to thrombus formation and obstuction of the disc. This problem was addressed by both Bjork and Shiley (1969) and Lillehei and Kaster (1970) the latter of whom moved the pivot point forward and replaced the cage with lateral guides (1965; Figure 3.4). Later modifications to the valve gave rise to the Ominscience (1978) and Ominicarbon (1984) valves which used abbreviated earlike guards in place of the retaining rails and replaced the flat disc with a slightly curvilinear disc in order to minimize turbulence, provide low flow resistance and minimize closing volume (energy) loss (Omniscience valve; Figure 3.4). Both the Lillehei-Kaster and Björk-Shiley valves were remarkable because, the discs totally occluded the valve orifice in the closed position and tilted to a given angle in the open position allowing nearly complete laminar flow with only minimal obstruction to the outflow but also reduced turbulence and produced a larger stroke volume. In addition, the occluder of the Lillehei-Kaster valve rotated within the housing during normal function evenly distributing potential wear around the circumference as well as during implantation to prevent interference with sub-annular abnormalities. Despite these improved haemodynamics both valves experienced problems such as absorbtion of moisture in the Delrin disc causing deformation post implant and valve obstruction and strut fracture at the weld joint leading to leaflet escape (Nair 2003). Furthermore, the Björk-Shiley valve also demonstrated thrombus formation on the outflow side of the valve. These problems were overcome by (a), replacing the Delrin disc with Pyrolyte (b), using a monostrut machined as an integral part of the orifice ring involving no weld joint

for the outflow retainer (c), increasesing the orifice area by changing the shape of the disc from flat (ie. plano) to a concave and (d), modifying the inlet and outlet struts to allow forward and downward movement of the disc thereby improving flow whilst decreasing turbulence around the minor orifice. However, reports of catastrophic valve failure of the Björk-Shiley Convexo-Concave (BSCC) valve soon began to appear. Early studies identified failure of the C-shaped outflow strut at the weld site caused by faulty welding, particularly in the larger sizes (ie. 29, 31 and 33 mm) and especially in younger patients as the cause (van der Graaf 1992). However, later studies have suggested the larger diameter valves placed an inappropriate 'leverage loading' on the centre of the small outflow strut as the leaflet closed causing the strut to fracture (Omar 2001). In the meantime and, in an effort to address these problems the valve was machined from a single solid piece of metal and the housing was reconfigured to include only one outlet strut and to increase the disc opening angle to 70º. The new Björk-Shiley Monostrut valve (Figure 3.4), which is still implanted today, was clinically introduced in 1983 and has a larger orifice area and reduced pressure gradients than its predecessor. This valve has proved to be durable with few valve-related complications in comparison (UKHVR 2007).

Despite the superior haemodynamics of the Björk-Shiley and Lillehei-Kaster valves compared with the caged-ball and disc valves, a study by Hall (1992) reported persistent problems with stasis and thrombus formation behind the disc and in the area of contact between the disc and valve ring in the open position. As a result help was sought to develop a tilting disc valve with a gap between the disc edge and valve ring which would increase flow volume and eliminate stasis and platelet aggregation and thus thrombus potential. The resulting valve, known as the Hall-Kaster valve (1977; Figure 3.4) later modified and renamed as the Medtronic-Hall valve (1987), used a centred perforation through which a guiding strut guided the disc during opening. This mechanism allowed the disc to move downstream eliminating areas of stasis during systole and inhibiting platelet aggregation by controlled washing during the closing cycle, the result of the non-

contact between the perforation and central strut. The ability to rotate the disc and housing within the sewing ring was also an important aspect of this valve because it allowed the surgeon to properly seat the valve to ensure a wide opening angle (ie. 80º) of the disc could be achieved. Follow-up studies of the Medtronic-Hall valve suggests it has achieved better haemodynamics with reduced level of thromboembolic complications, valve-related complications and good durability (Akins 1992; Svennevig 2007; UKHVR 2007).

Figure 3.4 Single-leaflet, tilting-disc valves

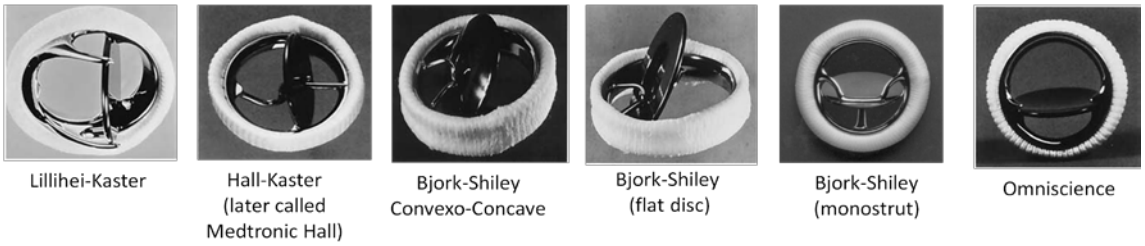

Björk-Shiley convexo-concave, Björk-Shiley flat disc valves: Gott (2003), permission granted July 2012 by RightsLink/Elsevier transaction to reproduce these images.

(d) Bileaflet valves

Investigations into the biocompatibility of materials conducted in the early 1960s led to the development of the first bileaflet prosthesis (Gott-Daggert Butterfly valve 1963; Figure 3.5) which was lower in profile than the cage designed valves. The valve also differed from existing mechanical valves because it used a hinge mechanism to secure two leaflets within the ring in place of the single free floating ball or disc. The leaflets, which protruded only slightly from the ring and therefore did not obstruct any other cardiac structures, were supported by open-ended struts projecting from the inside edge of the ring together with a bar located across the diameter of the disc and fused to the retaining ring giving it an appearance of a butterfly. The leaflet design and large effective orifice area were such that they allowed nearly normal flow, reduced turbulence

and washed the hinges during the closed phase thus preventing flow stasis and inhibiting mircro-thrombus formation. However, although coated with a thrombo-resistant material [21] (Gott 1972) the design was nonetheless susceptible to thrombus formation resulting from stasis distally between the superstrut used to capture the leaflets and the valve was subsequently withdrawn from the market in 1966.

In 1982 the Duromedics bileaflet valve was first clinially introduced. This valve was characterised by central flow and had a self regulating hinge mechanism to avoid stasis and thrombus formation in the critical circulation area. However, after only six years the valve was dramatically suspended following reports of leaflet escape (Radlick 1988). Subsequent investigations identified a number of contributory factors, the primary one being cavitation which caused pitting and micro-cracking of the pyrolitic carbon causing leaflet fracture (Baumgartner 1997). Furthermore, it was noted the Duromedics valve was more susceptible to cavitation compared with other valves, such as the Carbomedics or St Jude bileaflet valves (see below), because of its design for seating the lip which halted leaflet movement and subsequently caused high velocity microjets to form which eventually caused surface pitting, erosion and finally fracture (Richard 1994). Extensive modifications were made to the valve including modifying the radius of the seating lip, integrating a shock absorber into the sewing ring to reduce the impact of leaflet closure as well as, changes to the pivoting joints and porosity of the material. The valve was subsequently relaunched in 1990 as the Edwards Tekna valve.

Two of the most popular and enduring bileaflet valves, the St Jude Mechanical valve and the Carbomedics valve were first clinically implanted in 1977 and 1979 respectively. Originally designed with the help of Jack Bokros, known for his development of pyrolitic carbon and fabrication of monoleaflet valves, the St Jude mechanical valve has changed very little over the last 30 years. Manufactured from one piece of machined graphite and

[21] Vincent Gott and Ronald Daggert (1972) discovered colloid graphite sterilised in benzalkonium chloride and rinsed in heparin was resistant to thrombus formation.

coated with pyrolitical carbon without seams or welds the hinge mechanism has two leaflets restrained by two lateral protrusions at the leaflet edges fitting into two corresponding butterfly pivot recesses on the inner aspect of the valve ring. Coaptation occurs at an angle of 30º within the housing and the valve opens to an angle of 85º. Clot formation is inhibited by the washing effect of the blood as it flows across the space between the leaflets. As Figure 3.5 shows the Carbomedics valve differs from the St Jude valve in that it does not have pivot guards, struts or orifice projections and is therefore less likely to obstruct blood flow or reduce turbulence through the valve. In addition, the leaflets have a smaller opening angle (ie. 78º versus 85° (St Jude Mechanical valve)) but protrude further and, the rotatable sewing ring is carbon coated to reduce tissue ingrowth and valve obstruction potential. Follow-up studies nonetheless, report little difference in performance between the two valves although, there is a suggestion the Carbomedics valve has an increased rate of thrombo-embolism in comparison (Rosengart 1998; Kandemir 2006).

As previously mentioned the basic structure and leaflet design of the St Jude valve has remained unchanged since it was first clinically introduced. Modifications to the sewing ring to reduce its bulk and expanding the effective orifice area by 1.5 times that of the standard valve have been made resulting in the Haemodynamic Plus (HP) and Regent series of St Jude mechanical valves. In addition, although not a design modification per se, St Jude introduced a silver coating (ie.Silzone) to the sewing ring of its standard mechanical valve in the late 1990s in an attempt to inibit the development of prosthetic valve endocarditis. However, the AVERT clinical trial which aimed to evaluate the efficacy of Silzone in preventing prosthetic infection found valves treated with the silver coating performed poorly and demonstrated a higher incidence of reoperation compared with the control valves (Schaff 2002). In addition, the valve was reported as having increased risk of paravalular leak and thrombo-embolism early post-operatively (ie. $\leq$3 months) particularly in the mitral position and the manufacturer subsequently voluntarily withdrew the valve in January 2000 (Ionescu 2003; Grunkemeier 2004).

Despite our greater understanding of fluid mechanics of heart valves and heart valve design recent research suggests, bileaflet valves continue to demonstrate thrombus formation in the area around the hinges as a result of retrograde flow in these areas and, leakage through the b-datum (ie. the line where the two leaflets touch each other) which compromises blood cells and can lead to severe clot formation (Dasi 2009). The continuing problem of thrombogenicity of mechanical valves together with reservations about the potential harmful effects of implanting totally foreign material into the heart led to the development of alternative heart valves which would not require life-long anticoagulation and demonstrate fewer bleeding related complications. The next section of the chapter therefore focuses on the development of these biological tissue valves.

Figure 3.5 Bileaflet valves

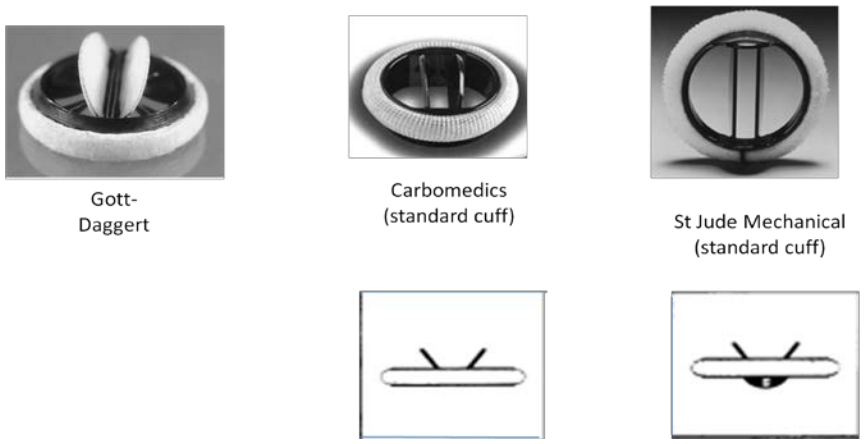

Gott-Daggert valve: Gott *(2003);* permission granted July 2012 by RightsLink/Elsevier transaction to reproduce these images.

3.1.2 Bioprostheses

(a) First generation bioprostheses

Early experimentation into the possibility of using natural heart valves taken from cadavers resulted in the first successful implant of an aortic homograft valve into the sub-coronary in 1962 (Ross Homograft flexible support). Following this and other successive procedures, Ross suggested using a patient's own healthy valve to replace one of their diseased valves (ie. autograft) arguing this type of replacement was a more viable option for children because of the ability of the translocated pulmonary trunk to continue growing with the child. In 1967 Ross performed the first autograft valve replacement (subsequently called the Ross procedure) by placing the pulmonary 'autograft' valve into the subcoronary position although in later procedures it was used for complete aortic root replacement. Although the haemodynamic and biological advantages of cadeveric heart valves were evident problems of maintaining an adquate blood supply as well as procuring a ready supply of homografts proved problematic. Consequently clinicians and engineers sought to identify other biological substitutes, experimenting with transplanted valves from other species such as sheep, calves, goats and pigs (ie.heterografts) as well as autologous fascia lata and dura mata (Ionescu 1970; Reid 1970). The first aortic valve replacements using heterografts preserved in mercurochrome-and-formalin and later formalin were performed by Binet and Carpentier in 1965 and 1966 respectively and although patients displayed a low thrombo-embolic risk and survived without anticoagulation durability was poor.

In these early days implantation was tedious and often difficult and prompted changes to the valve design. Structural supports were added to aid handling during the implantation procedure and one of the first designs, the Ionescu-Wooler heterograft support (1967) [22],

[22] Initially porcine valves were used but later fascia lata and heterologous pericardium valves also used in these valves.

used a rigid Dacron covered titanium stent with three legs and a sewing ring with cotton soaked in formaldehyde packed into the sinuses to ensure coaptation and maintain shape. Others opted for a slightly less rigid Teflon-coated stainless steel stent with two rings of Teflon cloth on which two suture lines could be used for implantation. This was later referred to as a stented bioprosthsis [23]. However, despite these enhancements initial results indicated free hand sewn homografts were more durable and less likely to demonstrate premature tissue failure than their new stented tissue valve counterparts. Subsequent research identified inadequate preservation methods combined with excessive stress forces on the tissues as the likely cause (Valente 1992). Carpentier attempted to address the problem by washing the tissue in a sterialising solution (e.g. Hanks' solution) with an oxidising agent and treating with glutaraldehyde, chosen because of its known resistence to enzymatic and chemical degradation and resulting denaturation of collagen and ability to reduce immunogenicity. First generation xenografts i.e. Carpentier Edwards standard porcine (1970), Ionescu-Shiley pericardial (1971) and Hancock Standard (1972) valves (Figure 3.6) initially demonstrated good mid-term results and increased durability. However, gluteraldehyde was found to cause calcification leading to tissue stiffness and stress relaxation (Duncan 1996) as well as tensile extensibility associated with shrinkage (Trowbridge 1986; Lee 1989; Schmidt 2000) at a faster rate than in fresh tissue. As a result these first generation bioprostheses began to fail five years post-implant (Oyer 1984; Wheatley 1994; Masters 1995). Furthermore, high pressure fixation techniques (i.e. 60-80 mgHH) were also found to cause tissue stiffening and non-compliance and kinks in the leaflets during opening (Broom 1979; Vesely 1988). Consequently, low-pressure fixation was introduced in the 1980s spawning a new generation of bioprostheses with an expected greater durability (see below).

First generation pericardial valves fabricated from flat sheets of pericardium (usually bovine) offered greater flexibility in design (ie. could be fabricated into uni- or bicuspid

[23] Carpentier referred to a bioprosthesis as a hybrid biological and mechanical structure whose durability was based on the stability of the tissue not on the regeneration of host cells. The term 'bioprosthesis was established for stented xenograft valves at the Bioprosthetic Cardiac Symposium (Munich) 1979.

valves) as well as improved hemodynamics over porcine valves. However, they were plagued by early structural failures associated with the mode of attachment to the stent and puncture sites within the tissue. Wheatley for example (1987; 1994) noted the origin of valve failure of the Inoescu-Shiley valve occurred close to the points where the sutures passed through the leaflets and, despite modifications to the fixation process the problem of cusp tearing persisted (Masters 1995). Thiene (1989), Hilbert (1992) and Butany (1992) for example, reported failure occurring at or near the alignment stitch, an area already weakened by increased membrane stresses resulting from the progressive loss of commissural tissue apposition and a significant reduction in mechanical properties (ie. 22%-59%) resulting from puncture holes created by the surgeon's needle. Furthermore, the size of hole was also found to be directly proportional to degree of compromise (Lim 1994). The impact on surgeon confidence in bioprostheses following these failures was significant, particularly in pericardial valves, and resulted in a marked decline in bioprosthetic implantation rates. In the UK for example, 46% of all heart valve replacements in 1986 were bioprostheses compared with 53% mechanical valves. Moreover, one-quarter of all bioprostheses were made from pericardial tissue (605/2399). By 1993 however, bioprosthetic implants had fallen to 27% (1491/5486) with a marked decline in pericardial valve implants to a low of $\leq$4% (50/1491) (UK Heart Valve Registry 2007). Demonstrable improvements in the long-term durability and freedom from structural valve deterioration demonstrated by second generation bioprostheses, such as the Hancock Modified Orifice valve, Carpentier Edwards Supra-annular valve, Carpentier Edwards pericardial valves, Medtronic-Hall Intact valve etc. have however, reversed this lack of confidence in bioprosthetic implants and data now shows a significant increase in the numbers of bioprostheses implanted annually (Gao 2004; UK Heart Valve Registry 2007).

As previously mentioned very few modifications to the design of xenografts have been made since the valves were first attached to stents. However, stents increase the valve's bulk effectively reducing its effective orifice area. In an effort to address this problem

and increase the valve's durability the geometry was modified by sewing the valve annulus into the supporting stent under slight longitudinal compression. The resulting low-profile valves (e.g. Liotta valve (formerly known as the BioImplant valve), Carpentier Edwards Supra-annular and Perimount valves, Mitroflow valve etc.)) had, as Figure 3.6 shows, a reduced height-to-diameter ratio which lessened the potential for impingement on the contracting myocardium. However, geometry-related stress problems compromised durability resulting in a number of early valve failures and led to the use of flexible stents in bioprostheses (e.g. Hancock II and Mosaic valve (Figure 3.6); Hamid 1986). A higher incidence of stent-creep and deformation during implantation or during the cardiac contraction as a result of long-term cyclical loading of certain polymers was also reported in these valves (Vesely 2003). As a consequence, manufacturers became more selective in the type of stent material used and also developed valves without the support structure which became known as stentless valves.

Figure 3.6 1st & 2nd generation bioprostheses

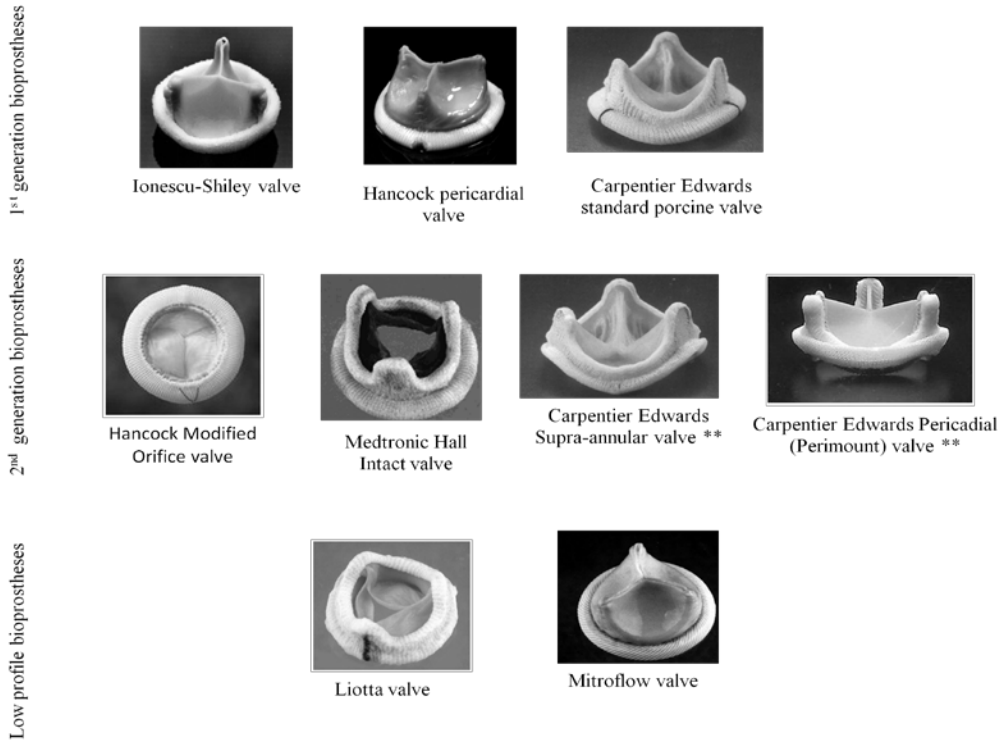

** The Carpentier Edwards Supra-annular and Carpentier Edwards Pericardial (Perimount) valves are also low-profile bioprostheses.

(b) Stentless bioprostheses

Stentless valves are similar to cryopreserved allografts except the tissue is usually fixed in gluteraldehyde. The whole porcine aortic tissue with its attached root is most commonly used and the lack of stent and associated sewing cuff gives a larger effective orifice area in the magnitude of approximately one to two sizes larger than the stented xenografts. As Figure 3.7 shows some designs of stentless valves are untrimmed giving the surgeon the option to trim the valve to fit the patient. However, implantation requires scalloping out the sinuses or, careful re-attachment of the coronary arteries as well as inflow and outflow suture lines making this technically very challenging and time consuming and requiring longer cross-clamps times. Consequently, initially surgeons have shown restraint in implanting stentless valves although, significant increases have been reported in the UK where numbers of valves implanted increased by 200% from 1,865 to 5,595 between 1987 and 2005 suggesting, increasing confidence associated with increasing experience in implantation skills (UK Heart Valve Registry 2007). However, the concept of the stentless valve has, as some such as Butany (2006) suggested, failed to live up to the biomechanical advantages and expectations.

Figure 3.7 Stentless bioprostheses

Freestyle valve | Prima valve | Prima Plus valve | Sorin Pericarbon valve | Biocor valve

(c) Tricomposite bioprostheses

Concerns about the potential patient mismatch and calcification of the aortic annulus (see Chapter 1) led to the development of a tricomposite valve constructed from three cusps, a non-coronary cusp from three different valves sewn together to create a single bioprosthesis (Figure 3.8). Theorectically, the risk of failure resulting from matching a non native single cusp from one valve with two existing cusps from another is high and, although initial results indicated good early and mid-term haemodynamic performance and durability later reports suggest long-term durability is a problem. Pavoni and colleagues' study evaluating the Cryolife O'Brien composite valve reported satisfactory results up until 8 years post implant after which, durability began to wane and the risk of structural valve deterioration (SVD) and reoperation increased significantly (Pavoni 2007). The authors noted freedom from SVD at five years was 91% but fell dramatically to 44% at 10 years with 18% (21/115) of patients suffering SVD within the first eight years compared with 36% (12/33) after eight years. Furthermore, out of the 17 patients who underwent reoperation for SVD the majority were found to have leaflet tears with the right coronary cusp the most common culprit. Pavoni also noted, from studies by Desai and Bach published in 2004 and 2005 respectively, the durability of the Freestyle and St Jude Toronto Stentless valves compared with the Cryolife O'Brien valve reported freedom from SVD at 10 years was far higher at 90% and 78% respectively than the Cryolife O'Brien valve. However, in contrast to these findings a study by O'Brien et al (2005) recorded only 1 failure as a result of SVD out of a total of 402 implants. Thus, uncertainty remains with regards to the durability of tricomposite valves and in particular the Cryolife O'Brien composite valve.

Figure 3.8 Tricomposite valves

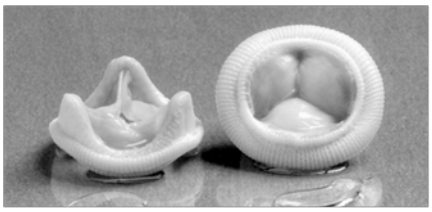

Labcor Syngergy ST valve

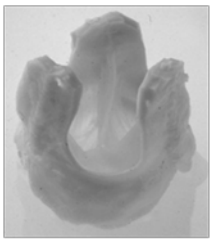

Cryolife O'Brien valve

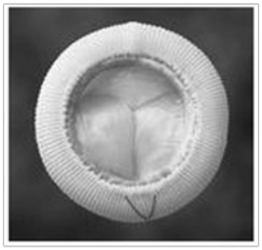

Hancock Modified Orifice valve

(d) Autologous bioprostheses

Valves fabricated from autologous tissues were expected to be superior to heterografts because of the atraumtic, non-thrombogenic and relative non-vascular nature of the tissue, its no-requirement for anticoagulation and because the tissue is nourished by penetration if transplanted as a heart valve replacement. Furthermore, because crosslinking of autologous tissue with gluteraldehye was not necessary it was assumed unfixed autologous tissue valves would be unlikely to calcify and should therefore demonstrate greater durability. However, despite encouraging initial results (Ionescu 1970; Talavilkar 1973) autologous pericardial tissue was found to show signs of shrinkage in response to haemodynamic forces, calcification and thrombo-emoblic potential (Welch 1971; Talavilkar 1973; Olson 1975; Cleland 1983). Scarring and tissue shrinkage was resolved by briefly immersing the tissue in gluteraldehyde which also made the tissue easier to handle since it became much stiffer although this negated any theoretical advantage it had with regards to calcification stimulating gluteraldehyde. Despite attempts to resolve the mechanical problems of autologous tissue valves their clinical performance was variable and there were many early failures. As a consequence, implantation using autologous valves ceased although, in more recent times newer designs have been clinically introduced (Edwards 2006; UK Heart Valve Registry 2007) and are being investigated further as part of the concept of tissue engineering.

3.2 Current developments for heart valve replacement

(a) Polymeric heart valves

Persistent concerns about the high risks of thrombo-embolic complications and associated life-time antigoculation requirements for mechanical valves together with, uncertain durability and increased risk of SVD in bioprostheses has shifted the focus of current research towards the possible use of different polymeric materials for heart valves. A number of polyurethanes are reknown for their good blood biocompatibility and also because of their potential to be moulded, rather than sutured, into a naturally geometrically similar trileaflet heart valve which could demonstrate central, less disturbed blood flow, good functionality and durability (Mackay 1996; Wheatley 2000). Wheatley (2000) for example, noted trileaflet polyurethane valves in animal studies demonstrated relatively low thrombogenicity and good haemodynamic function comparable with mechanical valves and although three valves became severely stenotic polyurethane valves were generally less stenotic after six months compared with bioprostheses.

(b) Tissue engineered valves

The lack of growth, repair and remodelling capabilities of current heart valve prostheses limit their use in certain patient populations, namely children with congenital defects. Thus, a replacement heart valve which incorporates these elements is something of a holy grail. To this end research has been conducted into engineering new 'tissue' from individual cellular components *in vitro* using a scaffold [24] for cells to attach to. However, decellurization is thought to compromise the mechanical properties of tissue, increase platelet activation and blood coagulation whilst cross-linking and gluteraldehyde toxicity

[24] This type of scaffolding is usually made from either biological (ie. donor human heart valves and decellularized animal derived valves) or syntehtic materials (such as polyglycolic acid (PGA) and polylactic acid (PLA)) fixed with guteraldehyde.

prevents celullar infiltration post implantation. The first tissue engineered decellularized porcine heart valve, the Synergraft ™ xenograft valve, was first clinically implanted in 2003. However, aggressive decellularization used in the technology led to catastrophic early valve failure (i.e. ≤1 year) as a result of structural failure and rapid degeneration associated with strong inflammatory response which occurred as early as two days post implantation with formation of a dense fibrous sheath around the graft, calcific deposition and zero host cell re-population on the valve matrix (Simon 2003). Despite this early failure and continuing problems with the mechanical strength required for functional performance, patients for whom conventional treatment is not an option will continue to act as the impetus for ongoing research into the field of tissue engineered heart valves (Vesely 2005).

(c) Percutaneous heart valves (PHV)

As previously mentioned some patients are deemed too high risk to undergo open heart surgery but the development of percutaneous technology presents a new sense of hope. Percutaneous valve replacement uses an expandable stent to percutaneously deliver a foldable heart valve. The procedure was first demonstrated by Anderson (1992) who successfully implanted a porcine bioprosthesis into the aortic site and a decade later Cribier performed the first successful human percutaneous implantation of an aortic valve (PAVR) (Cribier 2002). Although development of the percutaneous valve continues two distinct types are currently being used in clinical practice, the balloon-expandable trileaflet valve made from either equine (Cribier-Edwards) or bovine tissue (Edwards-Sapien) and the self-expandable porcine pericardium trileaflet valve (CoreValve; Figure 3.9). The balloon-expandable valves mounted within a tubular slotted stainless steel stent were initially delivered via the antegrade transseptal approach using large sheaths through the femoral vein under local anaesthetic. This approach eliminated the risk of arterial injury but appeared to increase the risk of anterior mitral valve leaflet injury likely to cause severe mR with haemodynamic collapse and death. Thus, attempts at retrograde

delivery using a steerable delivery catheter rather than a guide wire/catheter was attempted even though this required surgical cutdown and repair of the vascular site, as well as rapid right ventricular pacing (~200 beats/min) using a temporary pacemaker to arrest left ventricular flow so the valve could be accurately deployed. In addition, its use is unsuitable for patients with small and/or diseased iliofemoral arteries because of its large profile. As a result of these complications there has been a shift towards a transapical approach because it offers a more direct access to the aortic valve, eliminates the risk of arterial injury, reduces concerns about sheath size and has proved ideal for high risk surgical patients ± significant peripheral arterial disease (Chiam 2009). Unlike balloon-expandable PHV the self-expandable valve is mounted and sutured in a self-expandable nitinol stent with a length of 50 mm compared with 14-16 mm. The long sheath length is such that the lower (inlet) portion has a high radial force which expands and excludes the calcified aortic leaflets; the middle section houses the valve whilst the upper portion (outlet) is flared so the stent can be oriented and fixated in the ascending aorta. Moreover, haemodynamic support, rapid pacing, surgical 'cut-down' or access site vascular repair is not required. However, despite their differences a number of common complications and/or limitations have been reported for both types of PHV such as; accuracy in positioning the valve in the left ventricular outflow tract, the need to interrupt coronary flow during implantation, removal of the native diseased valve, risk of valve migration, the size and dimensions of the PHV and delivery route, severity of disease pathology and tissue friability, patient selection and operator skills (Coats 2007; Kidane 2009; Chiam 2009). In addition, there is also the question about their application to diseases other than calcific stenosis. Thus, there still appears to be a considerable amount of work to be done on developing these types of valves and their application.

Figure 3.9 Percutaneous heart valves

Cribier-Edwards heart valve

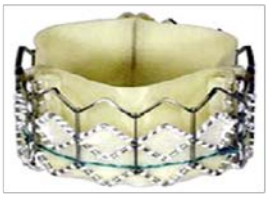

Edwards-Sapien heart valve

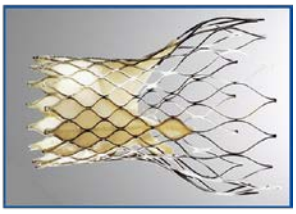

CoreValve heart valve

3.3 Chapter summary

In conclusion, Chapter 3 provides a brief history and description of the development of replacement heart valves following the introduction of the heart-lung machine in the 1950s. Early attempts to replicate the heart's natural valves identified the need for biocompatible, durable and chemically inert materials and a design which was responsive to pressure gradients, function rapidly, maintain directional flow, prevent regurgitation and stasis, be easily implantable and remain fixed in place. However, in spite of the different designs and the use of different materials all replacement valves without exception, have demonstrated some form of complication or failure. Persistent thrombo-embolic complications and life-long requirements for anticoagulation have tempered the enthusiasm for mechanical valves and although bioprosthetic valves were seen as the answer to the bleeding complications associated with mechanical valves and the lifelong anticoagulation requirements, problems of long-term durability as well as structural valve failures have persisted. Early replacement with homograft valves proved biologically and haemodynamically advantageous without the requirement for life-long anticoagulation but supply proved problematic. Autologous tissue failed because it proved unable to withstand the strong haemodynamic forces generated by the heart and resulted in tissue shrinkage, calcification and increased thrombo-embolic potential. Although animal tissue valves proved more compatible with human implantation poor durability of first

generation bioprostheses resulted in number of early valve failures. However, improved preservation and fabrication methods as well as, modifications to valve geometry has given rise to low-profile valves and the use of flexible stents which have significantly increased durability and valve performance.

The 21st Century has heralded new methods of implantation and the possibility of growing new biological valves from cells. Self- and balloon-expandable valves delivered percutaneously via a catheter is a simple concept but this is a technically difficult procedure and requires a robust yet flexible valve capable of withstanding strong compressive forces yet flexible and precise enough to unfold into the precise geometries required for function and durability. Despite complications associated with valve delivery, maintaining continuous haemodynamic function during implantation, patient selection, disease pathology and tissue friability etc. percutaneous transcatheter valve replacement continues to promise hope for a minority of otherwise surgically inoperable patients. Continuing concerns about bleeding complications, lifelong anticoagulation requirements, structural valve failure, durability and the inability of any current cardiac valve prostheses for growth, self-repair or remodeling has led to experimentation into tissue engineering a heart valve from living cells which offer the promise of being able to grow *in vitro* and *in vivo* [25] from transplanted autologous cells. However, attempts to translate the theory into a functionally engineered tissue valve has so far been retarded by problems associated with gluteraldehyde toxicity and inflammatory responses to decellurization. The use of different polymeric materials are also being investigated and early results using animal models suggest certain polymeric valves have shown good blood and biocompatibility, good haemodynamics and functionality in comparison to mechanical valve performance and are generally less stenotic than bioprostheses.

Improvements in the performance and durability of cardiac valve prostheses together with increases in the longevity of patients has resulted in an increased probability prosthetic

[25] The term *in vivo* in this document refers to studies which reference heart valves within the living heart and body.

cardiac valve patients will be referred for radiological diagnostic investigations such as magnetic resonance imaging (MRI). The next chapter therefore looks at the basic principles of MRI with particular reference to the interaction of MR associated magnetically induced forces with biological systems and heart valve prostheses.

CHAPTER 4

Magnetic resonance imaging.

Basic theory, bio-effects and interaction with biomedical implants

4. Introduction to MRI

The previous chapters introduced one of two main components to this thesis, the artificial heart valve, and discussed some of the common diseases affecting the cardiac valves which lead to heart valve replacement surgery with a prosthetic heart valve. In addition, these preliminary chapters also charted the development of the artificial heart valve and mentioned the types of materials used in their design and construction. Chapter 4 now introduces the second of the two major components to this thesis, magnetic resonance imaging and discusses its relevance to this study and the assessment of the interaction of MR induced magnetic forces on heart valve prostheses. The chapter begins with a description of the basic theory of MRI so the reader may gain a fundamental understanding of how strong magnetic forces influence the behaviour of nuclei and thus, why and how magnetic forces induced during MRI may interact with certain materials in artificial heart valves. The chapter then discusses the relationship between magnetism, materials and biological systems and presents a review of the potential hazards associated with MRI with particular reference to the three types of magnetic resonance (MR) associated magnetic fields. This aim of this review is to provide the reader with an insight into why anxieties about exposure of patients with biomedical implants to MRI persist amongst clinicians.

4.1 Basic MR Theory

MRI has its roots in nuclear magnetic resonance imaging (NMR) which was first discovered in the 1930s. Two independent investigators looking at the direction, rate and frequency of nucleic spin in a magnet noted precessing nuclei produce a detectable oscillating signal and electromagnetic energy produced during this precession is absorbed by a material at this resonant frequency [26]. However, it was not until the 1970s before it

[26] Felix Bloch, a Swiss born American physicist was jointly awarded the 1952 Nobel Prize for Physics with the American physicist Edwards Mills Purcell for their work on the development of nuclear magnetic

was suggested NMR could also be used to produce images of the body and a further decade before the first commercial clinical imagers were built and NMR became known simply as MRI. MRI is now regarded as one of the most important developments in medical diagnosis since X-rays were first discovered over 100 years ago [27]. However, unlike X-ray it does not employ ionizing radiation and other advantages are: it is non-invasive, has a unique ability to produce images in numerous planes without repositioning the patient, produces 3-dimensional images of the body's anatomical and functional internal organs with high quality spatial resolution and, can discriminate between types of tissue in an image simply by varying the way the image is formed. Thus, MRI can be tailored to specific clinical applications and as a result its popularity has soared rapidly. Between 1995 and 2006 for example figures for the UK show the percentage annual increase in MRI procedures was 26% compared with a 5% increase in ultrasound and 14% rise in computer tomography (CT) (Smith-Bindman 2008; Baker 2008). Furthermore, during this period the number of MRI procedures performed tripled compared with 40% increase in the ultrasound procedures and a doubling of CT scans (Smith-Bindman 2008). Current estimates indicate approximately 60-80 million MRI examinations are performed annually worldwide (Moser 2009).

4.1.1 Magnetism caused by atomic motion

MRI can be described as a combination of classic and quantum physics and is reliant on the spinning motion of specific nuclei, known as MR active nuclei which are present in all biological tissue. Hydrogen is the most important example of MR active nuclei because of its abundance in the human body and because of its ability to produce a significant magnetic vector. As we know, every atom consists of a central spinning nucleus and negatively charged electrons spinning on their own axis and orbiting the

resonance method of measuring the magnetic fields of the nuclei of atoms and the discoveries that resulted from these investigations.

[27] The first MR image was published in 1973, the first cross-sectional image of a living mouse was published in January 1974 and the first studies performed on humans in 1977. In comparison, the first human X-ray was take in 1895.

nucleus. It has been suggested the relevance of this, in terms of MRI is, when a charged particle spins it generates a small magnetic field that has both direction and magnitude and causes the nucleus to act as a small bar magnet as depicted in Figure 4.1. The direction and magnitude of the field can be represented by a vector known as the nuclear magnetization vector (NMV) [28].

Figure 4.1 Bar magnet with associated magnetic field

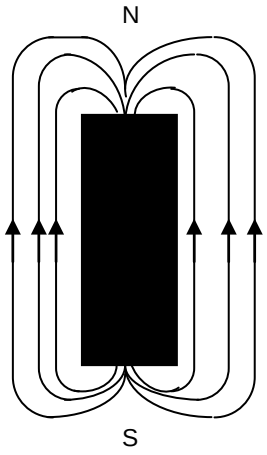

4.1.2 Precession and the Larmor equation

When hydrogen nuclei are exposed to a strong uniform magnetic field an interaction occurs between the field and the nuclei producing an additional nucleic spin and causing a 'wobble' of the NMV around the field. As Figure 4.2 shows the NMV traces out a cone shape as the nuclei 'wobble' and this secondary spin or precession, causes the magnetic moments to follow a circular path around the magnetic field (i.e. precessional path) at a

[28] The nuclear magnetization vector (NMV) is also known as the magnetic moment of the nucleus.

frequency measured in megahertz (MHz) [29]. Each type of MR specific nucleus has its own specific angle of precession and precessional frequency, often referred to as the Larmor frequency, which is determined by the Larmor equation (see Equation 1 below) as well as its own specific gyro-magnetic ratio, which is a constant of proportionality [30]. Thus, the B_0 field is proportional to the Larmor frequency and if B_0 increases, so too does the Lamor frequency and vice versa.

Equation [1]:

the precessional frequency $(\omega_0) = B_0 \, x \, \gamma$

where:

B_0 is the magnetic field strength of the magnet, and

γ is the gyro-magnetic ratio.

[29] 1 Hertz (Hz) is the equivalent of one cycle per second and 1 MHz is therefore 1 million cycles per second.

[30] The relationship between the angular momentum and the magnetic moment of each MR active nucleus is known as the gyro-magnetic ratio and is expressed as the precessional frequency of a specific MR active nucleus at 1.0 T. The unit of gyro-magnetic ratio is MHzT. The gyro-magnetic ratio of hydrogen for example is 42.57 MHzT and because the precessional frequency changes depending on the field strength it is exposed to, the precessional frequency of hydrogen at 1.5 T and 4.7 T respectively is 63.86 MHz (ie. 42.57 MHz x 1.5 T) and 200.08 MHz (ie. 42.57 MHz x 4.7 T).

Figure 4.2 Nuclear spin and precession

(a) Nucleus with net spin **(b) Nucleus demonstrating precession**

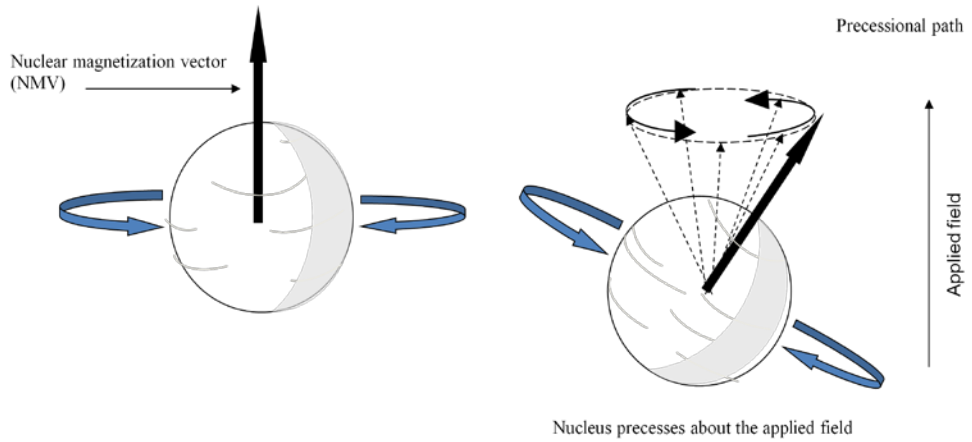

4.1.3. Alignment to the magnetic field

MR active nuclei align their axis of rotation to an applied magnetic field but are otherwise randomly orientated if the magnetic field is absent (Figure 4.3a). The laws of electromagnetic induction however, dictate that when nuclei spin and have a net charge [31] they acquire magnetic moments which allow them to align with the external magnetic field [32]. Alignment of hydrogen nuclei in the magnetic field is dependent also on its thermal properties (i.e. energy levels) as well as its strength. MR active nuclei possess two energy states, low and high energy known as spin-up and spin-down nuclei respectively. As Figure 4.3b shows low energy nuclei, which are more abundant than high energy nuclei, lack sufficient energy to oppose the magnetic field and therefore align their magnetic moments parallel to the magnetic field. In contrast high energy nuclei

[31] A net charge occurs when there is either an even number of neutrons and an odd number of protons or vice versa.

[32] The external magnetic field is denoted by B_0 and in MRI B_0 is equivalent to 1 Tesla (T) or 10,000 Gauss. The earth's magnetic field is approximately to 0.5 Gauss and is therefore 30,000 times weaker than a 1.5 T MR system.

have sufficient energy to oppose the magnetic field and consequently their magnetic moments align in an anti-parallel direction.

Figure 4.3 Alignment of the external magnetic field

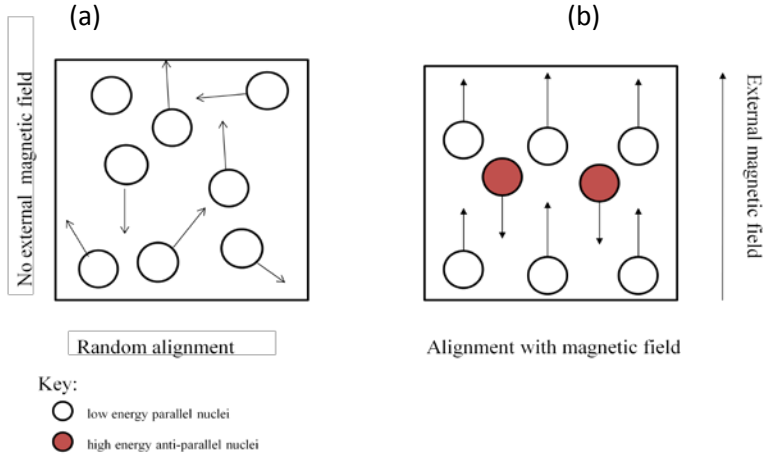

4.1.4. Resonance, net magnetization vector and the MR signal

As previously mentioned the magnetic field surrounding each nucleus has both direction and magnitude and is represented by NMV. When a large number of these individual NMVs interact however, they create a larger vector known as the net magnetization vector (M) which has two components: one parallel to the applied magnetic field (M_z) and the other perpendicular to the field (M_{xy}). When, as Figure 4.4a shows more nuclei are parallel to the applied field than anti-parallel M_z is positive. However, when precessing nuclei are excited by radiofrequency (RF) and absorb energy a decrease in the proportion of parallel low energy nuclei occurs as they gain sufficient energy to 'flip' over into the high energy anti-parallel state. As a result M moves away from B_0 and when the proportion of nuclei in the parallel and anti-parallel states is equal M_z is zero (Figure 4.4b). If the proportion of nuclei in the anti-parallel state exceeds that of the parallel state, M_z becomes negative (Figure 4.4c).

Figure 4.4 Orientation of a net magnetization vector

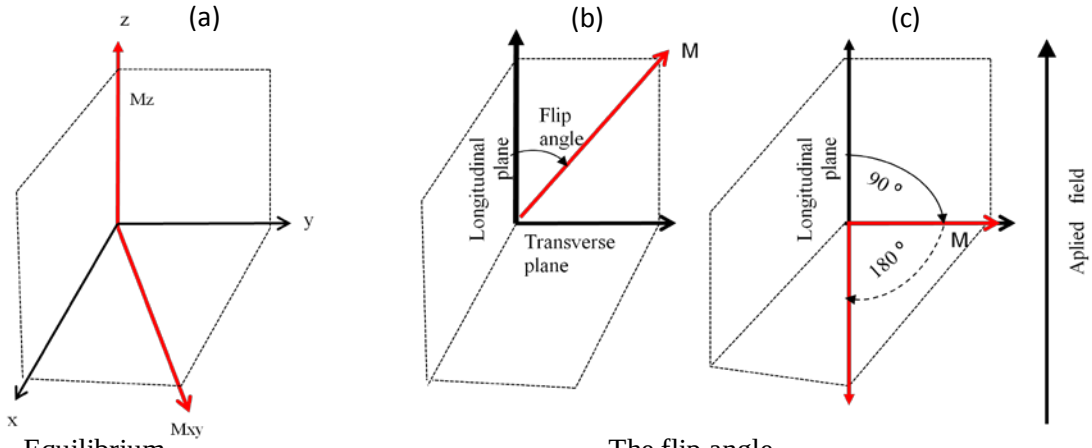

Equilibrium The flip angle

The angle of displacement of M away from B_0 can be controlled by the application of an RF pulse of an appropriate amplitude and duration. Two angles commonly used to produce these effects are 90º and 180º (Figure 4.4c) and are known as the 90º and 180º pulses [33,34]. As field strength and energy absorption increase the magnetic moments of nuclei in the transverse plane move into phase with each other and precess around B_0 (Figure 4.5) and as M precesses in phase a voltage is induced in the receiver coil and a signal with a frequency equivalent to the Larmor frequency is produced. When the pulse is withdrawn however, the nuclei in the surrounding area gradually lose energy (*relaxation*) and M_{xy} realigns itself one again to equilibrium parallel to B_0. As the level of magnetization in the longitudinal plane gradually increases exponentially with time (T1 recovery [35],[36]) the amount of magnetization in the transverse plane gradually

[33] When the net magnetization vector moves outs of alignment away from B_0 the resultant angle is called the flip angle and B_0 is now referred to as the longitudinal axis/plane. When the plane is perpendicular to B_0 (ie. 90° to B_0) it is called the transverse plane.

[34] The larger the flip angle the greater the RF energy deposition required to generate excitation.

[35] Recovery is also referred to as *spin lattice relaxation.*

[36] The rate of recovery is an exponential process with a time constant (T1) which corresponds to the time it takes 63% of the longitudinal magnetization to recover in the tissue.

decreases, also exponentially with time (T2 decay) so too, the magnitude of the voltage induced in the receiver coil. This reducing signal is known as free induction decay (FID) signal and the FID collected during and after the application of RF pulses and magnetic field gradients (i.e. pulse sequences) is responsible for producing magnetic resonance images. T1 recovery is always longer than T2 decay of the transverse magnetization and it is these differences in the relaxation parameters of the varying types of biological tissue which means MRI can produce clear images which distinguish and emphasize the natural contrast between them.

Figure 4.5 Phase of magnetic moments around their precessional path

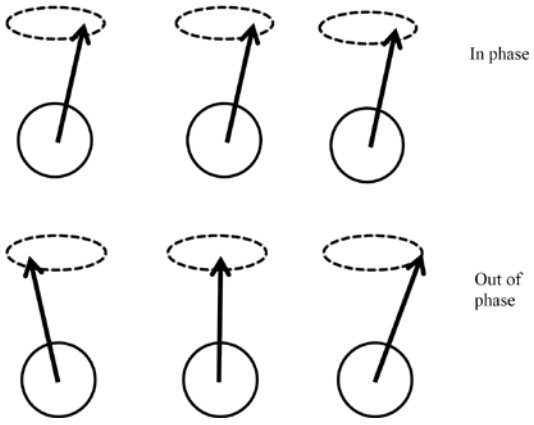

Magnetism is a fundamental property of all matter and the amount of magnetism demonstrated by any substance depends on its magnetic susceptibility (χ) [37]. There is of course, a spectrum of magnetism the most well known being ferromagnetism which has a high positive susceptibility and demonstrates a constant magnetic field, strong attraction and alignment to the magnetic field and retains its own magnetism. Paramagnetic substances on the other hand have a low positive susceptibility, are only weakly attracted to an external magnetic field and are only temporary. Once the external magnetic field is

[37] Magnetic susceptibility refers to how easily a substance can be influenced by the magnetic field.

removed and the field drops to zero a paramagnetic material loses it magnetism. At the far end of the spectrum are diamagnetic substances which have a low negative susceptibility and are repelled by the applied magnetic field. Although the focus of this research relates primarily to the interaction of MRI associated magnetic field interactions with prosthetic heart valves the next section of Chapter 4 includes broader issues with regards to patient safety.

4.2 Potential hazards of MRI

Despite an estimated 60-80 million MR procedures performed annually worldwide relatively few major incidents are reported and the vast majority of patients who undergo an MRI investigation do not appear to suffer any injury or long-term side-effects. It may therefore be reasonable to suppose MRI is inherently safe. Guidelines outlining the maximum acceptable limits for safe exposure to the magnetic fields induced during MRI have been defined (MHRA Device Bulletin DB2007(3). However, these are regarded as arbitrary and, anxieties about the hazards intrinsic to MRI including the potential bio-effects associated with exposure to the static magnetic field (B_0), time-varying magnetic field gradients (dB/dt), radiofrequency fields ((RF coils), B_1)) and, the interaction of certain biomedical implants with MR associated magnetically induced forces persist.

4.2.1 Static magnetic field (B_0)

Every individual is exposed to the Earth's magnetic field and is therefore continuously exposed to the naturally occurring static magnetic fields. However, some individuals are also exposed to additional, man-made static magnetic fields as a result of their involvement in and/or exposure to certain industries (e.g. welding), power-generating processes (e.g. rail transport (magnetic levitation known as MAGLEV trains)) and medical procedures (e.g. MRI). Unlike man-made magnetic fields the magnetic field within the MR environment is always present even when the scanner is not imaging.

However, a stray field, which extends to the surrounding space and results from a decrease in field strength with increasing distance from the bore's iso-centre exists and creates a large spatial gradient field (dB/dx). Particular concerns associated with exposure to B_0 field relate to the: potential physiological effects on human tissue, possibility an external object may become a dangerous projectile within the dB/dx field, potential for any magnetisable object *in vivo* to move, become dislodged or oppose the original magnetic field thereby impeding function and exposing the patient to a serious risk of harm or death (see below).

(a) Biological effects

All living tissues are known to be weakly magnetic or diamagnetic with a low χ which determines their interactions with B_0 field. The influence of strong magnetic forces associated with the B_0 field upon biological systems has stimulated considerable interest since clinical MRI was first used and it has been suggested for example, certain iron rich tissues such as haemoglobin and ferritin, possess a greater χ and may therefore be attracted to the applied magnetic field (Melville 1975; Brook 1998; Kinouchi 1988, Schenck 2000, Schenck 2005). Schenck (2000) for example, suggested erythrocytes, which are rich in haemoglobin,[38] are attracted towards regions with a stronger magnetic field although, the attractive force exerted on these cells is less than 4% of the gravitational force and therefore poses no risk to patients undergoing MRI even in the highest-field whole-body magnets. Critics of Schenck's calculations on χ of erythrocytes have however, criticized his emphasis on the use of calculations to determine specific behavior of biological systems and argue, biological systems do not always behave in an expected linear fashion therefore, it is unsafe to apply mathematical calculations to active systems in order to determine their interaction with the B_0 field (Hore 2005). Schenck also suggested certain macromolecules and organelles possess different anisotropic magnetic χ which result in a torque that attempts to minimize the magnetic energy and

[38] Each haemoglobin molecule contains four iron atoms.

align the molecules in the direction of the magnetic field (Schenck 2005). The torque effect for single *in vivo* molecules exposed to an applied magnetic field is negligible. If however, anisotropic macromolecules or cells cluster together their volume increases thereby increasing the magnitude of χ. These effects have been demonstrated *in vitro* with erythrocytes in sickle cell anaemia where the abnormal haemoglobin molecules aggregate and polymerize to form fibres and gel-like structures which bind together and orientate themselves in the same direction. However, the shear forces present in blood flow are greater than those demonstrated by magnetic orientation and as a result this effect can only be observed *in vitro* (Brody 1985; Schenck 1992).

Plasma membrane is innately diamagnetic and is therefore likely to interact with the B_0 field. Indeed, research has shown this interaction can lead to re-orientation of the molecular domains and rotation of the phospholipid membrane (Rosen 2003) which in turn, affects Ca^{2+} flux, cell shape, cytoskeleton arrangement, ion flux, receptor distribution etc. (Rink 1990; Teodori 2002, Chionna 2003; Teodori 2005, Silva 2006). Investigators have found exposure to B_0 field can result in a cell becoming less flat and more rounded and elongated with many irregular lamellar microvilli and membrane roughness and blebbing (Chionna 2003; Teodori 2005; Dini 2005). Cell death is thought to be strongly influenced by Ca^{2+} which acts either as a trigger for or, defense against apoptosis (Galli 1995; Dini 2005). Thus, any changes in Ca^{2+} flux resulting from exposure to the B_0 field will strongly influence the rate of apoptosis. Tavascoli et al (2009) suggest an increase in Ca^{2+} flux promotes the rate of apoptosis. However, others argue this is not the case and any increase in Ca^{2+} reduces the rate of cell death by apoptosis (Fanelli 1999). Despite the effects mentioned research has shown cell growth and survival, under normal culture conditions, is not compromised in the long-term when exposed to B_0 field regardless of magnetic density (Miyakoshi 2005).

The B_0 field is also thought to influence certain chemical reactions, namely the dissociation of the binary (AB) molecule in a solvent when joined by a non-magnetic

electron pair bond. When the electrons A and B are bound together they have opposite spins and form a single state with a total spin equaling zero. However, if AB attempts to spontaneously dissociate into separate radicals (A* and B*), this process is inhibited by the surrounding solvent molecules which act like a cage stopping each radical from completely separating from one another. If A* and B*, still in their singlet state, then recombine before separation is complete the 'caged' product AB is formed. However, if diffusion is successful an escaped product, A* and B* is formed. Should the magnetic moments of the two radicals in an applied field however not be the same, the spins of the two separating radicals precess at different rates and are unlikely to successfully re-bond although the yield of escape products will be increased (Brocklehurst 2002). The use of radical pair magnetic field effects to measure chemical and biochemical reactions is well recognized (Boga 1990; Brocklehurst 2002) although certain conditions must be met in order to detect magnetic field effects on any enzymatic reaction. However, the difficult and exacting requirements suggest many enzymes lack all the necessary criteria and therefore fail to produce magnetic field-induced reactions (Grissom 1995).

(b) Sensory effects

Several common transient sensory sensations including nausea, vertigo, metallic taste and magnetophosphenes[39] have also been reported during exposure to B_0 field (Formica 2004; de Vocht 2006; Weintraub 2007; Glover 2007). Studies suggest nausea and vertigo may be the result of a conflict between position sensing apparatus in the inner ear and visual systems resulting from the magnetic interaction with the inner ear's vestibular apparatus such that, when the head moves the inertia of the fluid in the ear (i.e. endolymp) causes the cupula to deflect and initiates a signal in the sensory epithelium. Excitation of the epithelium by B_0 field is perceived as an extraneous head rotation which does not correspond to visual inputs and therefore produces a sensation of nausea or vertigo

[39] Magnetophosphenes are visual flashes/sparks caused by excitation of the optic nerve and are sometimes reported by patients undergoing MRI.

(Schenck 1992). An alternative theory suggests these effects may result from field-induced direct depolarisation of sensory cells or, from diamagnetic anisotropy in the cupula which, when the head moves produces a torque and deflection of this structure (de Vocht 2006; Glover 2007). One suggestion offered as a solution to this problem is to reduce the speed of movement within the MR environment. De Vocht (2006) for example noted employees from an MR manufacturing environment who moved more rapidly, thereby generating a stronger dynamic field, reported more complaints of sensory effects than individuals who moved more slowly.

A metallic taste in the mouth during exposure to B_0 field was originally thought to result from electrolysis of the mercury in the amalgam fillings in the teeth (Chakeres 2005). However, this has been largely discounted and current theory suggests the likely cause is the generation of small electrical currents on the surface of the tongue when it is moved within a magnetic field (Winther 1999; de Vocht 2006). Visual disturbances in the form of phosphenes have been noted from movement through the B_0 field and are thought to result from the interaction of the magnetic field with the diamagnetic retinal rods in the eye which, when rotated cause a slight torque resulting in the illusory stimulation known as magnetophosenes (Kanal 1990). Although these sensory effects may be disturbing for the patient, vary between person to person and be potentially more significant during exposure to higher field strengths they have nonetheless, been found to be short-term with no long-term bio-effects with exposures up to and including <4 T (Beischer 1964; Schenck 1992).

Although a number of bio-effects at molecular and cellular level as well as sensory effects have been reported much of the research and results obtained have been conducted on cell cultures and/or animal investigations over significantly longer exposure times than we would expect to see during patient procedures and therefore such methodologies are difficult to extrapolate to human subjects. Thus, caution should be practiced when interpreting these results.

(c) Projectile risk

As mentioned previously, increasing distance from the magnet's iso-centre extends the B_0 field outward, decreasing its strength and producing a large spatial gradient (i.e. dB/dx) of magnetic force with accelerating potential. Thus, any ferromagnetic object within the B_0 field could potentially be accelerated towards the iso-centre becoming a projectile with sufficient velocity to cause injury to a patient or any person in its path. Serious incidents involving the "projectile effect" have been documented and include objects such as: gas cylinders, chairs, respirators, intravenous (IV) poles (Malott 1987; Chaljub 2001; Colletti 2004; Ulaner 2006) and researchers in the US have estimated there are 17 incidents per year and one serious incident every three years in every MRI facility in the US (i.e. approximately one incident in every 100 to 1000 scans (Chaljub 2001)). Furthermore, more than half of the institutions participating in the study reported serious incidents of this nature. Thus, despite an assumed understanding of these potential hazards reports of incidents involving ferromagnetic projectiles continue.

(d) Implants

Safety concerns pertaining to the attractive forces exerted by the B_0 field not only include collision hazards, as described by the "projectile effect" above, but also the risk of movement, dislodgement and/or altered or negated functioning of a biomedical implant or device as a result of translation forces, the tendency of the object to attempt to align with the magnetic field (i.e. torque effect) (Shellock 1988; Boutin 1994; US Food & Drug Administration 1997; Kangarlu 2000; Shellock 2002, 2004) and the induction of currents on metal components moving through the B_0 field which oppose the change in flux (i.e. Lenz Effect) [40]. The relative strength of translation and rotational forces depends on the

[40] Lenz Law which states "an induced current is always in such a direction as to oppose the motion or change causing it"

amplitude of the B_0 field, its spatial gradient [41] as well as the implant's degree of ferromagnetism, its dimensions, mass, orientation, χ and amount of fibrosing tissue securing it in place. Of these two effects torque is considered the greater hazard. The torque produced by the B_0 field acts to align the long-axis of long slender needle-like implants parallel to the magnetic field. In contrast, thin flat plate-like implants will attempt to turn their flat surfaces parallel to the field lines. Research conducted by Schenck (2000) suggests a substantially greater force is required by the body's tissue to prevent a non-spherical implant from aligning with the B_0 field than it does to prevent it from undergoing translational movement. Thus, a patient with a needle-like implant (e.g. aneurysm clip) which is longer than its width is at greater risk of injury because the implant is more likely to attempt to rotate than deflect.

However, as previously mentioned fibrosing tissue serves to anchor the implant in place and in addition, other counteractive forces such as the constant haemodynamic forces from the beating heart, resultant blood flow and the use of sutures also play a major role in securing the implant and protecting it from any form of unwanted movement. On the other hand, little is known about what happens if these counteractive forces are compromised. The aging process is known to decrease bone mass, muscle strength and immune responses to infections and as a result tissue strength and flexibility is reduced. Estimates suggest the body reaches peak efficiency at aged 30 after which it begins to decline. It is therefore estimated the average rate of tensile strength of muscle in the cardiovascular system for example, decreases by 7% in the 30-39 year olds and 21% in the 60-70 year olds (i.e. standard is 0.11 MPa [42] (Duck 1990; Yamada 1970). Therefore, by the time an individual reaches age 80 years their heart muscle will be expected to be functioning at only two-thirds its peak strength. Furthermore, a study by Edwards et al (2005) which assessed the force required to cause partial or total cardiac valve dehiscence

[41] Translational forces are greater at the opening of the bore and decrease with increasing proximity to the region of imaging inside the magnet. In contrast, rotational forces are greatest nearer the magnet's iso-centre and the axis of the implant at 45º to the z-axis.

[42] MPa (i.e. mega pascal) is a unit of measurement commonly used to measure stiffness or tensile strength of materials and is equal to perpendicular force per unit area (i.e. 1 Newton per square metre or N/mm^2).

reported, tissue samples known to have had a recent episode of infective endocarditis yielded at significantly lower forces than other samples which had not been recently exposed to infection. These results suggest the risk of partial or total valve dehiscence is very high in patients with, or at increased risk of, developing prosthetic valve endocarditis such as the elderly and those with multiple valve prostheses. However, there were a number of limitations to the study such as the small number of samples used and the heterogeneity of the sample, a factor which could not be controlled for. Nonetheless, these limitations should not minimize the suggestion of a relationship between weakened tissue and valve dehiscence and the potential for strong magnetically induced forces associated with MRI to cause movement/dislodgement of an implant and pose a serious risk to patient safety.

The interaction between the B_0 field and implants containing metal components has not been widely investigated and, to date is still only theory. Research conducted by Condon (2000) and Robertson (2000) suggests implants containing metal create their own magnetic field when moving through the B_0 field (the Lenz Effect) and can, in the case of heart valves containing metal within the occluding disc for example, potentially slow down the opening and closing of the occluders thereby increasing the risk of regurgitation and reducing cardiac output. The initial investigation by Condon (2000) suggests this resistive effect can, in the mitral position, be activated at low field strengths (i.e. $\leq$1.5 T) and increases linearly with field strength. Although Robertson (2000), in a follow-up study agreed the Lenz Effect can potentially cause a torque of the moving metallic components of a heart valve and subsequently impede function, this does not pose a significant risk to patients undergoing MRI in field strengths $\leq$1.5 T for which the magnetic effect is $\leq$1% of the pressure effect for both the mitral and aortic valves. However, patients exposed to higher field strength MR systems (e.g. $\geq$3 T) may be subjected to greater risk of valve impedance because the magnetic effect is nearly 10% for mitral and aortic valves.

4.2.2 Time-varying magnetic field gradients (dB/dt)

Another component of MRI are rapidly changing (ie. pulsed) gradient fields or time-varying fields. Time-varying fields are spatial variations in the B_0 field whereby the gradient magnetic field (B), which typically varies with time (t) at some rate (dB/dt), align with the B_0 field to produce resonant frequencies corresponding with spatial position. dB/dt is an essential element of spatial localization of the signal within the body which is achieved by performing selective excitation of protons in the patient. The highest additional magnetic field strength provided by the gradients is several times (usually at least 20 times) weaker than the B_0 field and is thought to exert no additional risk in terms of field strength. However, the sudden rapid switching of the field gradients up and down can, according to Faraday's law of induction, induce voltages and a current with sufficient intensity to heat body tissue and metallic implants, even when motionless and, stimulate nerves. This next section looks at the effects of time-varying magnetic field gradients on biological tissue and biomedical implants and the potential risks these present to patient wellbeing.

(a) Thermal effects

Induced ccurrents generated during the "ramp up" and "ramp down" of the gradient times are dependent on the time rate of change of the magnetic field, the cross-sectional area of the conducting tissue loop and, the conductivity of the tissue. Thus, heating of tissue may occur if either the tips of the conductor are close enough and the induced voltage is great enough to cause arcing and/or, if the conductor is a closed loop allowing a current to flow through it. However, these thermal effects are assumed to be negligible (Kanal 1990).

(b) Stimulation of sensory tissue

Non-thermal bioeffects, resulting from interference of the normal function of nerve cells and muscle fibres, include peripheral nerve and muscle stimulation and these are considered to be potentially more serious. Less serious of the non-thermal bioeffects is visual stimulation of the retina causing 'flashes of light' (ie. magnetophosphenes) caused by stimulation of the retina by the electrical currents. Like the B_0 field however (see above), magnetophosphenes reported in these fields have also been shown to be non-hazardous. The more serious and potentially more injurious to the patient is magnetostimulation of the nerve and muscle tissues. Tissues in the human body are known to act as conductors. Thus, induction of a high enough current in the body directed along a nerve fibre initiates an action potential which propagates along the fibre and, depending upon the type of fibre (ie. afferent or efferent)[43] results in a perception of a sensation and/or a mechanical movement of that muscle. Stimulation of the nerve and muscle tissue during exposure to dB/dt fields not only depends on nerve type [44] but also on the pulse shape and its repetition rate.

Research has shown that at sufficient exposure levels, peripheral nerve (PNS) and muscle stimulation is perceptible as 'tingling' or 'tapping' sensations (Bushong 1993; Hoffman 2000; Wahab 2008) but at higher exposure levels (i.e. 50% - 100% above perception threshold (frequencies ≥5 kHz)) this may be sufficient to cause pain and discomfort and

[43] Afferent or sensory nerves lead from receptor cells (eg. pressure, temperature) to the central nervous system (CNS) and stimulation of these nerves results in an action potential propagating to the CNS where it is perceived as a sensation. Efferent or motor nerves lead from the CNS to the muscles and an action protential resulting from stimulation of these nerves results in a single contraction of the muscle ie. a twitch. A muscle twitch can also result from direct induction of a muscle contraction through local activation at the level of the muscle endplate or membrane.

[44] Stimulation thresholds differ according to the type of fibre involved, peripheral nerves, for example have the lowest sensitivity, respiratory nerves have a greater sensitivity in comparison and those found in the cardiac conduction system the highest sensitivity (Reilly 1992). Furthermore, motor nerves generally exhibit a lower stimulation threshold than sensory nerves and are therefore more sensitive to stimulation through magnetic induction.

in some cases, may result in limb movement (Schaefer 2000; Hoffman 2000). At extremely high levels (i.e. 10 Hz and 100 Hz) cardiac stimulation may occur although, it is thought this is very unlikely because the magnitude of the gradient fields required to achieve this are greater than those currently available (Reilly 1991). Thresholds for PNS have been found to vary according to the gradient fields being applied on different axes and orientation with the field and either singularly (i.e. x-, y- or, z-gradient [45]) or in combination (Ham 1997; Bourland 1999; Hebrank 2000; Zhang 2003). As Table 1 shows stimulation of PNS in the transverse gradients (x and y axes) appear more common than in the longitudinal gradient (z-axis) and excitation along the y-axis causes the most stimulation for the body coil (Chronik 2001; Zhang 2003). Although it has been established dB/dx fields can induce sufficient current in body tissue to cause stimulation of the PNS the use of different terms of reference, for defining "ramp duration", and sinusoidal "ramp duration" have made direct comparisons difficult. Furthermore, gradient coils with different dimensions as well as shielded and non-shielded gradient coils have been used by the different researchers adding to the difficulties of equating research findings to one another.

[45] The x-axes refers to the vertical (ie. left/right) magnetic axis; y-axes refers to the parallel (ie. superior/inferior) magnetic axis and the z-axes refers to the perpendicular (ie. anterior/posterior) magnetic axis

Table 1 PNS stimulation sites of gradient fields

x-axes	y-axes	z-axes
Nose	Scapula	Scapula
Left thorax	Right thorax	Thorax
Iliac crest	Iliac crest	Iliac crest
Left thigh	Upper arms	Xyphoid
Buttocks	Shoulder	Abdomen
Lower back	Hip	Upper & lower back
	Hands	
	Upper back	

(c) Thermal effects on implants

Although dB/dt fields have a greater potential to result in bioeffects it has been noted they can also interact with biomedical implants and devices. Research has shown induced gradient currents tend to be concentrated on the conducting component of the implant/device and this appears to be further influenced by the shape and size of the implant. An implant/device containing a long wire or forming a closed loop of sufficient size, such as a lead used for a neurostimulation system, cardiac pacemaker or guidewire could, for example, potentially generate a significant concentration of the gradient currents and result in nerve stimulation (Smith 2001). Functional ability of active medical devices may also be compromised within these fields as induction of a current in

the device induces a magnetic moment and a resultant torque induced by the B_0 field. The implant then becomes subject to a high-frequency vibration (Hartwell 1997).

4.2.3 Radiofrequency field (B_1)

The third component of the MR environment is the RF magnetic field (B_1) which is a non-ionising electromagnetic radiation in the frequency of 0 to 3,000 GHz. When B_1 is applied perpendicular to the B_0 field hydrogen nuclei gain energy and precess at the Larmour frequency. As previously mentioned (see above) cessation of this pulse results in the hydrogen protons gradually returning to their natural alignment within the magnetic field and releasing their excess stored energy causing the signal emitted to be detected by the coil and sent to the computer system for conversion into an image. Deposition of RF energy as heat in the body is a by-product of this process and results primarily from the magnetic rather than the electric field. Bio-effects associated with exposure to the B_1 field relate to the thermogenic qualities of the field (see below).

(a) Specific Absorption Rate (SAR)

An RF pulse applied during MRI causes an oscillating magnetic field and the induced electric currents generated within the body are capable of generating heat within biological tissue (Kanal 1990; Shellock 2000a). The dosimetric term used (measured in units of watts per kilogram (W/kg)) to quantify energy absorption resulting from exposure to RF radiation during MRI is the specific absorption rate (SAR) and refers to the accumulation or storage of heat together with an elevation in local and/or overall tissue temperatures. Calculation of SAR is complex and is influenced by a number of factors such as strength of the MR magnetic field, type of RF pulse used (e.g. 90º or 180º), repetition time, type of RF coil used, volume of tissue contained within the coil, configuration of the anatomical region exposed, orientation of the body in the field, duration of exposure, rate or energy deposition etc. Current UK guidelines suggest

values below those listed (Table 2) should be adhered to in order to minimise the risks to patients undergoing an MR examination (MHRA 2007).

Table 2 Patient & volunteer SAR limits (W/kg) for B_1 field exposure

National Radiological Protection Board (NRPB)	Uncontrolled [46]	Upper[47]	Uncontrolled Peak SAR		
Body part Exposure time (t)	Whole body (i)	Whole body (i)	Head/ Fetus (ii)	Torso (ii)	Limbs (ii)
≤15 mins	2	4	4	8	12
≥15 t ≤30 mins	30t	60/t	60/t	120/t	180/t
≥30 mins	1	2	2	4	6

Note: (i) Averaged over any 15 minute period
(ii) Averaged over any 6 minute period

The rate of RF energy absorption and dispersion within the body is non-uniform and depends on the dimensions and configuration of the tissue in relation to the incident wavelength as well as blood flow. A tissue size of approximately 50% of the incident wavelength is known to result in the most efficient RF energy absorption but, if the tissue size is large relative to incident wavelength energy is absorbed at the surface whilst small tissue sizes result in little RF power absorption (Shellock 2000a). Surface and peripheral tissue demonstrates greater heat dissipation than central body tissue (Shellock 1986,

[46] Uncontrolled level – for periods of exposure ≥30 minutes and under moderate environmental conditions (relative humidity (RH) ≤50%, ambient temperature ≤22°C) restricting the whole-body SAR to an average of 1 W/kg will avoid a rise of more than 0.5°C in the whole body temperature of patients. The SAR limit depends on time limit.

[47] If the patient or volunteer is monitored the SAR limit can be relaxed according to body part and exposure time referenced in this table.

2000a) and avascular tissue takes longer to dissipate heat. Certain organs, such as the eyes, scrotum and testes are less capable of regulating and dispersing heat and are therefore more susceptible to harmful effects of RF exposure during MRI (Shellock 1987). Research conducted on the effects of energy induced heating on testicular function (eg. reduction or cessation of spermatogenesis, impaired sperm motility, degeneration of seminiferous tubules etc.) for example, suggest temperature increases which raise the temperature of the tissue between 38ºC to 42 ºC may be detrimental (Adair 1989). However, research measuring scrotal skin temperature in human volunteers exposed to MRI recorded a maximum temperature of 34.2 ºC, well within the threshold known to impair testicular function (Shellock 1990).

The majority of studies evaluating thermoregulatory reactions to tissue heating associated with exposure to RF radiation during MRI are however, based on animal models which are unable to mimic or simulate human factors, such as anatomy, tissue volume including subcutaneous fat, physical condition, age etc. (Adair 1986; Adair 1989; Shellock 2000a). Furthermore, the body responds to thermal challenges and the need to maintain thermal homeostasis by attempting to lose heat by means of convection, conduction, radiation and evaporation. Failure of any one of these thermoregulators because of an underlying health condition, use of medications (Rowell 1983; Drinkwater 1979; Fennel 1969; Barany 1955; Buskirk 1965; Jauchem 1985) and/or environmental factors (Formica 2004) to dissipate heat load results in an accumulation or storage of heat and an elevation in local and/or overall tissue temperature (Gordon 1987).

(b) Thermal effects on implants

Biomedical implants and devices are also known to undergo heating when subjected to B_1. (Davis 1981; Shellock 1994, 1995, 1996, 1998, 1999, 2001; Sawyer-Glover 2000; Sommer 2000; Levine 2007) However, certain implants and devices, such as electrodes, leads, guide-wires and certain types of catheters which have an elongated structure, are

more prone to act as receiving and re-transmitting "antenna" especially if they are the right length (Nitz 2001; Pictet 2002; Dempsey 2001). Laboratory studies using phantoms to assess heating-induced temperature increases in implants and devices associated with B_1 have suggested in addition to lead length the resultant heating is dependent on a number of other factors such as the presence of loops, the position, structure and geometry of the implant inside the phantom, thickness of the external lead insulation, shape and size of the phantom and position of phantom inside the coil (Dempsey 2001; Nyenhuis 2005; Mattei 2008; Pictet 2002; Sommer 2000; Muranaka 2007). A review of the literature by Nyenhuis (2005) of temperature rises *in vitro* in deep brain stimulator leads (DBS) noted the presence of loops could be used as a practical method for reducing temperature increases. Moreover, Mattei (2008) demonstrated maximum heating is produced when leads are sited close to the edge of the phantom, regardless of whether they are unipolar or bipolar, and towards the edge of the coil because of the greater electric field intensity at the periphery of the phantom adjacent to the inner wall of the RF coil. Although Luechinger (in Nyenhuis 2005) found temperature rises in unipolar leads were greater than bipolar leads, Mattei (2008) noted that if placed in close proximity to the edge of the phantom temperature increases were lower. However, if unipolar leads were centrally placed in the phantom heating was greater than in bipolar leads. Mattei however, cautions against making any general assumptions because these results were based on a limited number of positions and lead paths. The degree of heating in internal leads is also influenced by the presence and thickness of the insulation sheath. Un-insulated short (i.e. <15 cm) straight wires have been shown to demonstrate higher induced temperatures compared with insulated wires of the same shape and length. Furthermore, as the thickness of insulation increases the degree of heating decreases (Mattei 2008).

(c) Thermal effects on external device leads

B_1 has been shown to be responsible for focal heating of external medical devices such as physiological monitoring devices (e.g. electrocardiographic leads and electrodes, fingertip attachments, Swan-Ganz catheters, halo pins, transdermal patches etc.) during MRI. In the worst cases this has caused thermal injuries to patients, especially if direct contact between the patient's limbs or other body parts and the RF body coils, transmit coils or, if skin-to-skin contact occurred (Shellock 1996; Knopp 1996; Keens 1996; Hall 1992; Brown 1993, Dempsey 2001; Dempsey 2001; Kim 2003; Karch 2004; Haik 2009). RF used in MRI induces voltages in conductive media such that electric currents are produced and power loss is by ohmic or induction heating. Assessment of the heating effects of conductive media during MRI on implants and devices have worked on the theory loops or circuits created by monitoring cables and the patient's skin amplify the circuit's inductance as well as, the current's intensity causing increases in the temperature of the cable which in turn, causes thermal injury. However, results suggest evidence to the contrary. Studies have found heating resulting from electromagnetic induction alone is insufficient to cause significant temperature increases and therefore thermal injury (Buchli 1988; Davis 1981; Chou 1997; Dempsey 2001). An alternative theory suggested by Demsey (2001) is, if a large enough loop is sited in or near resonance it can induce sufficient electrical energy to break down the capacitive component of the circuit resulting in burns. Furthermore, and as mentioned earlier in this section, a cable of the right length (i.e. resonant length) can act as an antennae and as such, is sensitive to the electric rather than the magnetic component of B_1 and may therefore cause thermal injury (Pictet 2002; Dempsey 2001). However, as with internal implants and devices this effect depends on a number of variables such as, orientation of the loop not just cable length. Under normal imaging conditions currents are induced in the human body but, if loops are created a concentrated conduction of current creating a high current density in the tissue under the electrode can occur causing thermal injury at the site.

4.3 Chapter summary

Despite its many advantages and overall paucity of accounts reporting harmful effects of MRI anxiety persists about the intrinsic hazards associated with human exposure to strong magnetic fields as well as the interactions between certain biomedical implants and magnetically induced forces generated during MRI. Particular concerns about the B_0 field and its large spatial gradient relate to latent physiological effects on human tissue, the potential for objects to become projectiles, the attractive/repulsive possibility of implants to the field causing movement, dislodgement or functional impedance *in vivo* and, the potential for thermal injuries to occur. Although the dB/dt fields are several times weaker than the B_0 field and are therefore unlikely to pose any significant risks to patients the sudden 'ramping up and down' of the field gradients may induce voltages and currents with sufficient intensity to heat body tissue and metallic implants and cause nerve and muscle stimulation. Research however, indicates these bio- and sensory effects appear to be transient and are more disconcerting for the patient rather than harmful. More serious are the thermal injuries caused by exposure to the B_1 field either as a result of induced currents and subsequent heat generation within tissue or, heating of implants and devices particularly those with the right resonant length and structure causing them to act as re-transmitting 'antenna'.

Although the potential collision hazard risks have been evaluated and are more readily understood little if anything is known about the *in vivo* movement of implants exposed to magnetically induced forces associated with MRI. Results from *ex vivo* assessment of the translation and rotational responses to the B_0 field have been applied and assumptions made about the possible behaviour of implants *in vivo* and the associated risk to the patient of injury or death. Research however suggests the retentive forces which preserve an implant may be weakened by the aging process and/or disease thus increasing the risk of unwanted implant movement or dislodgement. Moreover, these risks may be further increased as increasing numbers of higher field strength MR systems are used for clinical

diagnosis. In addition, the interaction between the B_0 field and metallic components in implants and the potential for implant malfunction as a consequence has not been investigated but only surmised. It is therefore essential we investigate more fully the interaction of biomedical implants with the B_0 field at both low and high field strengths to identify: movement of a retained implant, the direction and degree of displacement as well as the applied force and, assess whether functional valve performance is impeded by the change in flux as the implant moves through the B_0 field. The focus of this study aims to address the lack of information pertaining to the interaction between the B_0 field with prosthetic heart valves in an effort to evaluate the potential for movement or functional valve impedance resulting from induced translation and rotational forces. The next chapter describes the methods used to assess magnetic field interactions associated with the 1.5 T and the 3.0 T MR environments with restrained heart valve prostheses *ex vivo* and *in vitro*.

CHAPTER 5

Materials and Methods

5. Introduction

As previously mentioned increased longevity and advances in medical technology has led to a significant rise in both heart valve replacement surgery with a prosthetic valve and, the demand for ultra-fast MR techniques (see Chapters 2 & 4). Consequently, there is an increasing probability patients with prosthetic heart valves will become candidates for MRI procedures. However, despite existing research on the safe exposure of heart valve replacement patients to the MR environment there is a lack of empirical evidence relating to the impact of MR associated magnetically induced forces acting on the prosthesis as it moves through the B_0 field and its associated gradient magnetic field (ie. dB/dx). Researchers have for example, theorised magnetic fields induced by certain components within the valves themselves may cause retardation of the valve's leaflets/occluder and thus increase the risk of regurgitation and reduction in cardiac output. This chapter therefore describes a novel method for detecting and recording *ex vivo*, movement of 9 different heart valve prostheses exposed to the B_0 field and the functional valve performance *in vitro*. The chapter is divided into three sections. Part I discusses the Materials and Methodology of the preliminary investigations which provided the basis to the research described in the main body of this thesis. In addition, the section also discusses the limitations identified with regards to the preliminary research apparatus and methodology and what attempts were made to improve these.

Parts II and III describe the Materials and Methods used to address the question posed by this thesis and test the hypothesis. Part II describes the specially designed test apparatus fabricated to detect and record (a), the movement of a prosthetic heart valve placed statically within and, as it was continuously advanced through the B_0 field (b), the direction and magnitude of detected movements and (c), any changes in the dynamic profile of a valve prosthesis indicating an interaction of the valve's leaflet(s)/occluder with the induced magnetic field. Part III describes the methodology employed for mapping the magnetic gradient fields of the two MR environments, calibrating the

experimental test equipment for both the *ex vivo* and *in vitro* experiments and, conducting the baseline and experimental test measurements.

Part I

Preliminary investigations to measure the interaction between MR associated magnetically-induced forces and prosthetic heart valves

5.1. *Study I*

(a) Measurement of translational (displacement/deflection) force

As part of the process for evaluating the interaction of heart valve prostheses with MR associated magnetically induced forces, I conducted a number of preliminary investigations *ex vivo* at 1.5 T and 4.7 T using an adaption of the methodology first presented by New et al in 1983 and subsequently adopted as an international standard (ASTM FF1542-94; ASTM 2052-06 [48]). In each of the studies a prosthetic heart valve was attached to a piece of lightweight thread (0.3 m in length) and suspended from the centre of an MR compatible test rig (Figure 5.1). The rig was placed at the position within the MR system(s) where the spatial gradient of the magnetic field was determined to be at its maximum based on measurements recorded at intervals along the z-axis using a gauss meter and axial probe. The angle at which the heart valve prosthesis deflected from the vertical was determined by taking multiple measurements which were then averaged.

In the first of these three investigations, 32 different heart valves were tested at 1.5 T (Table 3). As Figure 5.1 shows the prosthetic heart valve was suspended from the 0º indicator of a 180º non-ferromagnetic protractor positioned on the right-hand side of a Perspex stand. The 0º indicator was orientated vertically. The test rig was positioned 35 cm inside the bore of a magnet (General Electric Medical Systems, Milwaukee, WI) and at an off-axis position where the highest spatial gradient of the magnetic field had been

[48] American Society of Materials Testing (ASTM) is the recognized body for developing standard test methods for assessing the safety of medical devices and implants in the MR environment.

determined. However, although the accuracy of the measuring device was calculated as ±0.5º, the confined space of the bore of the magnet made precise reading of the protractor difficult. Furthermore, during testing it was noted some valves were repulsed by the B_0 field and therefore deflected away from the protractor. Thus, because the protractor was not fully 360° full circle any measurement of deflection away from the iso-centre required the test rig to be partially dismantled, the protractor re-positioned and the valve remounted so measurements could be recorded. Since there was no indication, prior to exposing the valves to the magnetic field, which ones would be repulsed from B_0 field this interfered with the order of testing the valves and proved time very consuming. As a result of these shortcomings modifications were made to the test apparatus to improve the accuracy and ease of taking measurements and reduce the margin of error (Figure 5.2).

Figure 5.1 Diagram of test rig used to measure displacement forces @ 1.5 T

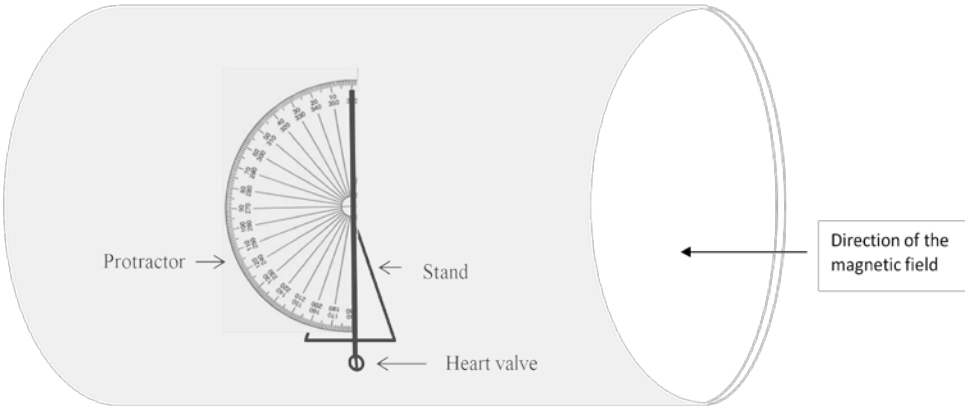

(b) Measurement of rotational (torque) force

Assessments of magnetic field interactions for rotational forces were conducted in conjunction with the evaluation of displacement forces. Although attempts to quantitatively measure torque by suspending an implant by a silk thread held in tension

by a lead weight and measuring the angle of deflection from the vertical had previously been reported (New 1983; Schueler 1999), the accuracy of these measurements was relatively low. Schueler (1999) for example, calculated the error rate to be approximately 20%. Furthermore, he argued only forces or torques acting perpendicular to gravity could be measured particularly if the implant did not have a well-defined axis of alignment. Thus, given the recognised problems associated with the accuracy of this test method as well as the lack of recognised published standard methods for measuring magnetically induced torque it was decided to assess torque force by applying a qualitative scale of measurement to un-weighted heart valve prostheses. In the first of the series of studies each prosthetic heart valve was suspended from a thin piece of thread held between the investigator's two fingers whilst positioned inside the bore of the magnet. The valve was rotated in 45º increments through 360º rotation to observe the effects of torque. A five point qualitative scale of torque previously described by Shellock was used to define the result (Shellock 1998; Table 4). However, during the execution of these measurements I identified a number of limitations of the method and scale of measurement which increased the potential for error. Firstly, the cramped conditions inside the bore of the magnet and the way in which the investigator was positioned made it difficult for the heart valve prosthesis to be held in a steady position for sufficient time to record any movement resulting from rotational forces. Moreover, use of the investigator to hold the heart valve meant it was very difficult to ensure movement of the valve resulted from interaction with magnetic forces and not accidental movement by the investigator. Thirdly, because all measurements were carried out and recorded by only one investigator there was an increased risk of possible human error. Furthermore, determining the speed at which any alignment towards the magnetic field was highly subjective and was thus open to future inter-investigator variation. In order to reduce this margin of error and improve the accuracy of the test equipment and methodology modifications to both the test apparatus and investigator methods were therefore made. The subsequent study is now described.

Table 3: List of heart valve prostheses evaluated for MR safety @ 1.5 T & 4.7 T

No	Prosthesis name	Group	Type	Site	Model	Size (cm)	Mass (g)	Materials	Field strength 1.5 T	Field strength 4.7 T
1	AorTech	Mechanical	Single leaflet	Aortic	3800	23	3.28	Pyrolitic carbon, Grade A-70 titanium, knitted Teflon	✓	
2	AorTech	Mechanical	Single leaflet	Mitral	4800	25	4.05	Pyrolitic carbon, Grade A-70 titanium, knitted Teflon	✓	
3	Aspire	Bioprosthesis	Animal tissue	Mitral	M55	27	4.94	Porcine tissue, Dacron, PTFE		✓
4	ATS Medical	Mechanical	Bileaflet	Mitral	500DM	29	5.30	Pyrolitic carbon, Teflon	✓	
5	ATS Medical	Mechanical	Bileaflet	Aortic	501DA	18	3.68	Pyrolitic carbon, Teflon	✓	
6	ATS Medical	Mechanical	Bileaflet	Aortic	500 FA	25	4.39	Pyrolitic carbon, titanium, Dacron, Teflon		✓
7	Beall	Mechanical	Caged disc	Mitral	Unknown	29	15.41	Pyrolitic carbon, pyrolitic carbon with Dacron	✓	✓
8	Biocor	Bioprosthesis	Animal tissue	Aortic	H3636	23	3.35	Porcine tissue, Celon, Dacron	✓	
9	Björk Shiley conical disc	Mechanical	Single leaflet	Mitral	MBUP	21	4.46	Pyrolitic carbon, chromium cobalt alloy, Teflon	✓	✓

10	Björk Shiley conical disc	Mechanical	Single leaflet	Mitral	MBRP	21	4.07	Pyrolitic carbon, chromium cobalt alloy with Teflon	✓	✓
11	Björk Shiley monostrut	Mechanical	Single leaflet	Mitral	MBUM	25	4.43	Pyrolitic carbon, chromium cobalt alloy, Teflon	✓	✓
12	Björk Shiley monostrut	Mechanical	Single leaflet	Aortic	ABMS	17	3.57	Pyrolitic carbon, chromium cobalt alloy with Teflon	✓	✓
13	Björk Shiley monostrut	Mechanical	Single leaflet	Mitral	MBRMS	23	5.75	Pyrolitic carbon, chromium cobalt alloy with Teflon	✓	✓
14	Björk Shiley monostrut	Mechanical	Single leaflet	Mitral	Unknown	33	7.54	Pyrolitic carbon, chromium cobalt alloy with Teflon		✓
15	Björk Shiley spherical disc	Mechanical	Single leaflet	Mitral	MBP	31	7.29	Pyrolitic carbon, chromium cobalt alloy with Teflon		✓
16	Björk Shiley 60º cc	Mechanical	Single leaflet	Aortic	ABC	27	4.06	Pyrolitic carbon, chromium cobalt alloy with Teflon		✓
17	Björk Shiley 60º cc valve graft	Mechanical	Single leaflet	Aortic	AGVCM	25	7.84	Pyrolitic carbon, chromium cobalt alloy with Teflon		✓
18	CarbonArt	Mechanical	Bileaflet valve graft	Aortic	AVP27/30	27	11.67	Pyrolitic carbon, T9614V, Carbofilm, pyrolitic carbon, polyacetal, PTFE, PTE		✓
19	Carbomedic standard	Mechanical	Bileaflet	Aortic	500	21	2.83	Pyrolitic carbon, titanium, Dacron, biolite		✓

20	Carbomedics supra-annular (Top Hat)	Mechanical	Bileaflet	Aortic	S500	23	3.23	Pyrolitic carbon, titanium, Dacron, biolite		✓
21	Carbomedic standard	Mechanical	Bileaflet	Mitral	700	31	6.25	Pyrolitic carbon, titanium, Dacron, biolite		✓
22	Carbomedics SuMit	Mechanical	Bileaflet	Mitral	S700	29	5.88	Pyrolitic carbon, titanium, Dacron, biolite		✓
23	Carbomedics valve graft	Mechanical	Bileaflet valve graft	Aortic	AP500	34	-	Graphite, pyrolitic carbon, titanium, Dacron, biolite		✓
24	Carpentier Edwards	Bioprosthesis	Animal tissue	Aortic	2625	31	6.63	Porcine tissue, Elgiloy, Teflon		✓
25	Carpentier Edwards	Bioprosthesis	Animal tissue	Mitral	6900	33	6.31	Bovine pericardium, Elgiloy, PTE cloth, polyester, silicone		✓
26	Carpentier Edwards supra-annular	Bioprosthesis	Animal tissue	Mitral	6650	31	7.42	Porcine tissue, Elgiloy, PTE cloth, silicone rubber, PTFE cloth		✓
27	Contegra	Bioprosthesis	Animal tissue	Pulmonary	200	18	3.94	Bovine pericardium, polypropylene		✓
28	Duromedics [49]	Mechanical	Bileaflet	Aortic	3160	27	7.97	Pyrolitic carbon, satellite, Dacron, Biolite		✓
29	Duromedics	Mechanical	Bileaflet	Mitral	9120	29	5.61	Pyrolitic carbon, satellite, Dacron, Biolite		✓
30	Durafic	Human	Human tissue	Aortic	AD	33	2.97	Human tissue + unknown stent/ring materials	✓	✓

[49] This valve is also referred to as the Edwards Tekna valve

31	Durafic	Human	Human tissue	Mitral	MD	23	4.08	Human tissue + unknown stent/ring materials	✓		✓
32	Elan	Bioprosthesis	Animal tissue	Aortic	AV33/P	22	3.49	Porcine xenograft, porcine pericardium.			✓
33	Elan valve graft	Bioprosthesis	Animal tissue	Aortic	RE80/P	23	6.23	Porcine xenograft, porcine pericardium			✓
34	Freedom	Bioprosthesis	Animal tissue	Aortic	PF	25	2.59	Bovine pericardium, Carbofilm			✓
35	Freestyle	Bioprosthesis	Animal tissue	Aortic	995MS	27	8.39	Porcine xenograft, polyester			✓
36	Hancock pericardial	Bioprosthesis	Animal tissue	Mitral	T410	25	4.99	Bovine tissue, Haynes alloy, polyester	✓		✓
37	Hancock Modified Orifice	Bioprosthesis	Animal tissue	Aortic	250	21	4.19	Porcine tissue, Dacron, Hayes alloy #25, polypropylene, Stellite, silicone rubber			✓
38	Hancock II Modified Orifice	Bioprosthesis	Animal tissue	Aortic	T505	25	5.23	Porcine tissue, acetal homopolymer, polyester, Haynes alloy #25			✓
39	Intact	Bioprosthesis	Animal tissue	Aortic	A805	19	3.18	Porcine tissue, Acetyl copolymer, Dacron	✓		✓
40	Intact	Bioprosthesis	Animal tissue	Mitral	M705	25	5.94	Porcine tissue, Acetyl copolymer, Dacron	✓		✓
41	Ionescu Shiley	Bioprosthesis	Animal tissue	Aortic	ISA	23	5.62	Bovine pericardium, titanium, Dacron, Teflon			✓

42	Jyros	Mechanical	Bileaflet	Mitral	J1M	30	7.22	Pyrolitic carbon, boron carbide, carbon	✓	✓
43	Jyros	Mechanical	Bileaflet	Aortic	J1A	26	5.29	Pyrolitic carbon, boron carbide, carbon	✓	✓
44	Labcor Synergy	Bioprosthesis	Animal tissue	Aortic	TLPB-A	21	3.58	Porcine pericardium, composite co-polymer, silicone		✓
45	Labcor Synergy	Bioprosthesis	Animal tissue	Mitral	TLPB-M	25	5.12	Porcine pericardium, composite co-polymer, silicone		✓
46	Liotta	Bioprosthesis	Animal tissue	Aortic	MA783	23	4.94	Porcine tissue, Acetyl resin, Delrin, Dacron	✓	✓
47	Medtronic	Mechanical	Single leaflet	Aortic	A7700	23	2.96	Pyrolitic carbon, titanium, Teflon		✓
48	Medtronic	Mechanical	Single leaflet	Mitral	M7700	23	4.19	Pyrolitic carbon, titanium, Teflon		✓
49	Medtronic	Mechanical	Single leaflet	Mitral	MHK	29	5.74	Pyrolitic carbon, titanium, Teflon		✓
50	Mira	Mechanical	Bileaflet	Mitral	9600	27	7.21	Pyrolitic carbon, Carbofilm, titanium, polyester		✓
51	Mitroflow	Bioprosthesis	Animal tissue	Aortic	11A	25	3.59	Bovine tissue, Delrin, Dacron, silicone	✓	✓
52	Mitroflow	Bioprosthesis	Animal tissue	Mitral	11M	29	4.19	Bovine tissue, Delrin, Dacron, silicone	✓	

53	Mitroflow	Bioprosthesis	Animal tissue	Aortic	14A	25	3.23	Bovine tissue, Delrin, Dacron, silicone	✓	
54	Mitroflow	Bioprosthesis	Animal tissue	Aortic	141	25	3.23	Bovine pericardium, Delrin 500, Dacron, silicone		✓
55	Mitroflow	Bioprosthesis	Animal tissue	Mitral	121	29	4.19	Bovine pericardium, Delrin 500, Dacron, silicone		✓
56	Mitroflow Synergy	Bioprosthesis	Animal tissue	Aortic	12A	21	3.17	Bovine pericardium, acetal homopolymer, polyester, silicone		✓
57	MØre	Bioprosthesis	Animal tissue	Aortic	PN	19	2.25	Bovine pericardium, polyacetal resin, PET, Carbofilm		✓
58	Mosaic	Bioprosthesis	Animal tissue	Aortic	305	29	6.23	Porcine tissue, acetal homopolymer, polyester		✓
59	Omniscience	Mechanical	Single leaflet	Mitral	2522	25	4.35	Pyrolitic carbon, titanium, Dacron		✓
60	On-X	Mechanical	Bileaflet	Aortic	ONXA	19	3.21	On-X ™, pyrolitic carbon, PTFE		✓
61	On-X	Mechanical	Bileaflet	Mitral	ONXM	31-33	7.62	On-X ™, pyrolitic carbon, PTFE		✓
62	Smelloff Cutter	Mechanical	Caged ball	Aortic	SA	21	9.74	Silicone rubber, titanium, polyester, Teflon	✓	✓
63	Sorin Allcarbon	Mechanical	Bileaflet	Mitral	MTR-AS	29	6.00	Pyrolitic carbon, Teflon, Carbofilm	✓	
64	Sorin pericabon (stented)	Bioprosthesis	Animal tissue	Mitral	SM	33	7.73	Bovine tissue, polyacetal resin, tantalum, PET Carbofilm	✓	✓

65	St Jude Masters	Mechanical	Bileaflet	Aortic	AJ -501	25	4.22	Pyrolitic carbon, Dacron	✓	
66	St Jude Standard	Mechanical	Bileaflet	Aortic	AEC	27	2.60	Pyrolitic carbon, Dacron		✓
67	St Jude Standard	Mechanical	Bileaflet	Mitral	MEC	25	4.23	Pyrolitic carbon, Dacron		
68	St Jude Regent	Mechanical	Bileaflet	Aortic	AGN-751	17	1.23	Pyrolitic carbon, Dacron	✓	
69	St Jude Regent	Mechanical	Bileaflet	Aortic	AGN-751	25	4.23	Pyrolitic carbon, MP35N, Dacron		✓
70	St Jude valve graft	Mechanical	Bileaflet valve graft	Aortic	CAVG	27	5.55	Pyrolitic carbon, Meadox, Hemasheild, velour polyester		✓
71	Starr Edwards	Mechanical	Caged ball	Mitral	6120	32	11.78	Stellite alloy #21, barium sulphate, silicone rubber, Teflon, polypropylene cloth	✓	✓
72	Starr Edwards	Mechanical	Caged ball	Mitral	6320	32	11.93	Stellite alloy #21, metal studs, polypropylene, Teflon	✓	✓
73	Starr Edwards	Mechanical	Caged disc	Mitral	6520	26	7.46	Polyethylene, titanium, Stellite alloy #21, Teflon, polypropylene		✓
74	Tascon	Bioprosthesis	Animal tissue	Aortic	Unknown	23	8.81	Porcine tissue, Elgiloy, polyester	✓	✓
75	Toronto stentless	Bioprosthesis	Animal tissue	Aortic	SPA-101	25	4.32	Porcine tissue	✓	
76	Toronto root	Bioprosthesis	Animal tissue	Aortic	Root	27	8.93	Porcine, BiLinx ™ AC, polyester		✓
77	Ultracor	Mechanical	Single leaflet	Aortic	3800	23	3.28	Pyrolitic carbon, grade A-70 titanium, Teflon		✓

78	Ultracor	Mechanical	Single leaflet	Mitral	4800	25	4.05	Pyrolitic carbon, grade A-70 titanium, Teflon			✓
79	Wessex	Bioprosthesis	Animal tissue	Mitral	WAV10	31	7.21	Porcine tissue, Acetal polymer, silicone rubber, Teflon	✓		✓
80	Wessex	Bioprosthesis	Animal tissue	Aortic	WMV20	25	5.53	Porcine tissue, Acetal polymer, silicone rubber, Teflon	✓		✓
81	Xenofic	Bioprosthesis	Animal tissue	Aortic	AP80	23	6.67	Bovine tissue, Teflon, stainless steel	✓		✓

Valve manufacturers (valve numbers): Alliance Medical, UK (11-14); Aortech Ltd, UK (1-2, 78-79); ATS Medical Inc, USA (4-6); Axion Medical Ltd, USA (42-43); Bolton Medical, UK (60-61); Coratomic Inc. USA (7); Cutter Laboratories; USA (62); Edwards Lifesciences , USA (24-26, 28-29, 50,71-73); Heart Institute, Sao Paolo Brazil (74); Implantes Medicos, Spain (81); Koehler Chemie, UK (3, 32-33); Medical Incorporated Inc, USA (59); Medtronic Ltd, USA (27, 35-40, 47-49, 58); Mitroflow International Inc, USA (51-53); Pfizer Inc, USA (16-17); Shiley Inc, USA (9-10, 15, 41); St Jude Medical Ltd, UK (8, 6, 65-70, 75-76); Sorin Biomedica Cardio SpA, Italy (18, 34, 44-45, 54-57, 63-64 79-81); Sulzer Carbomedics, UK (19-23).

Table 4 Qualitative scale of measurement for rotational forces

Measurement scale	Definition	Description
0	No torque	
+1	Mild torque	The device changed orientation slightly but did not align to the magnetic field.
+2	Moderate torque	The device aligned gradually to the magnetic field.
+3	Strong torque	The device showed rapid and forceful alignment to the magnetic field.
+4	Very strong torque	The device showed very rapid and very forceful alignment to the magnetic field.

5.2 Study II

(a) Measurement of translational (displacement/deflection) force

In this second investigation 81 heart valve prostheses were assessed for interactions with MR induced magnetic forces associated with a 4.7 T MR system (Table 3). The basic methodology remained the same as before with regards to plotting the spatial gradient of the magnetic field and positioning the valve on the test rig. However, modifications were made to the test apparatus and included, constructing a T-shaped wooden stand and attaching a rectangular glass plate which, in order to avoid parallax error had been etched with a 360º circular protractor for measuring the angle of deflection from the vertical regardless of the direction of the displacement (ie. attractive/repulsive). In addition, a mirror was positioned at 45º to the test rig to allow the investigators to accurately read and record the angle of deflection without the need to be positioned inside the bore of the magnet (Figure 5.2). Furthermore, two persons were employed to independently read and record the angle of deflection of each heart valve. Although

changes in the design of the equipment proved successful in reducing the time required to perform each measurement and made reading and recording the angle of displacement of the prosthesis in either direction along the z-axis easier, there was only a small reduction in the recorded rate of error (ie. accuracy was ±0.2º). Nonetheless, this degree of error was considered acceptable.

Figure 5.2 Diagram of test rig used to measure displacement forces @ 4.7 T

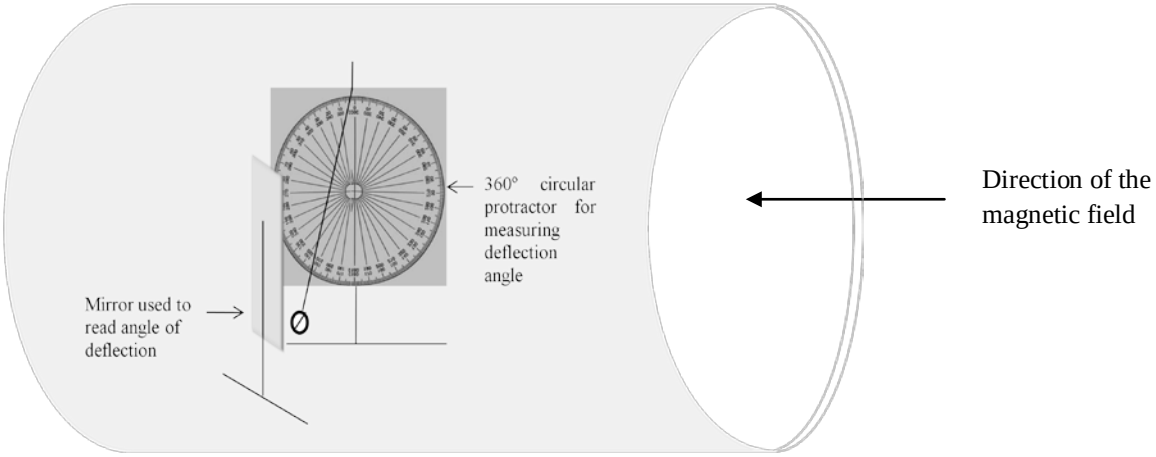

(b) Measurement of rotational (torque) force

Given the limitations identified in the first investigation to assess rotational forces an attempt was made in this study to simplify the methodology and scale of measurement in order to improve accuracy and repeatability. The method employed required each heart valve to be vertically suspended from the test rig (see above assessment of displacement force) either parallel (i.e. 180º) or perpendicular (i.e. 90º) to the long axis of the magnet's bore from a lightweight thread before being placed in the centre of the MR system (Magnex, Oxford). A three point qualitative scale of measurement which aimed to assess occurrence and degree of re-alignment with the B_0 field was then applied (Table 5). However, despite these modifications limitations of this measurement scale

were acknowledged. Although a concise and simpler scale of measurement it was nonetheless still a subjective measurement tool and failed to provide quantitative data for analysis and the calculation of actual applied force. As a result the type of analysis which could be performed was limited.

Table 5 Revised qualitative scale of measurement for rotational forces

Measurement scale	Definition
0	Zero torque
+1	Alignment or rotation of >0º to 45º from the starting position
+2	Alignment or rotation of >45º to 90º from the starting position

The methodology used for these early investigations limited the type of analysis which could be performed. In the first investigation a descriptive analysis of the translational and rotational forces displayed by the prostheses was possible (see Chapter 6, Part I). However, no further analysis was undertaken with regards to the assessment of magnetic field induced interactions. In the subsequent investigation a more detailed analysis of the translation force (F_{trans}) in the z-direction -was given by:

Equation [2]: $F_m = mg \tan\alpha$

Where m is the mass of the prosthesis, g is the gravitational constant (ie. 9.81 meters/second^2 (m/s^2)) and tan α is the tangential angulation of the thread from the vertical. –If the value for α is less than 45° F_m is found to be less than the gravitational force acting upon the device and therefore the patient is not considered to be at risk of harmful injury (ASTM 2006). The sense of deflection was dependent upon whether the

prosthesis was diamagnetic (negative susceptibility (χ)) or paramagnetic (positive χ). In addition, the mechanical forces of the beating heart (M_F) were also calculated for each prosthetic valve taking into account the valve's size (ie. annulus diameter (mm), weight (g) and anatomical position (ie. aortic or mitral) using mean aortic pressure and peak left ventricular pressure accordingly and calculated using the following equation:

Equation [3]: $M_F = 1.047 \times 10^{-4} \times P \times d^2$

where 1.047×10^{-4} is the constant, P is pressure measured in mmHg and d is the diameter of the valve ring (mm).

5.3 Limitations of these early investigations

Despite the modifications to the test apparatus and methodology and, although analysis of the results allowed calculation of the actual applied magnetic displacement force on the prosthetic heart valve in comparison to the mechanical forces of the beating heart (Table 7 Chapter 6) a number of limitations remained. Firstly, all investigations conducted were *ex vivo* and therefore did not take into account the *in vivo* conditions including the correct anatomical position and orientation of the heart valve. The test apparatus did not provide any reaction torque thus the valve was free to rotate and therefore no account was made for the retentive and counteractive forces such as, endothelialized tissue, sutures, haemodynamic flow etc. keeping it in place. All measurements recorded were one dimensional and only taken at static positions along the z-axis. Thus, any movement of the valve in any plane as the patient was moved in and out of the magnet was therefore missed. Finally, the use of a qualitative scale of measurement for magnetically induced torque force was subject to a variable degree of error. Nonetheless, as previously mentioned these and other investigations have provided us with some knowledge of the magnitude of the applied magnetic displacement force acting on a prosthetic heart valve placed statically within the B_0 and dB/dx field of a 1.5 T and 4.7 T MR environment. As a result, it may therefore be

possible to assess the risks of movement or dislodgement of the prosthesis *in vivo* within these environments as long as the patient remains motionless. However, the lack of empirical evidence means we do not know whether these risks or the risk of valve impedance are increased as the valve moves through the magnetic field and whether these are sufficient to pose a significant risk of harm to the patient. Nor do we know whether any movement of the valve is strictly one dimensional or whether it is likely to exhibit movement along another plane. Finally, the lack of empirical quantitative data on the impact of rotational forces on a prosthetic heart valve placed within the MR environment has made it impossible to assess the risks of movement or dislodgement due to torque force which, as Chapter 4 suggests, is potentially more hazardous to the patient. As a result of the limitations identified in these and previous studies the next part of research sought to design a novel method for detecting and measuring magnetically induced forces on prosthetic heart valves exposed to the B_0 field within the MR environment.

The questions raised therefore are:

(a) What is the direction and magnitude of any prosthesis movement within the MR environment as it advances through the B_0 field ?

(b) Are these forces sufficient to cause harmful movement or dislodgement of the prosthesis or impede valve function ?

(c) Are MR associated magnetically induced forces sufficient to pose a significant risk of harm to a prosthetic heart valve implant patient ?

5.4 Study aims & objectives

This study seeks address these questions and has thus identified the following as the aims and objectives of this investigation.

5.4.1 Aims

- design an MR compatible device with the sensitivity and capacity to:
    - detect and record, *ex vivo*, any movement of a prosthetic heart valve placed statically within and, as it is moved continuously through the B_0 field associated with a 1.5 T and a 3.0 T MR environment,
    - identify where in the B_0 field prosthesis movement occurred,
    - detect and record any changes in the hydro-dynamic flow of the prosthesis,
- evaluate the device's ability to achieve the above.

5.4.2 Objectives:

- compare and review baseline profiles for the apparatus at 1.5 T and 3.0 T with prosthesis profiles for static and dynamic placement to determine:
    - prosthesis movement within the MR environments,
    - location within the B_0 field prosthesis movement occurred,
    - differences in hydro-dynamic flow and thus functional valve performance.

5.5 Hypothesis:

Thus the hypothesis of this investigation is:

H_0: This novel device will lack the sensitivity and capacity to detect and record the occurrence, frequency, direction and magnitude of prosthetic valve movement and, valve function as the valve moves through the dB/dx and B_0 field associated within the MR environment;

and the alternative hypothesis states:

H_1: This novel device will have the sensitivity and capacity to detect and record the occurrence, frequency, direction and magnitude of prosthetic valve movement and, valve function as the valve moves through the dB/dx and B_0 field associated within the MR environment.

The next section of this Chapter describes the Materials and Methodology used to address the above questions and achieve the aims and objectives of this investigation. The first part, Part II, describes the materials used which are common to both and specific to the *ex vivo* and *in vitro* tests. Part III describes the methodology employed and begins with a description of the methods for calibrating the test apparatus and plotting the dB/dx and B_0 fields for the 1.5 T and the 3.0 T MR environments. This is followed by a description of the methodology used for each investigation to identify *ex vivo* any movement of the prosthetic heart valve as it travels through dB/dx and B_0 field and any interaction *in vitro* of the magnetic field with the valve leaflets/occluder thus impeding valve function.

Part II

Experimental investigations

Materials

5.6 Introduction

Part II of the Materials and Methods chapter begins with a description of the components of the test apparatus common to both investigations and includes the different heart valve prostheses, the Heart Valve Motion Analysis System and the MR systems. A description of the apparatus employed for each type of investigation i.e. *ex vivo* and *in vitro* concludes this section of the Materials segment.

5.6.1 Heart valve prostheses:

Nine different models of prosthetic heart valves implanted in the United Kingdom between 1974 and 2005 (unpublished data; UK Heart Valve Registry data 1986 – 2007) were evaluated for interactions with the magnetic fields at 1.5 Tesla (T) and 3.0 T (Table 6, Figure 5.3). There were six mechanical valves and three bioprostheses. Three valves within the mechanical group were caged housing design valves. These were the Starr Edwards caged-ball valve (x2) and Starr Edwards caged-disc valve (x1). Two valves, the Björk Shiley 60° convexo-concave valve and Medtronic Hall valve were tilting disc/single-leaflet valves and one valve, the Edwards Tekna valve was bileaflet. The remaining three valves were bioprostheses; the Carpentier Edwards supra-annular porcine valve, Hancock Modified Orifice II porcine valve and the Carpentier Edwards pericardial valve. Five out of nine valves were aortic and four were mitral with valve sizes ranging from 26 mm to 32 mm. Table 6 provides full information on the type, make, model, site and size of heart valve prostheses and the materials used in their construction.

Table 6 List of heart valves evaluated for safety @ 1.5 T and 3.0 T

No	Valve name	Valve type	Site	Model	Size (mm)	Housing	Sewing ring
1	Björk Shiley 60° Convexo-Concave (cc) valve	Mechanical tilting disc	Aortic	ABC	27	Pyrolitic carbon, chromium cobalt alloy	Teflon
2	Carpentier Edwards Supra-Annular valve	Tissue porcine xenograft	Aortic	2625	29	Flexible Elgiloy ® (cobalt nickel alloy)	Knitted porous Teflon
3	Carpentier Edwards Pericardial valve	Tissue bovine pericardial	Aortic	2900	29	Flexible Elgiloy ® (cobalt nickel alloy)	Polyester, silicone
4	Edwards Tekna valve	Mechanical bileaflet	Mitral	9210	29	Pyrolitic carbon, stellite	Dacron ® coated with Biolite
5	Hancock Modified Orifice II valve	Tissue porcine xenograft	Aortic	T510	31	Acetal homopolymer, polyester	Haynes #25 alloy, polyester
6	Medtronic Hall valve	Mechanical tilting disc	Aortic	A7700	31	Pyrolitic carbon on graphite substrate, titanium	Knitted Teflon ®
7	Starr Edwards caged-ball valve	Mechanical caged ball (silastic rubber)	Mitral	6120	32	Silicone rubber, barium sulphate, stellite alloy #21	Porous knitted Teflon + polypropylene cloth
8	Starr Edwards caged-ball valve	Mechanical caged ball (metal ball)	Mitral	6320	32	Stellite alloy #21, cloth interrupted with metal studs, polypropylene over Teflon	Knitted Teflon + polypropylene
9	Starr Edwards caged-disc valve	Mechanical caged disc	Mitral	6520	26	Polyethylene & titanium, stellite alloy #21	Knitted Teflon + polypropylene

Figure 5.3 Heart valve prostheses

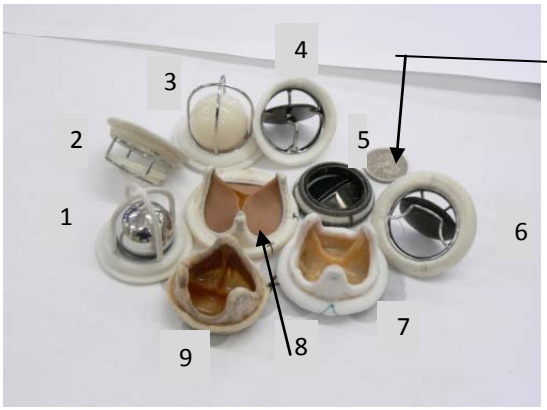

Key:

5 pence piece coin

[1] Starr Edwards metal caged-ball valve
[2] Starr Edwards caged-disc valve
[3] Starr Edwards silastic caged-ball valve
[4] Medtronic Hall valve
[5] Edwards Tekna valve
[6] Björk Shiley 60° cc valve
[7] Hancock Modified Orifice II valve
[8]Carpentier Edwards Supra-annular porcine valve
[9] Carpentier Edwards Pericardial valve

Manufacturers listed by valve numbers:
[1-3,5,8-9] Edwards Lifesciences (USA), [4,7] Medtronic Limited (USA), [6] Shiley Incorporated (USA)

5.6.2 Heart Valve Motion Analysis System (HVMAS)

A motion analysis system (Heart Valve Motion Analysis System (HVMAS)) was specially designed to detect and record any movement *ex vivo* of a prosthetic heart valve and leaflet performance in an *in vitro* test (ie. dynamic test) during exposure to a 1.5 T and a 3.0 T MR environment (see below). The HVMAS comprised four main components: a valve holder (*ex vivo* test) or valve chamber (*in vitro* test), piston pump (*in vitro* test), a Whetstone full bridge strain gauge indicator and recorder (Vishay Precision Group, Pennsylvania, USA) and a data acquisition system (Biopac Systems Inc. Goleta, USA) held on laptop computer (Figures 5.5 – 5.7). In addition, a jointed clear plastic stand was designed to hold the valve holder during the *ex vivo* test (Figures 5.5 - 5.6). A pump was used to regulate stroke volume and flow during the *in vitro* test and a clear isolation chamber was used to house the valve compartment and ensure safety and protection of the MR system (Figure 5.10). All components of the test equipment

exposed to the MR systems had been specifically designed to be MR compatible and did not contain any ferromagnetic materials. However, some components such as the piston pump, strain gauge recorder and laptop computer contained ferromagnetic materials which could not be substituted. These components of the test apparatus were therefore sited in the adjoining control room.

5.6.3 Magnetic Resonance Imaging Systems

Magnetically induced field interactions were assessed at two different field strengths using a 1.5 T Signa NVi (GE Milwaukee USA) and a 3.0 T Signa HD (GE Milwaukee USA) MR system. Both imaging systems were superconducting actively shielded short bore scanners and were housed at the Institute of Neurological Sciences, Southern General Hospital Glasgow (Figure 5.4). These two fields strengths were chosen to reflect current MR systems common in clinical use.

Figure 5.4 Signa GE magnetic resonance imaging systems

Signa NVi 1.5 T MR system

Signa HD 3.0 T MR system

5.6.4 Ex vivo test apparatus

Figure 5.5 shows the equipment used for the *ex vivo* test. Comparisons of this apparatus with the apparatus used in previous investigations (Figures 5.1 - 5.2) shows a number of significant differences are apparent. Firstly, unlike previous methodologies including attempts to quantitatively measure magnetically induced torque (ASTM F2213-06; D'Avenio 2007), the valve did not have unlimited freedom of movement but was retained in place by the valve holder which was analogous to the retentive structures *in vivo* (see below for method of valve insertion). Secondly, the valve could be angled and raised to the height of the *in vivo* position (Figures 5.5 - 5.6) and finally, the apparatus was designed to capture and record movement in more than one plane as the valve moved continuously through the magnetic field (Figures 5.7 - 5.8).

The *ex vivo* test apparatus comprised a clear plastic stand with valve holder designed to fit valves with a diameter between 26 mm and 32 mm, the strain gauge recorder and laptop computer (Figure 5.5). As previously mentioned the stand was jointed (ie. two joints) to allow positioning to the correct height and orientation of the heart in the chest cavity. The valve holder was designed to fit into the aperture in the upper plate of the stand which could be separated from the lower half by unscrewing two plastic screws thus allowing the valve holder to be removed (Figure 5.6). Interaction of the valve with magnetically induced forces was captured by four strain gauges mounted on cantilevers attached to the inside surface of the valve holder and positioned at 90° intervals along the z-axis (Figure 5.7). Early models of the valve holder attempted to use strain gauges bonded to the inner surface with the connector cables passing through small apertures in the walls of the holder (Figure 5.9). However, this design experienced continuing problems with the long-term attachment of the strain gauges to its smooth inner surface. Although the problem was resolved by scoring the inner surface of the valve holder to provide a key this significantly reduced the strain gauges' sensitivity and ability to demonstrate tension and compression. Thus, remodelling of the valve holder was

undertaken and resulted in the strain gauges being mounted on cantilevers. This improved sensitivity to tensile and compressive forces and increased accuracy in capturing movement in any one of the two axes across three planes (Figure 5.8). Revisions were also made to the way the connector cables fed back to the strain gauge recorder.

Prior to executing the study phase, pre-testing of the apparatus was undertaken to confirm MRI safety and compatibility as well as sensitivity. The equipment was exposed to a 1.5 T actively shielded MR system ((Philips Intera, Best, The Netherlands) at the Hammersmith Hospital, London. The results of the apparatus tests confirmed the MR system did not exert any influence on the strain gauge assembly. Furthermore, when pressure was exerted on the strain gauges within the B_0 field using a hand held puffer there was a measured output but the profile remained unchanged inside and outside the field.

Figure 5.5 Schematic of Heart Valve Motion Analysis System (HVMAS)

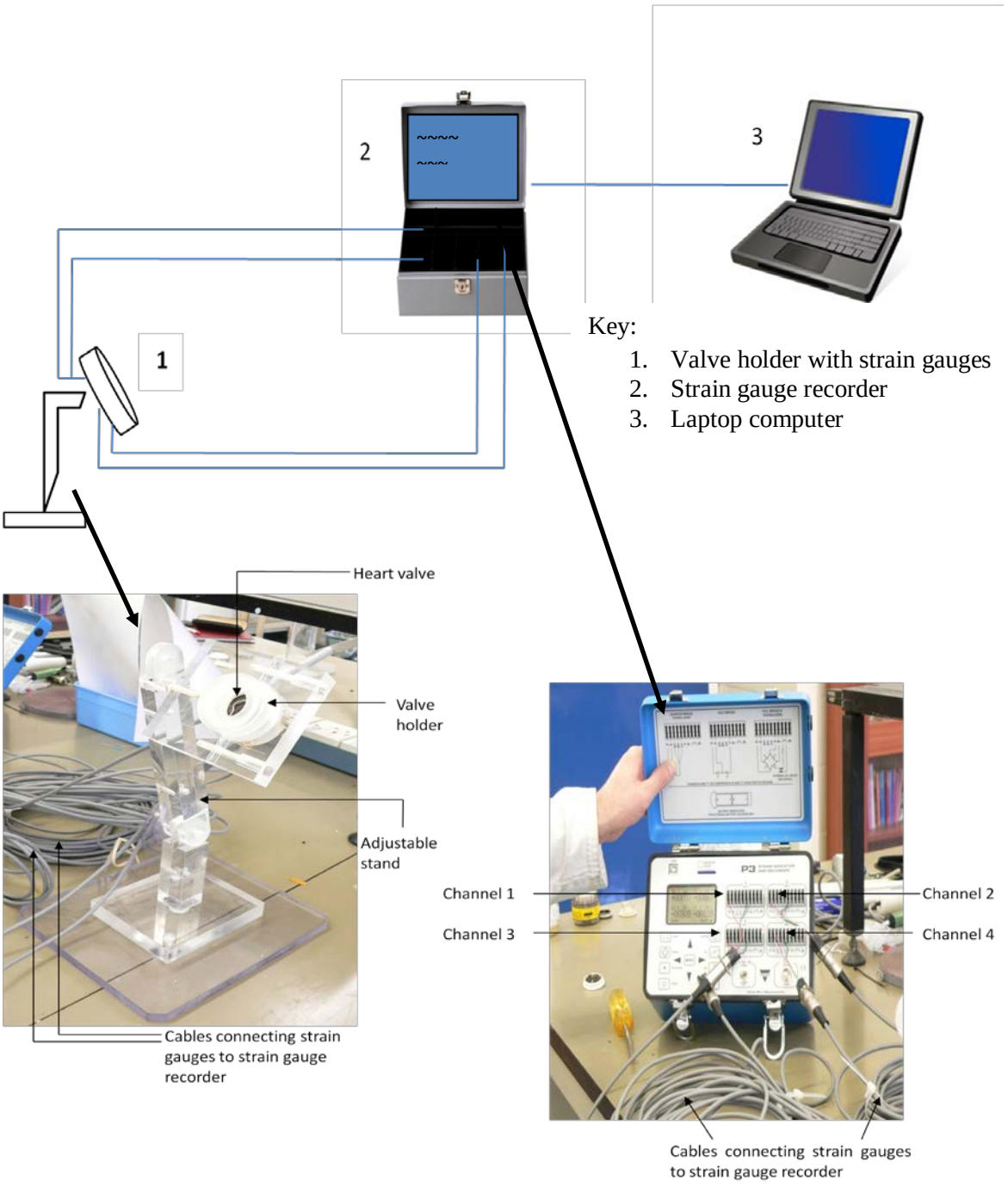

Figure 5.6 Valve holder positioned within valve holder plate

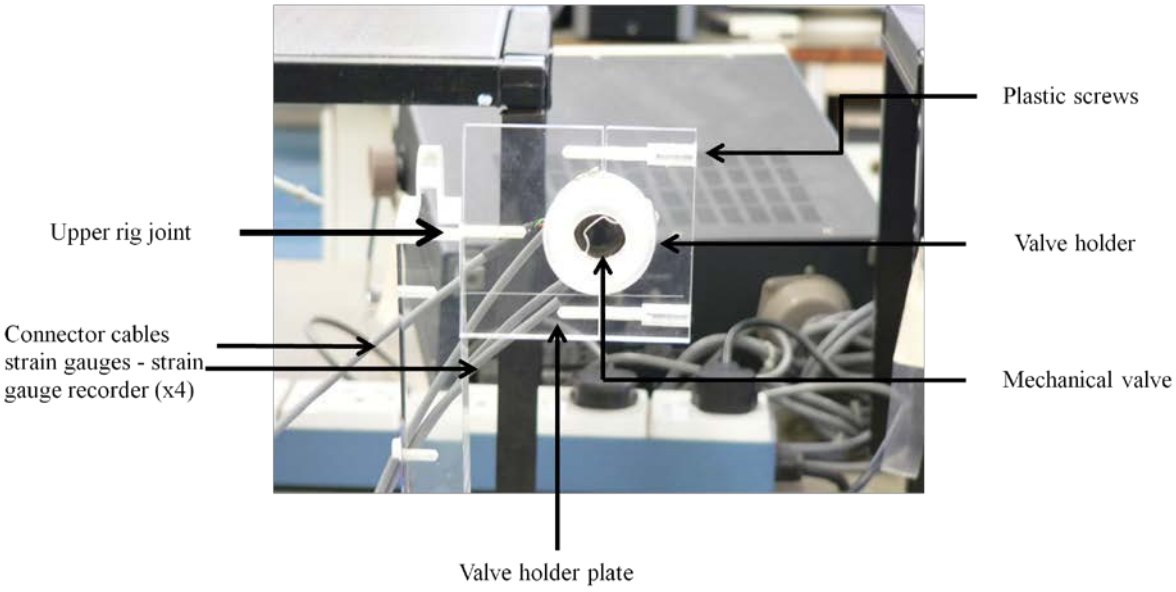

Figure 5.7: Valve holder with strain gauges positioned on the z-M and x-y axes

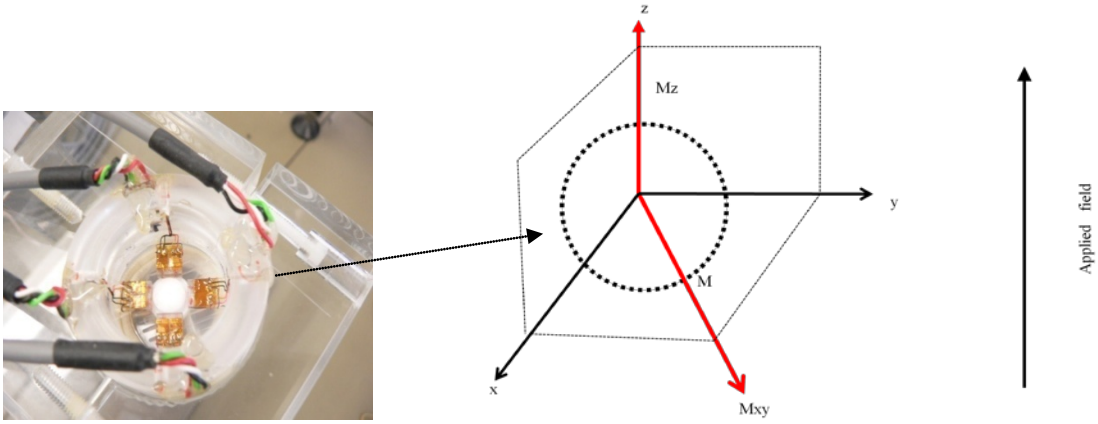

Figure 5.8: Directional movement of the strain gauges

(a)

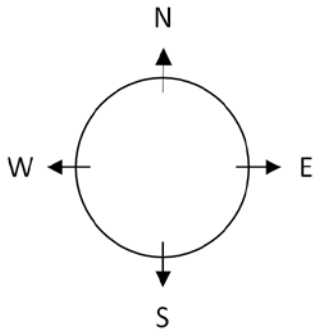

The arrows show the positive direction for each of the N/S/E/W strain axes.

(b)

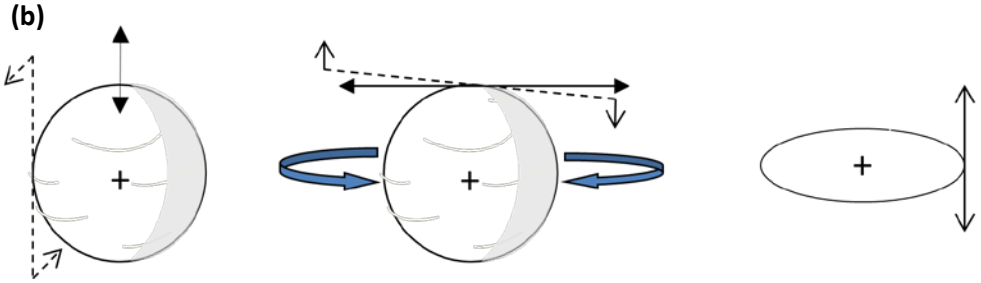

① Valve ring moves up or down the page in plane of the ring or tilts along the N-S axis.

② Valve ring moves left or right, rotates around the centre or tilts along the W-E

③ Valve ring pivots about an axis in the plane of the ring so the edge moves up or down.

Figure 5.9 Early model of the valve holder

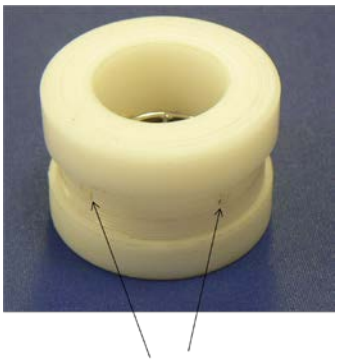

Openings to allow the cables connecting the strain gauges to the strain gauge recorder

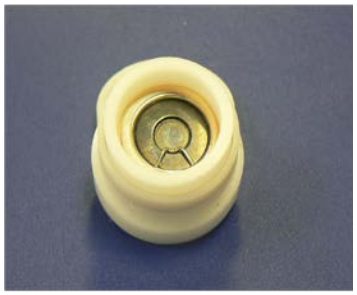

A view from overhead showing the valve placed inside the bottom half of the valve holder

5.6.5 In vitro test apparatus

The *in vitro* test rig was designed to measure any change in the fluid profile as a result of interaction of the valve's leaflets/occluder with the MRI induced magnetic forces. As Figure 5.10 shows the pump comprises a motor, gearbox and speed regulator. The motor drives the piston and is connected to the drive wheel which is perforated with a series of small radii used to regulate frequency and stroke volume. Certain other components of the *in vitro* test apparatus are also common to the *ex vivo* test (see above) and are therefore not described again. The hydraulic system used for the in *vitro* test comprised a simple circuit originating in a reservoir which supplied atrial filling and consisted of a simple piston pump, valve chamber with inlet and outlet tubes and isolation chamber. Four different sized valve ring holders were designed to fit inside the mid section of the valve chamber and hold the valve securely in place during fluid flow to prevent the valve ring from moving (Figure 5.11a). Each ring holder comprised an applicator and male and female ring (Figure 5.11b). The applicator was used to separate the male from the female ring so the heart valve could be placed between the two (Figure 5.11c). It was then used to couple the two rings together and secure the valve in place (Figures 5.11d-f). The valve chamber was secured in a wooden stand, the top half of which could be loosened to allow the chamber to be removed if required (Figure 5.12). The two parts of the chamber (inflow/outflow) could be separated and reassembled at the mid-section by unscrewing the chambers (Figure 5.12b-c) thus allowing the valve ring holder to be inserted (Figures 5.12d-f). In addition, the anterior side of each chamber housed a socket for the manometer lines to connect the valve chamber and electro-dynaphramatic pressure transducers (Figure 5.12f; see below). Finally and as previously mentioned this hydro-pneumatic test apparatus was contained within an isolation chamber to safe-guard against leakage and/or spillage during the dynamic flow and thus prevent damage to the MR system (Figure 5.10).

The major consideration in the design of the pump was simplicity and it was accepted at the start some components used in its construction would not be MR compatible. Therefore this piece of the hydro-pneumatic test apparatus remained outside the imaging suite. Other components also had to remain outside the MR suite because of the potential to cause damage to the MR system. Concerns about the fluid reservoir for example and its potential to cause water damage within the MR suite meant it too was located within the nearby control room. However, this created a number of complications. Firstly, a 10 m length of plastic tubing was required to carry water from the fluid filled reservoir to the valve chamber. Consequently concerns were raised about the length of the tubing and the potential to cause a significant drop in fluid pressure as a result of sheer stresses acting against tubing walls and the distance between the fluid reservoir and the valve chamber. These problems were overcome by using high shore hardness PVC tubing to reduce the potential for dissipation of energy resulting from friction of the fluid against the tube's walls and, by locating the fluid reservoir at a height above the valve chamber thus ensuring a consistent fluid pressure (Figure 5.10). In addition, concerns about the potential for induction of electrical currents caused by magnetic flux in the cable (please refer to Chapter 4) connecting the strain gauge apparatus with the strain gauges mounted in the valve holder were also raised. It was considered such inductions may be capable of causing irreparable damage to the sensory apparatus. However, time-varying magnetic field gradients nor RF were being employed thus it was thought it highly improbable currents would therefore be induced. Nonetheless, as an added precaution the maximum length of cabling (i.e. 6 m) known to be safe was used and efforts were made to ensure it did not become coiled during the experiment.

Figure 5.10 Schematic of Heart Valve Motion Analysis System (HVMAS)

In vitro test rig

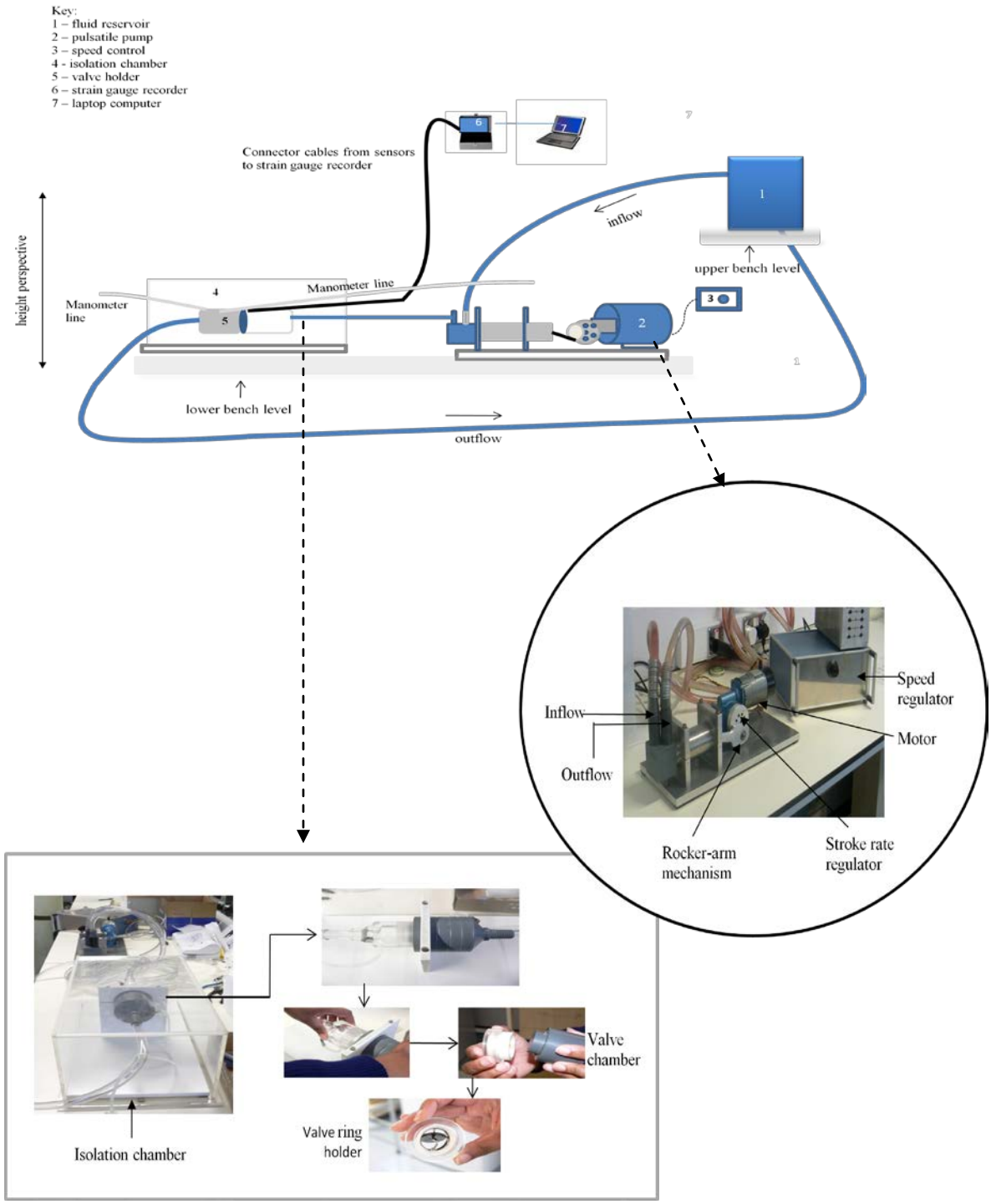

Figure 5.11 Valve ring holder – sequence for inserting the valve

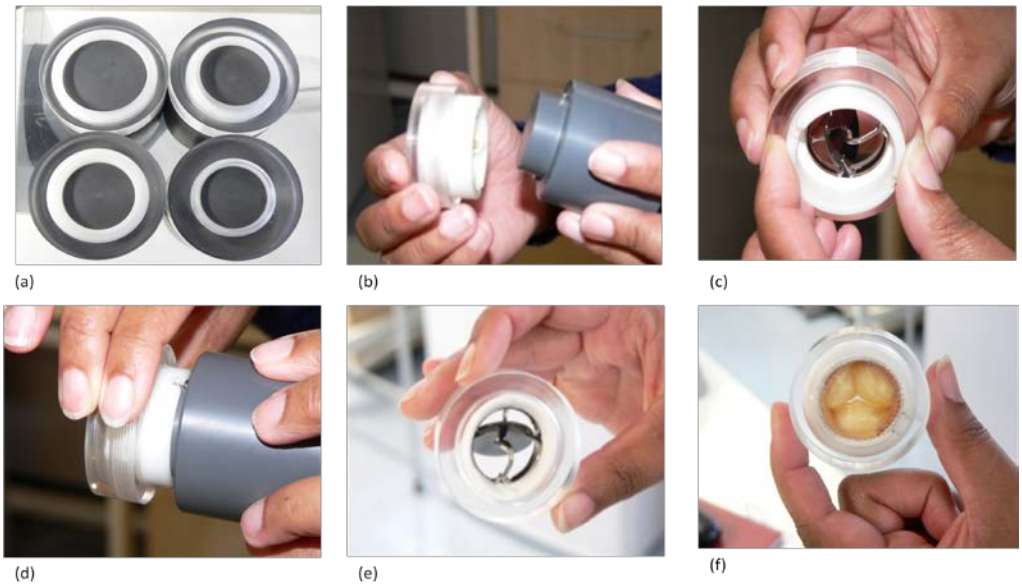

Figure 5.12 Detaching/re-assembling the valve chamber

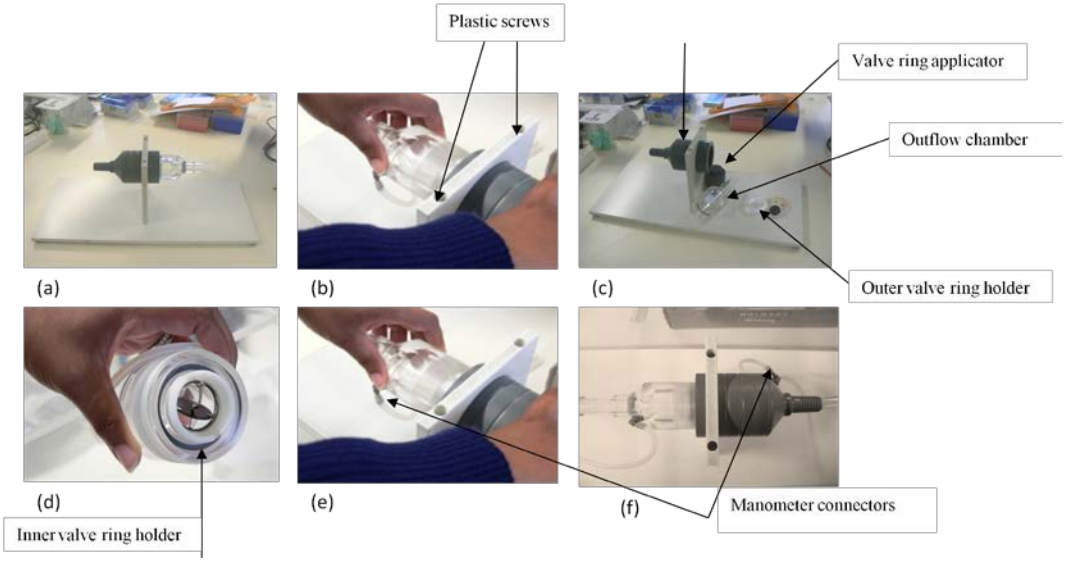

5.7 Section summary

In summary, this part of the Chapter described the components used in the experimental procedure to assessment the interaction of prosthetic heart valves with magnetic fields strengths of 1.5 T and 3.0 T and discussed what improvements had been made to the design of the test apparatus in comparison to prior investigations. In addition, limitations identified with this test apparatus were discussed in conjunction with the solutions employed to resolve these issues. The next part of the Chapter concludes the chapter on Materials and Methods and focuses on the methodology employed to conduct the study.

Part III
Experimental investigations
Methods

5.8 Introduction

The final part of this chapter on Materials and Methods describes the methodology employed to calibrate the test apparatus, plot the B_0 field of the 1.5 T and the 3.0 T MR systems and conduct the *ex vivo* and *in vitro* investigations. The first part of the section focuses on the methods for calibrating the pump and strain gauge apparatus and plotting the B_0 fields. Finally, the chapter concludes with a detailed description of the methodology used to conduct the assessment of the magnetic field interactions with the different prosthetic heart valves *ex vivo* and *in vitro* at the two field strengths.

5.9 Calibrating the apparatus

The following section describes the methods used to calibrate the test apparatus, define frequency and fluid output for the *in vitro* component of the apparatus, plot the B_0 fields of the 1.5 T and the 3.0 T MR systems and determine the velocity of the MR bed.

5.9.1 Calibration of the strain gauge apparatus

The strain gauge apparatus was calibrated by applying a spring balance with a known force (i.e. between 0 and 1 Newton (Nwt)) separately to each cantilever and the linearity of each strain gauge was evaluated by applying the spring balance in both directions (i.e. forward and reverse). Displacement of the strain gauge was recorded on the laptop computer and a set of data was produced for each of the four strain gauges for force (i.e. dependent variable) against displacement (i.e. independent variable). These data were plotted using Microsoft Excel (Microsoft Office 2007, USA) and a polynomial curve was constructed. Conversion of force measured in microstrain (μstrain) into force in Newtons

was achieved by substituting the known values (ie. dependent variables) into the polynomial equations for the respective line graphs.

5.9.2 Calibration of the pump

Calibration of the pump was performed to create an accurate impulse which corresponded to the shape of the average ventricular pressure pulse. Flow speed and stroke rate were regulated by the speed regulator and by altering the position of the drive wheel (ie. 1-10 positions) respectively (Figure 5.10).

5.9.3 Determining frequency

The average heart rate for a healthy adult is 75 beats per minute (bpm). Thus, for this investigation the apparatus needed to be set at a similar frequency (revolutions per minute (rpm). To determine the correct settings of the speed regulator and drive wheel the following steps were performed. The drive wheel and the speed dial were set at Position 1 respectively. A stopwatch was used to time a 20 second period from the start of the pulse during which time rpm was counted and recorded. At the end of the 20 second period the stopwatch was stopped and zeroed and the procedure repeated a further two times. The rpm recorded for each of the three 20 second timed periods was added together and the average calculated to give average rpm for Position 1, Speed 1. The speed dial was then advanced to Position 2 but the radii on the drive wheel remained the same as before. The procedure for counting and recording the rpm for three 20 second timed periods was repeated and the results recorded accordingly. The average rpm was then calculated using the same procedure as previously. This procedure was repeated for each speed for Position 1 on the drive wheel. Once all measurements had been recorded for Position 1 the speed regulator was returned to the start position (i.e. Position 1) and the position of the drive wheel was changed to Position 2. The procedure for recording three 20 second timed periods was then repeated as before and the average rpm calculated

for each speed at that position. This procedure was then repeated for each position of the drive wheel at each speed until the average required stroke rate of 75 rpm had been achieved (see Chapter 6, Part II).

5.9.4 Measuring fluid output

To achieve the required average fluid output of 5 l/m, the equivalent average cardiac output of a healthy adult the following procedures were performed. The drive wheel and the speed dial were set at Position 1 respectively. A fluid reservoir was connected to the pump's inlet connector and fluid pumped through the valve chamber, output was collected in a measuring cylinder (ml) and the measurement recorded. The measuring cylinder was then emptied. A stopwatch was used to time fluid output for a period of 1 minute. This procedure was repeated a further two times and the results from the three separate timed periods were added together and the average fluid output calculated. The speed regulator was then advanced to Position 2 but the position of the drive wheel remained unchanged. The fluid output was recorded for three 1 minute timed periods using the technique described. Once all measurements had been recorded for this position and speed the speed regulator was returned to the start position (i.e. Position 1) and the positioning of the drive wheel was changed to Position 2. The process was then repeated for each speed in this position. Fluid output was recorded separately for each position of the drive wheel and each speed until the average fluid output had been achieved. The results of the measurements for average heart rate and fluid output were then tabulated and the following equation applied to identify the corresponding tabulated result:

Pump output (Q) was therefore defined as:

Equation [4]:

Q = stroke volume (SV) x frequency (rpm) *[1]*

SV = 66 mL/frequency and average HR = 75 rpm

therefore:

Q = 66 mL/frequency x 75 rpm = 4950 ml/m *[2]*

= 5 l/m

5.9.5 Plotting the B_0 gradient field

The B_0 field is measured at the precise iso-center of the magnet where the three intersecting orthogonal planes (x, y and z) meet and where imaging begins. At this point the magnetic field gradient is at its maximum. However, as the distance from the iso-centre increases and the field is extended outward and covers an increasing spatial volume the B_0 field drops off rapidly. This creates a large spatial gradient of magnetic force with accelerating potential. In order to relate the forces exerted on the heart valve prostheses as they moved through this field two separate maps were plotted, one for the 1.5 T system and another for the 3.0 T MR system. A Hirst GM05 Gauss meter and axial probe (Magnetic Instruments Ltd) was used to measure the force (gauss) at intervals along the z- and x-axes (Table 10, Chapter 6). Measurement of the magnetic field along the z-axis commenced at the laser position (ie. 0 cm) and extended to 65 cm inside the bore of the magnet (ie. to the iso-centre where the magnetic field had levelled out and

was static) and 210 cm outside the bore to the five gauss line [50]. Measurements of the magnetic field along the x-axis were taken from the laser position to 30 cm bilaterally outside the bore. The distance along the axes was marked off in 5 cm increments. However, incremental changes along the z-axis towards the 5 gauss line increased after 60 cm to 30 cm intervals as the field became weaker in comparison and denoted the smallest magnetic field gradient.

The B_0 field of the 1.5 T MR system was measured first with measurements taken from the gauss line towards the iso-centre. The Hirst GM05 Gauss meter was already pre-calibrated by the manufacturer and therefore did not require additional calibration. All measurements on the z-axis were taken along the mid-line of the axis at the approximate height of the *in vitro* heart. The gauss meter was zeroed and axial probe orientated perpendicular to the direction of the field [51], the strength of the field was then measured and recorded. The gauss meter and probe were then advance 30 cm towards the laser and the gauss meter again zeroed, the probe orientated in the direction of the magnetic field as before and the strength of the field at this point measured and recorded. These steps were repeated up to 60 cm from the laser position after which the distance between measurements decreased to 5 cm apart and ended at iso-centre. Measurement of the magnetic field along the x-axis commenced at 30 cm outside the bore of the magnet and to the right of the entrance, measurements were taken at 5 cm intervals in the direction of the laser point (i.e. 0 cm) and extending 30 cm beyond this point. The same procedure was used to measure the magnetic field for the 3.0 T MR system.

[50] The magnetic field strength is described in units of gauss (G) and tesla (T) and 10,000 G is equal to 1 T. The earth's magnetic field is approximately 0.5 G and current safety standards therefore consider 0.5 G (also referred to as the 5 gauss line) to be the safe levels of MRI magnetic field exposure for the general public. The location of the 5 G line however, depends on the strength of the magnet.

[51] This probe was sensitive only to the magnetic force when positioned perpendiculr to the direction of the field. Orientation of the probe parallel to the direction of the magnetic field would have resulted in no measurements being captured.

The following equation was used to calculate the highest magnetic field gradient for the 1.5 T and 3.0 T MR systems:

The equation for the gradient (M) is:

Equation [5]: $M = (y2 - y1) / (x2 - x1)$

Where y is the field strength and x is the position in space relative to the laser.

5.9.6 Calculating the velocity of the MR bed

Calculation of the velocity of the MR beds for the two MR systems was performed to ensure all measurements were recorded at the exact same points on the z-axis for both magnetic fields. The method used to calculate both velocities was same for each MR system. A marker was placed at the approximate position on the MR bed where the human aortic valve would be if the patient's head was lined up with the laser. This was calculated to be approximately 68 centimetres (cm) from the laser position and is subsequently referred to in the remainder of the study as the aorta position. A second marker was placed at the iso-centre of magnet (see above). This was the point within the magnet the bed was stopped and reset to return to the starting position. The distance from the starting position to the iso-centre was also measured in centimetres (cm) using a non-ferromagnetic ruler. The MR bed was then advanced from the starting position to the iso-centre and a stopwatch was used to record the "turnaround time" in seconds (secs) of the bed at the iso-centre so these could be incorporated into the final velocity calculation. A series of three separate measurements of the "turnaround time" [52] of the MR bed were recorded using the methods described and the average time calculated. The MR bed was then returned to the starting position and a stopwatch used to time the progression of the bed from the starting point to the iso-centre. At the start of each timed sequence the

[52] The 'turnaround time' refers to the time it took for the MR bed to stop at the iso-centre and start its return journey measured in seconds.

stopwatch was zeroed and started at the same moment the button was pressed to start the progression of the bed and stopped when the bed returned to the starting position and the time recorded. Three separate timed sequences of the MR bed's progression from the aorta position to the iso-centre and back were recorded and the average time calculated. The velocity of the MR bed was then calculated using the equation given below.

Equation [6]: $v = \frac{d}{t}$

Where v is the velocity, d is the distance and t equals the time.

The same procedure was repeated to calculate the velocity of the MR bed at 3.0 T.

5.10 Ex vivo test

The *ex vivo* test was conducted to detect and record any movement of a prosthetic heart valve during exposure to strong magnetic forces associated with MRI when placed statically within the magnetic field and when the valve continuously moved through the field. Figure 5.5 shows the apparatus used in this part of the investigation.

5.10.1 Baseline measurements

Prior to conducting the experimental test procedure baseline measurements of the test apparatus (ie. without a prosthetic heart valve attached) were taken at 1.5 T and 3.0 T to confirm the sensitivity of the apparatus to measure any potential interaction of the apparatus with the magnetic field. The test procedure for measuring and recording the baseline measurements and for all measurements involving the heart valve prostheses were the same. The arm of the stand was adjusted at the lower joint (Figure 5.5) to the approximate height and orientation of the native *in vivo* aortic heart valve (Figure 5.13). The cabling connecting the strain gauges to the recorder was secured to the MR bed with

tape to ensure they did not become looped, kinked or displaced. At the beginning of each test period the strain gauge recorder was zeroed. Four positions along the z-axis were marked for points of reference within the B_0 field. All measurements were taken from laser position as follows: laser to the gauss line (+188 cm), laser to the aorta (+68 cm), laser (0 cm) and laser to the iso-centre (-65 cm) (see Table 9). Static measurements of the test apparatus only were recorded at each of these four positions along the z-axis for timed periods of fifteen seconds each and the measurements stored on the laptop computer. After all static measurements had been taken the test rig advanced continuously through the B_0 field from the gauss line towards the iso-centre and back. Any movement of the apparatus detected was recorded and stored on the laptop computer.

Figure 5.13 Diagram of position of the native aortic valve

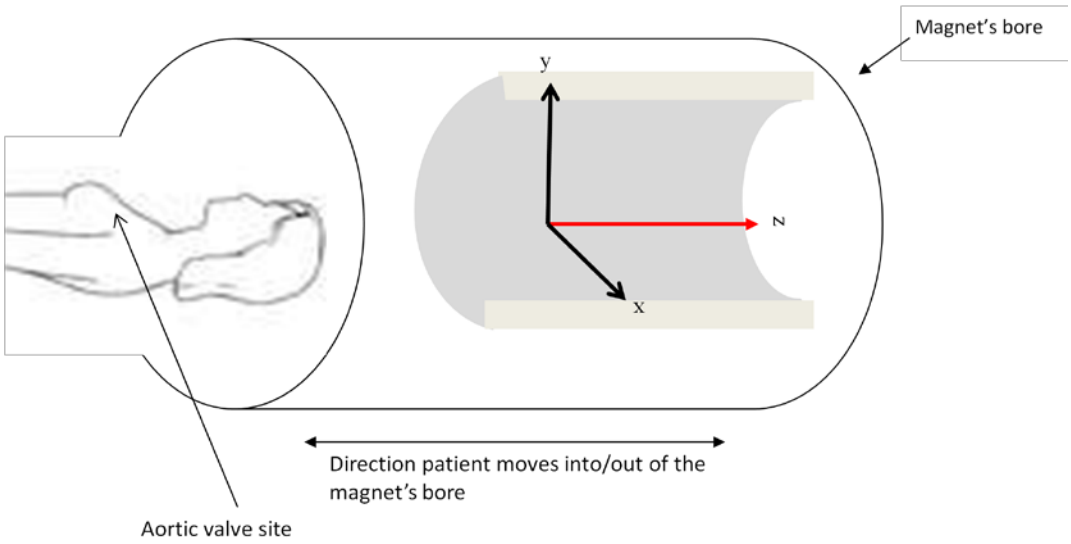

5.10.2 Experimental measurements

The experimental procedure for detecting and recording any interaction of a prosthetic heart valve with MR associated magnetically induced forces was the same as that described above for baseline measurements. Each valve was exposed to the 1.5 T MR system and measurements recorded. The same procedures were then followed for the 3.0 T MR system. Each prosthesis was placed in the valve holder ensuring the valve ring was in contact with all four strain gauge sensors and the leaflets/occluder were oriented according to the natural flow of blood. The valve was secured in place by screwing the male and female parts of the valve holder together. The holder was then secured in the flat plate of the test rig positioned midline of the MR bed. Data recorded for the first static measurement at the gauss line was saved using a unique identifier denoting the valve and test phase. The test rig was then moved to the aorta position for the second of four static measurements and the same procedure was repeated for measuring, recording and saving the data as before. This procedure was also repeated at the laser and iso-centre positions along the z-axis. On completion of these static measurements the test rig was returned to the gauss line and the procedure for resetting the strain gauge amplifier and recorder was again followed. The strain gauge recorder was started as the MR bed and test rig was continuously advanced to the iso-centre and returned to the starting position at which point the recording was stopped and the data saved onto the laptop computer using a unique identifier denoting the valve and test phase. After the static and dynamic tests had been completed the valve was removed from the valve holder and the next valve inserted as described above. The procedures for conducting the static and dynamic tests respectively were repeated for the next valve until all prosthetic heart valves had been tested at both field strengths.

All experimental data was adjusted for baseline measurements to compensate for any valve independent effects. This was achieved by deducting baseline measurements measured in μstrain from experimental data for each of the respective channels and

converting the results into Newton force as described above. Thus, all experimental results report accurate movement of the heart valve prosthesis within the magnetic field because the potential for error resulting from the combined interaction of the test apparatus and the valve prosthesis with the magnetic field have been excluded.

5.11 In vitro test (hydro-pneumatic investigation)

The first of the nine valve prostheses was secured in the valve holder apparatus as described in the Materials section above and placed inside the isolation chamber (Figures 5.11 - 5.12). The test apparatus was then positioned on the MR bed at the gauss line (Figure 5.14). As Figure 5.10 shows fluid was pumped from the fluid reservoir by the pumping system to the valve holder via 10 m of high shore hardness PVC tubing which connected the pump to the isolation chamber and valve holder apparatus. A fixed rate flow of 5 l/min at 1.166 Hz synonymous with the clinical setting environment was pumped through the valve and fluid pressures were measured using electro-dynaphramatic pressure transducers connected to the inlet/outlet valve holder using standard clinical manometer lines. Signals from high frequency pressure transducers were recorded using national instrument pressure recording apparatus and lab view software and pressure drops across the valve were assessed using time correction superimposition. The delta p across the valve was assessed as a marker of any MRI induced alteration in leaflet performance. Measurements were recorded for a 1 minute timed period at this position and the data saved onto the laptop computer using a unique identifier denoting the valve, position along the z-axis and phase of the test. The MR bed was advanced to the second position along the z-axis and stopped, the pressure recording system zeroed and a 1 minute timed period at the aortic position started. Data captured was saved and stored onto the laptop computer as before. This procedure was repeated a further two times i.e. at the laser position and the iso-centre (Figure 5.14). The test rig was then returned to the gauss line and the pressure recording system zeroed. The MR bed was then advanced continuously from this position to the iso-centre and returned to

the start position. A continuous recording was made throughout this period and the data saved as before. This procedure was repeated for all nine valves listed in Table 6 at 1.5 T and 3.0 T.

Figure 5.14 Diagram showing the direction of movement of the MR bed and the four reference points along the z-axis

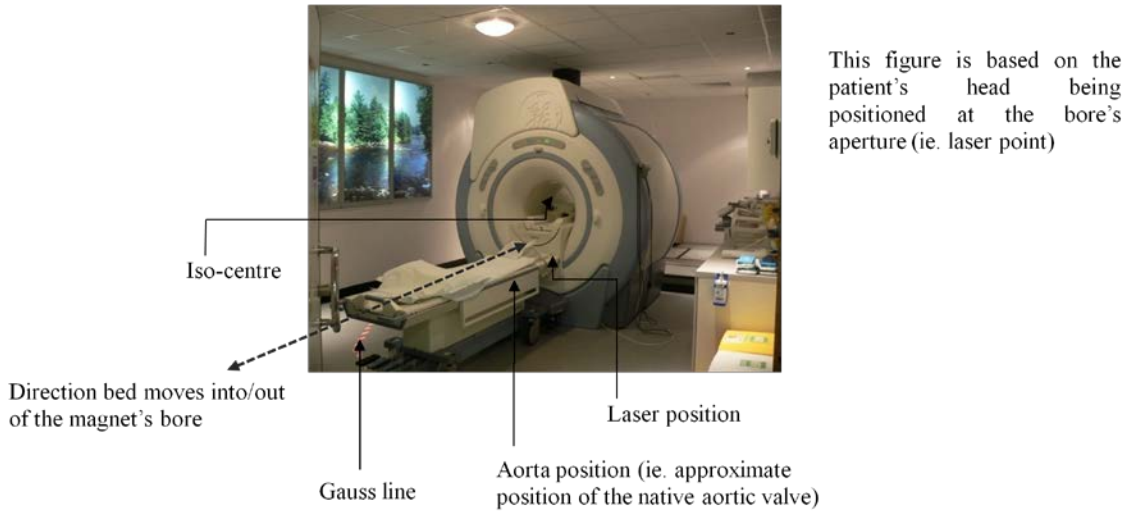

5.12 Chapter summary

This chapter has endeavored to identify and quantitatively measure for the first time any movement of a prosthetic heart valve *ex vivo* and *in vitro* as a result of the interaction with induced magnetic forces associated with MRI as it was in continuous motion through the B_0 gradient field. The following chapters present the results of the data and discuss these findings with respect to existing knowledge of the impact of MR induced magnetic forces on heart valve prostheses and implications for patient safety.

CHAPTER 6

Results

6. Introduction

Chapter 6 presents the results and analyses of the study's findings. Part I briefly describes the results from the first series of static *ex vivo* investigations assessing the interaction of heart valve prostheses with MR associated magnetically induced forces at 1.5 T and 4.7 T. These earlier experiments formed the foundation studies for this thesis. Parts III-IV of the Chapter report the results of the core investigation to assess the interaction of nine heart valve prostheses exposed to MR field strengths of 1.5 T and 3.0 T using apparatus specially designed to detect valvular movement across two axes and as the valve was placed statically within the field and, as it moved continuously through the field. The first part of the next section (Part II) details the results of the calibrations performed on the *ex vivo* test apparatus and maps the B_0 gradient fields of the 1.5 T and the 3.0 T MR systems used in the study. In addition, baseline data were recorded for comparison with the experimental data. The data are thus presented as the precursor to the main experimental data which focuses on the measurements recorded by the strain gauge apparatus at the different positions along the z-axis statically and, as the valve continuously progressed through the magnetic field.

Part III presents the results of the *ex vivo* experimental data in which the nine heart valve prostheses were exposed to magnetic field environments of the 1.5 T and 3.0 T MR systems and incorporates the static and dynamic exposure to these fields. The final section (Part IV) reports the results of the *in vitro* investigations and in particular, any interaction of the valve's leaflets/occluder with induced magnetic forces. The section evaluates the individual fluid profiles of each heart valve at specific points along the z-axis when the valve was static and as it moved through the magnetic field. Any differences in waveform, magnitude and complex formation compared with the baseline measurement at both field strengths are reported.

(Part I)

Preliminary investigations

6.1 Assessment of magnetic field interactions at 1.5 T

Table 7 presents the results for magnetic field interactions on 32 prosthetic heart valves evaluated at 1.5 T using the test apparatus shown in Figure 5.2, Chapter 5. As the Table shows only five valves showed an interaction with displacement forces and displayed deflection angles ranging from 0.5° to 5° and of these five valves three were mechanical and two made from human tissue. In contrast, nearly half of all valves (ie. n=13) displayed an interaction with rotational forces and measurements recorded using the five point qualitative scale described in Chapter 5 range from +1 to +2. Ten of the valves were single leaflet valves and displayed torque forces of +1. One of the three caged disc valves in this study, the Smelloff Cutter valve exhibited a stronger reaction to torque force in comparison with all other mechanical valves and recorded a qualitative measured rotational force of +2. The Durafic human tissue valves also recorded a measurement of +2 on the torque scale. However, although the leaflets were fashioned from dura mater the stent and/or sewing ring materials of this valve contained an unknown metal and it was thought this material interacted with the magnetic field causing the deflection and torque responses shown in Table 7. The results also show those valves which demonstrated the highest deflection angles also exhibited the higher torque force. These findings suggest therefore the type of materials used in the manufacture of these prosthetic heart valves were either non-ferromagnetic or weakly ferromagnetic relative to the 1.5 T MR environment. These responses however, fall within the ASTM operational definition for non-ferromagnetic implants [53] which deem implants safe for individuals in a $\leq$1.5 T environment if the deflection angle is $\leq$45°. In addition, as Table 7 shows the displacement force exerted on the heart valves causing them to deflect away from the

[53] The ASTM document actually referred to an aneurysm clip (ASTM 1994).

vertical were significantly smaller than gravity as well as the mechanical forces of the beating heart. Furthermore, whilst the torque ranged from 0 to +2 both the quantitative and qualitative findings are not believed to present a hazard or risk for these heart valve prostheses.

Table 7: Results of MR safety tests for 32 heart valve prostheses @ 1.5 T [54]

No.	Valve name	Deflection angle (°)	Torque	Magnetic force (N)	Magnetic susceptibility (χ)	Mechanical forces beating heart (N)
1	AorTech	0	+1	0	-	3.9 – 4.7
2	AorTech	0	+1	0	-	5.9 – 9.1
3	ATS	0	+1	0	-	7.9 – 12.3
4	ATS	0	+1	0	-	2.4 – 2.9
5	Beall	0	+1	0	-	7.9 – 12.3
6	Biocor	0	0	0	-	3.9 – 4.7
7	Björk Shiley conical disc	0	0	0	-	4.1 – 6.5
8	Björk Shiley conical disc	3.5	+1	2.5×10^{-3}		4.1 – 6.5
9	Björk Shiley monostrut	0.5	+1	3.8×10^{-4}		5.9 – 9.1
10	Björk Shiley monostrut	0	0	0		2.1 – 2.6
11	Björk Shiley monostrut	0	0	0		5.0 – 7.3
12	Durafic (aortic)	5	+2	2.5×10^{-3}		8.0 – 9.7
13	Durafic (mitral)	2	+2	1.4×10^{-3}		-
14	Hancock pericardial	0	0	0	-	5.9 – 9.1
15	Intact	0	0	0	-	2.6 – 3.2
16	Intact	0	0	0	-	5.9 - 9.1
17	Jyros	0	0	0	-	6.4 – 9.9
18	Jyros	0	0	0	-	4.9 – 6.0
19	Liotta	0	0	0	-	3.9 – 4.7
20	Mitroflow	0	0	0	-	4.6 – 5.6
21	Mitroflow	0	0	0	-	7.9 – 12.3
22	Mitroflow	0	0	0	-	4.6 – 5.6
23	Smelloff Cutter	3	+2	5.0×10^{-3}		3.2 – 3.9
24	Sorin Allcarbon	0	+1	0	-	7.9 – 12.3
25	Sorin pericabon (stented)	0	0	0	-	10.2 – 15.9
26	St Jude Masters	0	+1	0	-	4.6 – 5.6
27	St Jude Regent	0	+1	0	-	4.6 – 5.6
28	Tascon	0	0	0	-	-
28	Toronto stentless	0	0	0	-	4.6 – 5.6
30	Wessex	0	0	0	-	7.0 – 8.5
31	Wessex	0	0	0	-	5.9 – 9.1
32	Xenofic	0	0	0	-	3.9 – 4.7

[54] See Table 1, Chapter 6 for full details of model, size and valve materials.

6.2 Interactions with magnetic forces at 4.7 T

The results from the second of the preliminary investigations using the test equipment and revised qualitative scale of measurement (Figure 5.3, Table 5) are presented in Table 8. Thirteen out of the 81 prosthetic heart valves displayed zero interaction with the magnetic field both in terms of deflection and torque forces but all other prostheses demonstrated some measure of interaction.

6.2.1 Interactions with displacement forces at 4.7 T

Deflection angles for all prostheses ranged from 0° to 7.5° although, it was not possible to obtain an angle of deflection for the Carbomedics valve graft due to the length of the root graft interfering with the freedom of movement of the valve. Overall, the mechanical group of valves demonstrated a greater number of interactions with displacement forces and displayed greater deflections compared with bioprosthetic valves. As Table 8 shows the range of deflections displayed by both mechanical and bioprosthetic valves were similar and ranged from 0° to 7.5° and 0° to 7° respectively and interaction of human tissue valves with translational forces recorded measurements of 2° and 6° and as such, were two of the highest recorded displacements within the heart valve group. Within the mechanical group of valves only four displayed a zero deflection and all others deflected between 0.5° and 7.5° from the vertical. All but one of the single leaflet/disc valves demonstrated a displacement force and as Table 8 shows, all Björk Shiley valves consistently exhibited some of the highest deflections overall with deflections ranging from 3° to 5°. Within the bileaflet group two valves the Carbomedics standard valve and the Mira valve displayed zero deflection but the remaining four Carbomedics valves demonstrated some degree of deflection though this was only very small ie. >1°. Displacement forces exerted on the remaining bileaflet valves resulted in deflection angles ranging from 1° to 7.5°. The highest deflections were recorded by the Jyros

aortic and mitral valves which deflected by 6.5° and 7.5° respectively. Of the caged ball valves two showed no interaction with displacement forces but the third, the Starr Edwards model 6320 which contained metal studs in the housing, showed a relatively high deflection from the vertical of 6.5°. The remaining mechanical valves, the Beall and Starr Edwards caged disc valves exhibited deflection angles of 2° and 4° respectively. Although a number of heart valves have demonstrated a deflection from the vertical the applied magnetic force calculated to cause this is, as Table 8 shows, significantly smaller than both gravity and the mechanical forces of the beating heart. Overall seven heart valves were attracted towards the iso-centre and highest magnetic field indicating they were slightly paramagnetic/weakly ferromagnetic. All other prostheses were deflected away from the iso-centre corresponding to diamagnetic behaviour (Table 8). Moreover, all valve prostheses demonstrated a magnetic acceleration significantly less than that due to gravity.

6.2.2 Interactions with rotational forces at 4.7 T

Twenty-one out of the 81 heart valves did not align or rotate towards the magnetic field. Table 8 shows that when placed parallel to the magnetic field 16 prostheses recorded a rotational movement of +1 on the qualitative scale of measurement defined in the previous chapter. This movement equated to an alignment or rotation of ≤45° towards the magnetic field. Nine prostheses attempted to rotate between 45º and 90° towards the magnetic field and recorded a measurement of +2. When the prostheses were positioned perpendicular to the magnetic field along the z-axis similar numbers attempted to rotate ≤45° ie. +1 in comparison to when placed parallel to the field. Twenty-three prostheses rotated between 45° and 90° (i.e. +2) when orientated perpendicularly to the magnetic field. This was true for mechanical, bioprosthetic and human tissue valves. Interaction of the prostheses with rotational forces was not however always accompanied by interaction with displacement forces.

Moreover, those prostheses which displayed greater deflections from the vertical did not necessarily also demonstrate higher rotational behaviour.

Table 8: Results - exposure of prosthetic heart valves to 4.7 T

Heart valves:

N	Prosthesis name	Size (cm)	Deflection angle (º0)	Magnetic moment (Am^2)	Torque (parallel)[55]	Torque (perpendicular)	Magnetic force (N)	Mechanical forces beating heart (N)
1	Aspire	27	0	-	0	0	0	6.9 – 10.7
2	ATS Medical	25	1	6.6×10^{-4}	1	0	7.5×10^{-4}	5.9 – 9.1
3	Beall	29	2	8.1×10^{-3}	2	2	5.2×10^{-3}	7.9 – 12.3
4	Biocor	23	0	-	1	0	0	3.9 – 4.7
5	Björk Shiley conical disc	21	3	4.6×10^{-4}	0	0	2.3×10^{-3}	4.1 - 6.5
6	Björk Shiley conical disc	21	3.5	4.9×10^{-4}	1	1	2.4×10^{-3}	4.1 – 6.5
7	Björk Shiley monostrut	25	5	7.6×10^{-4}	2	2	3.8×10^{-3}	5.9 – 9.1
8	Björk Shiley monostrut	17	4	4.9×10^{-4}	1	1	2.4×10^{-3}	2.1 – 2.3
9	Björk Shiley monostrut	23	5	9.8×10^{-4}	1	1	4.9×10^{-3}	5.0 – 7.7
10	Björk Shiley monostrut	33	4	1.0×10^{-3}	0	2	5.2×10^{-3}	10.2 – 15.9
11	Björk Shiley spherical disc	31	3.5	8.7×10^{-4}	1	1	4.4×10^{-3}	9.3 – 14.1
12	Björk Shiley 60º cc	27	5	6.9×10^{-4}	1	1	3.5×10^{-3}	5.3 – 6.5
13	Björk Shiley 60º cc valve graft	25	4	1.2×10^{-3}	2	2	5.4×10^{-3}	2.1 –10.3
14	CarbonArt	27	0	-	0	0	0	5.3 – 6.5
15	Carbomedic standard	21	0	-	1	1	0	3.2 – 3.9
16	Carbomedics supra-annular (Top Hat)	23	0.5	5.5×10^{-5}	1	1	2.8×10^{-4}	3.9 – 4.7
17	Carbomedic standard	31	0.5	1.1×10^{-4}	2	2	5.3×10^{-4}	9.3 – 14.1
18	Carbomedics SuMit	29	0.5	1.0×10^{-4}	0	2	5.0×10^{-4}	7.9 – 12.3

[55] Scale of measurement: 0, zero torque; +1 = alignment or rotation of >0° to 45° from starting point; +2 = alignment or rotation of >45° to 90° from starting point.

19	Carbomedics valve graft	34	-	-	2	2	-	8.5 – 10.3
20	Carpentier Edwards porcine	31	3	6.8×10^{-4}	0	0	3.4×10^{-3}	7.0 – 8.5
21	Carpentier Edwards pericardial	33	7	1.5×10^{-4}	1	1	7.6×10^{-4}	10.2 – 15.9
22	Carpentier Edwards supra-annular	31	2.5	6.3×10^{-3}	2	0	3.2×10^{-3}	9.3 – 14.1
23	Contegra	18	0	-	0	0	0	0.7 – 1.0
24	Duromedics	27	0.5	1.4×10^{-4}	0	2	6.8×10^{-4}	2.1 –10.3
25	Duromedics	29	1	1.9×10^{-4}	0	1	9.6×10^{-4}	7.9 – 12.3
26	Durafic	33	655	6.1×10^{-4}	0	2	3.0×10^{-4}	8.0 – 9.7
27	Durafic	23	2[54]	2.8×10^{-4}	0	1	1.4×10^{-3}	2.7 – 16.9
28	Elan	22	0	-	0	0	0	3.5 – 4.3
29	Elan valve graft	23	0	-	0	0	0	3.9 – 4.7
30	Freedom	25	0	-	0	0	0	4.6 – 5.6
31	Freestyle	27	0	-	0	0	0	5.3 – 6.5
32	Hancock pericardial	25	1	1.7×10^{-4}	0	0	8.5×10^{-4}	5.9 – 9.1
33	Hancock Modified Orifice	21	1	1.4×10^{-4}	2	0	7.2×10^{-4}	3.2 – 3.9
34	Hancock II Modified Orifice	25	1	1.8×10^{-4}	0	0	8.9×10^{-4}	4.6 – 5.6
35	Intact	19	2	2.2×10^{-4}	0	0	1.1×10^{-3}	2.6 – 3.2
36	Intact	25	2	4.1×10^{-4}	0	1	2.0×10^{-3}	5.9 – 9.1
37	Ionescu Shiley	23	1.5	2.9×10^{-4}	0	1	1.4×10^{-3}	–
38	Jyros	30	7.5[54]	1.6×10^{-3}	0	2	8.0×10^{-3}	4.9 – 6.0
39	Jyros	26	6.5[54]	1.4×10^{-3}	0	2	6.8×10^{-3}	8.5 – 13.2
40	Labcor Synergy	21	2	2.5×10^{-4}	1	1	1.2×10^{-3}	3.2 – 3.9
41	Labcor Synergy	25	2.5	4.4×10^{-4}	0	0	2.2×10^{-2}	5.9 – 9.1
42	Liotta	23	2	3.4×10^{-4}	1	0	1.7×10^{-2}	3.9 – 4.7
43	Medtronic	23	1	1.0×10^{-4}	1	2	5.1×10^{-4}	3.9 – 4.7
44	Medtronic	23	2	2.9×10^{-4}	0	2	1.4×10^{-3}	5.0 – 7.7
45	Medtronic	29	1	2.0×10^{-4}	0	2	9.8×10^{-4}	7.9 – 12.3
46	Mira	27	0	-	0	0	0	6.9 – 10.7
47	Mitroflow	25	2	2.5×10^{-4}	1	1	1.2×10^{-3}	4.6 – 5.6
48	Mitroflow	25	2	2.9×10^{-4}	2	2	1.1×10^{-3}	4.6 – 5.6

49	Mitroflow	29	2	2.2×10^{-4}	0	2	1.4×10^{-3}	7.9 – 12.3
50	Mitroflow Synergy	21	3	3.6×10^{-4}	0	0	1.6×10^{-3}	3.2 – 3.9
51	MØre	19	0	-	0	0	0	2.6 – 3.2
52	Mosaic	29	2	4.3×10^{-4}	2	1	2.1×10^{-3}	6.2 – 7.5
53	Omniscience	25	0	-	0	2		5.9 – 9.1
54	On-X	19	3	3.3×10^{-4}	0	0	1.6×10^{-3}	2.6 – 3.2
55	On-X	31-33	3	7.8×10^{-4}	0	0	3.9×10^{-3}	9.0 – 15.9
56	Smelloff Cutter	21	0	-	0	2	0	3.2 – 3.9
57	Sorin pericabon (stented)	33	1.5	4.0×10^{-4}	1	1	1.9×10^{-3}	10.2 – 15.9
58	St Jude Standard	21	3	2.7×10^{-4}	0	2	1.3×10^{-3}	3.2 – 3.9
59	St Jude Standard	27	3.5	5.1×10^{-4}	0	2	2.5×10^{-3}	2.7 – 16.9
60	St Jude Regent	17	2	8.5×10^{-5}	0	+2	4.2×10^{-3}	2.1 – 2.6
61	St Jude valve graft	25	2	3.8×10^{-4}	0	+2	1.9×10^{-3}	4.6 – 5.6
62	Starr Edwards	32	0	-	0	0	0	9.6 – 15.0
63	Starr Edwards	32	6.5[54]	2.7×10^{-3}	0	0	1.3×10^{-2}	9.6 – 15.0
65	Starr Edwards	26	4[54]	1.0×10^{-3}	0	1	5.1×10^{-3}	2.7 – 16.9
66	Tascon	23	6[56]	1.8×10^{-3}	0	1	9.0×10^{-3}	2.1 – 10.3
67	Toronto root	27	0	-	0	0	0	5.3 – 6.5
68	Ultracor	23	1	1.1×10^{-4}	0	2	5.6×10^{-4}	3.9 – 4.7
69	Ultracor	25	1	1.4×10^{-4}	0	1	6.9×10^{-4}	5.9 – 9.1
70	Wessex	31	2	4.9×10^{-4}	1	1	2.5×10^{-3}	7.0 – 8.5
71	Wessex	25	2	3.8×10^{-4}	0	1	1.9×10^{-3}	5.9 – 9.1
72	Xenofic	23	2	4.6×10^{-4}	0	1	2.2×10^{-3}	3.9 – 4.7

[56] These valves were attracted towards the centre of the magnet, all other valves deflected away from the isocentre.

6.3 Limitations of the preliminary test apparatus and methodology

The first part of Chapter 6 presents the results of preliminary *ex vivo* investigations evaluating the interaction of MR associated magnetically induced forces with 81 different heart valve prostheses at 1.5 T and 4.7 T. Although the test apparatus employed was simple and capable of detecting and measuring displacement from the vertical a number of shortcomings in the test apparatus and methodologies were nonetheless identified (see below):

1. an inability to quantitatively measure torque force,

2. failure of the apparatus to reflect the orientation and position of the prosthesis under clinical conditions,

3. limited data on the possible interaction of a valve prosthesis with the magnetic force in vivo as it continuously moves through the B_0 field and thus its behaviour in terms of:
   a. frequency,
   b. magnitude of applied force and
   c. direction of movements.

4. insufficient information about whether the valve's leaflets/occluder interact with the B_0 field and thereby compromise valve function and performance.

We are therefore unable to adequately assess the risks of potential movement, dislodgement, dehiscence or interference in valve function likely to cause harmful or fatal injury to the patient. Thus, a model which more closely mimics the clinical/physiological setting is required. The next part of this chapter therefore presents the results of the *ex vivo* investigation of nine prosthetic heart valves exposed to two different field strength MR environments using apparatus specially

designed to detect movement in one of four directions as the valves move continuously through the B_0 field.

Results (Part II)

Ex vivo investigations:
Calibration of the test equipment and baseline measurements

This section presents the results of the calibration of the *ex vivo* test apparatus, mapping of the 1.5 T and 3.0 T B_0 field and baseline measurements recorded during the static and dynamic exposure of the test apparatus to magnetic fields associated with 1.5 T and 3.0 T.

6.4 Calibration of the test apparatus

Figure 6.1 shows the results of the calibration of the strain gauges with graduated force. All four profiles show near straight line graphs which were further confirmed by construction of the polynomial line graph. As the Figure shows three out of the four strain gauges (ie. Channels 1, 3 & 4) displayed similar measured responses to the incremental forces applied. Channel 2 however, displayed slightly different measured responses to the same graduated forces compared with the other channels. The calibration procedure was repeated several times and recorded consistent results. One plausible explanation for these unexpected differential responses is the possibility of differences in the sensitivity of the transducers.

Figure 6.1 Calibration curves for *ex vivo* test apparatus

(a) Paired sensors 1 & 3

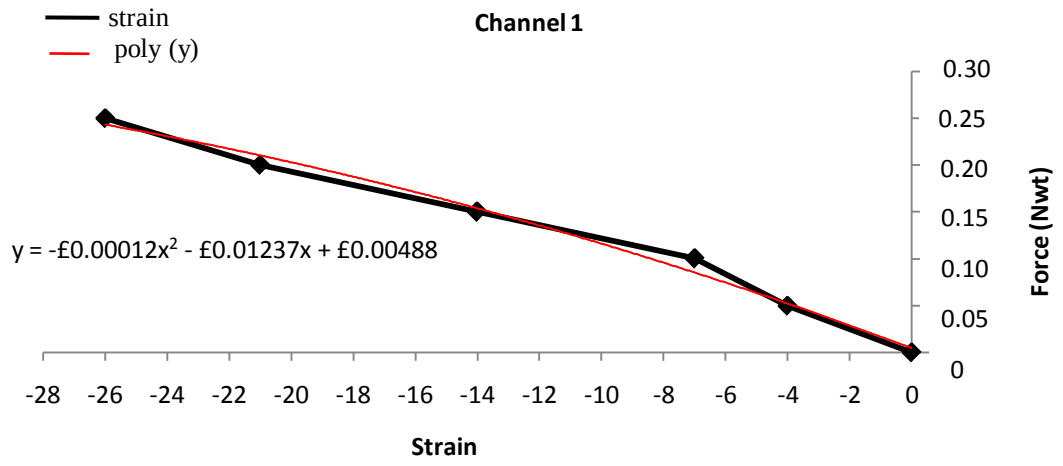

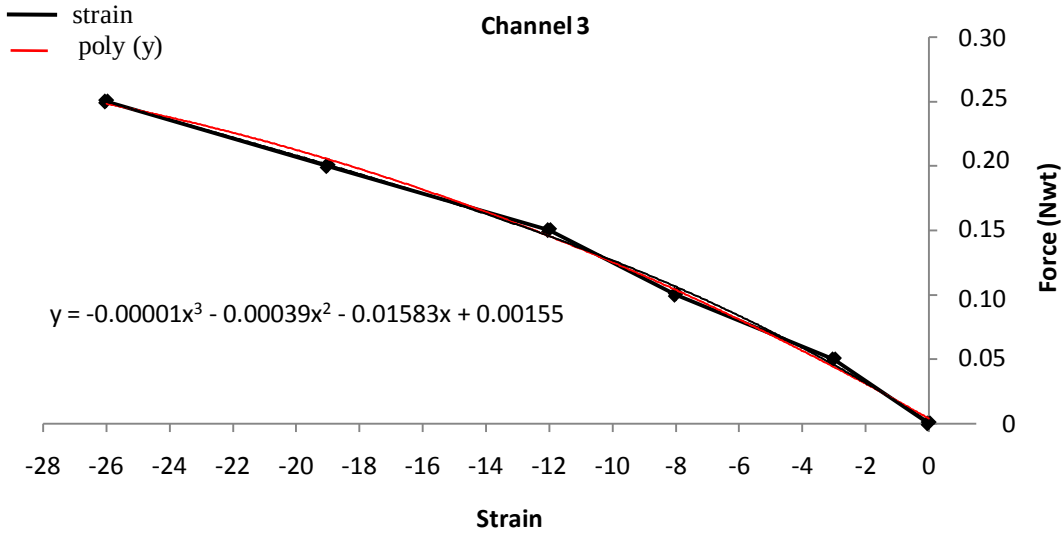

(b) Paired sensors 2 & 4

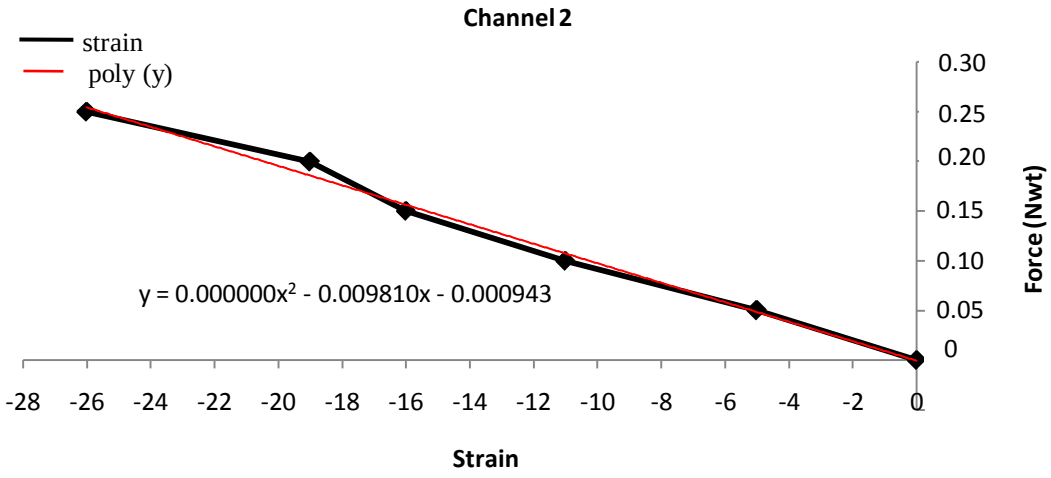

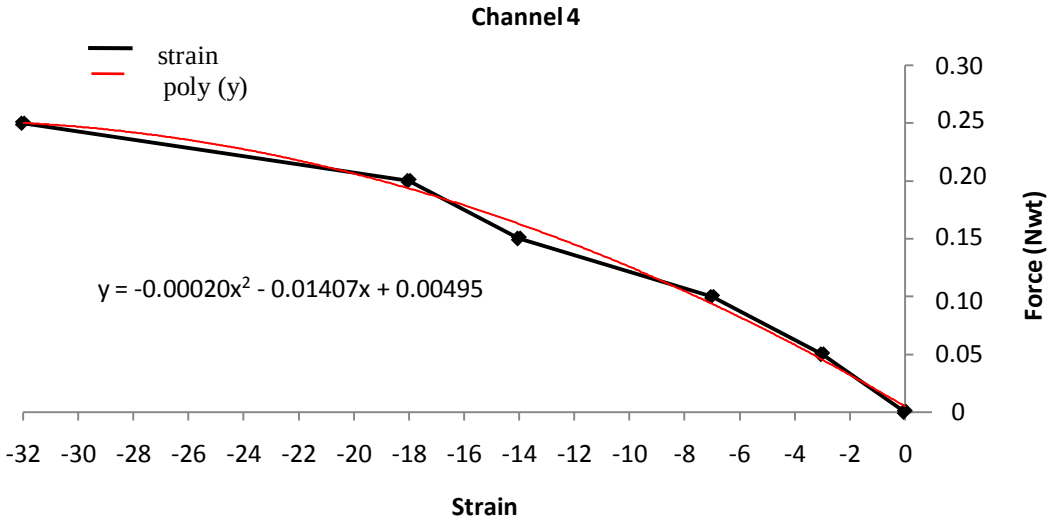

6.5 B_0 gradient field maps

Table 9/Figure 6.2 shows a series of plotted measurements taken at intervals from the fringe of the magnetic field towards the iso-centre along the z-axis for the 1.5 T and 3.0 T MR systems. The data shows the B_0 field along the z-axis increases with increasing proximity to the centre of the magnet where it becomes homogenous. The series of field strengths recorded for the 1.5 T MR system range from 0.002 T (20 G) at the fringe of the field to 1.5 T (15,000 G) at the iso-centre and, the highest magnetic field gradient was calculated to be 0.020 T/cm (200 G/cm) (see Equation [7]) and occurred between ±20 cm from the laser position. The varying field strength along the z-axis of the 3.0 T MR system ranged from 0.005 T (50 G) to 3.0 T (30,000 G) between the gaussline and the iso-centre and the highest magnetic gradient strength was calculated to be 0.037 T/cm (380 G/cm) (see Equation [7]). As Figure 6.2 shows the field strength falls off towards to the outer fringes of the z-axis creating a dome-shaped field. At the four reference positions along the z-axis (see Chapter 5 Figure 5.14) the strength of the magnetic field was measured as 0.003 T at the gauss line (ie. 30 G), 0.06 T (600 G) and 0.66 T (6,600 G) at the aortic and laser and positions respectively and 1.50 T (15,000 G) at the iso-centre for the 1.5 T MR system. Measurements taken for the 3.0 T MR system were recorded as 0.008 T (80 G), 0.19 T (1,900 G), 1.52 T (15,200 G) starting at the gauss line and moving towards the iso-centre and, 3.0 T (30,000 G) at the iso-centre.

Equation [7]:

If the field strength = 1.01 (y2) at position -15 (x2) and 0.39 (y1) at position +15 (x2) *[1]*

Then = (1.01 - 0.39) / (-15 - 15) *[2]*

= 0.62 / -30 = -0.020 T/cm (200 G/cm) [57]

[57] The negative sign indicates only that the gradient is decreasing outside the bore of the magnet

Similarly, at 3.0 T the highest magnetic gradient was calculated to be:

If the field strength = 2.11 (y2) at position -15 (x2) and 0.05 (y1) at position +15 (x2) *[1]*

Then = (2.11 - 0.95) / (-15 - 15) *[2]*
= 1.16 / -30 = - 0.038 T/cm (380 G/m)

6.5.1 Velocity of MR bed

Chapter 5 described the methodology employed to calculate the velocity of the two separate MR beds at 1.5 T and 3.0 T respectively. Of the three sets of measurements recorded the distance from the starting point to the iso-centre was found to be 253 cm for both MR systems respectively. The average time calculated for the MR bed to cover this distance in the 1.5 T MR system was 37.7 seconds and 34.0 seconds at 3.0 T. Thus, by substituting these data in the equation given below the average velocity of the MR bed(s) was determined to be 6.7cm/sec at 1.5 T and 7.4 cm/sec at 3.0 T.

Equation [8]: $v = \frac{253\ cm}{37.7\ secs}$ *=6.7 cm/sec @ 1.5 T*

and: $v = \frac{253\ cm}{34\ secs}$ *=7.4 cm/sec @ 3.0 T*

Table 9: B_0 gradient measurements along the z-axis

Position on z-axis	Distance from laser (cm)	Magnetic field strength (1.5 T)		Magnetic field strength (3.0 T)	
		Midline		Midline	
z-axis		z-axis	x-axis	z-axis	x-axis
Iso-centre	-65	1.50		3.0	
	-60	1.50		3.0	
	-55	1.50		3.0	
	-50	1.50	-	3.0	-
	-45	1.50	-	3.0	-
	-40	1.46	-	2.96	-
	-35	1.40	-	2.88	-
	-30	1.35	0.54	2.76	1.34
	-25	1.25	0.61	2.53	1.42
	-20	1.15	0.62	2.36	1.47
	-15	1.01	0.65	2.11	1.50
	-10	0.90	0.66	1.93	1.52
	-5	0.82	0.67	1.70	1.54
Laser	0	0.66	0.66	1.52	1.52
	5	0.56	0.64	1.32	1.54
	10	0.47	0.67	1.12	1.52
	15	0.39	0.66	0.95	1.50
	20	0.33	0.62	0.80	1.47
	25	0.27	0.56	0.67	1.39
	30	0.23	0.52	0.55	1.34
	35	0.20	-	0.48	-
	40	0.18	-	0.39	-
	45	0.15	-	0.30	-
	50	0.11	-	0.25	-
	55	0.09	-	0.20	-
Aorta [4]	60	0.06	-	0.19	-
	90	0.028	-	0.072	-
	120	0.013	-	0.034	-
	150	0.006	-	0.015	-
Gauss line [5]	180	0.003	-	0.008	-

[4] The aorta position was measured at 68 cm from the laser.
[5] The gauss line was measured at 188 cm from the laser.

Figure 6.2 B_0 gradient field map along the z-axis

(a) 1.5 T

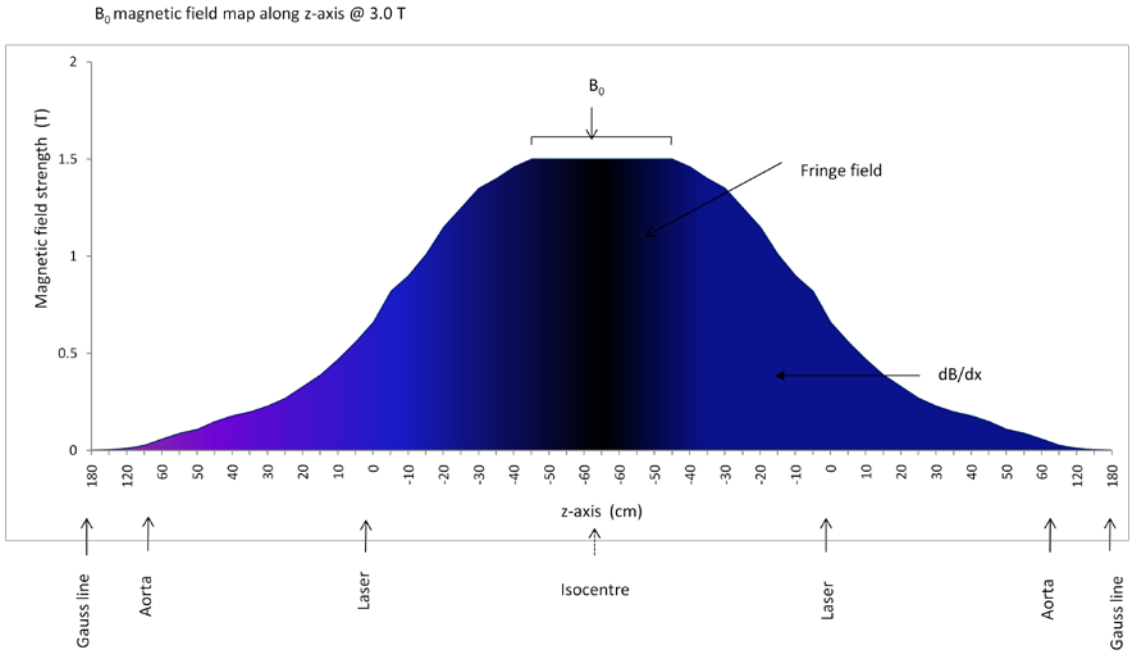

(b) 3.0 T

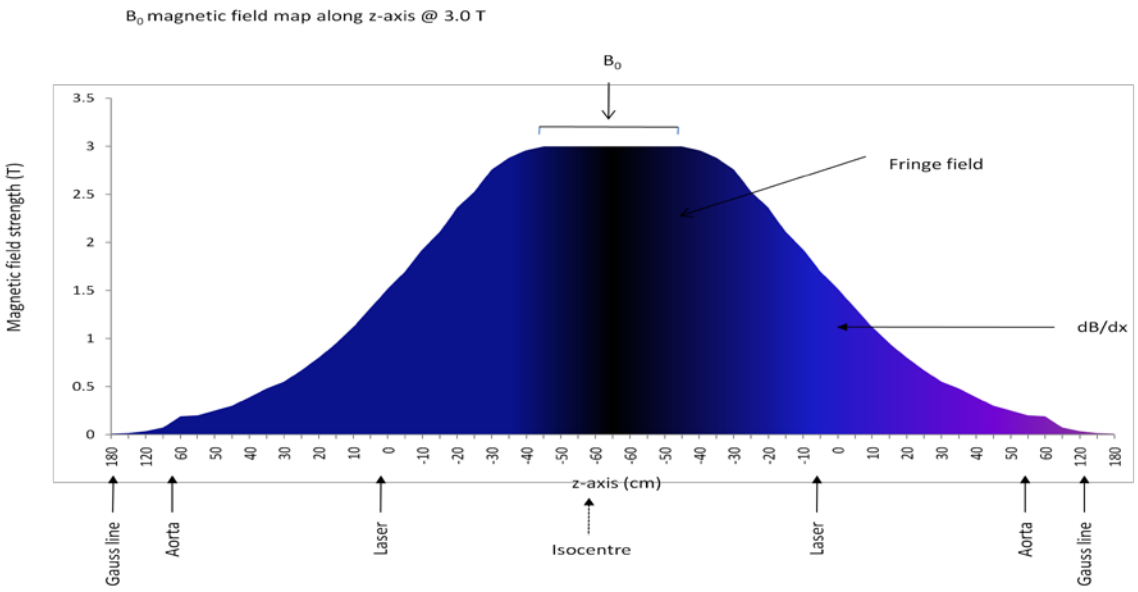

6.6 Baseline measurements

Baseline measurements, taken as part of the experimental test procedure to determine whether the test apparatus interacted with the magnetic field environment are presented in this next section. Data recorded for the static measurements of the test apparatus taken at the four points along the z-axis are presented in tabular format for entry and exit measurements by paired channels at both field strengths. Results are presented in both units of μstrain and Newton force to allow for comparison with previous studies. The second set of baseline measurements refer to the dynamic exposure of the test apparatus to the magnetic fields of the 1.5 T and 3.0 T MR systems as it was continuously advanced from the gauss line to the iso-centre and back. Measurements were recorded as the test apparatus passed through each of the four points on the z-axis on entry to and exit from the magnet.

6.6.1 Static test measurements

Table 10 presents the static baseline measurements recorded by the strain gauge apparatus as the test apparatus was placed incrementally at the four points on the z-axis in both MR environments. Overall, the measurements recorded are fairly uniform in both field environments. Some variation in entry and exit measurements has been recorded but, as the Table shows these are very small and likely to reflect expected 'noise' resulting from varying magnetic fields in the area enclosed by the signal circuit rather than actual movement of the test apparatus or, as previously mentioned possible differences in the sensitivity of the transducers.

Table 10 Static baseline measurements along the z-axis

	Force (μstrain)					Force (Nwt)			
Field strength	**N-S axis**		**W-E axis**			**N-S axis**		**W-E axis**	
	Ch 1	**Ch3**	**Ch 2**	**Ch4**		**Ch 1**	**Ch3**	**Ch 2**	**Ch4**
1.5T									
Gauss line entry	1	0	1	1		0.00	0.02	-0.02	0.01
Gauss line exit	1	0	1	1		0.00	0.02	-0.02	0.01
Aorta entry	1	1	1	1		0.00	0.00	-0.02	0.00
Aorta exit	2	1	0	2		-0.01	0.00	-0.01	0.00
Laser entry	3	1	2	2		-0.01	0.00	-0.03	-0.01
Laser exit	2	1	2	1		-0.01	0.00	-0.03	0.00
Centre	2	1	1	1		-0.01	0.00	-0.02	0.00
3.0T									
Gauss line entry	-2	0	-1	-1		0.04	0.02	0.00	0.03
Gauss line exit	-1	2	0	1		0.03	-0.02	-0.02	0.01
Aorta entry	-1	1	-1	-1		0.03	0.01	0.00	0.04
Aorta exit	-1	0	-3	-3		0.03	0.02	0.02	0.05
Laser entry	1	2	-2	2		0.01	-0.01	0.01	-0.01
Laser exit	0	0	-1	-1		0.02	0.02	0.00	0.04
Centre	0	2	0	2		0.02	-0.01	-0.01	-0.01

6.6.2 Dynamic test measurements

Figure 6.3 presents the profile for the baseline measurements recorded as the test apparatus moved continuously through the B_0 field along the z-axis of the 1.5 T and 3.0 T MR systems. As before the measurements were initially recorded in μstrain and converted into force in Newtons. The first set of paired profiles presented in Figure 6.3 presents the raw data recorded in μstrain at 1.5 T and 3.0 T respectively (Figure 6.3a, b, e, f). The subsequent sets of profiles show the converted raw data from μstrain to Newton force (Figure 6.3c, d, g, h). As the Figures show the profiles representing the raw data for the two field strengths are largely similar to their respective converted data graphs but in reverse. This 'mirror image' effect is thought to result from the calibrated spring balance being applied in two directions; forward and reverse pull [58] (see Chapter 5). Although as previously mentioned the somewhat unexpected variation displayed by Channel 2 is likely to reflect potential differences in the sensitivity of the transducers which have resulted in the larger variation in magnitude of oscillations shown.

The profiles show some movement of the test apparatus was detected by the strain gauges as the test rig continuously moved through the B_0 fields particularly at the higher field strength and, across Channels 2 & 4 (W-E axis). At 1.5 T little or no movement of the test apparatus within the field was detected across the N-S axis (Channels 1 & 3) and variations in the oscillations shown in Figure 6.3b/d are predominantly in Channel 2 (E). However, for reasons already mentioned movements recorded by this strain gauge may be subject to greater error and thus, caution needs to be observed when reviewing the profile representing Channel 2 although, experimental data has been adjusted for baseline measurements. Nevertheless, at 3.0 T as Figure 6.3e-h shows the increase in the frequency of oscillations across all four channels in comparison suggests some interaction of the

[58] Forward pull of the spring balance is a pull/deflection away from the strain gauge. A reverse pull is a pull of the spring balance inwards/towards the strain gauge.

test apparatus with the magnetic field at this strength. Movement of the test apparatus was confined primarily to the magnet ie. between the laser on entry to and exit from the magnet although, these movements were not confined to B_0 field only. The uni-directional profile of the oscillations across all four channels suggests overall the apparatus was subjected to a deflective force causing an upward/downward movement as described in Figure 5.8③. However, as the apparatus moved towards the laser on exit from the magnet the applied force caused a different response to that just described. As the profile shows on entry to the magnet diametrically opposing oscillations across all four channels suggest the force was acting upon the strain gauge apparatus in an S-E direction. However, as the apparatus exited the magnet this force was reversed to a N-E direction although, the uni-directional profile across the N-S-W axis indicates a force pushing down against the strain gauges across this plane.

Although these baseline measurements show some interaction of the test apparatus with the magnetic field they allow for the experimental data to be adjusted accordingly. Furthermore, the calculated rate of error determined the accuracy for this apparatus to be ±0.1. When this is compared with the recorded rate of error for the previous designs of the equipment used to detect movement of heart valves within MR associated magnetic fields (please refer to Part I of this Chapter) this shows an improvement in the accuracy rate for this test equipment.

Figure 6.3 Baseline measurements for *ex vivo* test apparatus

@ 1.5 T

Raw data

(a) (b)

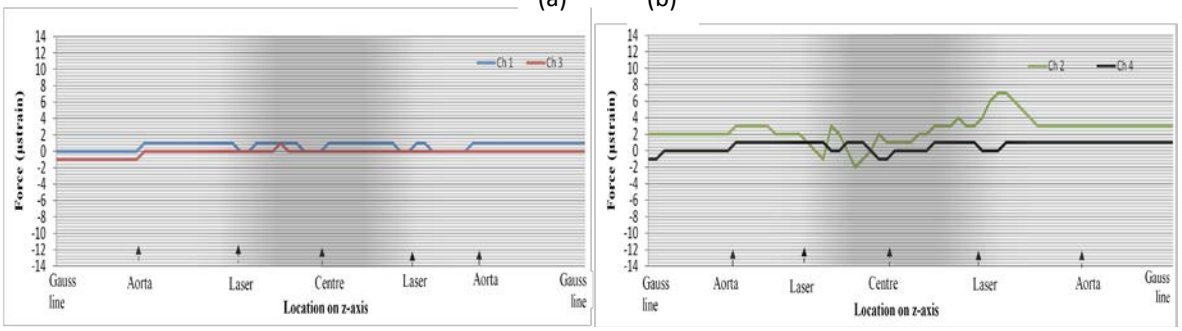

Converted data

(c) (d)

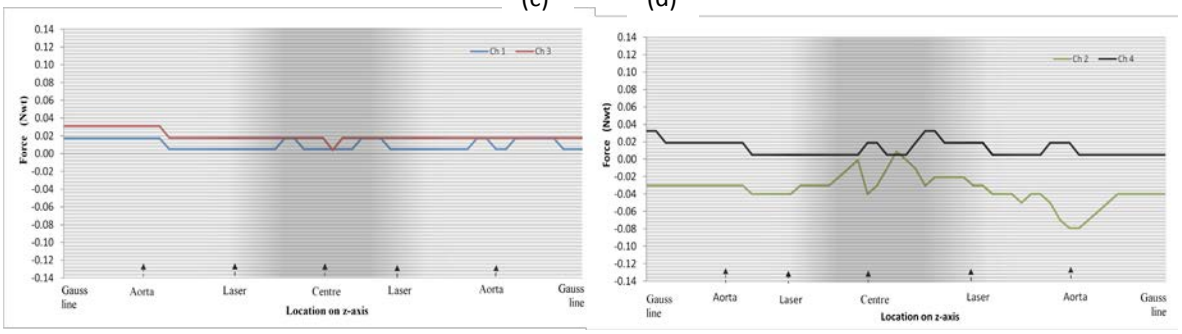

@ 3.0 T

Raw data

(e) (f)

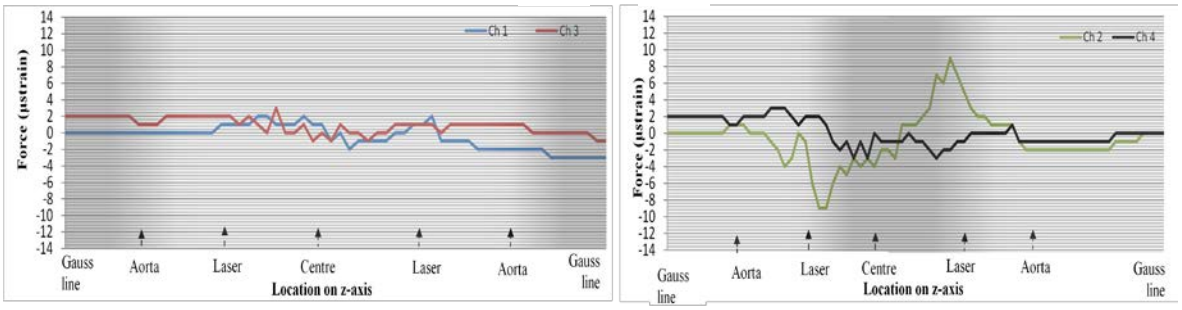

Converted data

(g) (h)

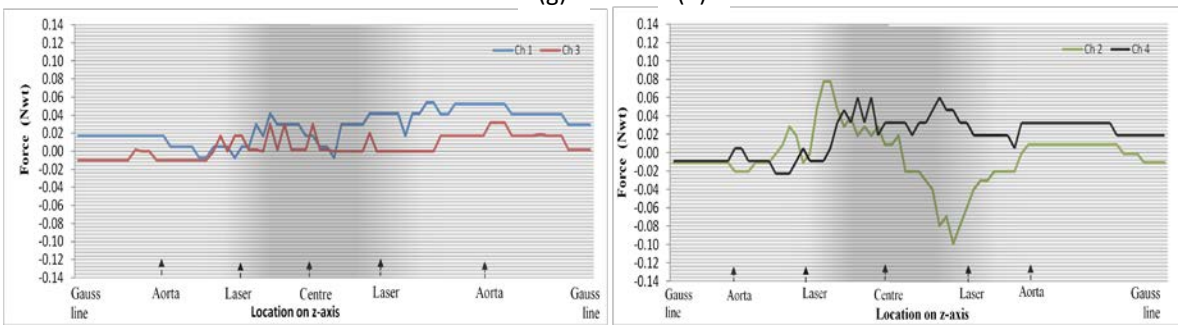

Part III

Experimental valve data

6.7 Magnetic field interactions with prosthetic heart valves

The next section of this Chapter focuses on the results of the experimental procedure to assess the potential interaction of the heart valve prostheses with magnetic fields associated with 1.5 T and 3.0 T. All experimental test data has been adjusted for baseline measurements to compensate for any valve independent effects and are thus reported accordingly. Furthermore, although the graphs show both the raw and converted data the results are discussed in terms of Newton force rather than μstrain for the reasons cited previously (please refer to Chapter 5 for conversion method). The section begins with an overall summary of the static and dynamic [59] measurements recorded e*x vivo*. Data are then presented separately for each of the valve prostheses detailing the movement of the valve in terms of frequency, magnitude and direction of movements detected in response to B_0 field.

6.7.1 Summary of field interactions with heart valve prostheses

Figures 6.4 – 6.12 show the results of the static and dynamic measurements recorded for each prosthetic heart valve exposed to both magnetic field environments. The data shows all nine heart valves interacted with both the 1.5 T and 3.0 T B_0 fields and displayed differences between the static and dynamic measurements at the same locations on the z-axis as well as different entry and exit profiles. Furthermore, there

[59] Static measurements in the ex vivo experimental test refers to stationary measurements recorded at (a) gauss line, (b) aorta position (ie. 68 cm from laser and outside the magnet), (c) laser and (d) iso-centre. The dynamic measurements refer to measurements recorded during continuous movement of the test apparatus ± heart valve prosthesis through these points on the z-axis (ie. from the gauss line to the iso-centre and back).

was no commonality between the valve groups or sub-groups in terms of frequency, magnitude, pattern or direction of oscillations.

6.7.2 Individual prosthetic valve results

The following figures (Figures 6.4 – 6.12) present the profiles of movements detected for each heart valve within two different MR associated magnetic fields. The data are presented in a series of three sets of paired profiles for each valve at both field strengths. The first pair of profiles labelled a, b and g, h refers to the raw data measured in μstrain. The second set of profiles labelled c, d and i, j refers to the raw data converted from force measured in μstrain to force measured in Newtons (see Chapter 5). The third and final set of profiles labelled e,f and k, l include both static and dynamic measurements and have been adjusted for the baseline data. Although the results are presented in this way all descriptions and discussions refer to the adjusted profiles only. Furthermore, for reasons already mentioned, any forces resulting in movement of the valve are described in Newton force.

(a) Björk Shiley valve

The response of the Björk Shiley valve to exposure to the B_0 fields of the 1.5 T and 3.0 T MR systems are displayed in Figure 6.4. Overall, the data show two very different profiles in terms of frequency, magnitude and pattern of movements detected as well as differences in the static compared with dynamic measurements recorded. Very little movement of the valve was detected at 1.5 T and these were confined to between the laser and iso-centre as the valve entered the magnet and, at the laser and aorta positions on the return journey from the iso-centre. Furthermore, there was greater movement detected along the W-E axis of the valve. In addition, Figure 6.4e-f shows a marked deviation in static measurements from the dynamic profile along the N-S axis compared with the W-E axis at the laser (entry) and iso-centre but vice versa between the aorta and gauss line on the return from the magnet. All other static measurements recorded more-

or-less corresponded with the dynamic profile measurements. In contrast, there was a conspicuous increase in the frequency and magnitude of oscillations displayed at 3.0 T and differences in the type of movement detected. The frequency of movements detected at this higher field strength however, was similar across both the N-S and W-E axes. Moreover, static measurements corresponded more closely to the dynamic profile on the N-S axis compared to those at 1.5 T although, those measured on the W-E axis consistently displayed a greater deviation from the dynamic profile in comparison.

At 1.5 T no movement of the valve was detected between the gauss line and aorta positions on the N-S axis and very little along the W-E axis. As Figure 6.4e-f shows the first movements detected for this single leaflet valve occurred at the aorta position as the valve moved towards the magnet. The uni-directional path of the oscillations suggests the valve was subjected to a deflective force causing the valve annulus to move downwards and press against the valve holder. This was seen more prominently in Channel 2 (E) which may also have coincided with an attempt by the valve ring to rotate away from the magnet. As the valve progressed along the z-axis and moved through a rapidly increasing gradient to homogeneous field a small series of plateau type oscillations can be seen in Figure 6.4e between the laser point and iso-centre. The pattern of oscillations, particularly those in Channels 2 & 3 suggest a tilting motion of the valve occurred along the S-E axis which continued until the valve began its return from the iso-centre at which point a change in orientation was noted and it rotated around the N-E-W arc. As the valve passed through the laser it underwent a rapid change in its orientation and this coincided with a deflective movement downwards as the valve ring was pushed against the valve holder. Movement of the valve continued to be detected as it advanced through the aorta position on the return to the gauss line and continued to tilt around the N-E-W arc. The overall pattern of oscillations displayed in this profile at 1.5 T suggests the flat plane of the valve ring was tilted away from the magnet and the B_0 field throughout its journey.

Comparison of the static and dynamic profiles at 1.5 T show static measurements on the N-S axis corresponded with the dynamic profile outside the magnet but, the reverse was true within the magnet particularly on entry from the laser to the iso-centre. On exit from the magnet at the laser position this deviation became less marked. In contrast, static and dynamic measurements on the W-E axis at each of the four locations along the z-axis between the gauss line on the approach to and, the laser position on the return from the magnet were more-or-less consistent with each other. However, between the aorta and gauss line following exit from the magnet Figure 6.4e-f shows a larger difference between these two types of measurement was recorded in Channel 2 (E). Nonetheless, despite differences between the static and dynamic profiles the overall profile for static measurements at each of the four points on the z-axis show little or no difference between entry and return measurements.

At 3.0 T the overall profile is dominated by a combination of deflective upward/downward movements of the valve, as those described by Figure 5.8 Chapter 5, and a similar frequency of movements across all four channels in contrast to its exposure to the 1.5 T MR field (Figure 6.4k-l). Little movement of the valve was detected between the gauss line and aorta positions as the valve moved towards the magnet. However, as with 1.5 T the first significant movement of the Björk Shiley valve was detected at the aorta position. In contrast to the movement at 1.5 T this movement however, was an upward deflection such that the valve annulus moved away from the valve holder as illustrated by the uni-directional movement of the oscillations across all four channels. Furthermore, the magnitude of the oscillation representing Channel 2 (E) suggests the valve may have also been subjected to a tilting movement as it attempted to rotate away from the magnet. This movement was followed by a tilt on the N-S axis and successive deflection of the valve in a downward direction which continued as the valve progressed through the increasing magnetic field from the aorta to laser position. At the laser point the valve's orientation along the N-S axis changed such that the tilt was on the S-E axis. Immediately after the valve moved through the laser however, a switch in

the W-E orientation occurred as the valve rotated around its northern plane to rest on a N-W tilt before changing again at the boundary of the dB/dx and B_0 field.

Movement of the valve at the iso-centre was marked by a very distinct uni-directional oscillation in three out of the four channels. This pattern of movement suggests the valve was subjected to strong downwards deflection causing the flat plane of the valve ring to attempt to rotate parallel to the direction of the field. As the valve moved across the boundary of dB/dx and B_0 field and continued to move through a decreasing magnetic field towards the aorta and gauss line it continued to be subjected to upward/downward deflective movements as well as a S-W tilt. Static measurements recorded at 3.0 T as previously mentioned, corresponded more closely with the dynamic measurements at the same points on the z-axis along the N-S axis compared with those on the W-E axis. Nonetheless, despite these greater deviations from the dynamic profile on this axis comparison of the entry/return measurements across all four channels shows an overall consistency in measurements in Channels 2 (E) and 3 (S) but, marked differences in Channels 1 (N) and 4 (W).

Figure 6.4 Björk Shiley valve

@ 1.5 T

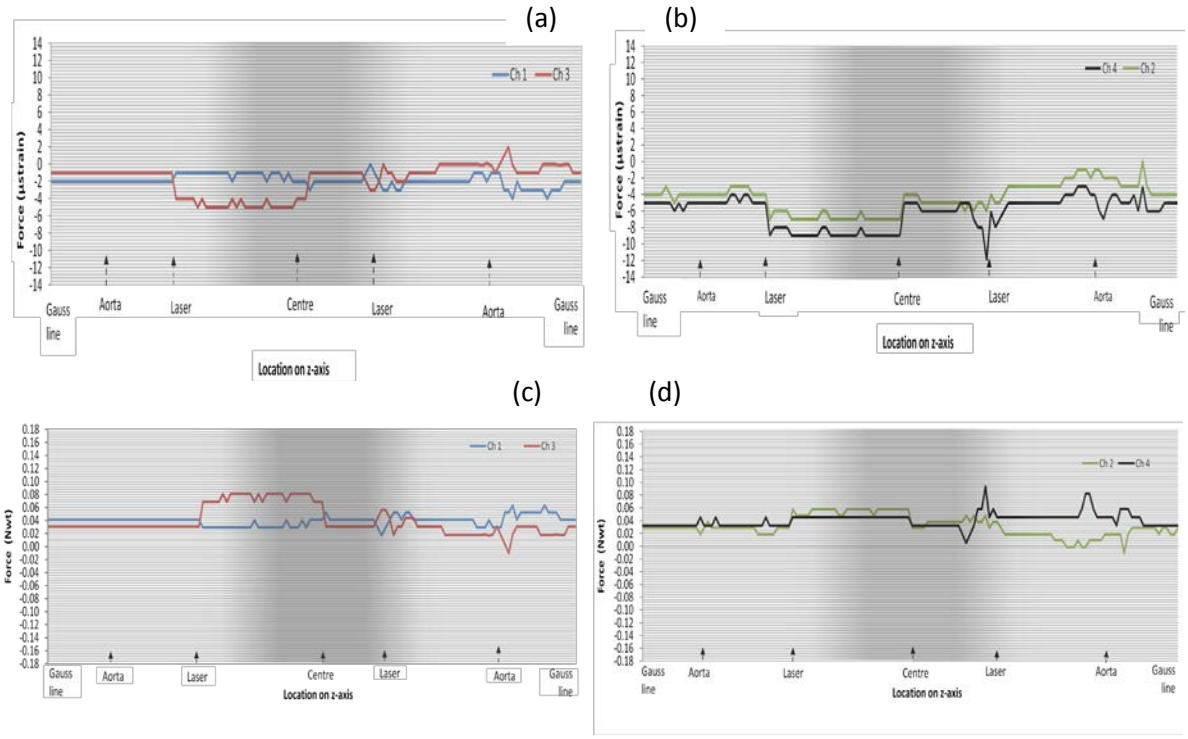

Adjusted for baseline data

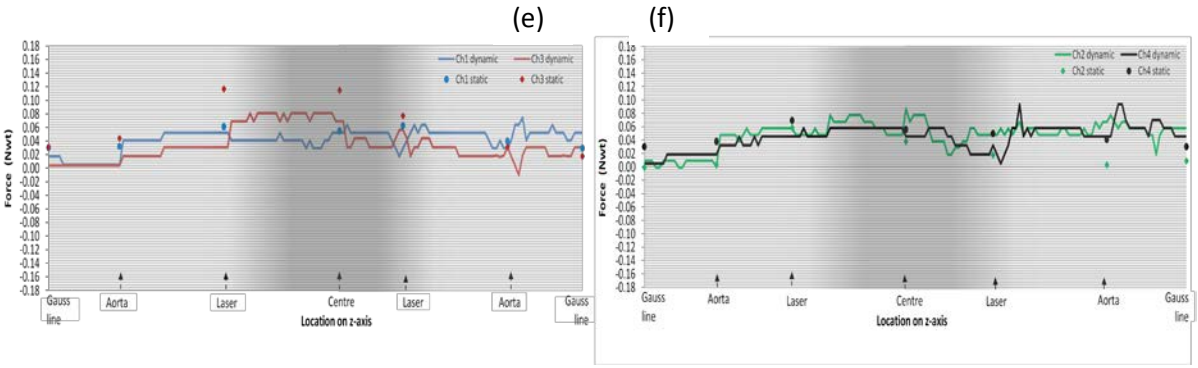

@ 3.0 T

(g)

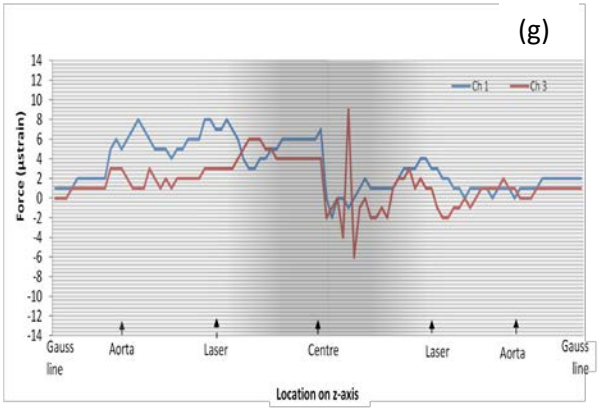

(h)

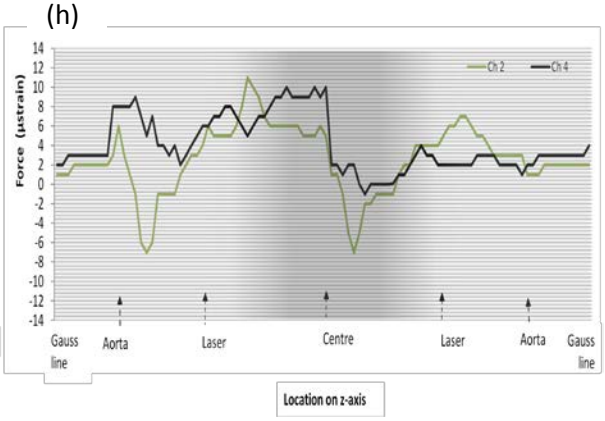

(i)

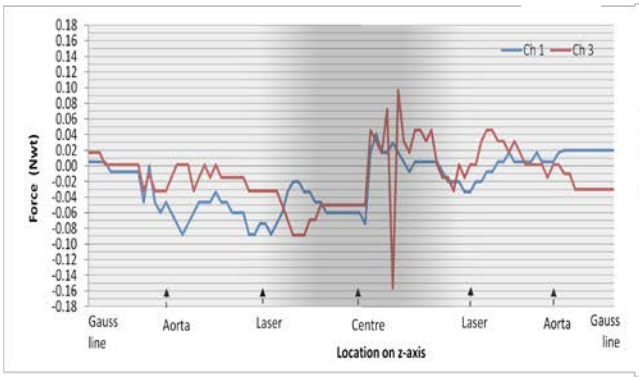

(j)

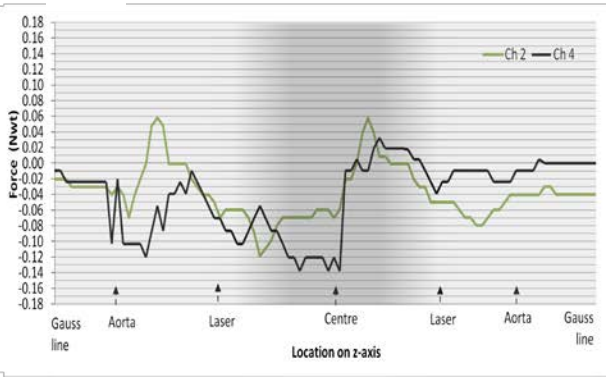

Adjusted for baseline data

(k)

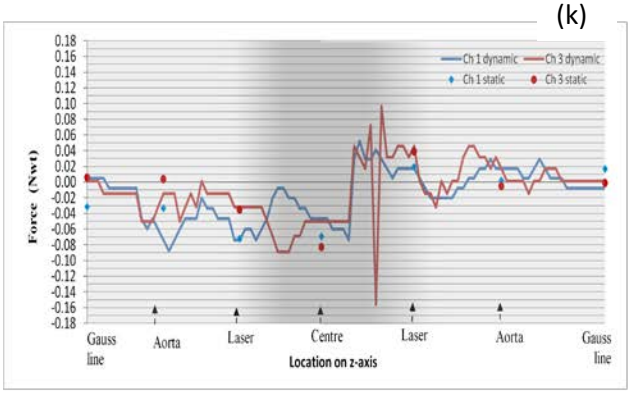

(l)

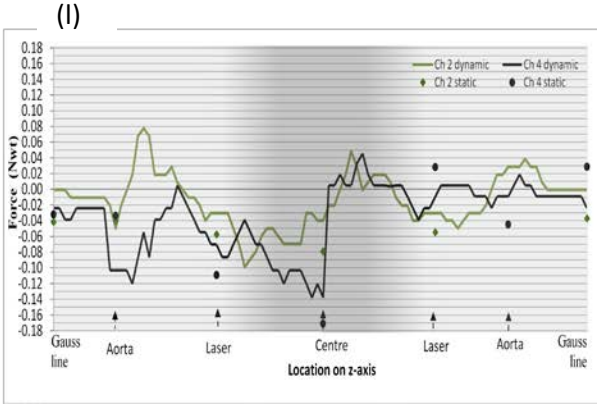

(b) Carpentier Edwards pericardial valve

Figure 6.5 shows two very different profiles representing detected movements of the only pericardial tissue valve included in this study. A greater frequency of movements were detected at 1.5 T compared with exposure of the valve at 3.0 T and movement was detected at an earlier point on the z-axis in the lower strength field. Furthermore, the type of movements recorded also differed compared with those at the higher field strength. At 1.5 T movements were predominantly deflective in an upwards/downwards direction along the x-y axis and as illustrated in Figures 5.8 ③ & 5.14. However, at 3.0 T Figure 6.5k-l shows the pattern of diametrically opposing oscillations suggests the valve was subjected mainly to two relatively strong tilting movements in addition to some degree of deflection. The profile for static measurements corresponds to the dynamic measurements captured at the same positions on the z-axis for both axes (N-S/W-E) at 1.5 T and thus displays different entry and return measurements for each of the four locations. This pattern of measurements occurs in three out of the four channels (ie. Channels 1, 2 & 4 (N, E & W respectively) although, the differences are relatively minor. In contrast, measurements recorded at 3.0 T are consistently different from the dynamic profiles across all four channels. Furthermore, these differences also reflect differences in the entry and return measurements of the valve particularly at the gauss line and laser points.

The profile of oscillations displayed in Figure 6.5e-f represent movements detected in the Carpentier Edwards pericardial valve at 1.5 T. As the profile shows movement of the valve was first detected near the aorta position as the valve travelled from the gauss line towards the magnet. A deflective force was recorded in all four channels although this was stronger across the N-S-E plane. Nonetheless, the uni-directional profile of these oscillations suggests, as the valve passed through this point on the z-axis the valve ring was being pressed downwards into the valve-holder on the N-S-E plane and thus, away from the magnet. Few movements were detected thereafter in Channels 2, 3 and 4

(S, W, E) until the valve reached the iso-centre and homogeneous field. However, in contrast the frequency of oscillations displayed by Channel 1 suggests the valve was subjected to a constant 'fluctuation' type motion in this plane. At the iso-centre and on its return through the homogenous field the valve's orientation changed multiple times suggestive of a rotation around the S-W-E plane whilst at the same time being subjected to a deflective motion along the N-S axis similar to that described in Chapter 5 Figure 5.8①. This type of rotational movement continued until the valve reached the aorta position at which point a second downward movement occurred causing the valve's annulus to press against the valve holder as it tilted away from the magnet.

The main features of the profile at 3.0 T for the Carpentier Edwards pericardial valve are the deflective movement of the valve between the aorta and laser positions causing the valve annulus to be pressed downwards against the valve holder such that the stents were being pulled in the direction of the x-axis. This was followed by a large rotation on the N-S axis with a slight tilt on the eastern axis as the valve passed through the rapidly changing gradient field at the laser point and moved towards the iso-centre. Once in the homogeneous field however, the valve was no longer subjected to these changing forces and therefore resumed its status quo. However, as it returned from the iso-centre and proceeded through the laser point a second large N-W/S-E tilt was detected. The pattern and differential magnitude of these oscillations however, suggest the valve may have been subjected to a rotational force such that the plane of the valve's annulus was parallel to the y-axis. Subsequent to this movement a smaller tilting motion on the S-W axis was detected as it passed through the aorta position and decreasing magnetic field towards the gauss line. Thereafter, no further valve movements were recorded by the test apparatus.

Figure 6.5 Carpentier Edwards pericardial valve

@ 1.5 T

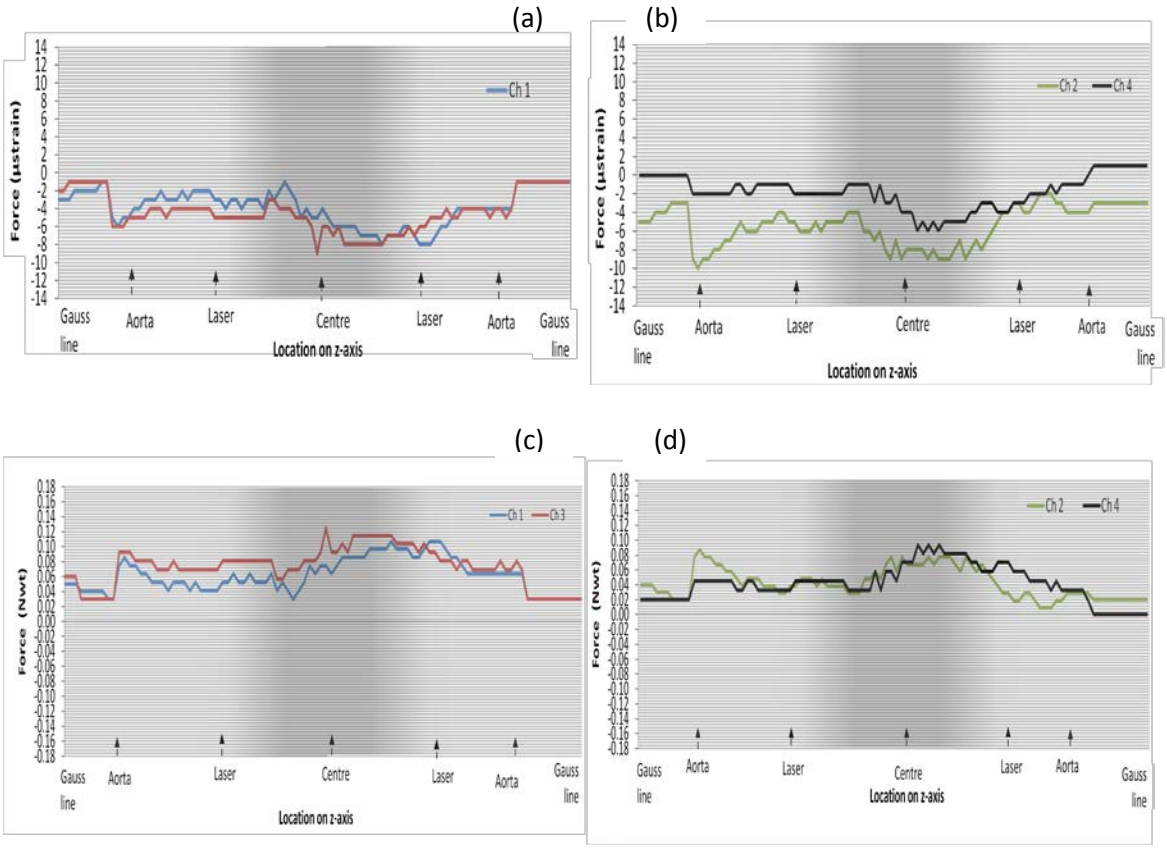

Adjusted for baseline data

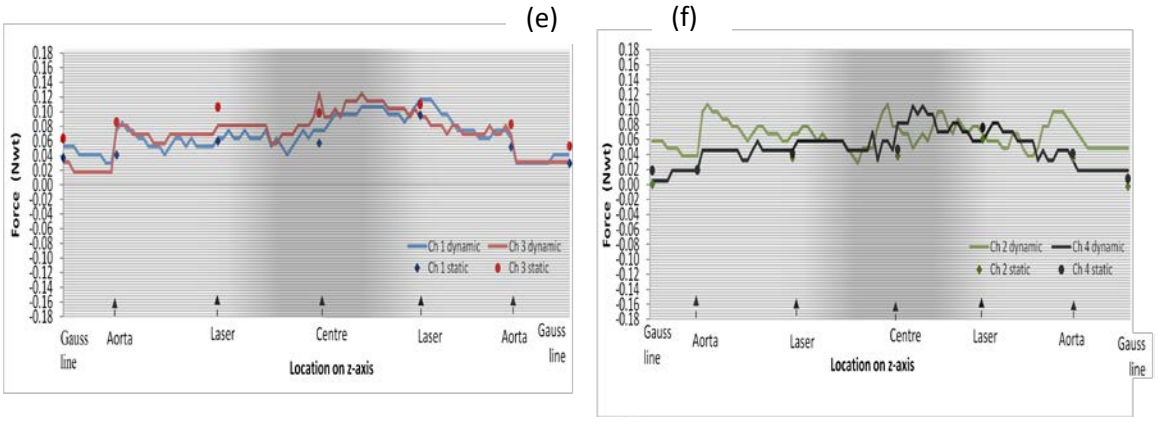

@ 3.0 T

(g)

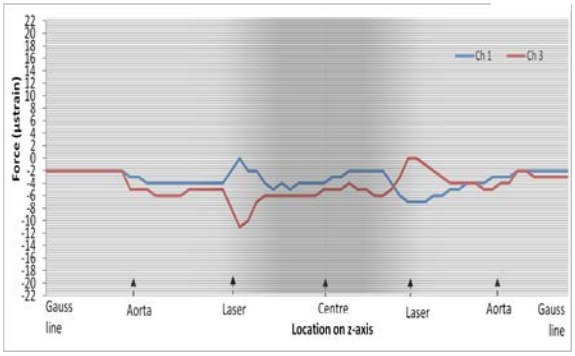

(h)

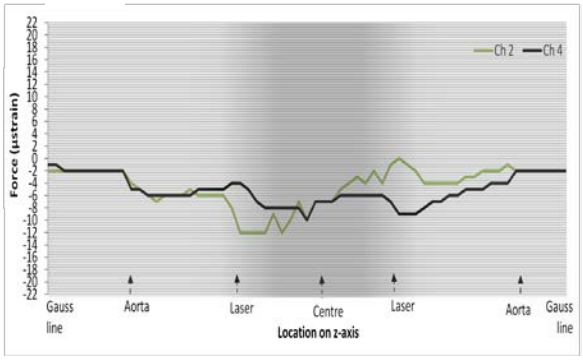

(i)

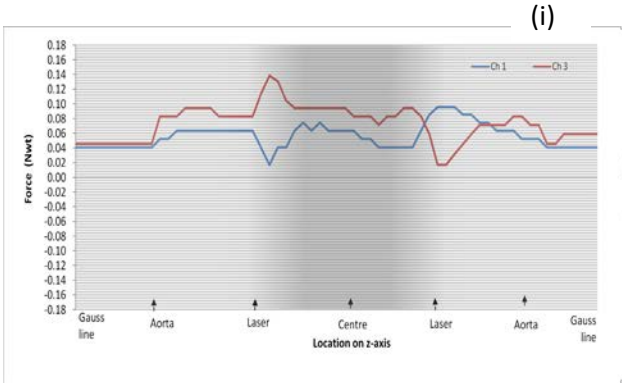

(j)

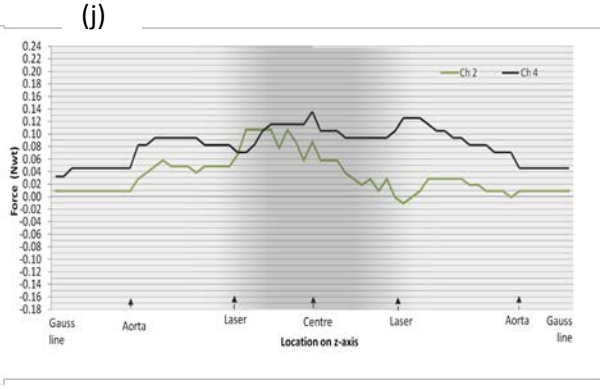

Adjusted for baseline data

(k)

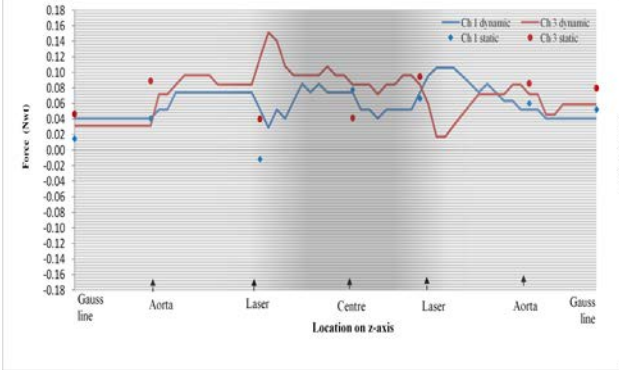

(l)

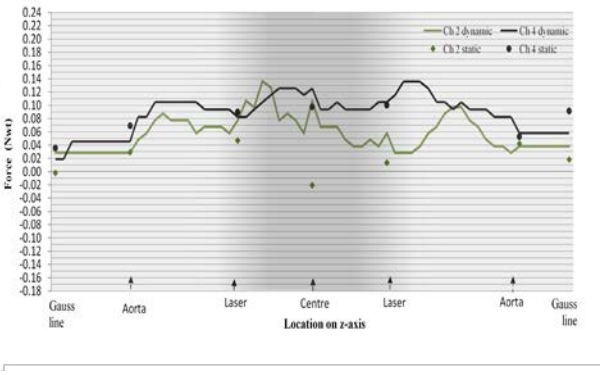

(c) Carpentier Edwards porcine valve

The first of the porcine tissue valves exposed to the experimental test procedure, the Carpentier Edwards supra-annular valve (Table 6/Figure 5.3) demonstrated different responses to exposure to the two different field strengths primarily on the W-E axis. Figure 6.6 shows that in both fields little movement in terms of frequency of valve movement was detected between the gauss line and the approximate boundary of dB/dx and B_0 field on entry to the magnet. However, on the return from the iso-centre the frequency of movements detected increased particularly in Channel 1. The profile at 1.5 T is dominated by the divergence of oscillations between the aorta on entry to and return from the magnet suggestive of a possible spin type/rotational movement (Figure 6.6f). However, movement of the valve was first detected at the aorta point. The upwards uni-directional oscillations across all four channels indicate the valve annulus was being pushed downwards against the valve holder along the x-axis and, this force continued to be applied to the valve until it began its return from the iso-centre. Between the iso-centre and laser point a second deflective movement of the valve occurred causing its annulus to be pressed upwards against the valve holder. However, this force was not sustained after the laser point on the return from the magnet. Nonetheless, the valve continued to rotate largely on the W-E axis but with a north-westerly tilt until it moved through the aorta position whereupon, a large deflective movement similar to that displayed at the entry aorta point in terms of direction and orientation and of similar magnitude was detected and recorded by the test apparatus.

Figure 6.6k-l displays the results of the exposure of the Carpentier Edwards porcine valve to the 3.0 T MR field. Overall, little or no movement of the valve was detected in either axes between the gauss line and boundary of dB/dx and B_0 field on entry to the magnet with the exception of a tilt around the N-E plane as the valve moved towards the magnet and passed through the aorta position. The direction of these oscillations suggests the valve's annulus was orientated slightly away from the magnet. As the valve crossed the boundary of dB/dx and B_0 field a change in its tilt along the N-S axis

occurred although, its orientation with respect to the magnet remained the same. As the valve began its return from the iso-centre and crossed the B_0 and dB/dx boundary it continued to tilt on its S-E axis but, as the oscillations show, it also underwent an upward/downward deflection similar to that described in Figure 5.8③. A change in orientation from N-W to N-E axis suggestive of a rotational movement around its N-W-E plane occurred as it progressed through the laser point and exited the magnet. Thereafter, although movement continued to be detected in Channel 1 as the valve moved further away from the magnet and closer to the gauss line no further movements were detected in any of the other three channels.

Comparison of the static with the dynamic profiles for this valve show some measure of difference between the two at both field strengths and across all four channels and, as Figure 6.6 shows these differences appeared more marked at the higher field strength. In addition, there were variations in the entry and return measurements recorded across channels, field strengths and different locations on the z-axis. For example, at 1.5 T differences in the entry and return measurements in Channels 2 (E) and 3 (S) were more marked at the aorta and laser points but similar measurements were recorded across all four points on the axis for Channels 1 (N) and 4 (W). However, at 3.0 T all four channels recorded inconsistent measurements between the entry and return journey of the valve. Channels 1, 2 & 3 for example displayed different entry and return measurements at the gauss line and laser position whilst Channel 2 (E) also demonstrated differences in the two measurements at the aorta position.

Figure 6.6 Carpentier Edwards porcine valve

@ 1.5 T

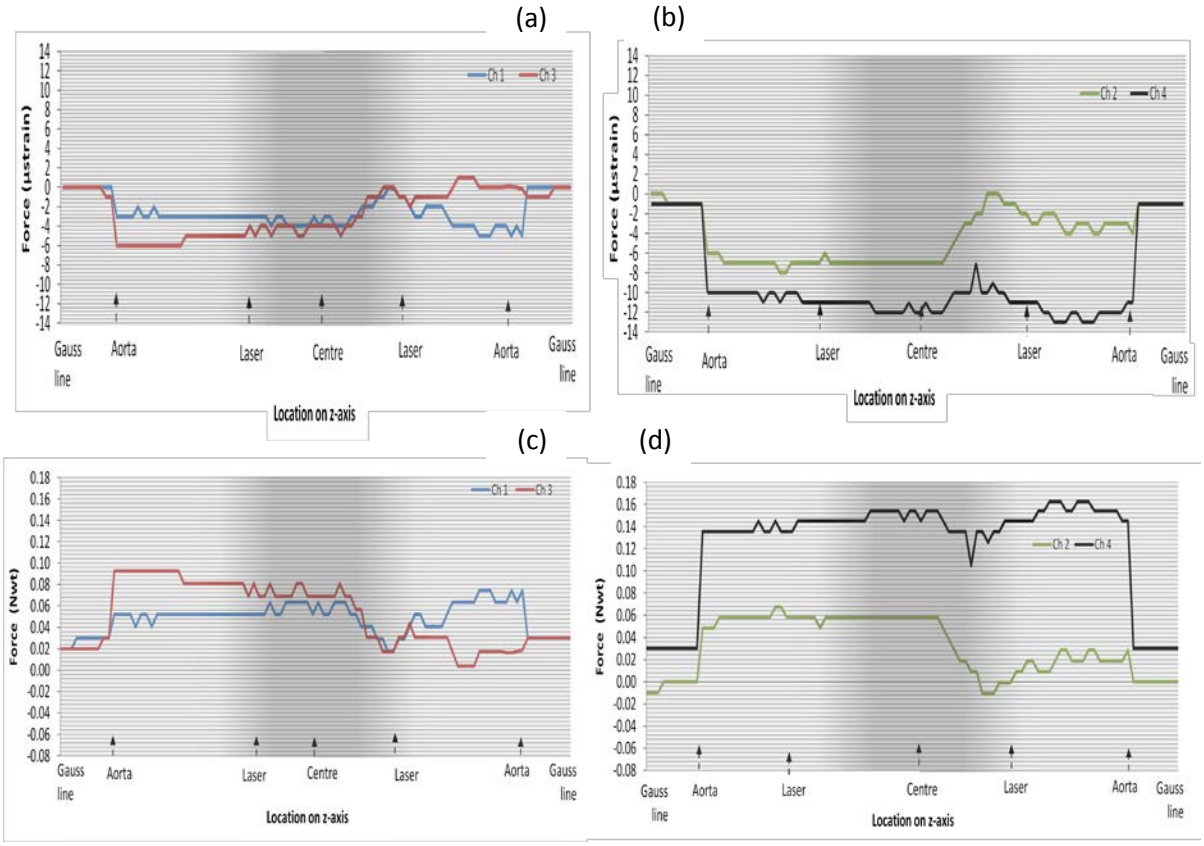

Adjusted for baseline data

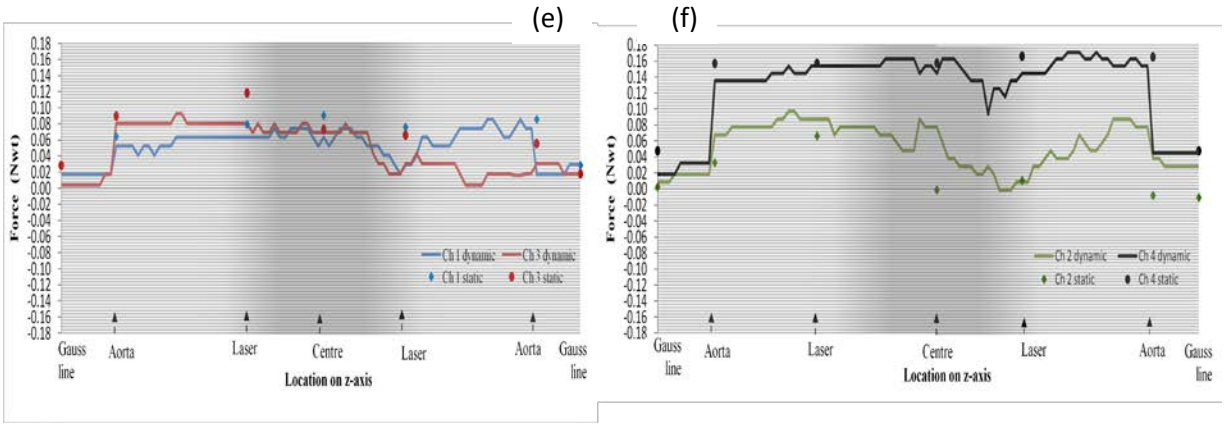

@ 3.0 T

(g)

(h)

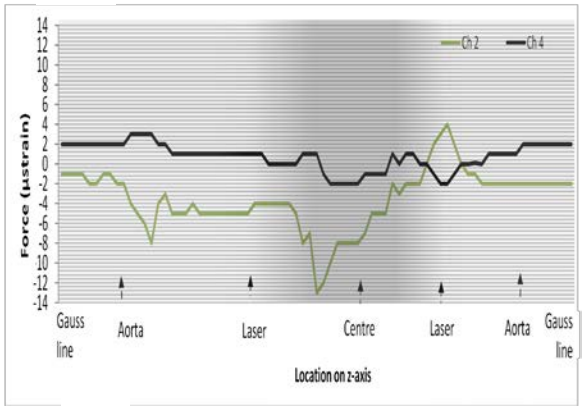

(i)

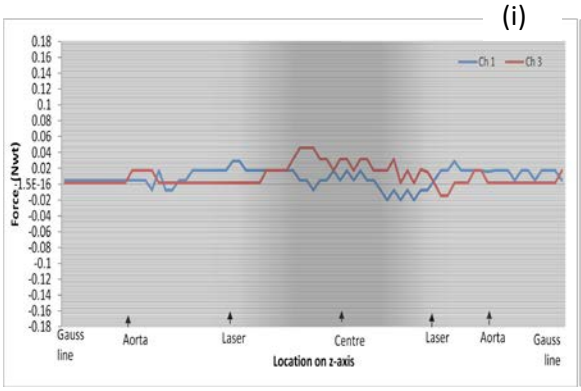

(j)

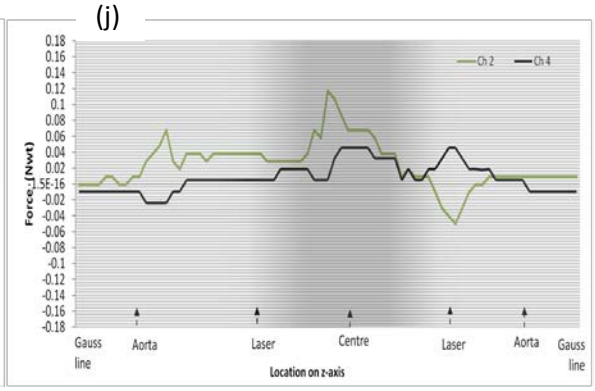

Adjusted for baseline data

(k)

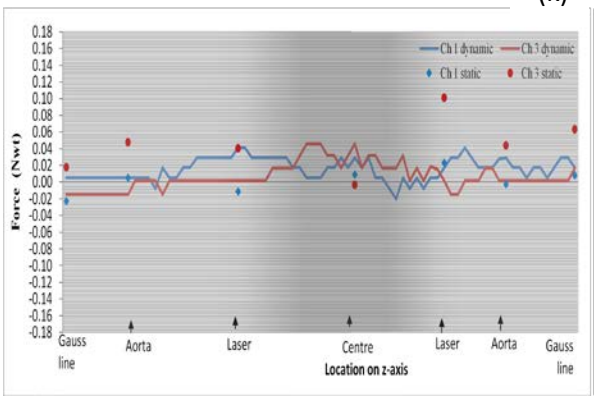

(l)

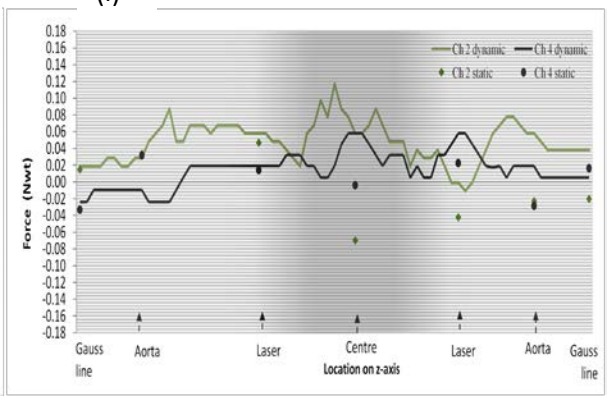

(d) Edwards Tekna valve

The predominant feature of the Edwards Tekna valve in response to exposure to magnetic field strengths of both MR systems is the similarity in the profiles of the N-S axis although, the magnitude of responses differed between the two as Figure 6.7 shows. Little movement of the valve was detected at either field strength between the gauss line and fringe of B_0 and dB/dx field until the valve's return from the iso-centre at either field strength along the N-S axis and, only after this point did the frequency of oscillations increase markedly. Some movement of the valve was detected from the laser point on entry to the magnet and the initial movement recorded was a downwards deflective movement which pushed the valve's annulus against the valve holder causing a tilt of the valve ring towards the magnet. This magnitude of the tilt increased causing a greater rotation of the valve along the S-W axis which then remained fairly static until the valve had passed through the iso-centre. As it returned and moved through the fringe of the B_0 and dB/dx field the tilt of the valve suggested the occurrence of a rotation around the W-S-E arc followed by a deflective movement away from the magnet as it exited the magnet. The S-E tilt of the valve away from the magnet was maintained as it moved towards the aorta. However, the increase in the magnitude of the tilt as it subsequently passed through the aorta suggests an even stronger rotation away from the magnet occurred. Thereafter, little significant movement of the valve was detected.

Similar to 1.5 T the first significant movement detected at 3.0 T was also a deflective movement. However, the movement differed in that it was detected at an earlier position on the z-axis and, the direction of the deflection was contrary to that displayed at 1.5 T (Figure 6.7k-l). An increase in the frequency of movements was recorded by the test apparatus as the valve began its return journey from the B_0 field and the iso-centre. The return journey was initiated by a large tilt on the N-S axis in conjunction with a switching of orientation along the W-E axis suggestive of a rotational movement around the W-E-S arc which decreased as it moved closer to

the exit of the magnet. However, there was an increase in this magnitude of movement as the valve approached the aorta position culminating in a rotational movement around the S-W-E arc and away from the magnet. Furthermore, the subsequent change in direction and magnitude of the oscillation representing Channel 1 (N) immediately after this rotation indicated a sudden rotation around the S-E-N arc. Thereafter, as the valve continued towards the gauss line the frequency of movement decreased significantly and no further movement was detectable on the S-E axis.

Differences between the static and dynamic measurements are also highlighted in Figure 6.7. Although these differences were common to both field strengths it was more marked at 3.0 T. Between the gauss line and laser locations consistently higher static measurements were recorded in comparison with dynamic measurements in all four channels at 1.5 T on entry to the magnet. Measurements recorded at the iso-centre were similar for both static and dynamic profiles and for Channel 4 on the return journey of the valve from the iso-centre to the aorta. Figure 6.7e-f shows the remaining three channels displayed some deviation of static measurements away from the dynamic profile on the return journey from the iso-centre and the pattern of deviations were different from the entry profile. Figure 6.7k-l shows the static and dynamic profiles at 3.0 T differ in terms of the N-S versus W-E axes. Static measurements recorded on the N-S axis for example closely corresponded with the dynamic profiles of their respective channels. However, in contrast those recorded by the W-E axis corresponded more closely with Channel 4 (W) only.

Figure 6.7 Edwards Tekna valve

@ 1.5 T

(a) (b)

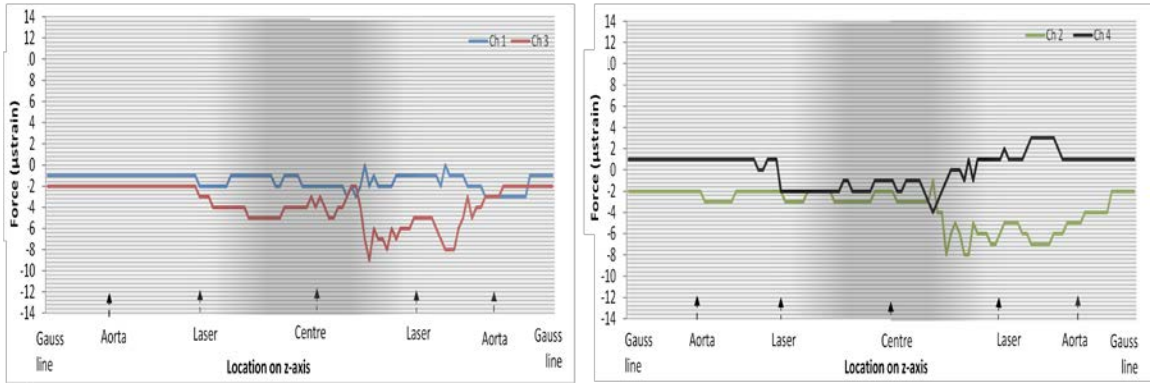

(c) (d)

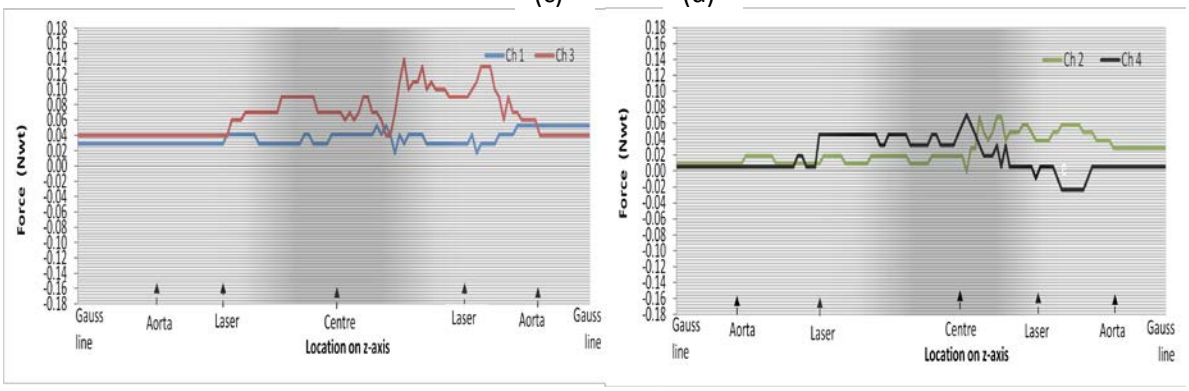

Adjusted for baseline data

(e) (f)

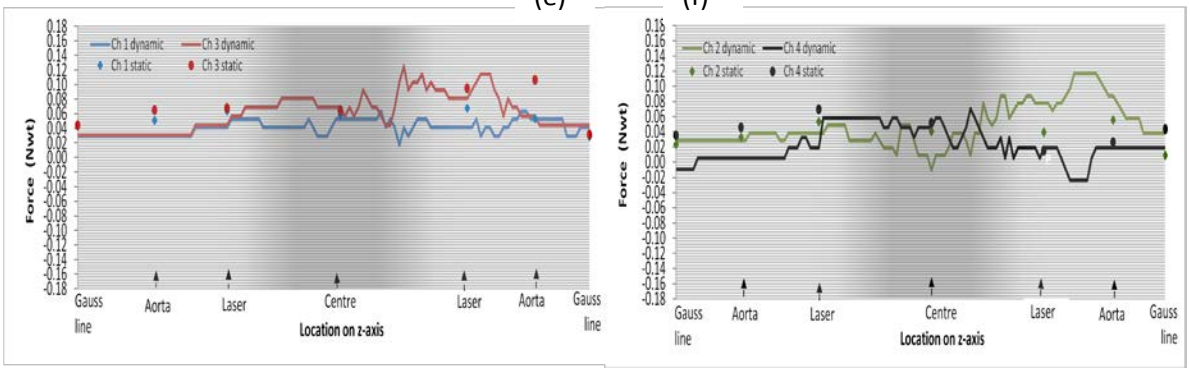

@ 3.0 T

(g)

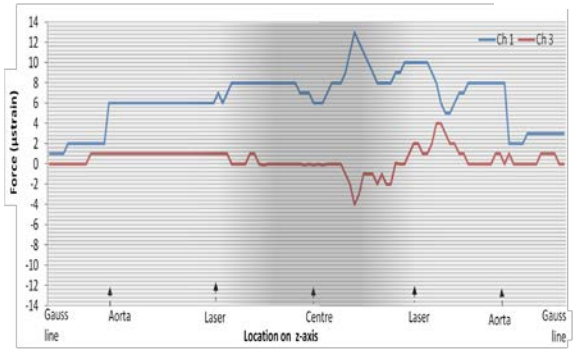

(h)

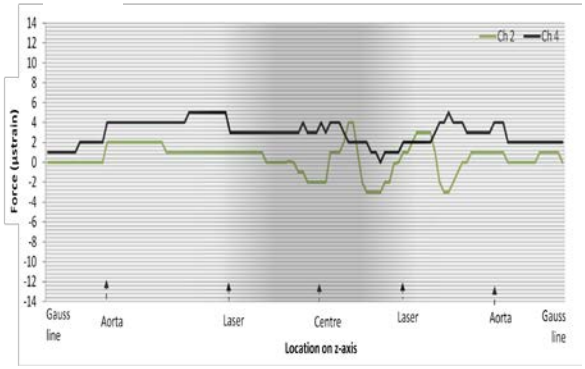

(i)

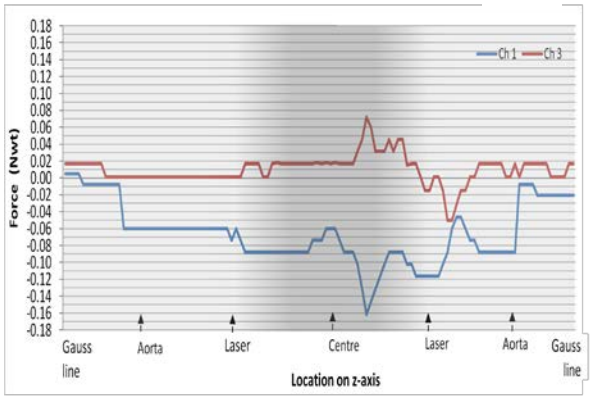

(j)

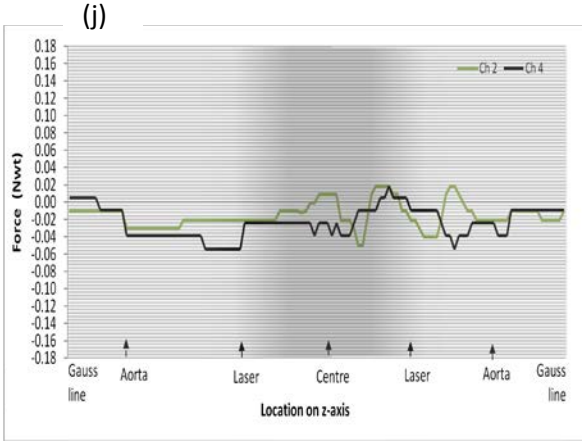

Adjusted for baseline data

(k)

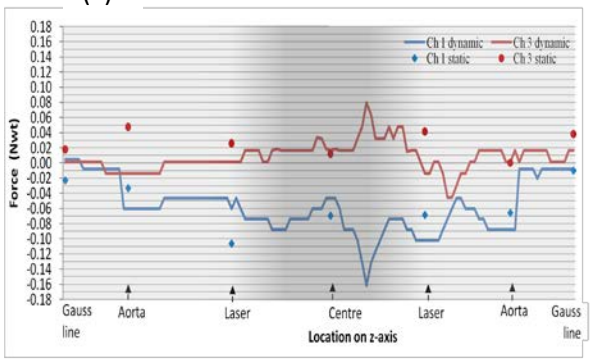

(l)

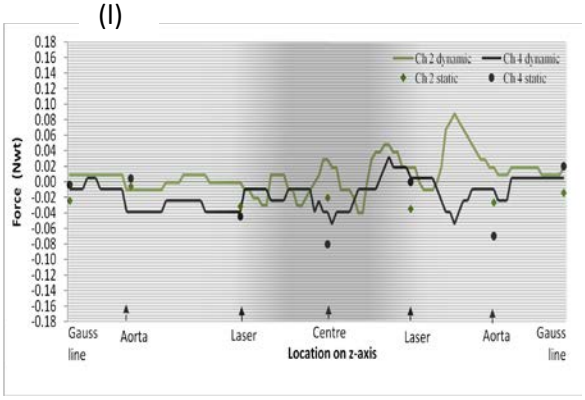

(e) Hancock II Modified Orifice valve

The Hancock II Modified Orifice valve was the second of the two porcine tissue valves subjected to the *ex vivo* test procedure. The profiles of the valve for the two field strengths show no commonality in terms of the shape, frequency or magnitude of oscillations although, there was some similarity with regards to position on the z-axis at which movement was first recorded on the N-S axis and the two deflective movements, one at the laser on entry to the magnet and the second at the aorta following exit from the magnet. Similarities between the static and dynamic profiles were also noted but these occurred at 1.5 T and predominantly on the W-E axis although, there were some differences between the two profiles on the N-S axis. At 3.0 T marked differences between the profiles was however noted. As Figure 6.8k-l shows between the aorta on entry to and return from the magnet there was a marked deviation of the static measurements from the dynamic profile for all four channels. In addition, differences between the static measurements are displayed at the gauss line, aorta and laser consistent with the dynamic profile.

Overall, at 1.5 T Figure 6.8e-f shows very little movement of the valve was detected. A downwards movement of the valve against the valve holder occurred at the laser point on entry to the magnet and is signified by the uni-directional profile of the oscillations corresponding to the four channels. Thereafter however, although some rotational movements around the W-N-E arc the profile of movement suggests movement of the valve was confined predominantly to a tilting motion along the W-E axis between the iso-centre and aorta point on the return journey. A second deflective movement was detected at the aorta point of the z-axis as the valve's annulus was pushed away from the valve holder after which no further movement was detected at this field strength. A greater frequency of valve movement was recorded by the test apparatus at 3.0 T on the W-E axis compared with the N-S axis. Movement on this axis was, as Figure 6.8k-l shows, restricted to the homogeneous field and the exit field near to the laser. On the approach to the magnet the valve's

orientation was mainly on its N-E axis and tilted towards the lesser field (E). At the boundary of dB/dx and B_0 field however, the valve's orientation switched backwards and forwards between the N-E/S-W axes before being maintained on the S-W axis until its exit from the magnet at which time, a large rotational movement was recorded. Following this no other significant movements were detected.

Figure 6.8 Hancock II Modified Orifice valve

@ 1.5 T

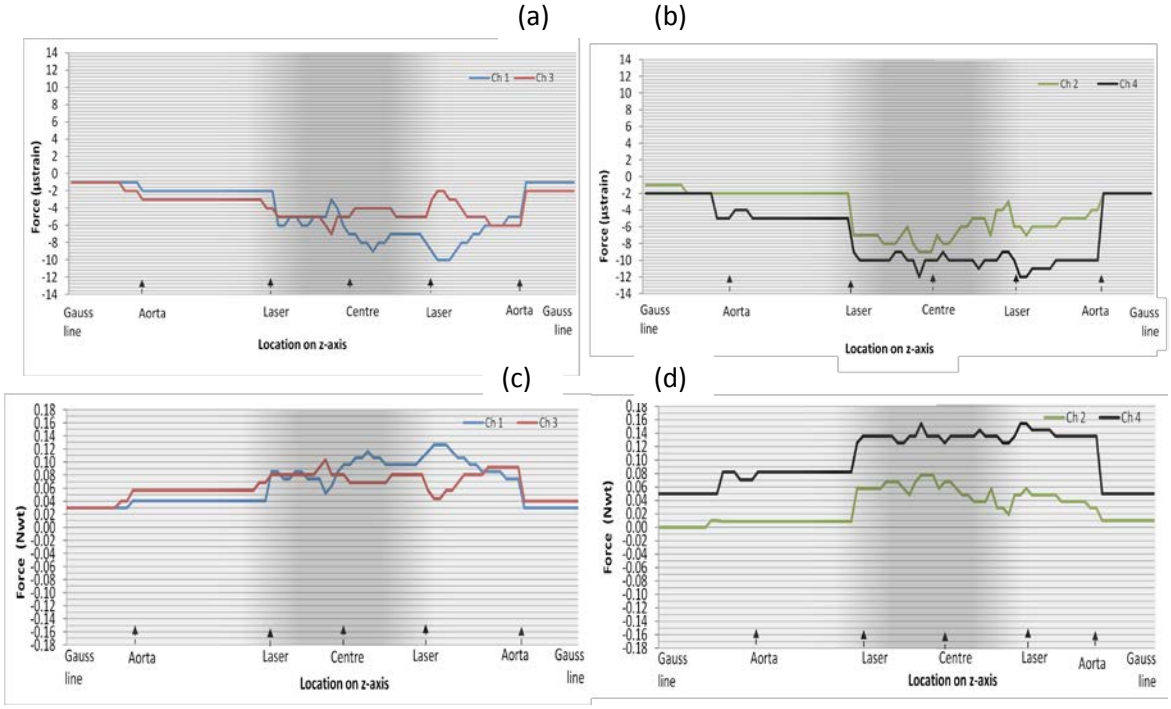

Adjusted for baseline data

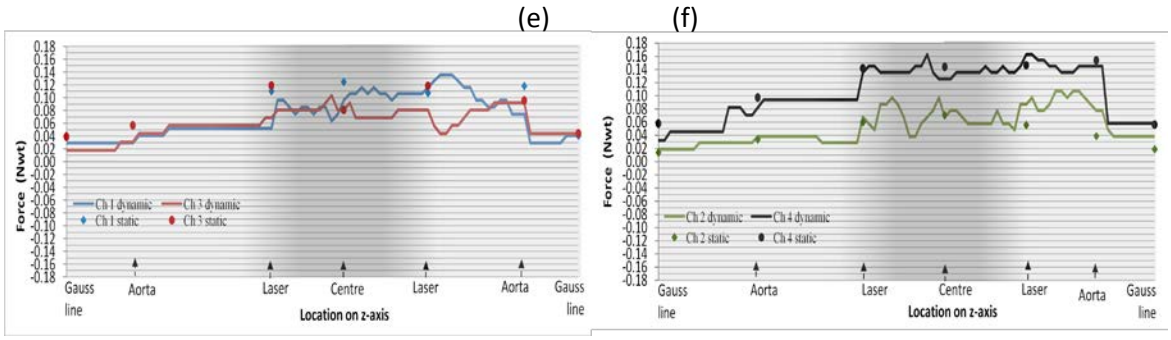

@ 3.0 T

(g)

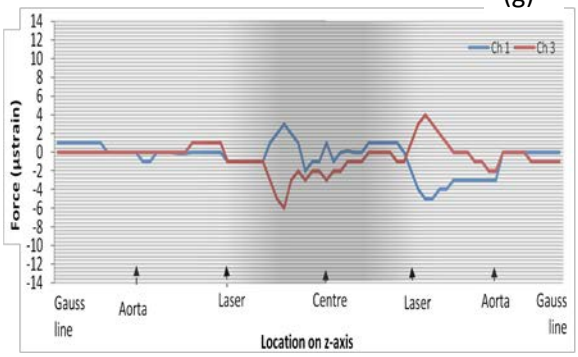

(h)

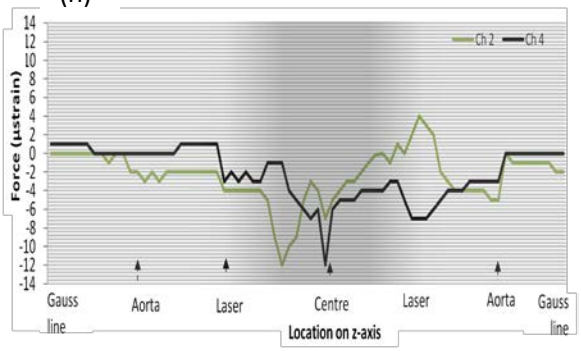

(i)

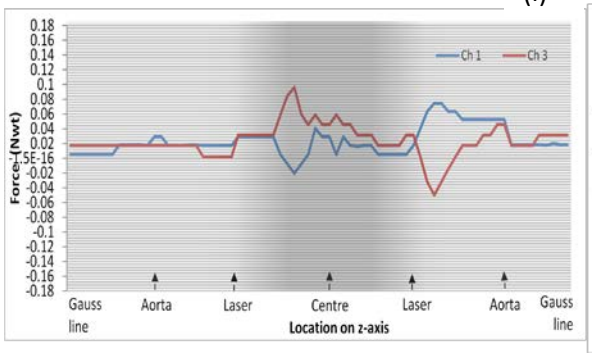

(j)

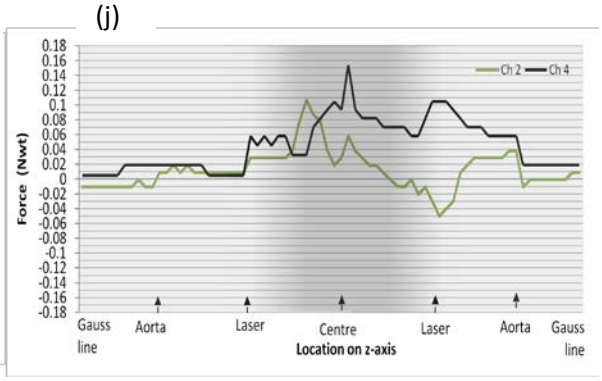

Adjusted for baseline data

(g)

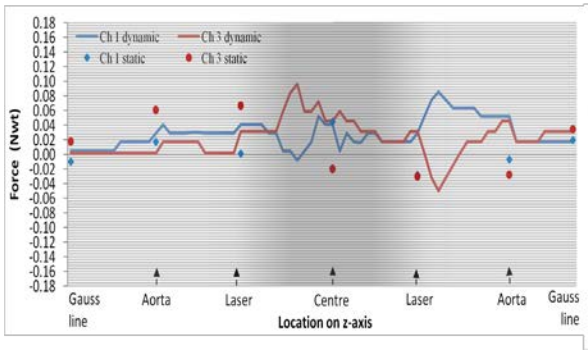

(h)

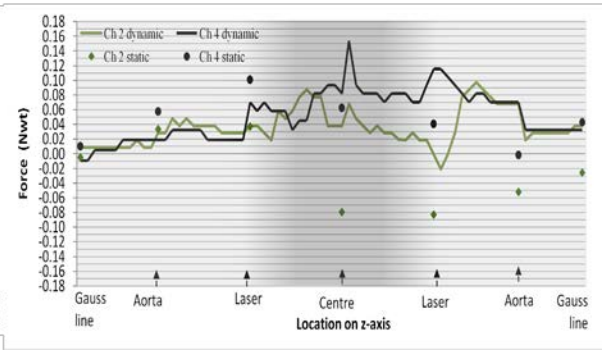

(f) Medtronic Hall valve

Movement of the Medtronic Hall single leaflet mechanical valve exposed the MR associated magnetic field environment is illustrated by Figure 6.9. Overall this valve displayed little or no interaction with the magnetic fields of the 1.5 T and 3.0 T MR systems. What little movement detected at 1.5 T occurred mainly along the W-E axis and between the laser upon entry to and, aorta following exit from the magnet (Figure 6.9e-f). At 3.0 T movement was confined to within the magnet but not solely the homogeneous field on the N-S axis and although the field of movement extended beyond the magnet on the W-E axis as the Figure shows the frequency of movement was limited. The profiles representing the static movements show differences between these and the dynamic measurements for the same points on the z-axis. The size of deviations of the static measurements from the dynamic profiles varied within and between the field strengths although most occurred outside the boundaries of the dynamic profiles. Moreover, entry and return measurements at the aorta and laser points were different in three out of four channels at both field strengths (ie. Channels 1, 2 & 4 @ 1.5 T; Channels 1, 3 & 4 @ 3.0 T)

At 1.5 T an upward/downward movement of the valve was recorded at the laser on entry to the magnet followed by a sideways deflection on the W-E axis towards the B_0 field as the valve entered the magnet. Within the homogeneous field the valve is seen to tilt such that the W-E axis attempted to rotate parallel to the x-axis. However, on its return and as it passed through the B_0 and dB/dx field a change in the N-S orientation tilted the valve onto its N-W axis. This however, was only a temporary position and the switch back to the S-E axis was maintained until a downward deflection occurred as the valve progressed through the aorta point on the return to the gauss line. Although the magnitude of oscillations displayed on the N-S axis in the profile for the 3.0 T magnetic field was larger compared with those at 1.5 T, the frequency of movements was comparable. In contrast, the magnitude of oscillations displayed on the W-E axis was smaller and the frequency less (Figure 6.9k-l). Movement of the valve at 3.0 T was

more-or-less confined to the area within the magnet though not solely within the homogeneous field. The first significant interaction of the valve with the magnetic field occurred at the boundary of the dB/dx and B_0 field. As the profile in Figure 6.9k-l shows a large N-S tilt occurred coupled with a sideways deflection towards the magnet on the W-E axis. However, within the homogeneous field at the iso-centre a reduction in this applied force was demonstrated causing a temporary reduction in the magnitude of valve's tilt and a deflection in the opposite direction. Though the directional movement of the oscillations indicate the direction of the deflection towards the iso-centre was maintained as the valve began its return journey, the increase in the divergence of oscillations on the N-S axis suggests there was a further increase in the applied force culminating in a relatively large second but opposite tilt on the N-S axis. However, a corresponding tilt also occurred on the W-E axis thus, causing the valve to tilt north-westerly. Although a switch in orientation was again recorded following its exit at the laser point no further valve movement was detected between the aorta and gauss line.

Figure 6.9: Medtronic valve

@1.5T

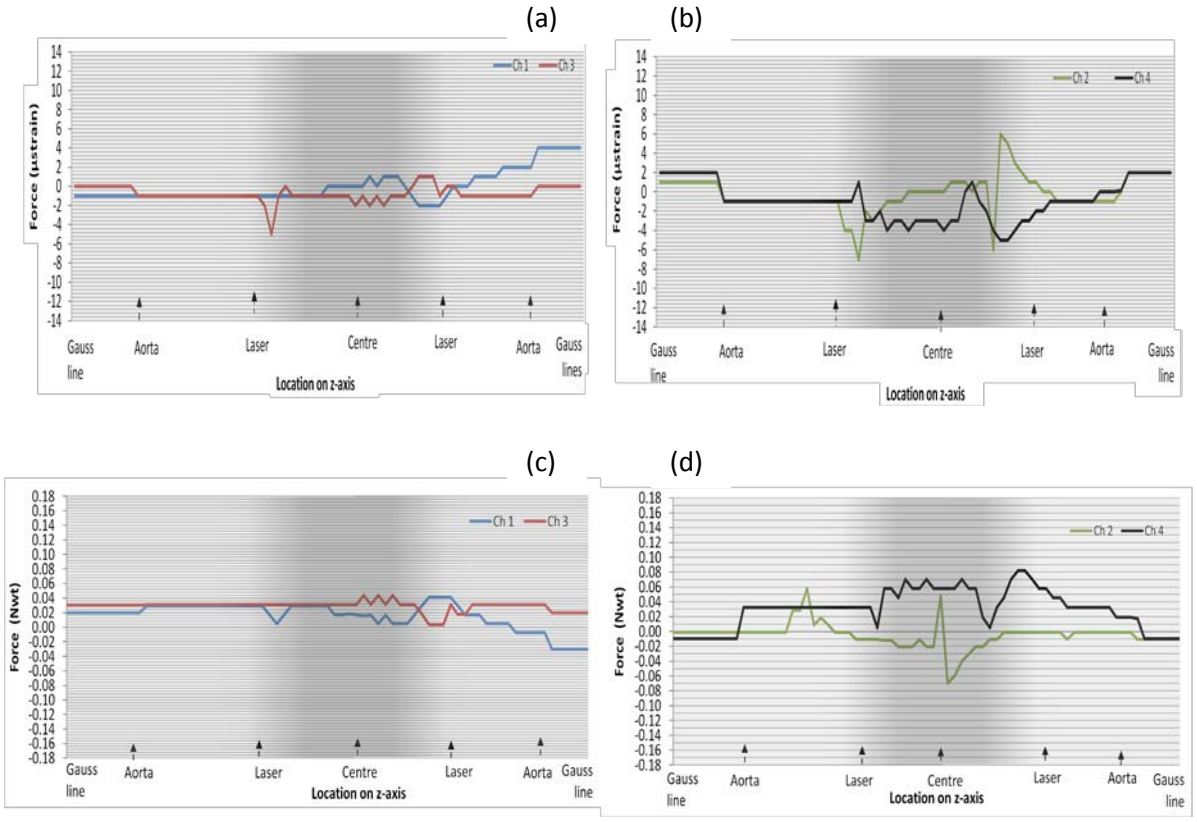

Adjusted for baseline data

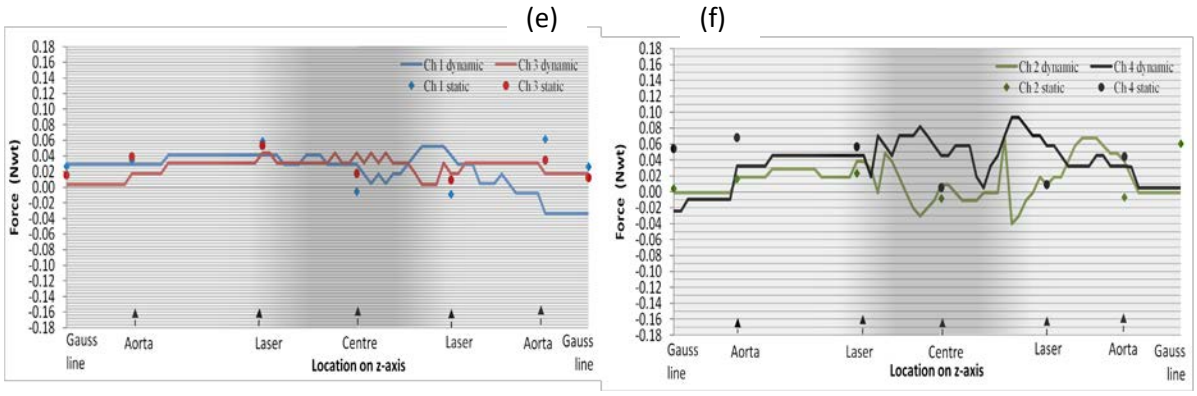

@ 3.0T

(g)

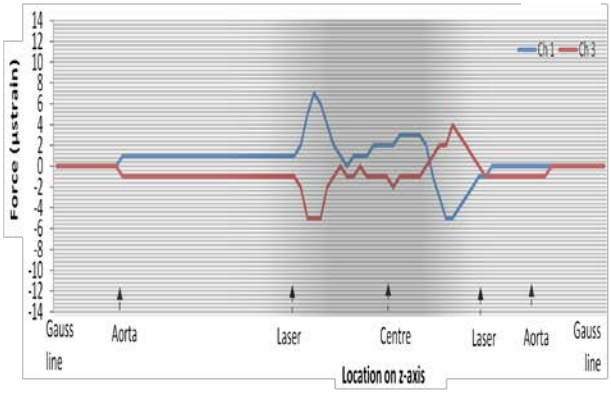

(h)

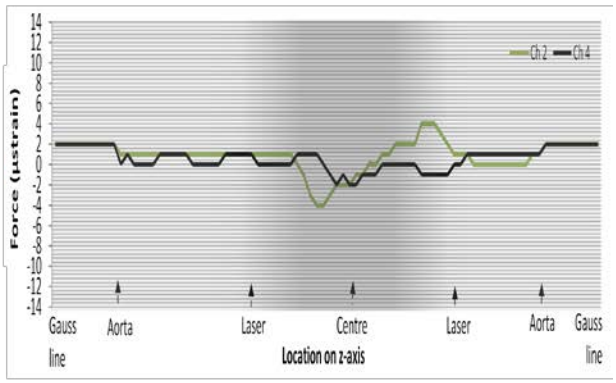

(i)

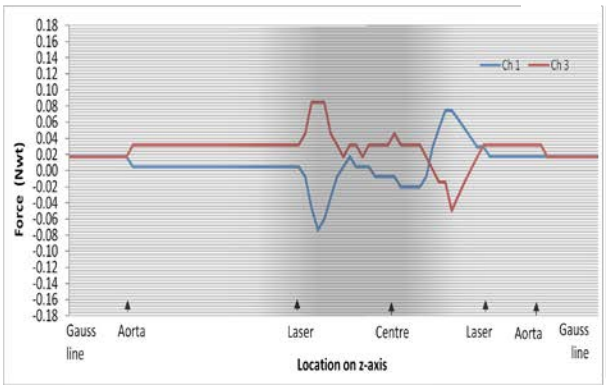

(j)

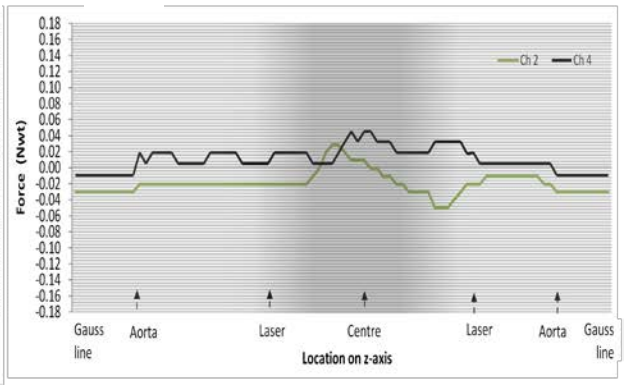

Adjusted for baseline data

(k)

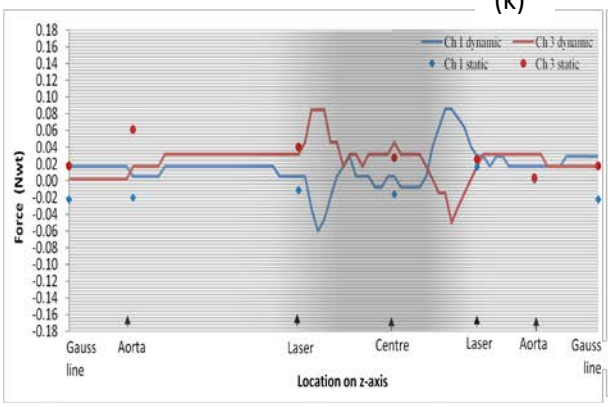

(l)

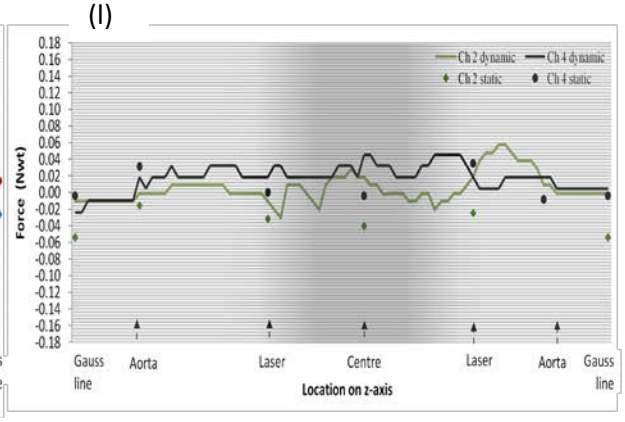

(g) Starr Edwards caged disc valve

The only caged disc valve included in this study demonstrated different patterns of behaviours to exposure to the two different field strength MR system as Figure 6.10 shows. Overall, the frequency of oscillations recorded at either field strength shows little movement of the valve was recorded at either field strength although an increase in the frequency of oscillations on the return journey from the iso-centre is demonstrated. This was true for both field strengths. Furthermore, static measurements appear to correlate more closely with the dynamic measurements for the same points on the z-axis at 1.5 T and in particular on the W-E axis. Differences recorded between the profiles at 3.0 T were however, relatively small.

At 1.5 T the movement of the valve was dictated by a rotational motion around the N-W-E arc in contrast to movement at 3.0 T in which the applied force caused the valve to tilt on its N-W axis. No movement of the valve was recorded between the gauss line and aorta point at 1.5 T but, at the aorta a deflective force, which was maintained until the valve exited the magnet, caused the valve's annulus to be pushed against the valve holder. In addition a temporary change in its N-S orientation occurred at the magnet's centre. At the start of the return from the iso-centre the magnitude of oscillations increased along both axes although more noticeably along the N-S axis. Moreover, the tilt of the valve also changed such that it tilted on its N-W axis until it had passed through the laser. Other movements of note at 1.5 T occurred between the laser and aorta on the return to the gauss line. An exaggerated tilt on the N-S axis occurred as the valve moved through the rapidly changing gradient field at the laser point and then, deflected upwards away from the valve holder as it proceeded through the aorta.

In contrast, interaction of the valve with the magnetic field at 3.0 T occurred primarily within the confines of the magnet. Figure 6.10k-l confirms virtually no movement was detected outside these boundaries and only limited movement particularly on the W-E axis. A small tilt on the N-W valve axis was detected at the laser point as the valve

entered the magnet and nothing of any significance was recorded thereafter until it reached the B_0 field and the iso-centre. A temporary change in the valve's orientation from N-W to S-W was recorded but this was rapidly reversed and immediately followed by a downwards deflection of the valve's annulus against the valve holder. This deflective force continued to act upon the valve until it again passed through the laser point whereupon, as at 1.5 T a relatively large tilting motion occurred along the N-S axis. Although minimal movement was recorded by Channel 2 no further movement of the valve was detected in any of the other channels as it moved between the aorta and gauss line in the decreasing magnetic field.

Figure 6.10 Starr Edwards caged disc valve

@ 1.5T

(a) (b)

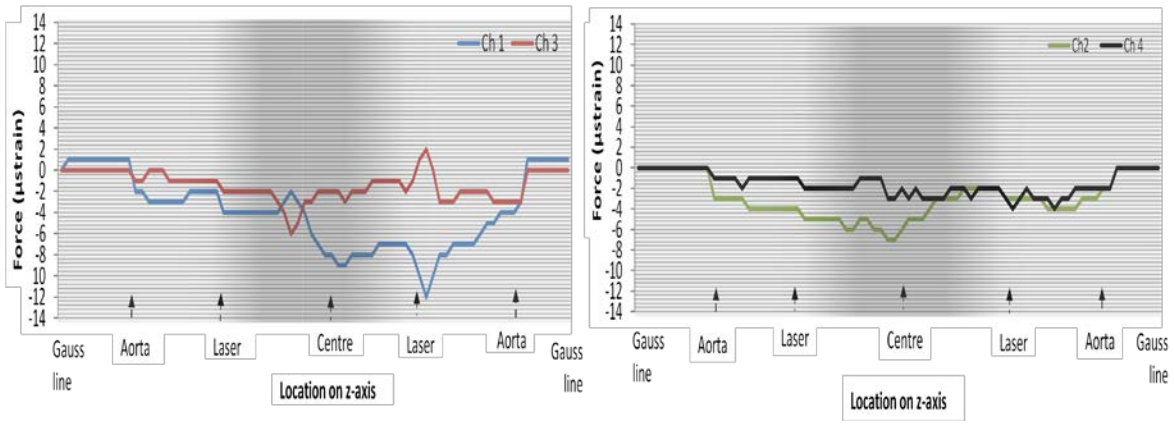

(c) (d)

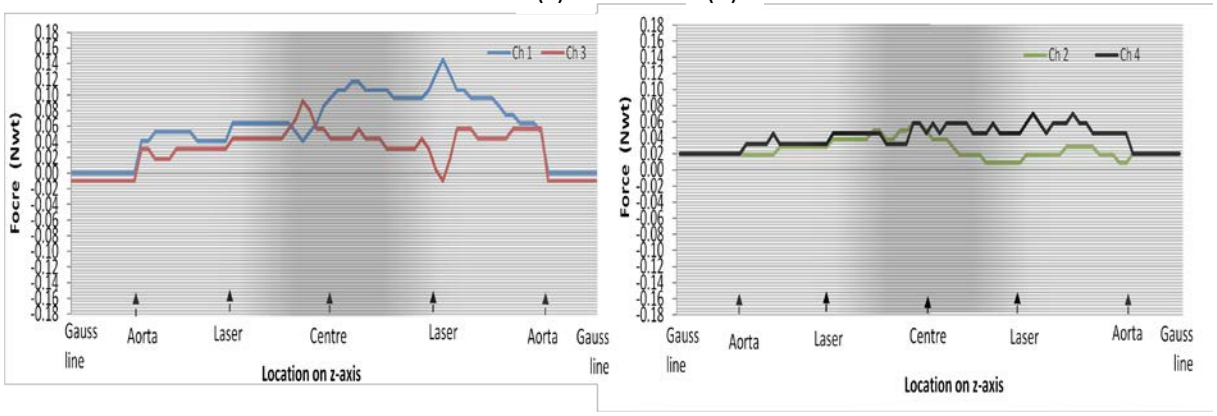

Adjusted for baseline data

(e) (f)

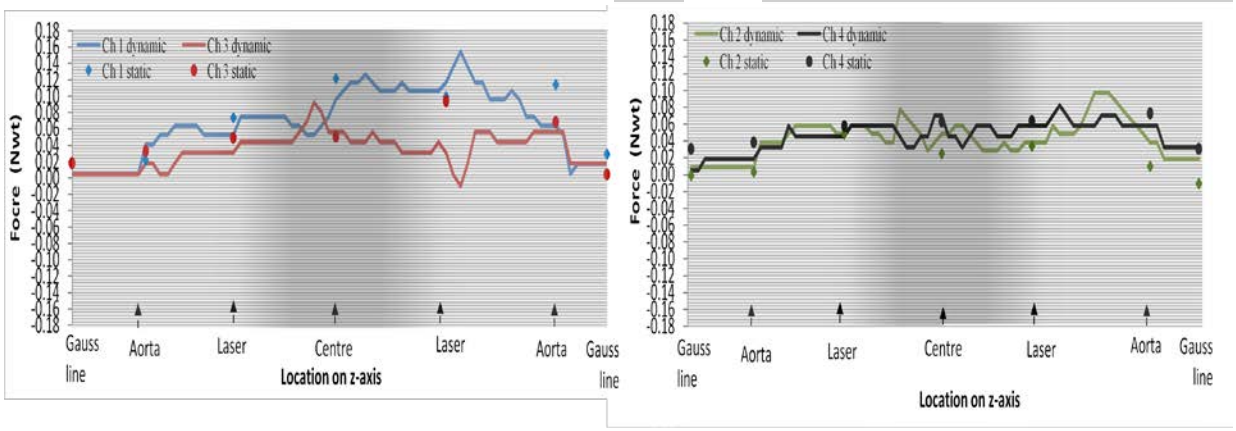

@ 3.0 T

(g)

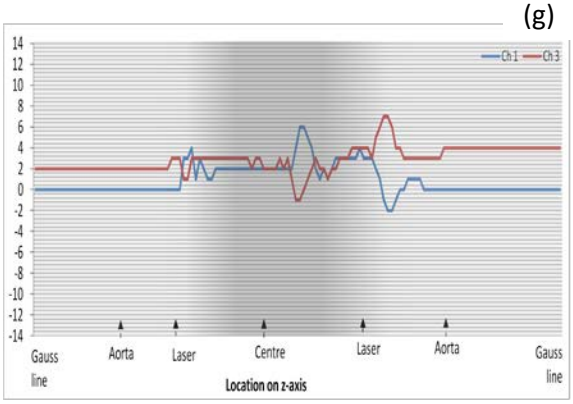

(h)

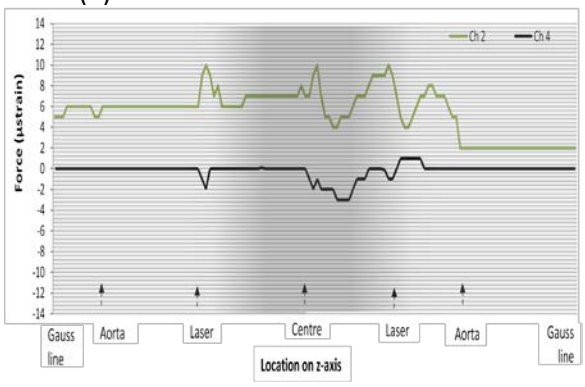

(i)

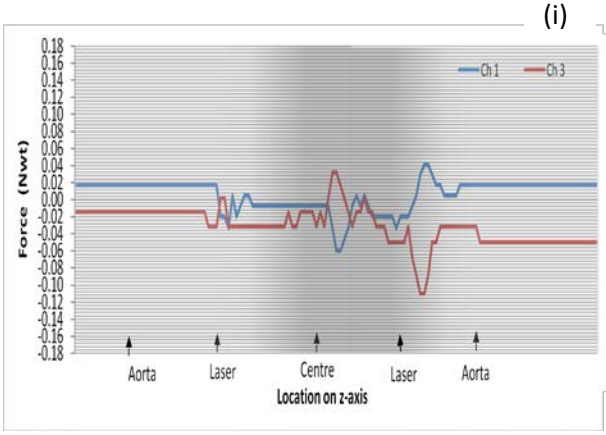

(j)

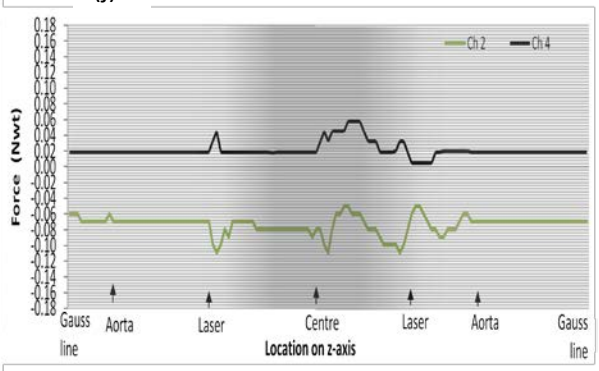

Adjusted for baseline data

(k)

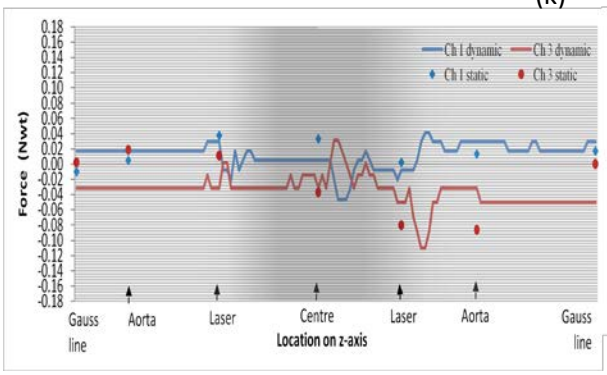

(l)

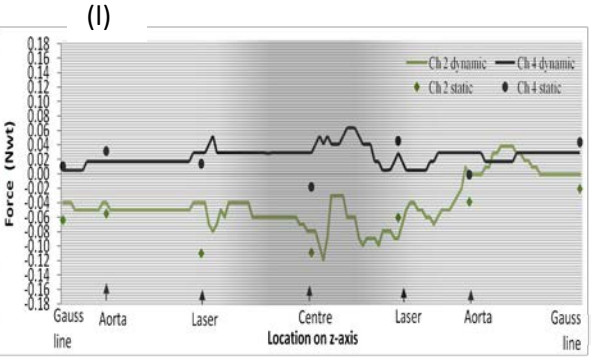

(h) Starr Edwards metal caged ball valve

Figure 6.11 displays the profile of one of the two mechanical caged ball valves evaluated in this study. Overall, the profiles for the valve at 1.5 T and 3.0 T show a similar frequency of movements between the two field strengths although, the magnitude and profile of oscillations differs. Furthermore, the orientation of the valve along the N-S axis is also different. Static measurements recorded at 1.5 T are closely correlated on the W-E axis and to some extent, along the N-S axis with some exceptions (Figure 6.11e-f). Although the static measurements recorded at 3.0 T did not deviate greatly from the dynamic profile overall, some differences between respective measurements and corresponding profiles were measured as Figure 6.11k-l shows.

Overall very little movement of the valve was detected at 1.5 T as the frequency of oscillations displayed in Figure 6.11e-f show. Some fluctuating movements were recorded in Channel 2 (E) in addition to a downward deflective movement (Figure 5.8③) on the return journey between the magnet's centre and laser point. A review of Figure 6.11 suggests the uni-directional profile of the oscillations across all four channels illustrates the downward force applied to the valve's annulus causing it to be pushed against the valve holder. However, this force was not maintained after it had passed through the aorta and progressed towards the gauss line. At 3.0 T no significant movement of the valve was recorded by Channel 4 (W). Stepwise incremental increases in movements detected can be seen in Figure 6.11k along the N-S axis as the valve moved from the gauss line to the laser point at which point the valve displayed a tilt on the N-S axis in a southerly direction. At the boundary of the dB/dx and B_0 field an increase in the force exerted on the valve caused an increase in the N-S tilt with some corresponding movement in Channel 2 (E). As the valve advanced from the magnet and through the laser point a small sideways

deflection of the W-E axis away from the magnet occurred followed by a temporary change in its orientation mid-way between the laser and aorta point after which no further movements of the valve were recorded.

Figure 6.11 Starr Edwards metal caged ball valve

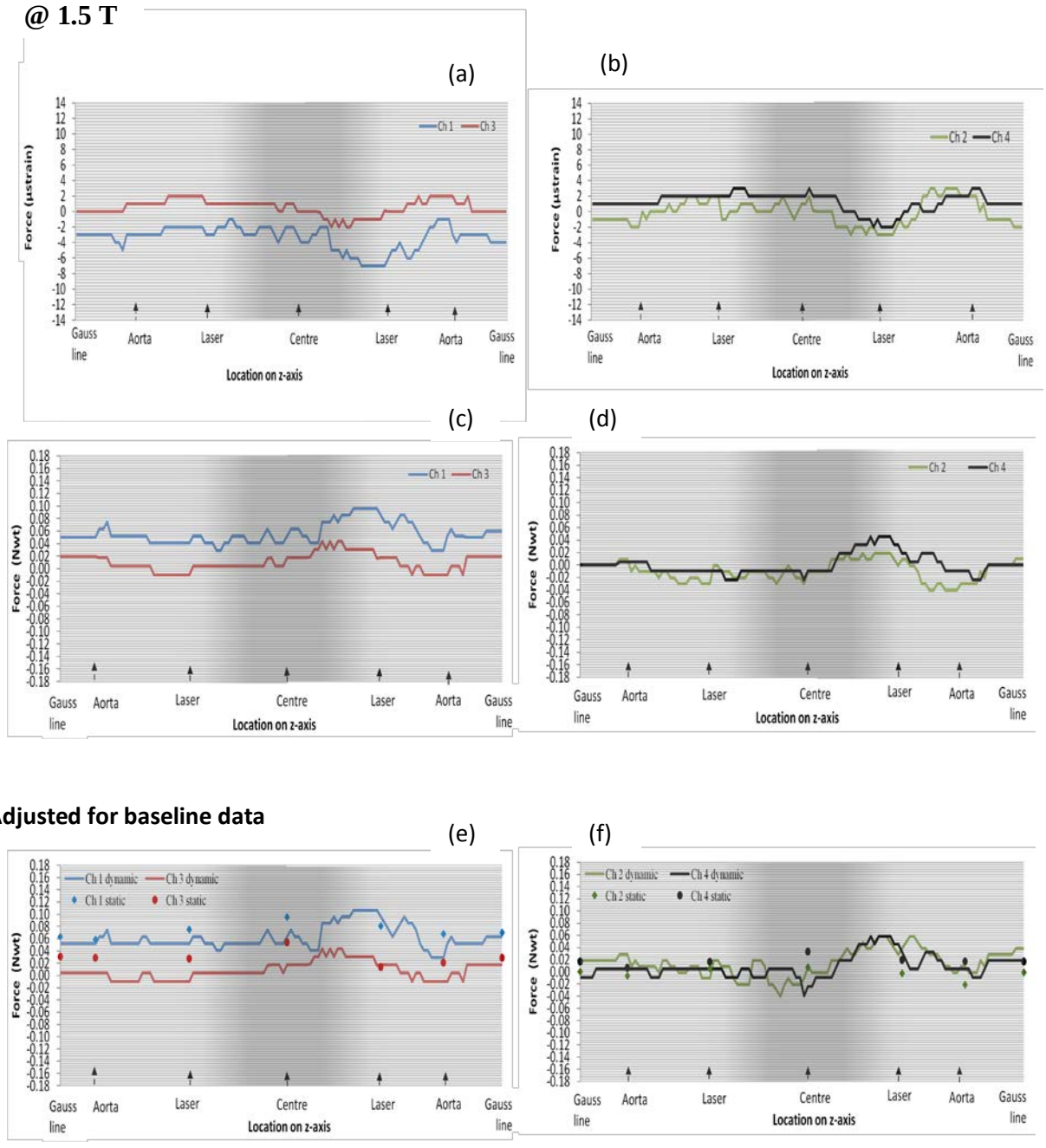

@ 3.0 T

(g)

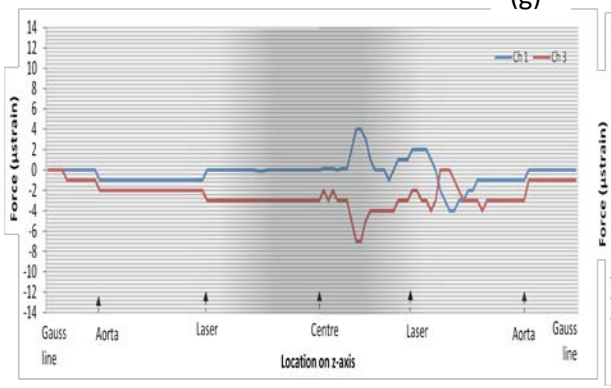

(h)

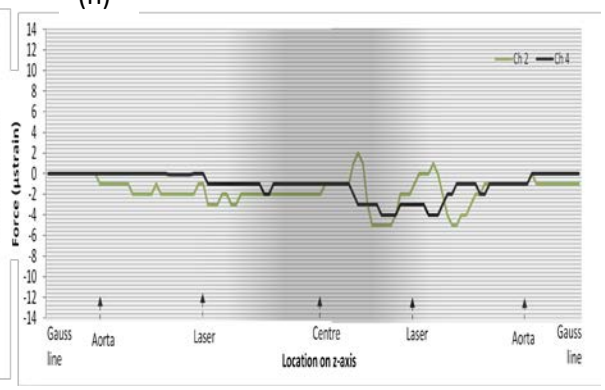

(i)

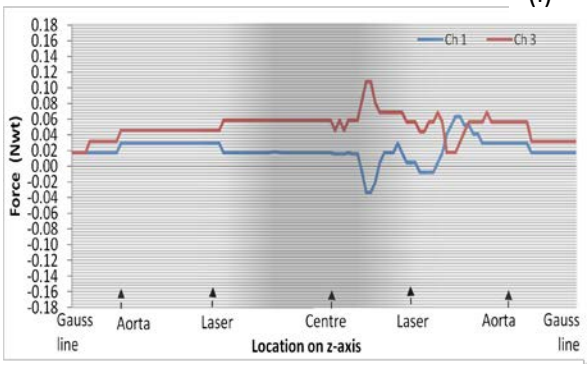

(j)

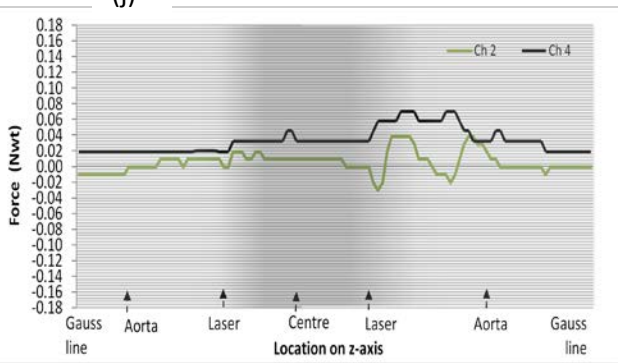

Adjusted for baseline data

(k)

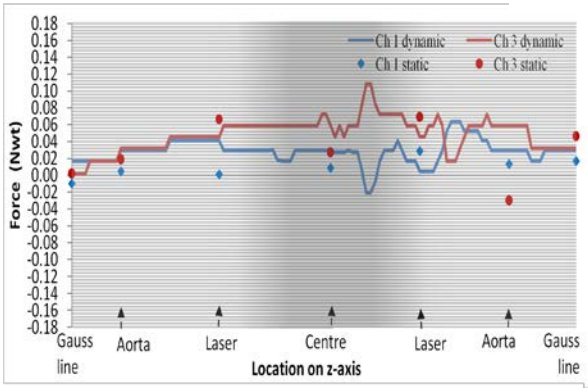

(l)

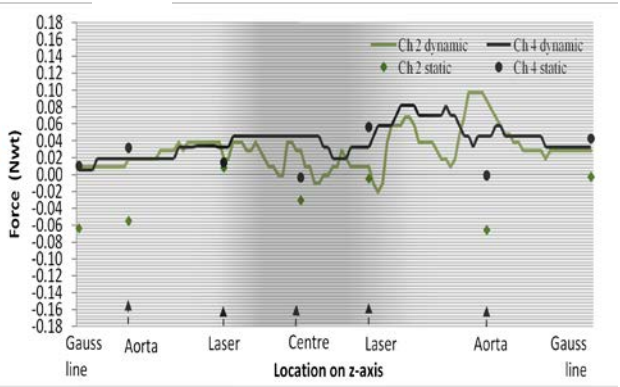

(i) Starr Edwards silastic caged ball valve

Two very different profiles denoted the interaction of the Starr Edwards silastic caged ball valve with the 1.5 T and 3.0 T MR environments as Figure 6.12 shows. The most striking feature of the profiles is the wide opposing parallel oscillations along the W-E axis at 1.5 T which suggests a 'spinning' type motion of the valve along this axis. This movement, as Figure 6.12f shows, also occurred in conjunction with a deflective force which occurred between the boundary of the B_0 and dB/dx field and aorta point as the valve returned from the magnet's centre. The few movements of the valve at 3.0 T were dominated by a tilting motion on the S-W axis at the boundary of the dB/dx and B_0 field on the entry to the magnet and a reverse (N-S) tilt as the valve exited the magnet at the laser point. Although the oscillations on the W-E axis displayed some degree of opposition they did not imitate those demonstrated at 1.5 T.

Overall, little or no movement in Channel 3 (S) was detected at 1.5 T until after the valve had reached the iso-centre. Moreover, in its paired opposite channel (N) although some movement was recorded between the laser and iso-centre the frequency of movements, as Figure 6.12e shows, was very low. An increase in the frequency of movements was recorded, mainly in Channel 1, as the valve continued to move through the boundary of the B_0 and dB/dx field on its return and this coincided with a change in direction of oscillations indicating a deflective movement of the valve. The applied force between these points on the z-axis caused the valve ring to be pressed against the valve holder. However, the force was not uniform and thus, the valve annulus was subjected to a series of small fluctuating movements as described in Figure 5.8③. As the valve moved closer to the aorta point and away from the magnet there was a reduction in the applied force such that it tilted on its S-E axis as though attempting to align the valve's annulus with the x-axis. Immediately thereafter, no further movement of the valve was detected.

As previously mentioned movement of the valve at 3.0 T was dominated by the two tilting motions on the N-S axis although, apart from these and a much smaller, almost negligible tilt at the aorta on the approach to the gauss line, no other movement along the N-S axis was recorded. Frequency of movement on the W-E was more consistent in Channel 4 (W) although not high. Forces acting on the valve appeared to increase causing the oscillations to diverge further from one another as the valve moved through the increasing gradient field from the aorta position towards the centre of the magnet, particularly once inside the magnet. However, this increase was not maintained and on the return from the magnet the oscillations converged and little or no movement was detected thereafter.

Similar to the other caged design valves included in this study the Starr Edwards silastic rubber ball valve also demonstrated a similar relationship between its static and dynamic profiles. Both profiles primarily corresponded closely with regards to their respective field strengths on the N-S axis although, static measurements recorded at 1.5 T for Channel 4 (W) also corresponded to dynamic measurements recorded at the same points on the z-axis. In contrast, those recorded for Channel 2 (E) displayed marked deviations from the dynamic profile. At 3.0 T static measurements along the W-E axis were consistently different from the dynamic profile and as the Figure shows the forces measured were generally lower.

Figure 6:12 Edwards silastic caged ball valve

@ 1.5 T

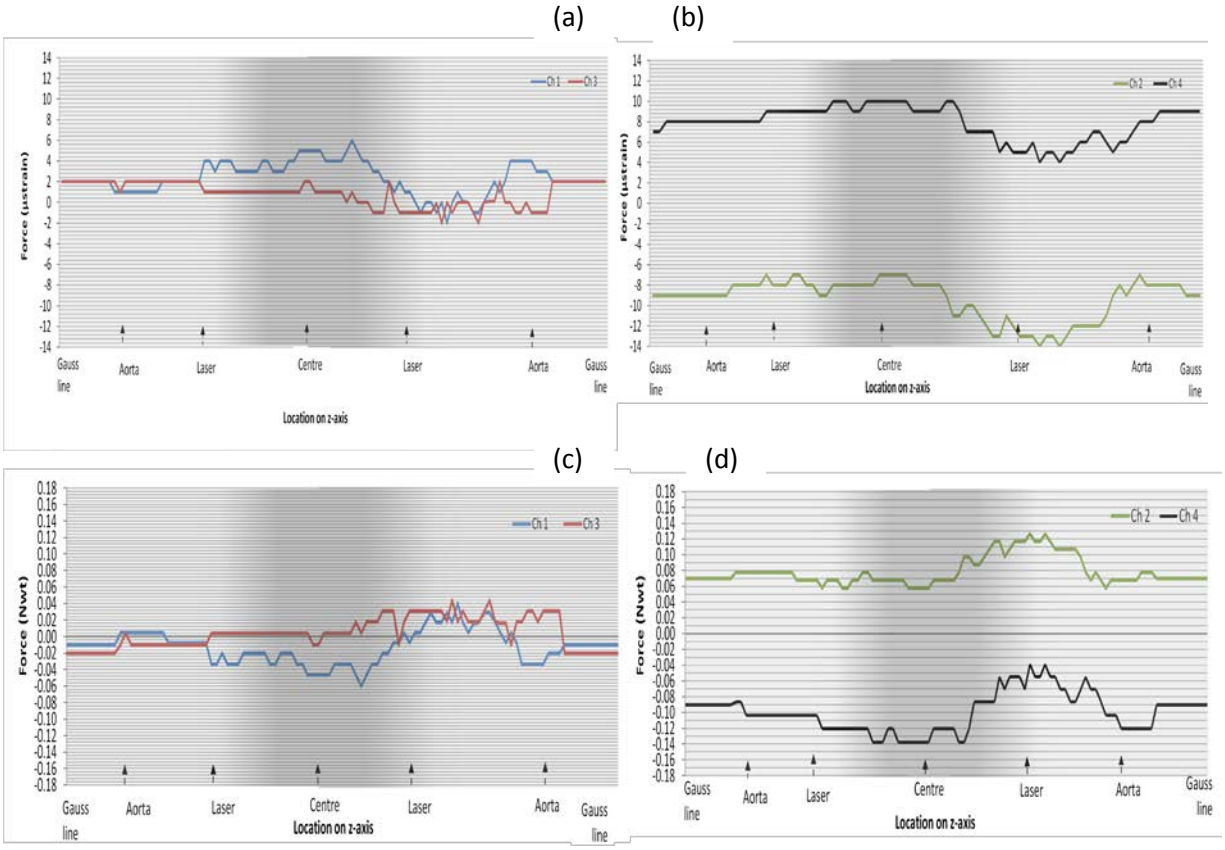

Adjusted for baseline data

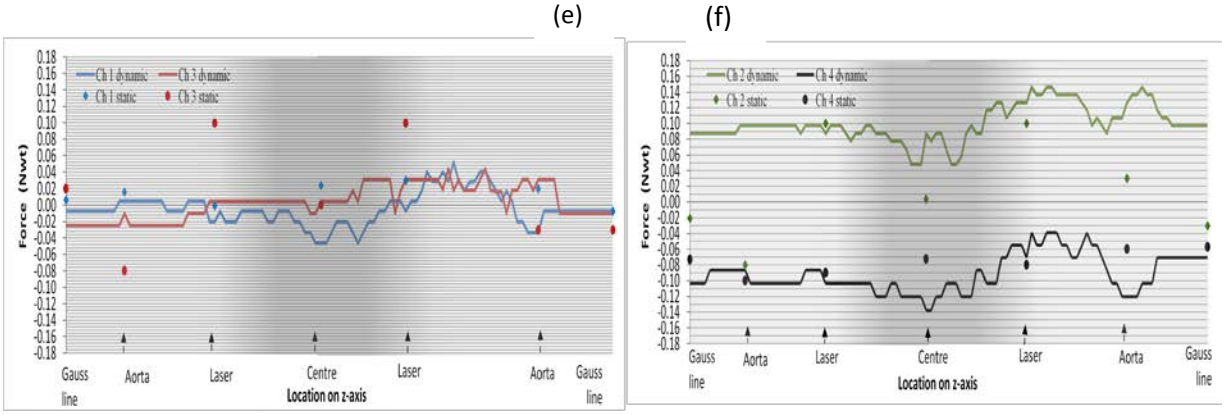

@ 3.0 T

(g)

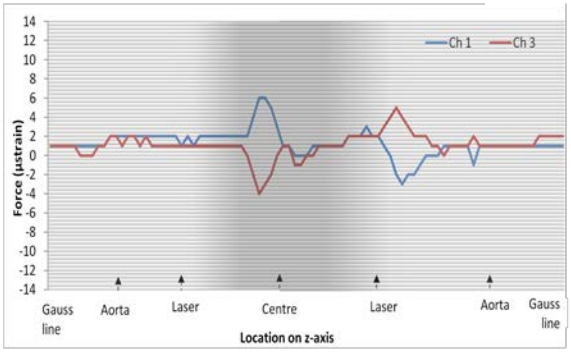

(h)

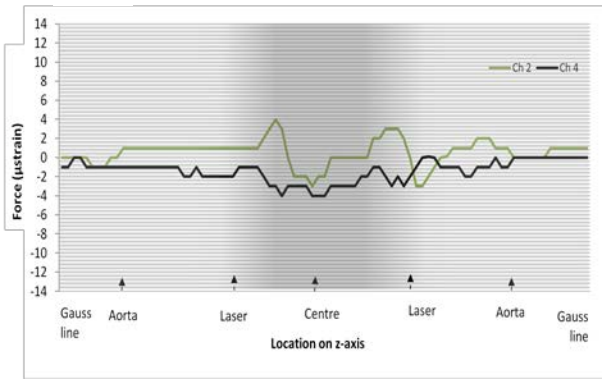

(i)

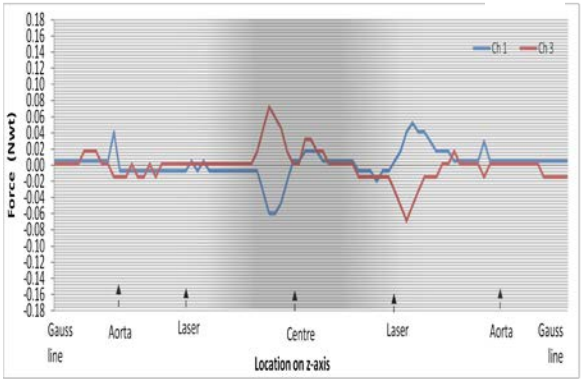

(j)

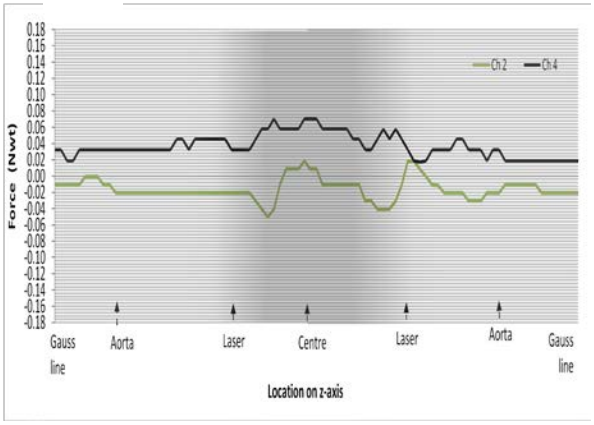

Adjusted for baseline data

(k)

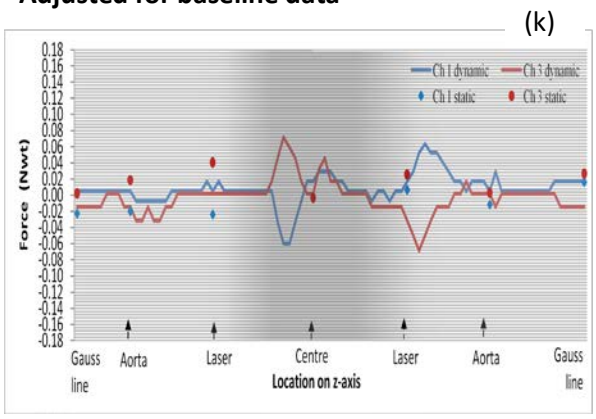

(l)

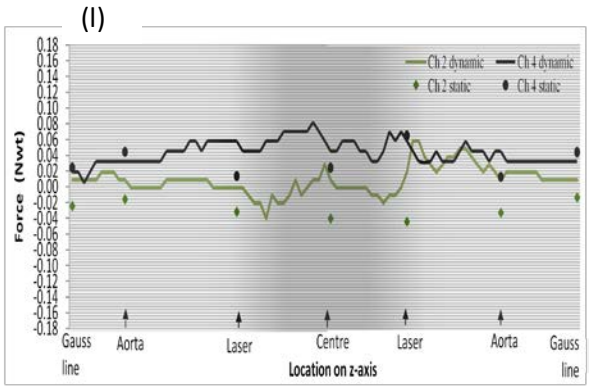

6.8 Section summary

In summary, although the data show some interaction of the test apparatus with the magnetic fields these results nonetheless confirm the sensitivity and competence of this device to detect and record movement of heart valve prostheses exposed, *ex vivo*, to MR associated magnetically induced forces. Moreover, the use of strain gauges afforded the apparatus the capacity to detect the frequency of valve movements together with the magnitude of applied force and differentiate between deflective, tilting and rotational movements such as those described in Figure 5.8. The individual valve profiles produced by this apparatus not only identified differences in the type, frequency and magnitude of movements between all valves and sub-groups but also differences in entry and return profiles which indicate magnetism is both induced and retained in a prosthesis during its continuous movement through the B_0 field. This concludes the presentation of the *ex vivo* test results. The next section of the Result Chapter (Part IV) focuses on the *in vitro* investigations and presents the findings of the influence of MR associated magnetically induced forces on valve function and performance.

Part IV

Hydro-pneumatic results

6.9 Introduction

This section reports the results of the fluid flow tests performed on the individual heart valve prostheses exposed to the B_0 field. Individual profiles are reviewed for any variations in pressure waveform compared with the baseline data and also for, within profile variations with particular reference to the different positions along the z-axis.

6.9.1 Calibration of the hydro-pneumatic test apparatus

Table 11 shows the results of the calibration of the hydro-pneumatic test apparatus. An average heart rate for a healthy adult (75 bpm) was achieved when the speed and stroke regulators were set at positions 5 and 9 respectively. However, as Column 7 in Table 11 shows the required fluid output of 5 l/min was not achieved at these positions. Repositioning of the arm of the stroke regulator to position 10 however, increased output sufficiently and the required fluid output of 5 l/min was thus achieved.

Table 11: Rate of fluid flow regulated by the pulsatile pump

Beats/minute (bpm)	Speed 1	Speed 2	Speed 3	Speed 4	Speed 5	Maximum fluid output at maximum speed (ml/min)
Position 1	30	35	45	56	65	(1360)
Position 2	33	40	49	58	68	(1620)
Position 3	36	42	49	58	70	(1980)
Position 4	36	42	49	59	70	(2480)
Position 5	36	43	51	60	71	(2720)
Position 6	36	43	51	60	71	(3300)
Position 7	36	43	52	63	73	(3580)
Position 8	36	43	53	65	73	(4170)
Position 9	36	43	54	65	75	(4310)
Position 10	36	43	56	66	75	(4950)

6.10 Baseline measurements at 1.5 T

The hydro-pneumatic test apparatus used in the study and described fully in Chapter 5 was designed to produce a consistent haemodynamic profile in order to investigate the influence of magnetic fields on prosthetic heart valves. A baseline profile of fluid flow through a valveless chamber as the apparatus proceeded through the B_0 field is presented in Figure 6.13. The overall profile produced shows a typical sinusoidal waveform with a frequency of 75 rpm (i.e. 1.25 Hz; Table 11). Measurements recorded as the apparatus moved through the magnetic field along the z-axis shows no differences in the shape or magnitude of the pulse waves thus confirming the test equipment did not interact with the magnetic field. Furthermore, the sensitivity of the test equipment was established when

inconsistencies in pulse waves (i.e. complexes) were identified at points in the profile when the MR bed was known to have experienced a juddering motion. Figure 6.14 for example, shows a series of irregular complexes at a position along the z-axis when the MR bed was known to have temporarily faltered (see also Figure 6.19d).

Figure 6.13: Baseline profile @ 1.5 T

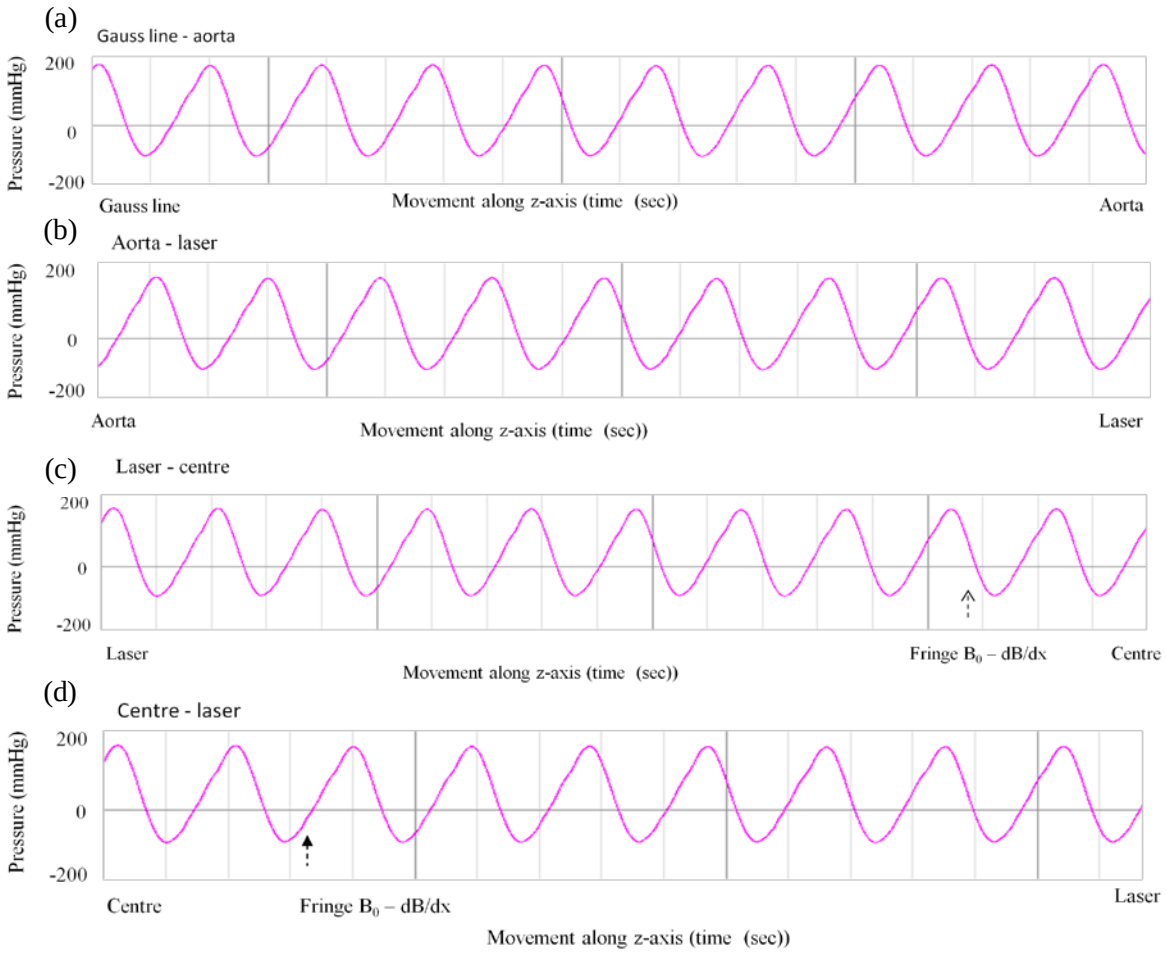

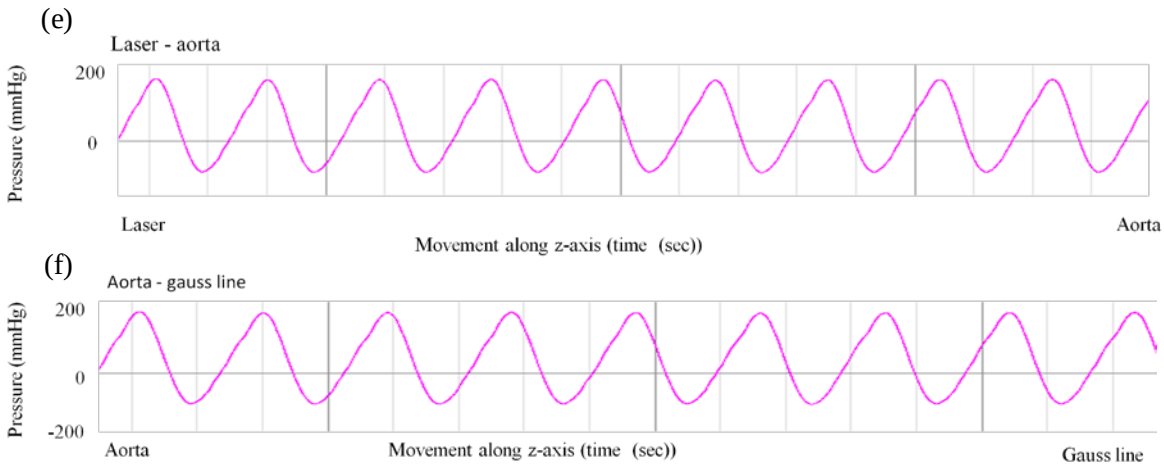

Figure 6.14: Illustration of sensitivity of hydro-pneumatic experimental apparatus

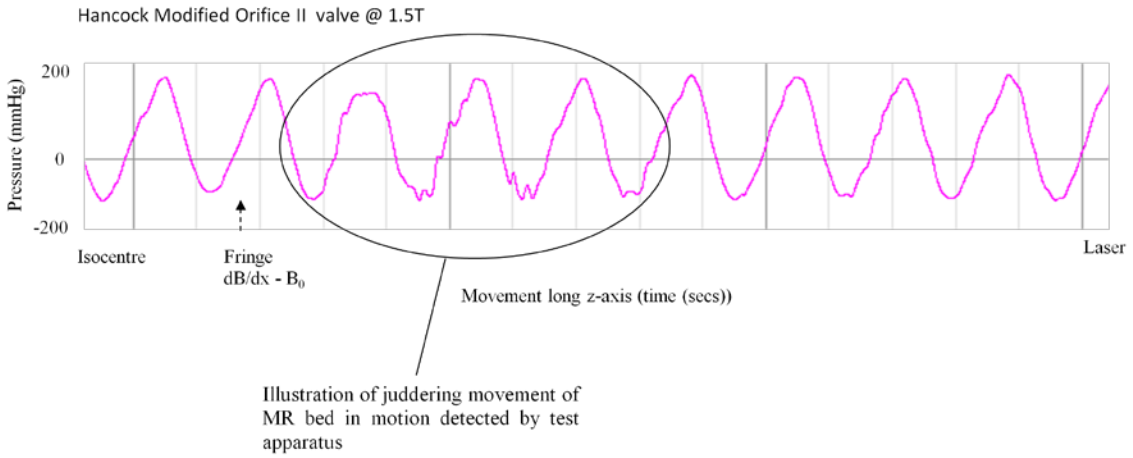

6.11 Overall results at 1.5 T

Comparison of the haemodynamic profiles of the nine prosthetic heart valves exposed to MRI at 1.5 T show all valves produced sinusoidal waveforms (Figures 6.15 - 6.23). Furthermore, no differences in the magnitude of waveforms for the individual valves compared with the baseline profile were detected. Although some profiles shared a

similarity in terms of the shape of the complexes for example, Carpentier Edwards pericardial and porcine valves (Figures 6.16, 6.17), Starr Edwards caged disc and silastic caged ball valves (Figures 6.21, 6.22), Björk Shiley, Edwards Tekna, Hancock II and Starr Edwards metal caged ball valves (Figures 6.15, 6.18, 6.19, 6.22) there was generally no consistency with the shape of the complex and valve type or sub-group. Furthermore, the consistent recurrence of specific patterns of complex shape in some profiles was thought to be associated with the closing mechanisms of the valve leaflets/occluder. Investigations of the closing dynamics of prosthetic heart valves have for example, shown such patterns reflect the water hammer effect caused by the sudden and instantaneous impact of the leaflets against the seat stop or guiding strut which creates a 'shock-wave' effect and is commonly associated with cavitation of the valve (Feng 2000; Nair 2003; Chapter 3). Thus, the recurrence of variations shown in the Figures 6.16, 6.17, 6.20, 6.21 and 6.23 suggest these are the result of the water hammer phenomenon rather than any interaction of the leaflets/occluder with magnetically induced forces. The next section of this chapter describes the results of the hydro-pneumatic tests on the individual valve prostheses.

6.12 Individual valve profiles

(a) Björk Shiley valve

Figure 6.15 shows the appearance on the Björk Shiley valve of a dicrotic notch. Although this is typically associated with the closure of the aortic valve this was unusual in this valve because it consistently occurred on the ascent and not the descent of the pulse wave. This suggests possible movement of the leaflet in response to the magnetic field. In addition, this valve also displayed further variations in the pressure profile beginning in the last three complexes (Figure 6.15d) and continuing until to the 5th complex after the aorta position despite a decreasing field strength (Figure 6.15f). Changes in the shape of the complexes were not confined to either the ascending or descending pulse wave but occurred with similar frequency in both. Furthermore, changes in the shape of the peak and base pressures were also observed. Although the

frequency of these variations began to decrease after the valve had passed through the return aorta position variations suggestive of an interaction of the leaflet with the magnetic field could also be observed in a very weak field near to the gauss line.

Figure 6.15: Björk Shiley valve @ 1.5 T

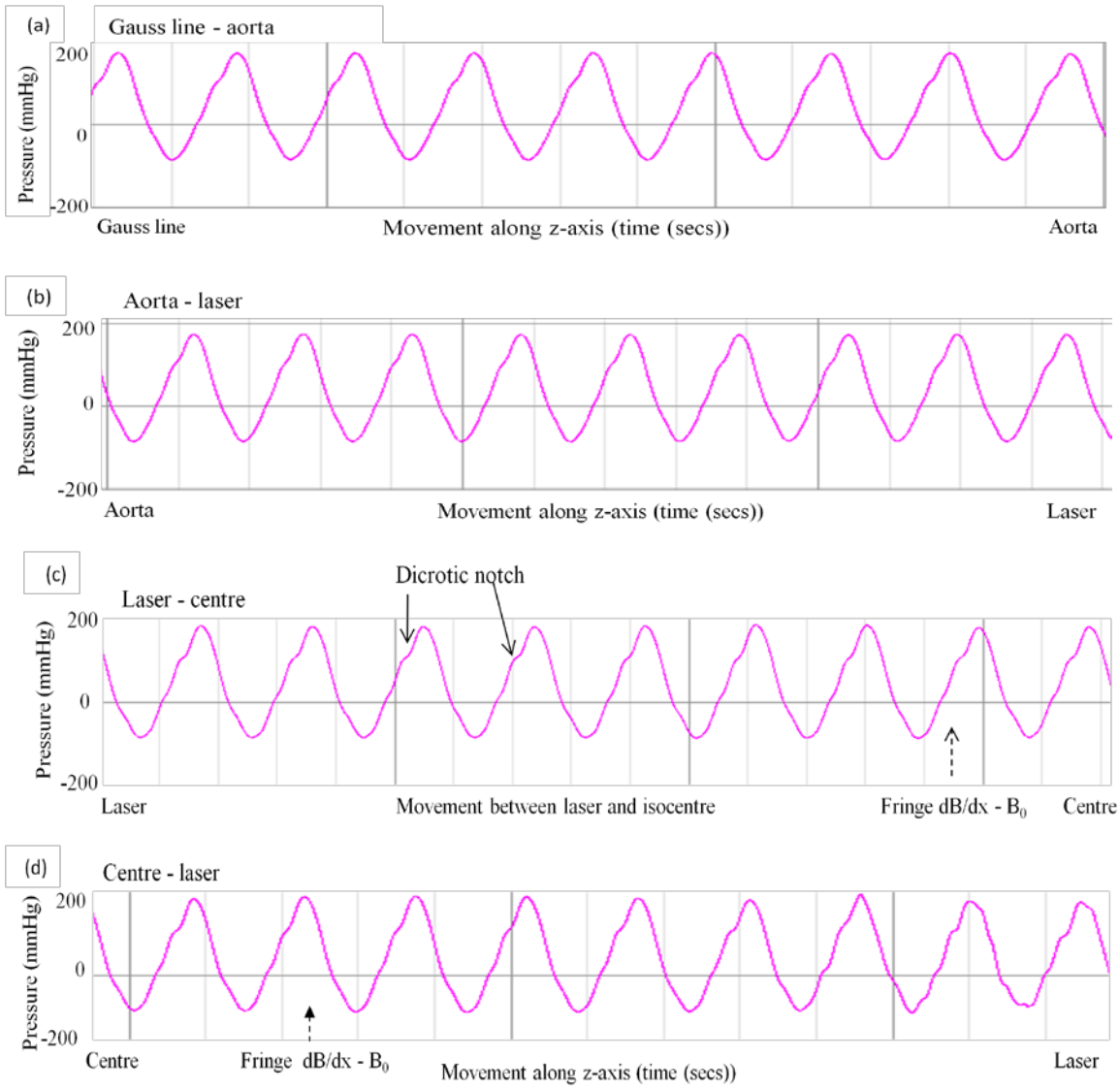

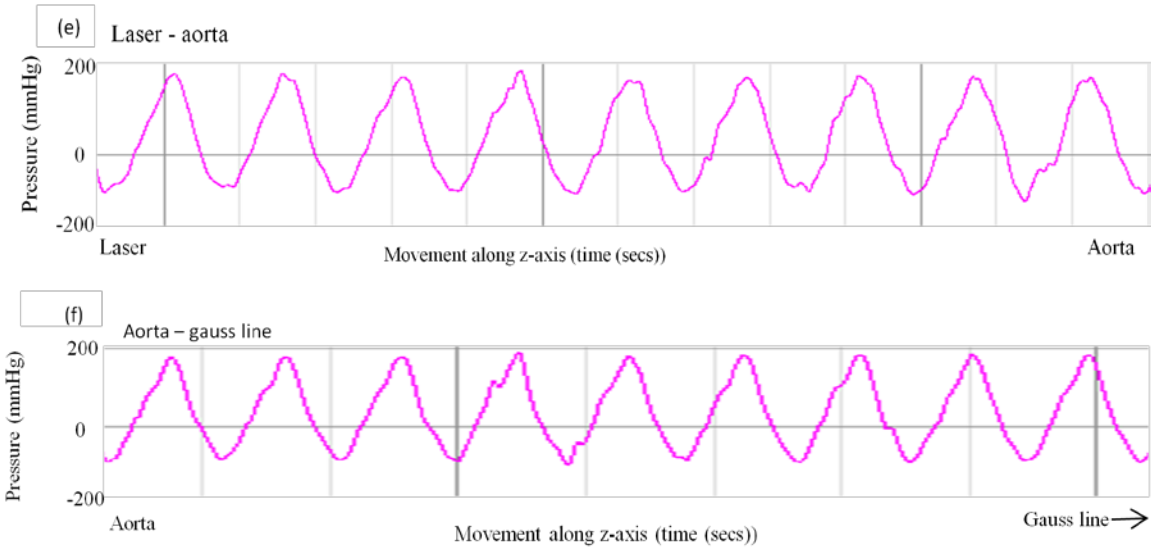

(b) Carpentier Edwards pericardial valve

The dynamic profile of the Carpentier Edwards pericardial valve is presented in Figure 6.16. The Figure shows a consistency in all the complexes as the valve moved through the B_0 field at 1.5 T which confirms no interaction of the valve's leaflet with the magnetic field on either entry or return between the gauss line and iso-centre occurred.

Figure 6.16: Carpentier Edwards pericardial valve @ 1.5 T

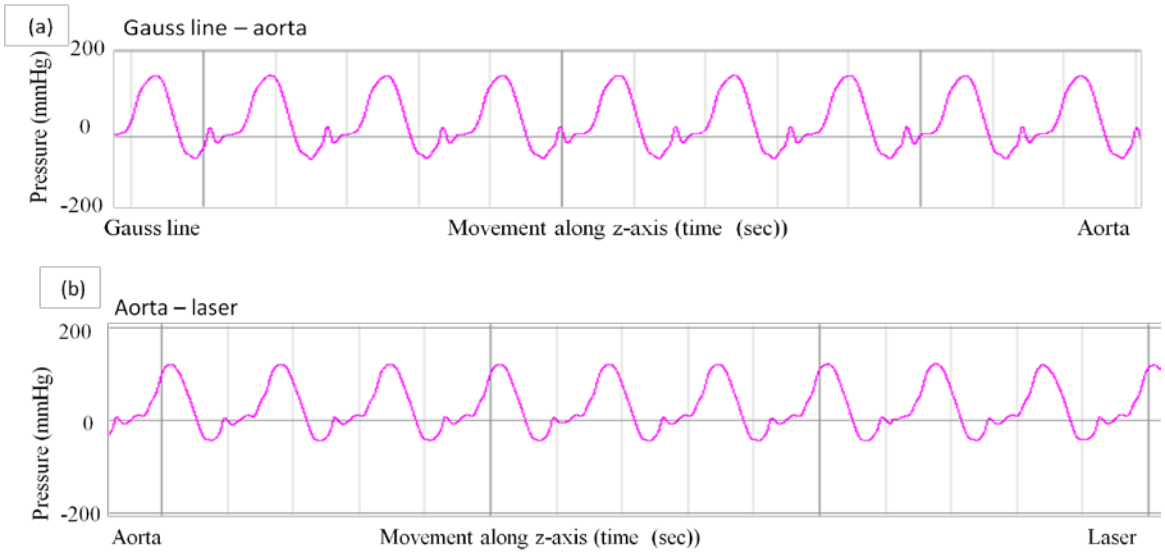

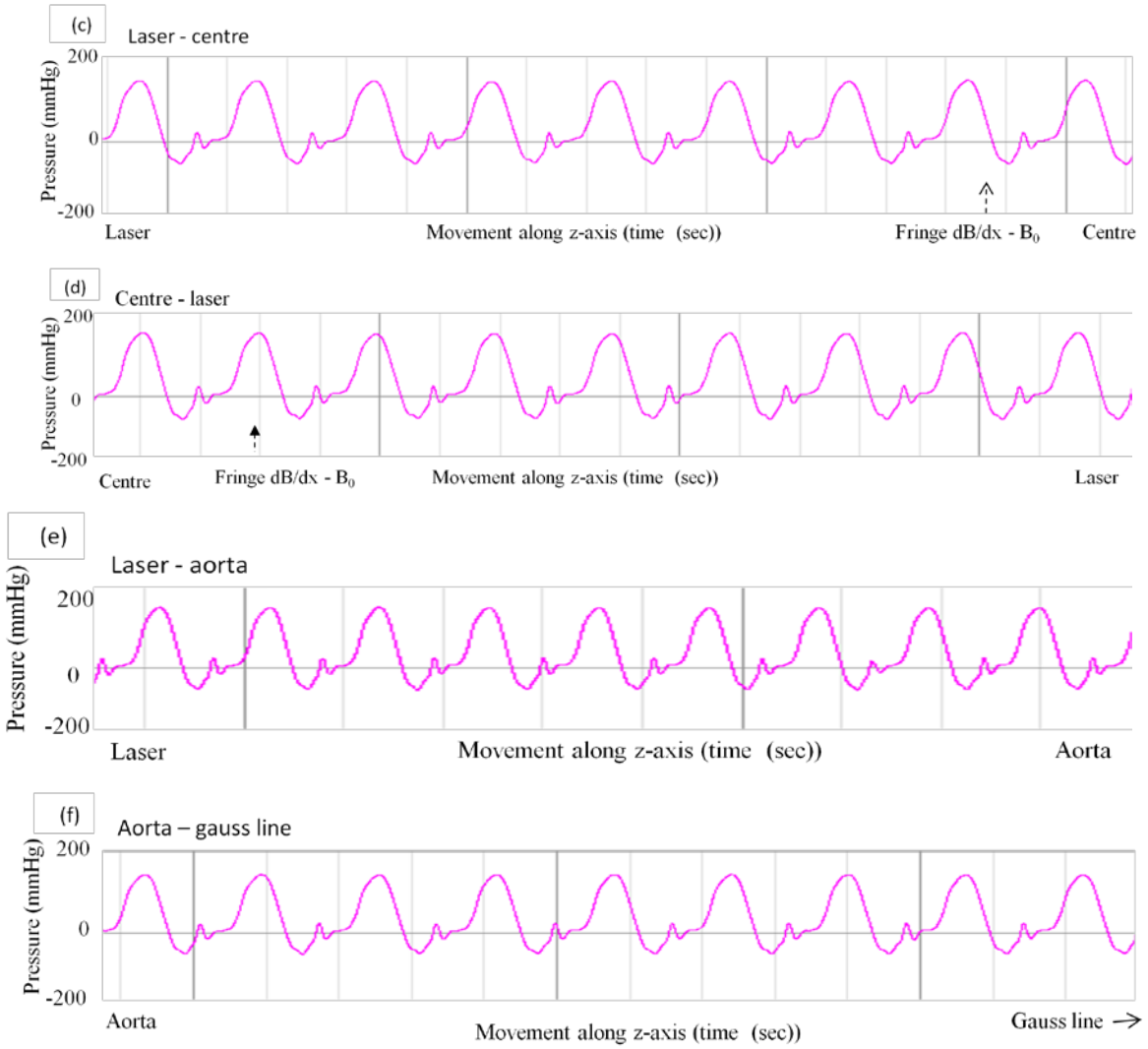

(c) Carpentier Edwards porcine valve

The shapes of the complexes displayed by the dynamic profile of this porcine valve (Figure 6.17) are similar to the Carpentier Edwards pericardial tissue valve. Again, the consistency in the shapes of the complexes is suggestive of a total lack of interaction of the valve's leaflets with the magnetic field at 1.5 T.

Figure 6.17: Carpentier Edwards porcine valve @ 1.5 T

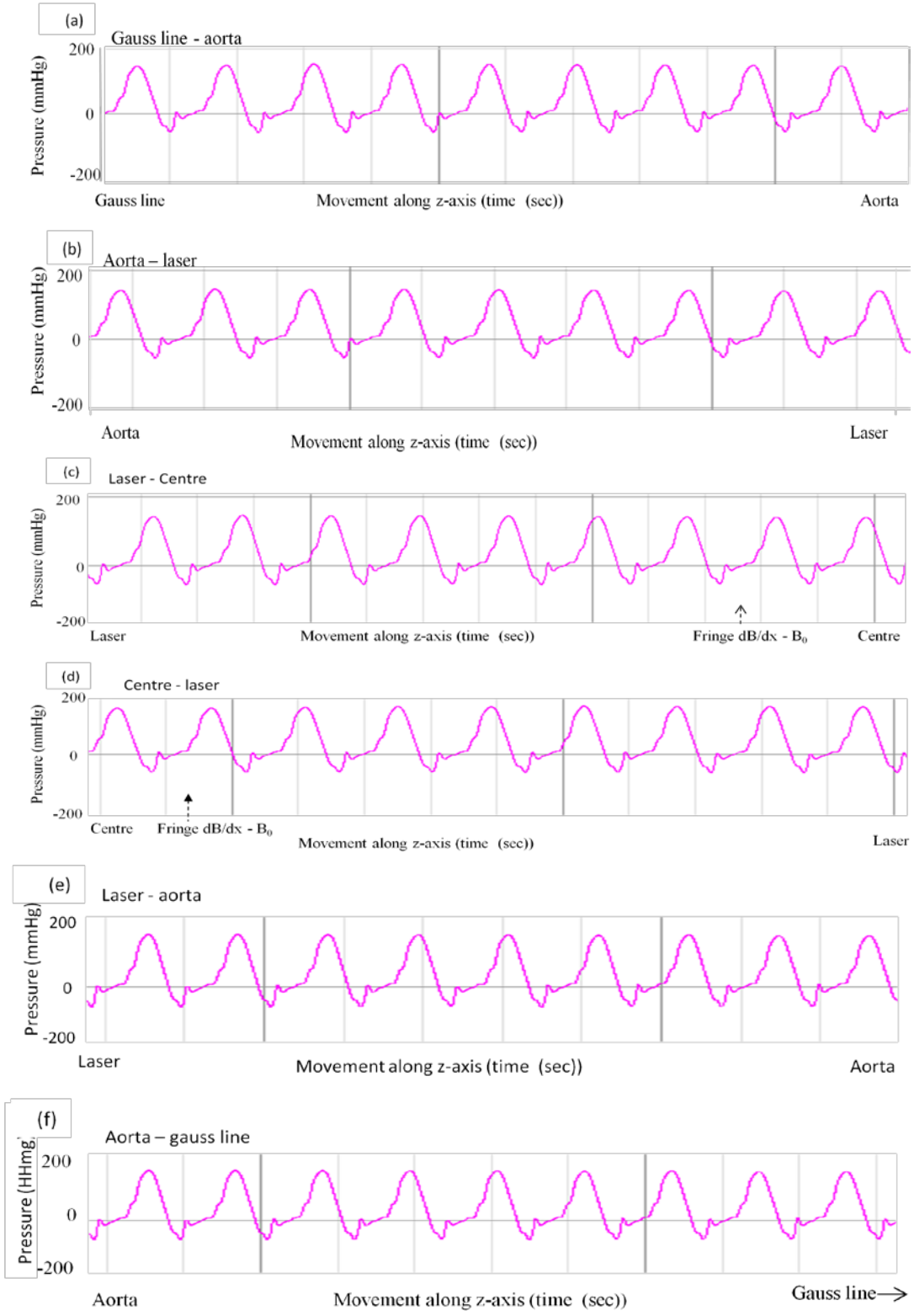

(d) Edwards Tekna valve

Figure 6.18 presents the pressure profile of the Edwards Tekna valve at 1.5 T and shows inconsistencies in the complexes. In addition, increases in the magnitude of some complexes were also observed on both entry and return from the magnet. As Figure 6.18c shows interaction of the valve's leaflets with the magnetic field was initiated at the entry laser position. Inconsistencies in the shape and magnitude of the pulse waves continued as the valve progressed towards the boundary of the dB/dx with B_0 field at which point there was a marked increase in the number of notches recorded in both the ascending and descending pulse waves (Figure 6.18c-d). Furthermore, interaction of the leaflets with the homogeneous field continued but the intensity of the interaction appeared to decrease after the valve had moved through the boundary of the B_0 and dB/dx field toward the return laser position. However, despite a continuing decrease in field strength the interactions of the valve's leaflet with the inhomogeneous field continued as illustrated by both the variable shape and magnitude of the pulse waves shown in Figure 6.18c-f.

Figure 6.18: Edwards Tekna valve @ 1.5 T

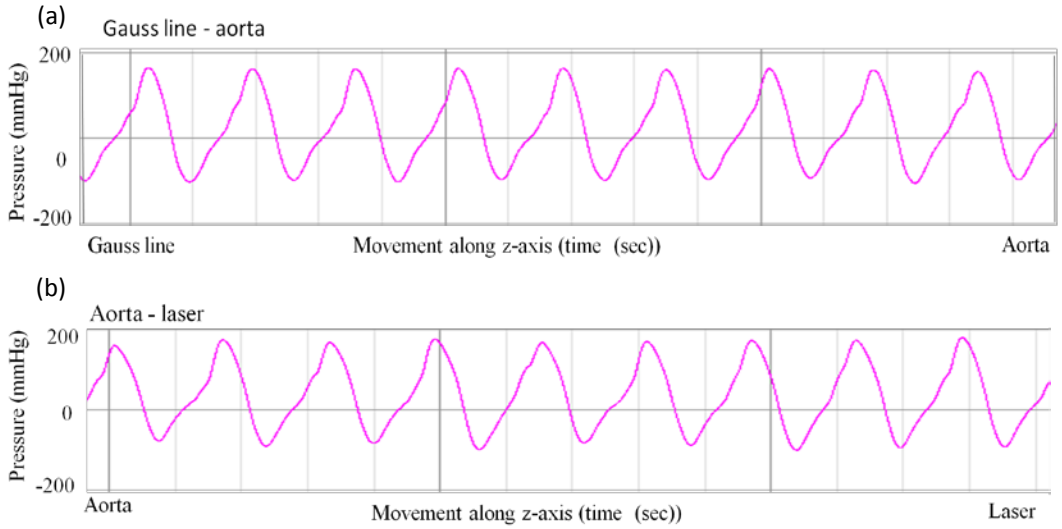

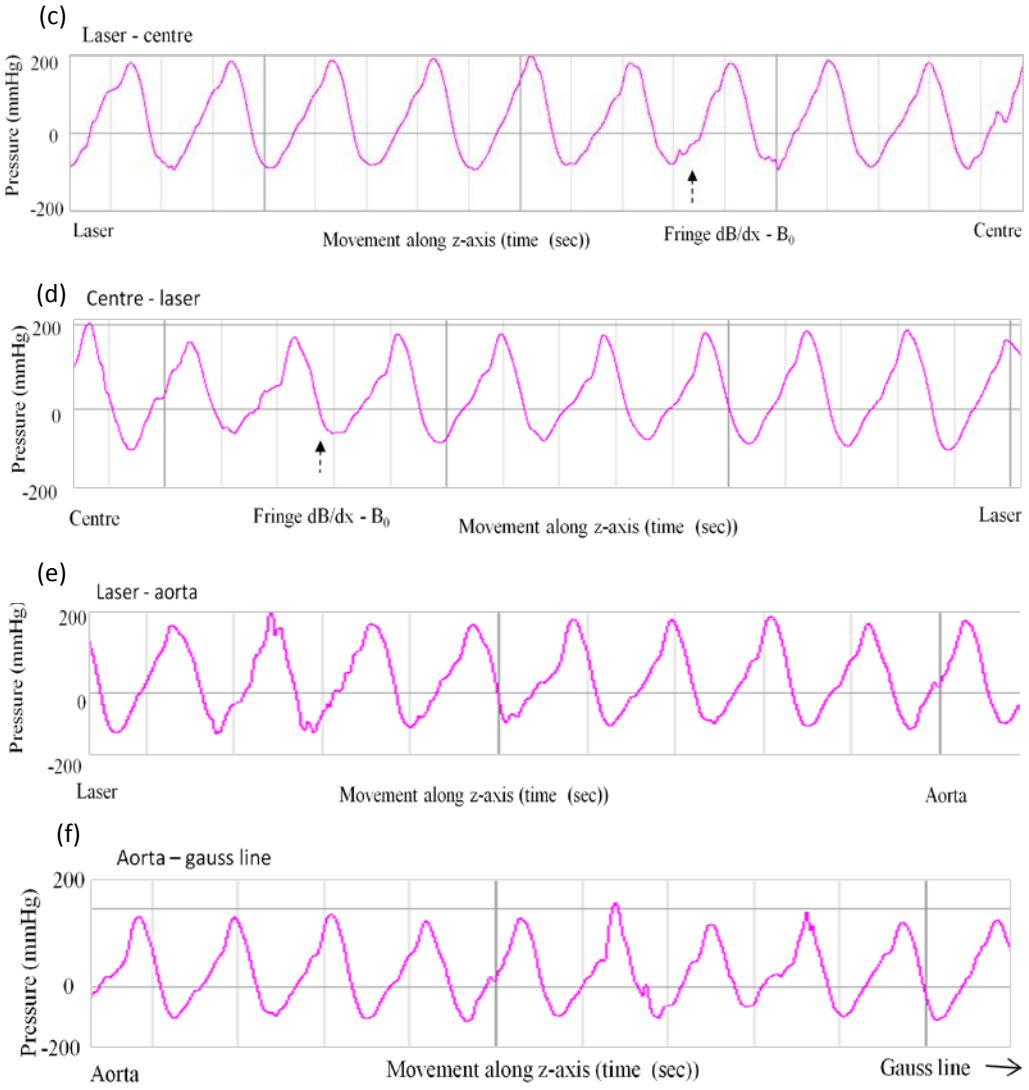

(e) Hancock II Modified Orifice valve

The general shape of the waveform for the Hancock porcine valve displayed in Figure 6.19 shows a similarity with that of the baseline profile shown in Figure 6.13. However, in contrast, it also shows some variation in the complexes suggestive of an interaction of the valve's leaflets with the B_0 field. As the valve returned from the iso-centre towards the gauss line for example, a number of inconsistencies in the complexes were detected (Figure 6.19d-f). Firstly, the experimental apparatus detected a series of irregular

complexes between the gauss line and the aorta on entry to the magnet. These irregularities were defined by an accentuated diocrotic notch on the ascending pulse wave. Secondly, irregular complexes were detected midway between the iso-centre and laser. However, as explained in an earlier paragraph these irregularities reflect an unexpected faltering of the MR bed which resulted in a 'juddering effect' (Figure 6.14). Between the laser and the aorta the test apparatus detected additional small irregularities in the complexes beginning with the 3rd complex from the laser position and continuing towards the gauss line. Although it has been suggested this type of movement is associated with the possible movement of the leaflets in response to the magnetic field this was in reference to a mechanical valve and not a bioprosthesis (see Björk Shiley valve). However, there is no evidence to suggest porcine tissue itself interacts with magnetically induced forces associated with MRI and therefore it might be suggested interaction occurred between the B_0 field and the stent materials which may also impact on the closing of the leaflets. Alternatively, it may be there was existing damage to the leaflets which inhibited closure. However, if this were the case a greater consistency of irregularities in the complexes would be displayed in the profile.

Figure 6.19: Hancock Modified Orifice valve @ 1.5 T

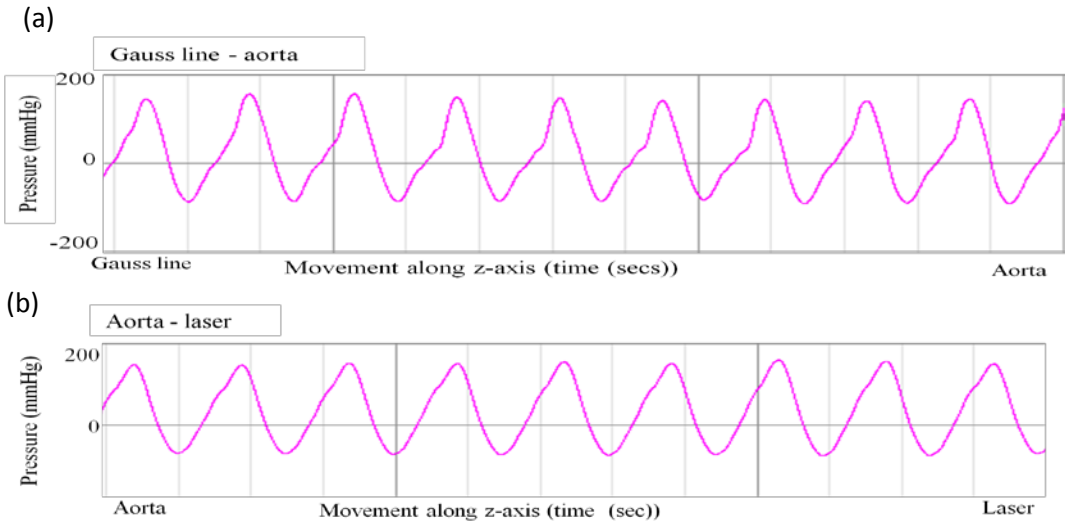

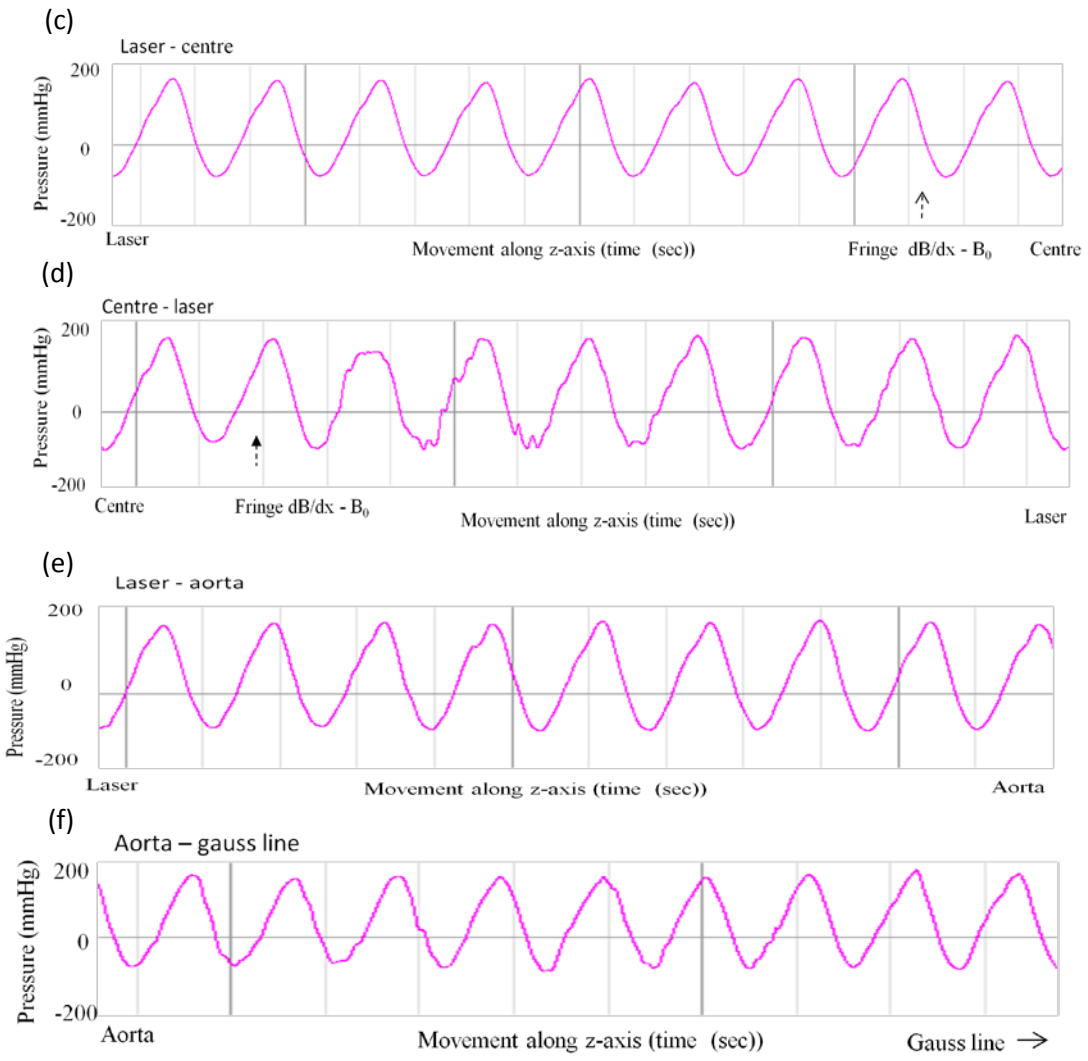

(f) Medtronic valve

Figure 6.20 shows the haemodynamic profile of the Medtronic tilting disc mechanical valve. The overall pattern of complexes in this profile is different to any other haemodynamic profile. Nonetheless, the consistency in the pattern of complexes displayed throughout the progression of the valve from the gauss line to the iso-centre and back indicates there was no interaction of the disc occluder with the magnetic field.

Figure 6.20: Medtronic valve @ 1.5 T

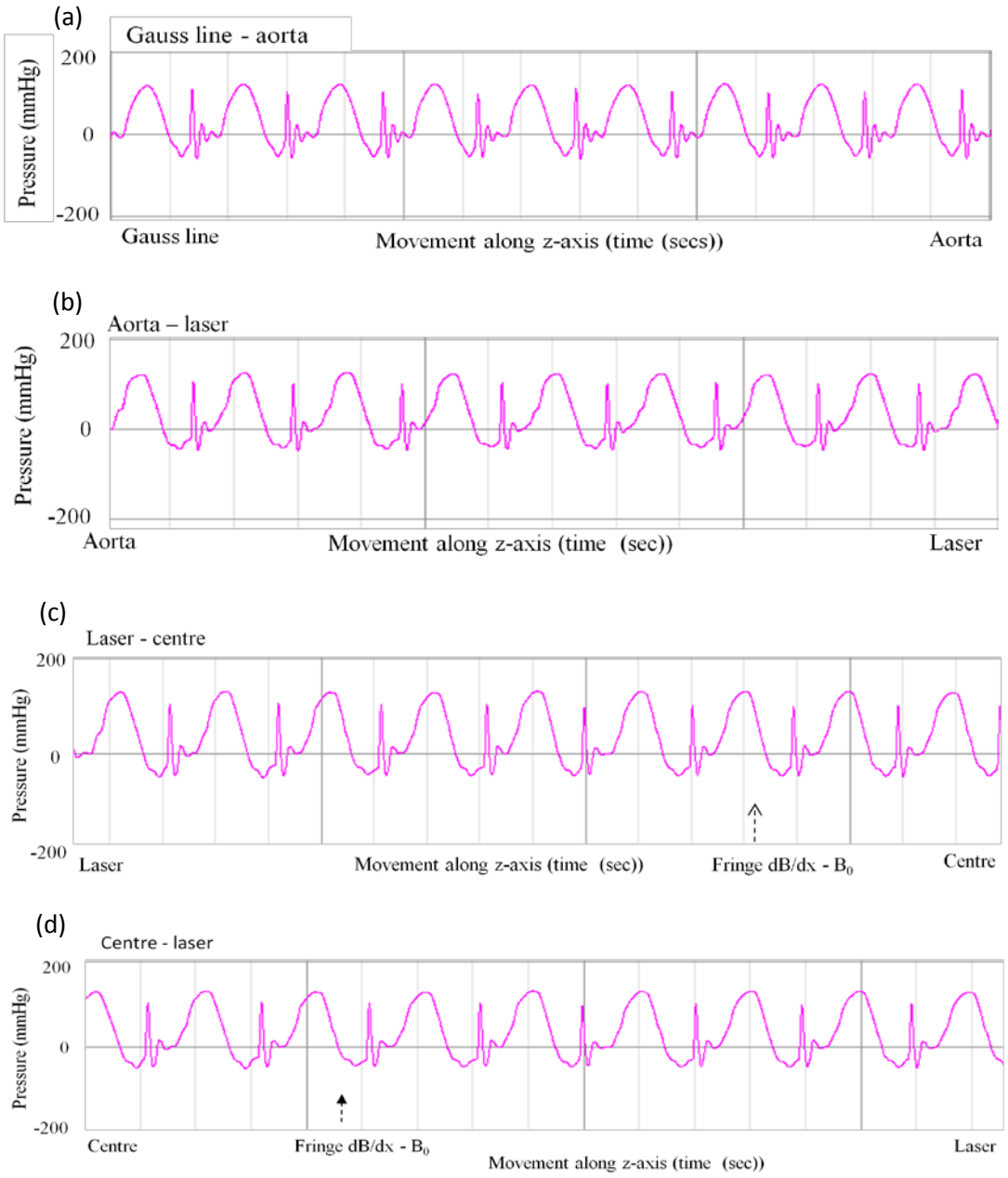

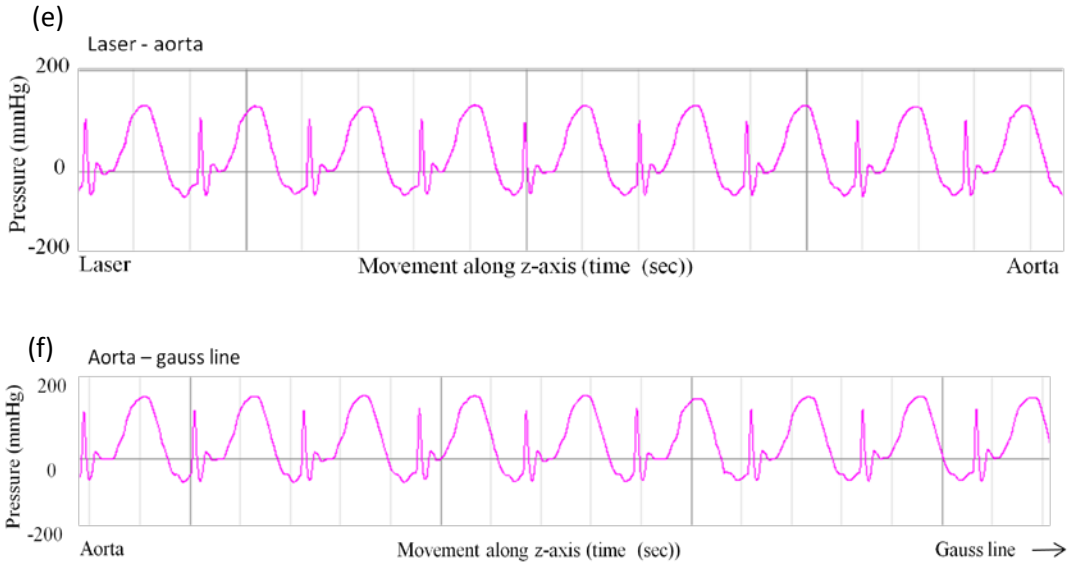

(g) Starr Edwards caged disc valve

The haemodynamic profile showing the response of the Starr Edwards caged disc valve to the magnetic field at 1.5 T is presented in Figure 6.21. The pattern of complexes is consistent throughout the progression of the valve through the magnetic field and indicates no interaction of the occluder with the magnetic field occurred.

Figure 6.21: Starr Edwards caged disc valve @ 1.5 T

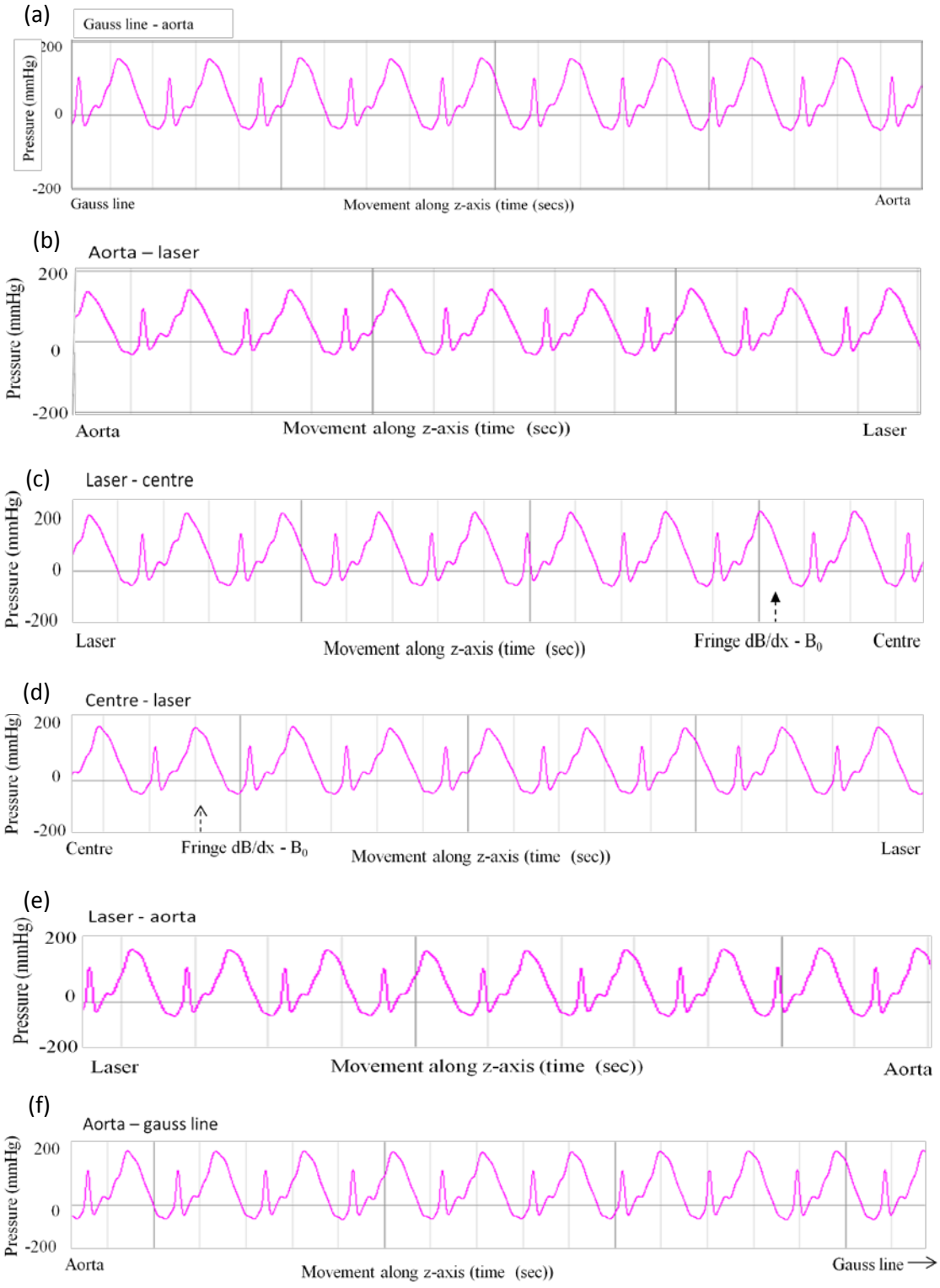

(h) Starr Edwards metal caged ball valve

The dynamic profile of the Starr Edwards metal caged ball valve shows interaction of the metal ball occluder with the magnetic field on the return from the magnet but only after it had advanced through the laser position and continued to progress towards the gauss line. Figure 6.22e shows changes in the shape and magnitude of pulse waves began on the first complex after the laser position. Notches in the ascending and descending pulse wave were observed and with increasing frequency as the valve neared the aorta position despite a decrease in the magnetic field strength (Figure 6.22e-f). Moreover, the shape of the notches between the 5th and 9th complexes in Figure 6.22e and 1st and 4th complexes in Figure 6.22f suggest the interaction of the ball occluder with the magnetic field during systole caused a sudden movement of the ball to the closed position resulting in shock waves (ie. similar to the water hammer effect).

Figure 6.22: Starr Edwards metal caged ball valve @ 1.5 T

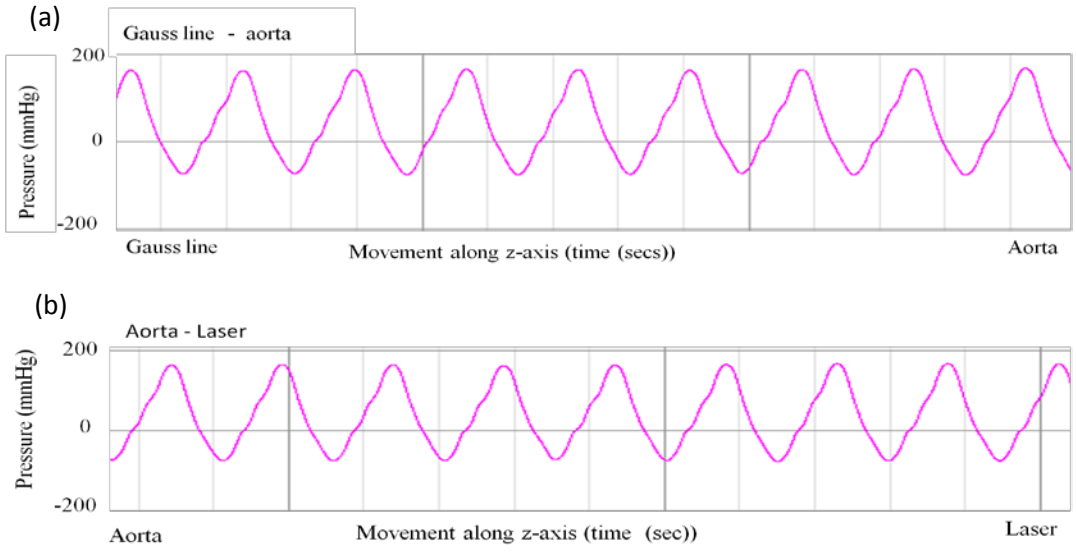

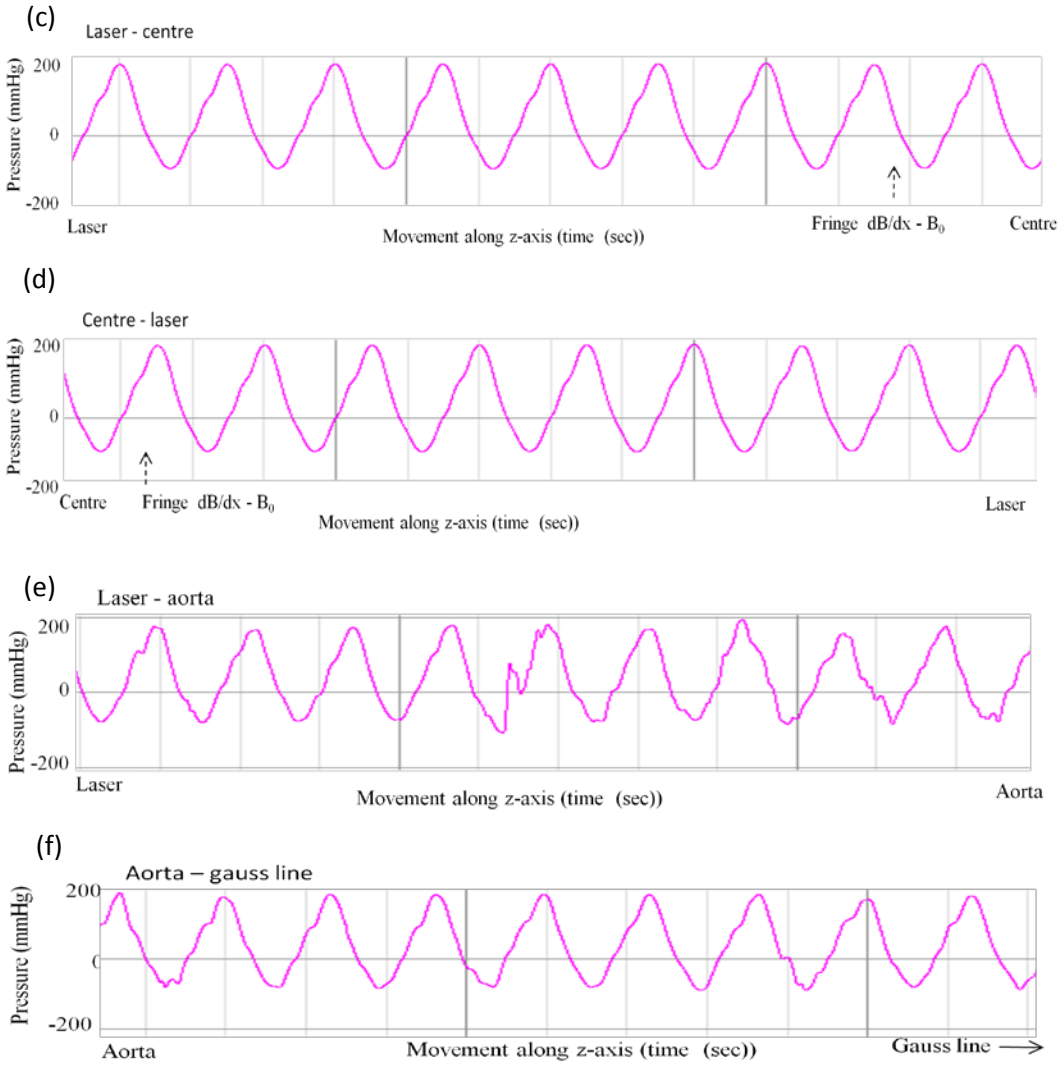

(i) Starr Edwards silastic caged ball valve

The consistent pattern of the waveforms displayed by the haemodynamic profile of the Starr Edwards silastic caged ball valve shown in Figure 6.23 suggests no interaction of this valve with the magnetic field associated with 1.5 T occurred.

Figure 6.23: Starr Edwards silastic caged ball valve @ 1.5 T

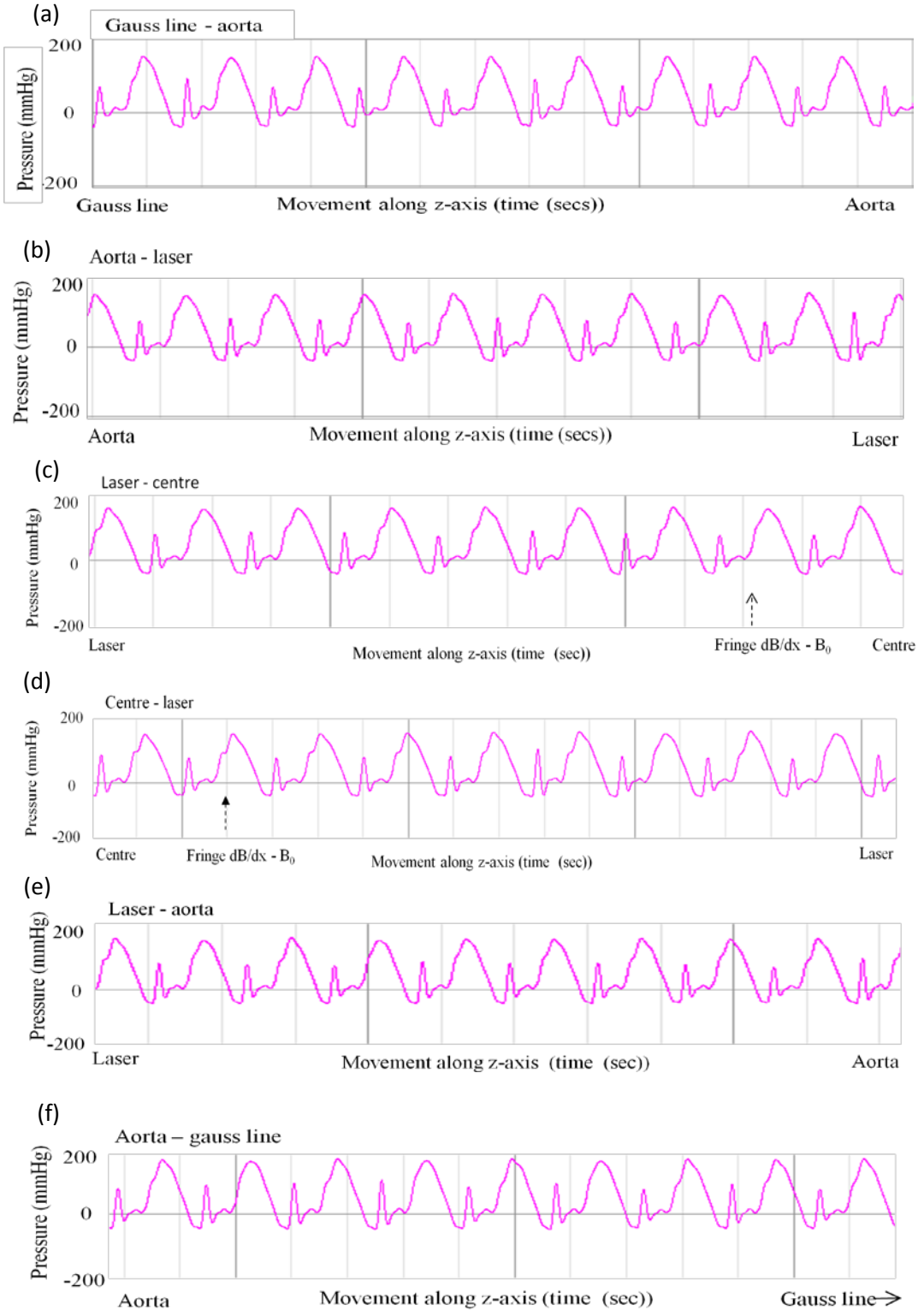

6.13 Overall results @ 3.0 T

There were considerable technical and environmental challenges which precluded the investigation of valve function using the hydro-dynamic test apparatus in the 3.0 T setting. The layout of the 3.0 T MRI suite resulted in the need for extremely long input and output tubing sections to feed the valve test element of the apparatus. Whilst this was technically possible to achieve, it resulted in an unacceptable level of "dampening" of the pressure waveform within the system, producing pressure profiles which were not physiologically representative in any meaningful way. A solution to this would have been to move the flow generating apparatus into the MRI suit, shortening the input and output tubing length however, the makeup of this element of the technology, which incorporates ferrous elements, was not compatible with MRI safety. Therefore the safe deployment of the device was not possible in the 3.0 T setting. Clearly this is a matter which requires further investigation and design consideration and forms an essential part of our future work.

6.14 Chapter summary

Chapter 6 presented the results of the *ex vivo* and *in vitro* evaluation of a novel device designed to be compatible with the MR environment and to detect and quantitatively measure movement and functional performance of 9 different heart valve prostheses exposed to the B_0 field associated with field strengths of 1.5 T and 3.0 T. The baseline data confirm, although there was some interaction of the *ex vivo* test apparatus with the B_0 field this was unlikely to be hazardous and had little impact on the experimental data which was adjusted accordingly. Thus, overall the MRI compatibility of both the *ex vivo* and *in vitro* components of this test apparatus was confirmed. Real-time three-dimensional dynamic movements of the valves were detected and the applied force quantitatively measured. Furthermore, despite difficulties experienced in conducting the hydro-dynamic test at 3.0 T the results obtained at 1.5 T confirm the ability of this apparatus to detect and measure changes in pressure across the valve which indicates the possibility of an interaction between the B_0 field and the valve's occluder/leaflets. The

overall the results of this investigation therefore corroborate the compatibility, sensitivity and capacity of this test apparatus within the MR environment and thereby confirm the aims and objectives of this study were met.

CHAPTER 7

Discussion

7. Introduction

Research suggests the aging and/or disease processes may compromise cardiac tissue strength sufficiently to cause an increase in the risk of unwanted prosthetic heart valve movement and/or dislodgement during exposure to strong magnetic fields associated with MRI (Edwards 2005). Moreover, as previously mentioned these risks may be further amplified with exposure to higher field strength MR systems which are becoming more commonplace in clinical practice today as technology continues to push the upper field limit. Little if anything is known about the *in vivo* movement of cardiac valve prostheses within the MR environment or whether the Lenz Effect restricts the valve's leaflets/occluder sufficiently to cause functional valve impedance. The limitations of existing test methodologies and apparatus have resulted in an inability to fully assess valve movement in terms of frequency, direction, magnitude and functional valve performance *in vivo* in which the valve is constrained by retentive and counteractive forces and is either stationary within or, in continuous motion through the B_0 field. As a result of the paucity of data questions about the potential risks of harmful or fatal movement, dislodgement and valve dehiscence in tissue already compromised by degrading and/or degenerative processes or, functional valve impedance have been raised. The aim of this study was to assess the sensitivity and capacity of a novel device intended to detect and measure *ex vivo* the frequency, direction and the magnitude of movements of prosthetic heart valves exposed to MR associated B_0 fields and, assess valve function *in vitro* as the valve(s) were advanced continuously through the B_0 field. This chapter reviews and discusses the results of this investigation and whether the study's aims and objectives were met. In addition, the limitations of the test apparatus and methodology employed are discussed and what contribution these study findings can make to our knowledge and understanding of the behaviour of heart valve prostheses *in vitro* during exposure to B_0 fields $\leq$3.0 T.

7.1 Addressing the limitations of existing methodology

Historically, assessment of MR associated translation and rotational forces on heart valve prostheses have been performed *ex vivo* using a piece of thread to suspend a heart valve from the vertical of a non-ferromagnetic frame and measuring the angle of deflection and by using a qualitative scale of measurement to assess torque force (Soulen 1985; Randall 1988; Frank 1992; Pruefer 2001; Shellock 1994, 2001; Chapters 5 & 6). Although these methods provide some indication of the type and magnitude of forces acting on the valve prostheses they are subject to a number of limitations. Firstly, uncertainty persists regarding the location within the B_0 field displacement measurements should be recorded. Soulen (1985), Frank (1992), Kagetsu (1991) and Shellock (1994) for example, measured displacement force at the entrance to the magnet where the flux line density is the greatest. In contrast, others have recorded displacement force at the point within the magnetic field where the spatial gradient is determined to be at its maximum (Randall 1988; Shellock 2001; ASTM 2006; Chapter 5). However, as Figures 6.4 - 6.6 and 6.10 - 6.11 show this novel apparatus recorded larger and potentially harmful magnetic forces at other locations within the magnetic field than previously reported at either the entrance to the magnet or the point of the highest spatial gradient with forces ranging from 3.0 Nwt x 10^{-2} to 1.4 Nwt x 10^{-1} at 1.5 T at the aorta position (Figure 5.14). In comparison, applied displacement forces reported by others at the magnet entrance and highest spatial gradient ranged from 9.6 Nwt x 10^{-5} to 1.1 Nwt x 10^{-3} respectively (Soulen 1985 Frank 1992; Pruefer 2001; see also Chapter 6). Furthermore, this study also found the highest magnitude of movement, and thus force, was not always recorded in the same location within the field for all valves. Thus, this investigation has shown the standard use of singular specific locations to measure the applied displacement force is unsatisfactory.

Other limitations of the existing test apparatus and methodology are, measurements were one-dimensional and therefore failed to detect or record other movements which may have occurred in the x- and the y- planes. Furthermore, with the exception of a thin

thread to suspend the heart valve prosthesis from the test apparatus the valves were unrestrained contrary to the *in vivo* state in which a heart valve prosthesis is usually secured by at least 14 sutures (discussed below). In addition, the apparatus was unable to position the valve in such a way it matched the *in vivo* height and orientation and as a consequence of these failings it has not been possible to properly assess the true risks of valve movement, dislodgement or dehiscence *in vivo* in a patient exposed to the B_0 field environment. The results of this investigation show the design of this apparatus successfully addressed each of these shortcomings. Although the heart valve was secured in the valve holder it was still free to move in response to interactions with the magnetic field and the data captured recorded three-dimensional movement across the x-, y- and z-axes. Furthermore, the jointed stand holding the valve holder allowed for the valve to be oriented according to the correct *in vivo* position and height. Moreover, unlike previous studies which only reported on statically placed heart valve prostheses within the B_0 field, this apparatus allows reporting on valvular movement of the statically placed valve and as it continuously advanced through the field. Thus, in light of this investigation's results it might be suggested our current use of static measurements of valve deflection and rotation to determine safe exposure of prosthetic heart valve patients to the B_0 field may be inappropriate because, as the data show the type and magnitude of the valve's response differs depending on whether the measurement was captured during static or dynamic recording.

Previous research was also limited in its ability to quantitatively measure torque force. Consequently, data on the actual magnitude of rotational force, which is potentially more harmful than translation force, was deficient. The cramped confines of the magnet also made it difficult for the investigator(s) to read the angle of deflection accurately thereby increasing the potential for investigator error. The use of a strain gauge system which independently recorded valvular movement eliminated this type of error and bias. However, although this apparatus measured the magnitude of displacement force it was incapable of measuring the distance of that displacement. As a consequence, it was not

possible to determine the degree of displacement and thereby apply this to current safety standards and subsequently determine comparable risk of harm to the patient.

Moreover, in addition to the potential for valve movement as a whole, as Chapter 4 mentions concerns have also been expressed about the potential for functional valve impedance as a result of metal components within the valve's occluder creating an associated yet separate magnetic field in opposition to the magnetic field of the MR system (Condon 2000; Robertson 2000). However, such concerns are primarily based on conjecture and there is, as yet, no empirical evidence to confirm the occurrence of the Lenz Effect *in vivo*. Therefore, one of the aims of this study and as described in Chapter 5 was to design and evaluate a device with the capacity to test this theory. Despite the difficulties experienced in analyzing these results this sensitive instrument was shown to be capable of capturing and recording leaflet 'flutter' which may impact, albeit temporarily within the MR environment, on the haemodynamic performance of the heart valve. This finding however, merits further investigation and application of a more refined analytical tool.

7.2 Rejecting the H_0

Overall, the experimental data presented in this study confirms both the sensitivity and capability of this test apparatus to detect and record movement of the valve's annulus within a retained structure as well as, changes in functional valve performance associated with the interaction of the valve's leaflets with magnetically induced forces. For the first time the frequency and magnitude of movements could be successfully captured in real-time, in three-dimension and on any and all points along the z-axis when the valve was either placed statically or as it moved continuously through the B_0 field associated with the 1.5 T and the 3.0 T environments. Furthermore, the use of strain gauges placed equidistant at intervals around the valve ring meant, not only were a range of movements detected but the apparatus was also able to differentiate between deflective, tilting and rotational movements occurring either concurrently or

simultaneously. In addition, unlike previous studies this apparatus was capable of recording the applied magnetic force at the time valve movement occurred and equally if not more importantly, provides a quantitative measurement of torque force which, as Chapter 5 mentioned, has historically been subjectively measured. Furthermore, by using a series of strain gauges connected to a strain gauge recorder and laptop computer this test apparatus was able to produce profiles showing real-time dynamic valve movements as they occurred in addition to, improving the accuracy of data capture. The sensitivity of the *in vitro* component of the test apparatus to detect changes in fluid flow was proven in the haemodynamic profiles. Unusual and irregular complexes, such as those displayed in Figure 6.15 clearly illustrate the ability of the apparatus to detect and record changes in pressure profiles of the complexes corresponding to unexpected movements or interaction of the valves leaflets with the magnetic field. The experimental data also confirms the compatibility of the test apparatus within the MR environment. Although, as discussed in Chapter 5 some components of the test apparatus contained ferromagnetic materials which could not be substituted and therefore had to remain in the control room, those elements which were directly exposed to the MR environment showed little or no interaction with the magnetic fields as illustrated by the *ex vivo* and *in vitro* baseline profiles (Figures 6.3; 6.14). Thus, the data shows the device possesses the sensitivity and the capacity to detect and record the occurrence, frequency, direction and magnitude of prosthetic valve movement and valve function as the valve moves through the B_0 field. Thus, the requirements of the H_0 have not been met and therefore this hypothesis must be rejected in favour of the H_1.

7.3 Limitations of this investigation

Although this investigation was successful in its efforts to design and evaluate a novel device which aimed to detect and record prosthetic valvular movement within the MR environment a number of problems and limitations of the apparatus and methodology were identified. One of the major obstacles in conducting this investigation was the significant cost. The budget for the study was very small but the cost of the equipment

was very high for example, a single prosthetic heart valve costs in the region of £2,000 to £3,000, the use of one of the MR systems at the Southern General Hospital, Glasgow has a daily cost of £2,000. Furthermore, the various components for the Heart Valve Motion Analysis System (HVMAS) including computer software added up to just under £30,000. Nine heart valve prostheses were used in the study and two MR systems. In addition, other resources such as specialist engineers were used for the fabrication of the HVMAS as well as MR professionals to operate the MR systems. The study was however extremely fortunate to receive donated prosthetic hearts valves for use in the study as well as free time on the MR systems and donated engineering capacity. Nonetheless, this lack of funds restricted the number of available heart valves for evaluation, access to the MR systems and also the number of times each prosthesis could be exposed to the magnetic field environments. Furthermore, the lack of available funds also meant the study was dependent on fitting in with the timetables and commitments of those key specialists who donated their time. As a consequence this had an impact on the execution of the investigation.

Other limitations of the study became apparent during the conduct of the study. During the *ex vivo* investigations insertion of the different valves into the valve holder was relatively quick and easy and certainly less cumbersome than in the preliminary investigations. However, the *in vitro* insertion of the prosthesis into the valve holder proved both awkward and time consuming as a result of having to partially dismantle the water-tight container and also the valve holder which was screwed together. This led to increased preparation time for each valve and resulted in unexpected delays in performing these experiments. As a result, this part of the experimental procedure took longer than originally planned. Some problems however did not become apparent until the analysis phase of the investigation. During the analysis of the *ex vivo* data for example, interpretation of the type and sequence of movements was sometimes difficult. This stemmed from the use of only four strain gauges on the valve holder which detected and recorded movements across only the N-S and W-E axes. Although movements occurring outside these axes were detected to some extent, the interpretation of rotational

movements in particular with regards to their direction and sequence (ie. clockwise versus anti-clockwise) was more difficult than originally envisaged. Analysis of the 3.0 T *in vitro* data proved very difficult as Chapter 6 described. During the execution of the *in vitro* investigations it was noted the distance between the control room and 3.0 T MR suite was slightly greater than between the control room and the 1.5 T suite. At the time this did not appear to cause any significant problems. However, this greater distance between the fluid reservoir and valve chamber caused an energy loss and subsequent pressure drop in fluid which was not detected at the time and as a result the data was subjected to considerable dampening effect.

In addition, one of the most significant limitations of the investigation identified was the inability of the device to detect and measure movement of the valve's annulus in conjunction with changes in the pressure profile denoting interaction of the valve's leaflets/occluder with the magnetic field. This shortcoming meant it was not possible to garner a comprehensive picture of the valve's full interaction with the magnetic field and therefore assess the risk of harm to the patient in those valve's which displayed both *ex vivo* and *in vitro* responses such as, the Björk Shiley valve, Edwards Tekna valve, Starr Edwards metal caged ball valve and the Hancock II Modified Orifice valve. Nonetheless, despite these limitations the device was able to successfully detect and record some very interesting and unexpected results but also provide for the first time, some insight into the actual behaviour of heart valve prostheses to the MR environment.

7.4 Interaction of valve prostheses within the dB/dx and B_0 field

The pattern of valve movements displayed *ex vivo* raises questions about the effects of translation and rotational forces on the anchoring mechanisms of the valve. Movement of the valve ring within the valve holder was shown to be neither static nor uncommon but a series of continuous dynamic movements. In addition, the response of the valve(s) to the B_0 field differs between the entry and the return journeys and these differences also extend to between field strengths. Deflective movements of the valve are expected

in the inhomogeneous field in response to translational forces and indeed, these movements were not uncommon and occurred both on entry and return from the B_0 field. However, a number of differences were detected by the apparatus compared with other studies. Firstly, very few deflections were lateral with most occurring in the x-y plane (ie. upwards/downwards; Figure 5.8③). The Björk Shiley tilting disc valve, the Medtronic single leaflet valve, the Starr Edwards caged disc valve and the two Carpentier Edwards tissue valves all deflected downwards against the valve holder as they passed through the aorta position on entry to the 1.5 T magnets. At 3.0 T three valves, the Björk Shiley, Carpentier Edwards pericardial and the Edwards Tekna bileaflet valve deflected at the aorta position but contrary to deflections at the lower field strength the force acting on the Björk Shiley and Edwards Tekna valves caused the valve rings to be deflected upwards and away from the valve holder. Secondly, deflective movements did not always occur in isolation but also occurred in conjunction with tilting and/or rotational motions. For instance and as previously mentioned, the Björk Shiley valve displayed deflections at entry and on the return from the magnet at the aorta point at 1.5 T and 3.0 T and, as Figure 6.4 shows these movements occurred in conjunction with simultaneous tilting motions causing the valve to rotate. At 1.5 T for example, the rotational movement caused the flat side of the valve's outflow structure to face perpendicular to the direction of the applied field but at 3.0 T, the flat side of the inflow structure was orientated perpendicular to the field lines as depicted in Figure 7.1. The Carpentier Edwards porcine valve and the Starr Edwards silastic caged ball valve both also displayed tilting motions at 1.5 T, although the pattern of oscillations suggest a different type of tilting motion more akin to a spinning-like movement along the W-E axis. In addition, the Starr Edwards valve displayed a rotational movement such that the cage of the valve was oriented towards the magnet as though attempting to align its long axis parallel to the magnetic field. The overall data shows there was little effect on valve function *in vitro* at 1.5 T although it is difficult to confirm any interaction between the B_0 field at 3.0 T and the cardiac valve prostheses for reasons already stated.

Figure 7.1: Illustration of the inflow and outflow aspects of a single leaflet heart valve prosthesis in relation to the direction of the applied field.

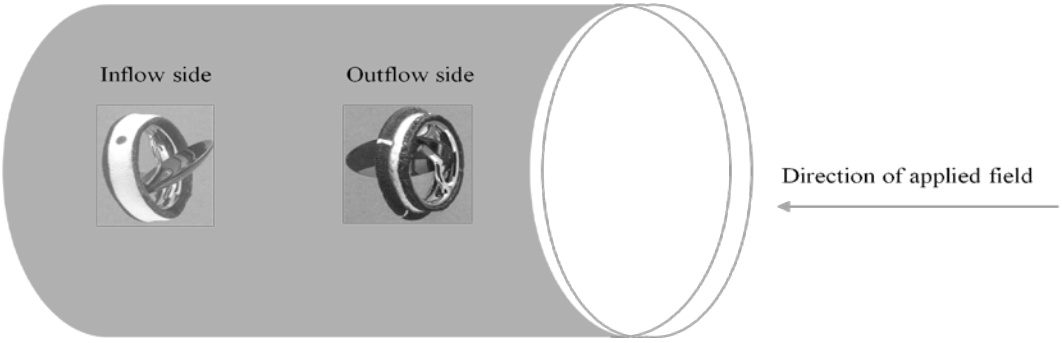

The magnitude of an implant's interaction with the B_0 field depends on its dimensions, mass, orientation, magnetic properties and χ as well as the quality of tissue anchoring it in place. Inherent to the amplitude of the field is its spatial gradient which changes over distance creating a differential translational force. Thus the types of movements displayed by these valves reflect the changes in these field gradients because the orientation of the valves in the field were such that the front part of the valves' annuli (ie. Channel 4 (W) remained in the slightly higher field than the back part (ie. Channel 2 (E) causing the valve to tilt along the W-E axis and deflect along the z-axis. Rotational movements are, on the other hand, associated with the homogeneous field. Thin flat spherical implants will, for example, attempt to turn their flat surfaces parallel to the field lines. In contrast, non-spherical implants which have a greater length than width will attempt to align their long axis with the direction of the magnetic field. Thus, thin flattish valves such as the Björk Shiley, Edwards Tekna and Medtronic valves should attempt to tilt/rotate their flat surfaces (ie. inflow side) in the direction of the applied field in contrast to the high profile valves which would align their long axes parallel to the field lines. At 1.5 T and 3.0 T the Björk Shiley appeared to adhere to this rule and tilt so that the outflow side was oriented towards the direction of the field lines. The Edwards Tekna valve also appeared to follow this rule with the exception that at 1.5 T its

inflow side was tilted towards the direction of the field but the reverse was true at 3.0 T. Only the Medtronic valve displayed some degree of orientation of its inflow side in the direction of the field lines at both field strengths. Of the higher profile valves neither the Starr Edwards metal caged ball or caged disc valves or, the Hancock porcine valve displayed any orientation of their long axes in the direction of the magnetic field. The Starr Edwards silastic caged ball valve and the two Carpentier tissue valves did however orientate their long axes in the direction of the magnetic field. Although all three of these valves had relatively large ring diameters the respective caged housing and stents increased their overall dimensions such that their lengths were greater than their widths and as a result they behaved like non-spherical implants (Figure 5.3/Table 6). Interestingly however, the Carpentier Edwards pericardial valve only oriented its long axis parallel to the direction of the field on entry to the magnet and not on the return and the porcine valve only orientated its long axis in the direction of the field at 3.0 T and not at 1.5 T.

As a result of these non-conformities to the rule it could be suggested an implant's other properties contribute more to its behaviour within the magnetic field. All the materials used in the manufacture of these heart valves are recommended for use in the manufacture of biomedical implants because of their biocompatibility, mechanical properties and good fatigue life (New 1983; Davis 2003). Many of these materials which include carbon-based material (eg. pyrolitic carbon), cobalt alloys (eg. Haynes Stellite-21, Haynes Stellite-25, Elgiloy), titanium alloys and polymers (eg. silicone rubber, polyester) (Table 6) are intrinsically non-magnetic but arguments about the potential to alter their magnet properties through handling, heat treatments and/or cold working (e.g., machining, melting, moulding, bending, solidification etc) for example continue. Cobalt and nickel alloys are it is argued, intrinsically ferromagnetic in their pure form but Assefpour-Dezfuly and Bonfield (1984) and Clerc and colleagues (1997) argue this magnetism is lost as a result of the manufacturing processes so the resultant alloys such as Elgiloy, are non-magnetic. However, a counter argument presented by Ho and Shellock (1999) suggests rather than being non-magnetic these alloys possess some

degree of magnetism and are paramagnetic as a result of a random mix of alloys occurring during solid formation which results in the nickel and cobalt combining to produce cluster formations which act as microscopic magnets. Additional mechanical or heat treatment/cold working is thought to increase the numbers and/or sizes of these clusters thereby increasing their potential and altering the magnetic properties of the implant.

Further support for this argument is provided by Kanal (1996) who reported some previously non-ferromagnetic aneurysm clips subsequently displayed weakly ferromagnetic properties and suggested induced magnetism may have resulted from the re-sterilization process prior to implantation, post-distribution handling or manufacturing differences. In addition, Kangarlu (2000) and Shellock (2003) reported interactions of implants containing Elgiloy with MR associated B_0 fields and, data presented by these initial investigations show bioprostheses containing Elgiloy interacted more strongly with the B_0 field than most other implants (Table 8). Moreover, pericardial tissue valves displayed one of the highest deflections recorded when exposed to the 4.7 T MR environment. This argument for the potential for induced magnetism in valve prostheses is given further credence by the data presented by Figure 6.2 which confirms the symmetry of the B_0 field in the two MR environments used in this investigation. These symmetrical profiles would suggest for example, valve movements within these fields should also display a corresponding level of symmetry. However, as Figures 6.4 – 6.12 show each valve profile is asymmetrical and shows an increased magnetism on the return from the magnet. Furthermore, this apparent induced magnetism is retained within the valve despite its return through a decreasing magnetic field although it is not known how quickly this takes to dissipate once away from the field exposure. Nevertheless, what is known is this cumulative effect continues at least for as long as the valve remains within the field.

Our understanding of the magnetic properties of materials is however, being continuously updated and materials which have always been considered without question

to be non-magnetic are now being subjected to investigations about whether and how their magnetic properties may be altered. Carbon for example, a baseline element used in many biomedical implants including the Björk Shiley and Edwards Tekna valves (Table 6) has always been considered a non-magnetic element. However, in recent years it has been shown to possess a transient magnetism which can be induced when it is closely exposed to other magnetised elements (Ohldag 2007). This research is however, still very much in its infancy and no firm conclusions can be made at this point about its true magnetic nature. Nevertheless, it introduces the possibility of a transient magnetism being induced in these passive implants.

Ideally knowledge about the χ of an implant would help us to determine whether it was dia-, para- or ferromagnetic and thus, provide some guidance on how it may interact with an external magnetic field and the potential to become magnetized during exposure to that field. Proportional increases in translational attraction and torque on implants resulting from increases in magnetic field strengths between 1.5 T and 3.0 T alter an implant's χ such that it becomes more pronounced at the higher field strength. Consequently, one would expect to see proportional increases in applied forces causing movement of the valve between 1.5 T and 3.0 T. However, one of the limitations of this study was its inability to determine the χ of each valve because movements were not one but three-dimensional across the x-, y- and z-planes and, rotational movements did not just occur in the homogeneous field. Nonetheless, it may be possible to make some very general assumptions about the valves' χ by using as a proxy, magnetic moments calculated at 4.7 T (Table 8) because magnetization is known to be directly proportional to the magnetic moment and χ is directly proportional to magnetization. Thus, the smaller the magnetic moment the less susceptible a valve will be to the applied magnetic field compared with valves with a higher magnetic moment. Three valves from the earlier study the Carpentier Edwards pericardial and porcine valves and the Starr Edwards metal caged ball valve demonstrated magnetic moments of a higher order of magnitude than the remaining five valves for which the magnetic moment could be calculated. The lack of interaction with translation force of the Starr Edwards silastic

caged ball valve resulted in a zero value for its magnetic moment. The data from these earlier studies suggest these three valves should show a greater propensity to interact with the magnetic field. However, as Figures 6.4 - 6.12 show this assumption is not borne out if one compares the frequency and direction of movements with the other valves at either field strength. Moreover, there is no evidence to suggest there were proportional increases in the magnitude of applied magnetic force resulting in valvular movement of the valves between the two field strengths.

The constant dynamic movements of the valve during magnetic field exposure coupled with spikes of intense magnetic force may have implications for the anchoring mechanisms of the valve, especially if the surrounding tissue has been significantly weakened by age, disease or puncture holes caused by suturing. Chapter 4 described how decreases in muscle strength and the body's immune responses to infections resulting from the natural aging process can lead to loss of tissue strength and flexibility by more than 20% by age 70 years. In addition, research has shown puncture holes associated with sutures can weaken tissue by as much as 22-59% (Butany 1992; Lim 1994; Wheatley 1987). Moreover, in a study conducted by Edwards et al (2005) tissue affected by infective endocarditis was found to yield and fully rupture at relatively small forces (ie. <0.2 Nwt). This low yield/rupture force did not however categorise patients as high risk of harmful valve movement or dehiscence because the applied forces causing valve deflections were calculated to be at least one-hundred times smaller than the yield force of infective tissue (Table 8; Frank 1992; Pruefer 2001; Soulen 1985). However, the magnetic forces detected and recorded by this test apparatus and shown in Figures 6.4 - 6.12 are considerably greater and only ten times less than the yield force. Though cardiac valves are customarily secured in place by at least 14 sutures patients with infective or prosthetic valve endocarditis are at increased risk of tissue tearing and rupture because they are more likely to develop paravalvular abscesses which can cause destruction of the valve annulus and also infiltrate other nearby supporting structures (see Chapter 1). Furthermore, patients may continue to be at risk of complications of the disease long after completion of their antibiotic therapy and the increased risk of

developing pseudo-aneurysms adds to the potential additional stresses exerted at the suture line and aortic wall and may therefore further increase the risks of rupture and metastatic abscess formation. What's more, as Chapter 4 noted Schenck (2000) suggested a substantially greater force is required by the tissue to prevent implants whose dimensions are such they are greater in length than width, from aligning with the B_0 field than it does to prevent it from responding to translation force. Thus, patients with high profile valves are therefore at greater risk of harmful valve movement than those with flat spherical valves and, those with a current or past history of prosthetic valve endocarditis are at even greater risk of partial or total valve dehiscence with potentially catastrophic consequences.

CHAPTER 8

Conclusions & further work

8.1 Summary of thesis achievements in relation to the objectives

In summary this thesis describes and evaluates a novel device designed to detect and measure valve movements *ex vivo* and functional valve performance *in vitro* of nine different prosthetic heart valves secured within a structure analogous to the retentive structures *in vivo* as they were continuously advanced through the B_0 fields associated with 1.5 T and 3.0 T. The results of this investigation show this design, though not wholly MR compatible displayed sufficient sensitivity and capacity to detect and record:

- three-dimensional movements in response to the B_0 field and differential B_0 gradient field when the valve was moved continuously through the magnetic field,

- valve movement(s) within the B_0 field,

- the frequency of valve movement(s) and the magnitude of the applied forces and,

- interference of the valve's leaflets/occluder by the B_0 field and thus functional performance during hydro-dynamic flow.

8.2 Rejecting the H_0

The results of this study show this thesis can confidently reject the H_0 hypothesis, which as Chapter 5 states, "will lack the sensitivity and capacity to detect and record the occurrence, frequency, direction and magnitude of prosthetic valve movement and valve function as the valve moves through the B_0 field associated with the MR environment" in favour of accepting the H_1. Thus, this thesis concludes this novel device is superior to existing experimental methodologies used to detect and record valve movement within MR associated B_0 fields.

8.3 Conclusions and implications for clinical practice

The data presented in this study shows this novel device has the technical sensitivity to capture, record and detect differences in cardiac valve prosthesis movement, quantitatively measure applied force and produce individual three-dimensional profiles illustrating valve behaviour. As a result it may be suggested we now have the technology to discriminate between valves moving through the MR environment and therefore provide MR clinicians and operators with sufficient information about the potential interaction of prosthetic heart valves with MR magnetically induced forces based on their materials, dimensions and the *in vivo* orientation. As a consequence of our increased knowledge we should therefore be able to more accurately assess the risk of harmful prosthesis movement in all patients and in particular, those with highly friable tissue where anchorage of the valve prosthesis can be highly precarious.

Concerns raised about the possible impedance of valve function due to the Lenz Effect have neither been proven nor disproven by this investigation and, although the study provides some evidence to show the apparatus' capacity to detect variances in leaflet function in response to the B_0 field problems identified with the test apparatus need to be addressed in order to further investigate Condon's (2000) and Robertson's (2000) theory of the –potential to interfere with functional valve performance and whether - resistive effects increase linearly with field strength.

8.4 Future work

The primary aim of this investigation was to make an MR compatible device capable of detecting and recording valvular movement and functional valve performance within the MR environment and, although this device has shown itself to be superior in comparison with others' devices it nonetheless highlighted the need for further development and

refinement. Design restrictions resulted in a technology which contained some ferromagnetic components which could not be exposed to the MR environment for safety reasons. Consequently the quality of the data captured was affected. In addition, there were difficulties in interpreting the *ex vivo* data which stemmed from having only four strain gauges attached to the valve holder. As a result it lacked the subtlety to record the magnitude of movements occurring between these strain gauges and also made the determination of the direction of movements, particularly rotational movements difficult if not impossible.

Future work would therefore aim to modify the design of the apparatus to incorporate an integrated wireless transmission system to control a pneumatic pump made from plastic materials and capable of communicating with the recording equipment and which could then be located within the MR suite thereby eliminating the need for metres of tubing and cables and thus reducing the potential for flow relationship issues and poor data quality. In addition, the strain gauges could be mounted around the entire circumference of the valve holder in order to capture any and all movements giving a complete 360° three-dimensional profile. Furthermore, these measurements could be further enhanced by attaching the valve holder to a gyroscope to allow greater freedom of movement of the valve holder in any direction in response to applied magnetic forces on the valve itself. Thus, by incorporating all of these refinements to the device its sensitivity and capacity to record valve movements will be significantly improved and interpretation of the resultant data will be made easier. Future work would also focus on combining both the *ex vivo* and *in vitro* components so that a full dataset could be captured during a single exposure to the B_0 field. This would significantly reduce the time it takes to conduct each exposure and thus reduce the costs of the investigation, intra and inter experimental variation and potential error and, would provide information on the combined risks to the patients of the possibility of harmful valve movement and functional valve impedance which is currently unavailable.

Although the main emphasis of this research has been the design of the device the data obtained on valve movements and functional valve performance within the B_0 field have highlighted the need for prosthetic valve profiling. The lack of a benchmark profile providing the limits for normal valve movements and function for comparison make it impossible to determine whether the individual valve profiles fall within normal parameters. This is further complicated because the profiles for each individual prosthesis, *ex vivo*, differs between the different field strengths. Thus, it is important to define a set of profiles for each prosthetic heart valve, including the new percutaneous heart valve prostheses for which no information is currently available, in order to provide a standard baseline profile and range of parameters to determine safe movement *in vitro* within the B_0 field and for all field strengths. This study would need to include each make and model of the different valve types of heart valves, for single and multiple exposures taking into account the length of time between exposures for those valves undergoing multiple exposures.

In summary, although significant modifications to this apparatus are required to improve its capacity to capture more readily analyzable data on valve movement and functional performance within the B_0 field, having tested this device we conclude it nevertheless introduces a new method for detecting and recording the interaction of prosthetic heart valves with magnetically induced forces associated with MRI. The data shows this device possesses the sensitivity and capacity to detect and record three-dimensional, real-time movement and functional valve performance of different heart valve prostheses exposed to the MR associated B_0 field during continuous progression through the magnetic field environment. Furthermore, unlike existing methodologies this device has the ability to simultaneously record quantitative measurements of applied magnetic force. Thus, this investigation shows this device provides a superior method of assessing magnetic field interactions between cardiac valve prostheses and MR associated translation and rotational forces and, the resultant data will provide MR operators and clinicians with accurate information on the safe exposure of prosthetic heart valve implant patients to the MR environment.

REFERENCES

Adair ER, Berglund LG. On thermoregulatory consequences of NMR imaging. *Magn.Reson.Imaging1986;4:321-333*

Adair ER, Berglund LG. Thermoregulatory consequences of cardiovascular impairment during NMR imaging in warm/humid environments. *Magn.Reson.Imaging 1989;7:25-37*

Akins CW. Review of the global experience with the Medtronic-Ha valve. *Eur J Cardio-thorac Surg 1992;6(1):S68-S74*

Alfieri O, Maisano F, De Bonis M et al. The double-orifice technique in mitral valve repair: a simple solution for complex problems. *J Thorac Cardiovasc surg 2001;122:674-681*

Allender S, Peto V, Scarborough P, Kaur A, Rayner M (2008). *Coronary heart disease statistics*. Oxford: British Heart Foundation Health Promotion Group, Department Public Health, University Oxford

American Standard for Testing and Materials (ASTM). Standard specification for the requirements and disclosure of self-closing aneurysm clips. *ASTM Designation Standard F1542–94:1-3. West Conshohocken, PA: ASTM International; 2000*

American Standard for Testing and Materials (ASTM). Standard test method for measurement of magnetically induced displacement force on medical devices in the magnetic resonance environment. *ASTM Designation Standard F2052-06. West Conshohocken, PA: ASTM International 2006.*

American Standard for Testing and Materials (ASTM). Standard test method for measurement of magnetically induced torque on medical devices in the magnetic resonance environment. ASTM Designation Standard F2213-06. *West Conshohocken, PA: ASTM International 2006.*

Anderson HR, Knudsen LL, Hasenkam JM. Transluminal implantation of artificial heart valves. Description of a new expandable aortic valve and initial results with implantation by catheter technique in closed chest pigs. *Eur Heart J 1992;13(5):704-708*

Anguera I, Del Río A, Miró JM, Matínez-Lacasa X, Marco F, Gumá JR et al. Staphylococcus lugdunensis of infective endocarditis: description of 10 cases and analysis of native valve, prosthetic valve, and pacemaker lead endocarditis clinical profiles. *Heart 2005;91:160-166*

Arom KV, Emery RW, Shettry VR, Janey PA. Comparison between port-access and less invasive surgery. *Ann Thorac Surg 1999;68:1525–1528*

Assefpour-Dezfuly M, Bonfield W. Strengthening mechanisms in Elgiloy. *J.Mater.Sci 1994;19;2815-2836*

Attman WG, El Tahan S. Minimally invasive closed mitral commissurotomy. *Tex Heart Inst J 1999;26:269-274*

Baker LC, Atlas CW, Afendulls CC. Expanded use of imaging technology and the challenge of measuring value. *Health Aff (Millwood) 2008;27(6):1467-1478*

Baldwin JC: Editorial (con) re Minimally invasive port-access mitral valve surgery. *Comment* on *J Thorac Cardiovasc Surg 1998:115(3):563-564*

Barany RF. Abnormal vascular reaction in diabetes mellitus. *Acta Med Scand Suppl 1955;304:556-624*

Bashore TM. Adult congenital heart disease right ventricular outflow tract lesions. *Circulation 2007;115:1933-1947*

Baumgartner FJ, Munro AI, Jamieson WRE. Fracture embolization of a Duromedics mitral prosthesis. *Tex Heart Inst J 1997;24(2):122-124*

Beers J. Biological effects of weak electromagnetic fields from 0 Hz to 200 MHz: a survey of literature with special emphasis on possible magnetic resonance effects. *Magn.Reson.Imaging 1989;7:309-331*

Beischer DE, Knepton JC Jr. Influence of strong magnetic fields on the electrocardiogram of squirrel monkeys (Saimiri Sciureus*). Aerosp Med 1964;35:939-944*

Belcher JR. The surgical treatment of mitral regurgitation. *Brit Heart J 1964;26:513-523*

Benyon RP, Bahl VK, Prendergast BD. Infective endocarditis. *BMJ 2006;333:334-339*

Bernal JM, Gutiérrez-Morlote J, Llorca J, San José JM, Morales Pontón A, Diaz B, Llorca J, García I, Srralde A, Diago C, Revuelta JM. Surgery for rheumatic tricuspid valve disease: A 30-year experience. *Ann Thorac Surg. 2008;136(2):476-481*

Bettadapur MS, Griffin BP, Asher CR. Caring for patients with prosthetic heart valves. *Cleveland Clinic Journal Medicine 2002;69(1):75-87*

Bigelow WE, Callaghan JC, Hopps JA. General hypothermia for experimental intracradiac surgery. *Ann Surg 1950;132:531-537*

Bizzarri F, Tudisco A, Ricci M, Rose D, Frati G. Different ways to repair the mitral valve with artificial chordae: a systematic review. *J Cardiothorac Surg. 2010; 5*: 22

Blackstone EH, Kirklin JW, Pluth JR, et al. The performance of the Braunwald-Cutter prosthetic valve. *Ann Thorac Surg 1977;23:302–18*

Bloch D, Vouhe PR, Poulain MH, Cachera JP, Aubry PH, Heurtematte Y, Loisance DY, Vernant P, Galey JJ. Long-term evaluation of bioprosthetic valves: 615 consecutive cases. *Eur Heart J 1984;5(suppl D):73-80*

Bloomfield P. Choice of heart valve prosthesis. *Heart 2002;87:583-589*

Boga E, Kádár S, Peintler G, Nagypál I. Effect of magnetic fields on a propagating reaction front. *Nature 1990;347:749-751*

Bonow RO, Carabello B, de Leon AC Jr. Edmunds LH Jr. Fedderley BJ, Freed MD et al. Guidelines for the management of patients with valvulvar heart disease: executive summary. A report of the American College of Cardiology/American Heart Association Task Force on Practice Guidelines (Committee on Management of Patients with Valvular Heart Disease). *Circulation 1998;98:1949-1984*

Boudoulas H. Etiology of valvular heart disease in the 21st Century. *Hellenic J Cardiol 2002;43:183-188*

Bourland JD, Nyenhuis JA, Schaefer DJ. Physiologic effects of intense MR imaging gradient coils. *Neuroimaging Clin N Am 1999;9:363-377*

Boutin RD, Briggs JE, Williamson MR. Injuries associated with MR imaging: survey of safety records and methods used to screen patients for metallic foreign bodies before imaging. *Am J Roentgenol 1994;162:189-194*

Boyle D. A comparison of medical and surgical treatments of mitral stenosis. *BMJ 1961;23:377-382*

Braunberger E, Deloche A, Berrebi A, Abdallah F, Celestin JA, Meimoun P, Chatellier G, Chauvaud S, Fabiani JN, Carpentier A. Very long-term results (more than 20 years) of valve repair with Carpentier's techniques in nonrheumatic mitral valve insufficiency. *Circulation 2001;104(suppl I):I-8 –I-11*

Broom ND, Thomson FJ. Influence of fixation conditions on the performance of glutaraldehyde-treated procine aortic valves: towards a more scientific basis. *Thorax 1979;34(2):166-176*

Brocklehurst B. Magnetic fields and radical reactions: recent developments and their role in nature. *Chem.Soc.Rev. 2002;31:301-311*

Brody as, Sorette MP, Gooding CA, Listerud J, Clark M, Mentzer WC, Brasch RC, James TL. Induced alignment of flowing sickle erythrocytes in a magnetic field: a preliminary report. *Invest Radiol 1985;20:560-566*

Brook RA, Vymazal J, Goldfarb RB et al. Relaxometry and magnetometry of ferritin. *Magn.Reson.Med* 1998;*40:227-235*

Brown TR, Goldstein B, Little J. Severe burns resulting from magnetic resonance imaging with cardiopulmonary monitoring. Risks and relevant safety precautions. *Am J Phys Med Rehab 1993;72(3):166-167*

Brunton L. Preliminary note on the possibility of treating mitral stenosis by surgical methods. *Lancet 1902;1:352*

Buchli R, Boesiger P, Meier D. Heating effect of metallic implants by MRI examinations. *Magn.Reson.Med 1988;7:255-261*

Budinger RF. Nuclear magnetic resonance in vitro studies: known thresholds for health effects. J *Comput Assist Tomogr 1981;5:800-811*

Bulckaen HG, Puisieux FL, Bulckaen ED, di Pompeo C, Bouillanne OM, Watel AA, Fauchais ALM, de Groote P, Millaire A. Antiphospholipid antibodies and the risk of thromboembolic events in valvular heart disease. *Mayo Clin Proc 2003;78:294-298*

Bushong SC. Radiologic Science for Technologists: Physics, Biology, and Protection. *5th ed. St. Louis, Mo: Mosby Year Book Inc; 1993:465-480*

Buskirk EF, Lundegren H, Magnusson L. Heat acclimation patterns in obsess and lean individuals. *Ann N Y Acad Sci 1965;131:637-653*

Butany J, Vanlerberghe K, Silver MD. Morphological findings and causes of failure in 24 explanted Ionescu-Shiley low-profile pericardial heart valves. *Human Pathol 1992;23:1224-1233*

Butany J, Collins MJ, Nair V, Leask RL, Scully HE, Williams WG, David TE. Morphological findings in explanted Toronto stentless porcine valves. *Cardiovasc Pathol 2006;15(1):41-48*

Cabell CH, Heidenreich PA, Chu VH, Moore CM, Stryjewski ME, Corey R, Fowler VG. Increasing rates of cardiac device infections among Medicare beneficiaries: 1990-1999. *Am Heart J 2004;147:582-586*

Cannegieter SC, Rosendaal RF, Briët E. Thromboembolic and bleeding complications in patients with mechanical heart valve prostheses. *Circulation 1994;89:635-641*

Carapetis JR, Steer AC, Mulholland EK, Weber M. The global burden of group A streptococcal diseases. *Lancet Infect Dis 2005;5:685-694*

Carpentier AF, Lessana A, Relland JY, Belli E, Mihaileanu S, Berrebi AJ, Palsky E, Loulmet DF. The "physio-ring": an advanced concept in mitral valve annuloplasty. *Ann Thorac Surg 1995;60:1177–1185*

Cavarocchi NC, Kolff J. Prosthetic valve endocarditis with annulus destruction: technique for reconstruction. *Tex Heart Inst J. 1983;10(1):49-52*

Cervera R, Khamashta MA, Font J, Reyes PA, Vianna JL, López-Soto A et al. High prevalence of significant heart valve lesions in patients with 'primary' antiphospholipid syndrome. *Lupus 1991;1:43-47*

Chakeres DW, de Vocht F. Static magnetic field effects on human subjects related to magnetic resonance imaging systems. *Progress in Biophysics and Molecular Biology 2005;87:255–265*

Chaljub G, Kramer LA, Johnson III RF, Johnson Jr. RF, Singh H, Crow WN. Projectile cylinder accidents resulting from the presence of ferromagnetic nitrus oxide or oxygen tanks in the MR suite. *AJR 2001;177:27-30*

Cheitlin MD, Sokolow M, McIlroy MB (1993) "*Clinical Cardiology*". 6th ed. New York. Lange Medical Publishers

Chiam PTL, Ruiz CE. Percutaneous transcatheter aortic valve implantation: Evolution of the technology. *Am Heart J 2009;157:229-242*

Chionna A, Dwikat M, Panzarini E, Tenuzzo B, Carla EC, Verri T, Pagliara P, Abbro L, Dini L. Cell shape and plasma membrane alterations after static magnetic fields exposure. *European Journal Histochemistry 2003;47:299-308*

Chou C, McDougall JA, Chan KW. RF heating of implanted spinal fusion stimulator during magnetic resonance imaging. *IEEE Trans Biomed Eng 1997;44:367-372*

Christ G, Diwan S. Chronic illness and ageing. Section 1. The demographics of aging and chronic diseases. *Council on Social Work Education. National Centre for Gerontological Social Work Education. Federal Interagency Forum 2008*

Chronik B, Rutt BK. A comparison between human magnetostimulation thresholds in whole-body and head/neck gradient coils. *Magn Reson Med 2001;46:386-394*

Cilliers AM. Rheumatic fever and its management. *BMJ 2006;333:1153-1156*

Cleland J, Molloy PJ. Thrombo-embolic complications of the cloth-covered Starr-Edwards prostheses No. 2300 aortic and No. 6300 mitral. *Thorax 1973;28:41-47*

Cleland WP. The evolution of cardiac surgery in the United Kingdom. *Thorax 1983;38:887-896*

Clerc CO, Jedwab MR, Mayer DW, Thompson PJ, Stinson JS. Assessment of wrought ASTM F058 cobalt alloy properties for permanent surgical implants. *J.Biomed Mater Res (Apl Biomater) 1997;38:229-234*

Coats L, Bonhoeffer P. New percutaneous treatments for valve disease. *Heart 2007;93:639-644*

Coletti D, Teodori L, Albertini MC et al. Static magnetic fields enhance skeletal muscle differentiation in vitro by improving myoblast alignment. *Cytometry Part A. 2007;71A:846-856*

Colletti PM. Size "H" oxygen cylinder: accidental MR projectile at 1.5 Tesla. *J.Magn.Reson.Imaging 2004;19:141-143*

Condon B, Hadley DM. Potential MR hazard to patients with metallic heart valves: The Lenz Effect. *J.Magn.Reson.Imaging 2000;12:171-176*

Connolly HM, Crary JL, McGoon MD, Hensrud DD, Edwards BS, Edwards WD, Schaff HV. Valvular heart disease associated with fenfluramine-phentermine. *N Engl J Med 1997;337:581-588*

Cooley DA: Antagonist's view of minimally invasive heart valve surgery. *J Card Surg* 2000;*15:3-5*

Cosgrove DM, Sabik JF. Minimally Invasive Approach for Aortic Valve Operations. *Ann Thorac Surg 1996;62:596-597*

Crawley F, Bevan D, Wren D. Management of intracranial bleeding associated with anticoagulation: balancing the risk of further bleeding against thromboembolism from prosthetic heart valves. *J Neurol Neurosurg Psychiatry* 2000;69:396–398

Cribier A, Eltchaninoff H, Bash A, Borenstein N, Tron C, Bauer F, Derumeaux G, Anselme F, Laborde F, Leon MB. Percutaneous transcatheter implantation of an aortic valve prosthesis for calcific aortic stenosis: first human case description. *Circ 2002;106:3006-3008*

Currie PF, Sutherland GR, Jacob AJ, Bell JE, Brettle FP, Boon NA. A review of endocarditis in acquired immunodeficiency syndrome and human immunodeficiency virus infection. *Eur Heart J 1995;16(B):15-18*

Cutler EC, Levine SA. Cardiotomy and valvulotomy for mitral stenosis. Exprimental observations and clinical notes concerning an operated case with recovery. *The Boston M & S Journal 1923;188:1023-1027*

D'Avenio G, Canese R, Podo F,Grigioni M. A novel method for measuring the torque on implantable cardiovascular devices in MR static fields. *J Magn Reson Imaging 2007;26:1368-1374*

Dahl CF, Allen MR, Urie PM, Hopkins PN. Valvular regurgitation and surgery associated with fenfluaramine use: an analysis of 5743 individuals. *BMC Med 2008;6:34*

Dasi LP, Simon HA, Sucosky P, Yoganathan AP. Fluid mechanics of artificial heart valves. *Clin Exp Pharmacol Physiol 2009;36(2):225-237*

David TE. Replacement of chordae tendineae with expanded polytetrafluorethyelene sutures. *J Card Surg 1994;4:286-290*

David TE. The surgical treatment of patients with prosthetic valve endocarditis. *Seminars Thorac Cardiovasc Surg 1995;7(1):47-53*

David TE, Ivanov J, Armstrong S, Christie D, Rakowski H. A comparison of mitral valve repair for degenerative disease with posterior, anterior and bileaflet prolapse. *J Thorac Cardiovasc Surg* 2005;*130:1242-1249*

Davis JR (2003). *Handbook of materials for medical devices*. Ohio. ASM International Materials Park.

Davis PL, Crooks L, Arakawa M, McRee R, Kaufman L, Margulis AR. Potential hazards in NMR imaging: heating effects of changing magnetic fields and RF fields on small metallic implants. *AJR Am J Roentgenol 1981;137:857-860*

Dempsey MF, Condon B, Hadley DM. Investigation of the factors responsible for burns during MRI. *J.Magn.Reson.Imaging 2001;13:627-631*

Dempsey MF, Condon B. Thermal injuries associated with MRI. *Clinical Radiology 2001;56:457-465*

de Oliveira JM, Antunes MJ. Mitral valve repair: better than replacement. *Heart 2006;92:275-281*

de Vocht F, van Drooge H, Engels H, Kromhout H. Exposure, health complaints and cognitive performance among employees of an MRI scanners manufacturing department. *J.Magn.Reson.Imaging 2006;23:197-204*

Dini L, Abbro L. Bioeffects of moderate-intensity static magnetic fields on cell cultures. *Micron 2005;36:195-217*

Drinkwater BL, Horvath SM. Heat tolerance and aging. *Med Sci Sports 1979;11:49-55*

Duck FA (1990). Mechanical properties of tissue. In: Academic Press Limited *Physical properties of tissue. A comprehensive reference book.* London: Academic Press Limited. 137-167

Duncan AC, Boughner D, Vesely I. Dynamic gluteraldehyde fixation of a porcine aortic valve xenograft. I. Effect of fixation conditions on the final tissue viscoelastic properties. *Biomats 1996;17:1849-1856*

Duran CG, Ubago JL. Clinical and hemodynamic performance of a totally flexible prosthetic ring for atrioventricular valve reconstruction. *Ann Thorac Surg. 1976 Nov;22(5):458-63*

Dűrrleman N, Pellerin M, Bouchard D, Hébert Y, Cartier R, Perrault LP, Basmadjian A, Carrier M. Prosthetic valve thrombosis: Twenty-year experience at the Montreal Heart Institute. *J Thorac Cardiovasc Surg 2004;127(5):1388-1392*

Edmunds LH Jr. Clark RE, Cohn LH, Grunkemeier GL, Miller DC, Weisel RD. Guidelines for reporting morbidity and mortality after cardiac valvular operations. Ad Hoc Liaison Committee for Standardizing Definition s of Prosthetic Heart Valve Morbidity of The American Association for Thoracic Surgery and The Society of Thoracic Surgeons. *J. Thorac Cardiovasc Surg 1996;112:708-711*

Edwards MB, Ratnatunga CP, Dore CJ, Taylor KM. Thirty-day mortality and long-term survival following surgery for prosthetic endocarditis: a study from the UK Heart Valve Registry. *Eur J Cardio Thorac Surg 1998;14:156-164*

Edwards MB. 25 years of heart valve replacements in the United Kingdom. A guide to types, models and MRI safety. *UK Heart Valve Registry 2000, London, United Kingdom*.

Edwards MB, Draper ERC, Hand JW, Taylor KM, Young IR. Mechanical testing of human cardiac tissue: some implications for MRI safety. *J. Cardiovasc. Magn.Reson 2005;7:835-840*

Edwards MB. Heart valve and annuloplasty ring implants in the United Kingdom 1974 – 2004. A guide to types, models and MRI safety. *UK Heart Valve Registry 2006, London, United Kingdom*.

Ellis LB, Harken DE, Black H. A clinical study of 1000 consecutive cases of mitral stenosis two to nine years after mitral valvuloplasty. *Circulation 1959;19:803-20*

Faggiano P, Antonini-Canterin F, Baldessin F, Lorusso R, A'Aloia A, Dei Cas L. Epidemiology and cardiovascular risk factors of aortic stenosis. *Cardiov Ultrasound 2006;4:27 doi:10.1186/1476-7120-4-27*

Fanelli C, Coppola S, Barone R, Colussi C, Gualaldi G, Volep P, Ghibelli L. Magnetic fields increase cell survival by inhibiting apoptosis via modulation of CA^{++} influx. *FASEB Journal 1999;13:95-102*

Fann JI, St. Goar FG, Komtebedde J, Oz MC, Block PC, Foster E, Butany J, Feldman T, Burdo TA. Beating heart catheter-based edge-to-edge mitral valve procedure in a porcine model: efficacy and healing response. *Circulation 2004;110:988-993*

Farivar RS, Cohn LH. Hypercholestermia is a risk factor for bioprosthetic valve calcification and explantation. *J. Thorac Cardiovasc Surg. 2003;126(4):969-975*

Fedak PWM, McCarthy PM Bonow RO. Evolving concepts and technologies in mitral valve repair. *Circulation 2008;117;963-974*

Feng ZG, Umezu M, Fujimoto T, Tsukahara, T, Nurishi M, Kawaguchi D. In vitro hydrodynamics of four bileaflet valves in mitral position. *Asian Cardiovasc Thorac Ann 2000;8:3–10*

Feldman T, Kar S, Rinaldi M, Fail P, Hermiller J, Smalling R, Whitlow PL, Gray W, Low R, Herrmann HC, Lim S, Foster, Glower D, for the EVEREST Investigators. Percutaneous mitral valve repair with the MitraClip System. Safety and midterm durability in the Initial EVEREST (Endovascular Valve Edge-to-Edge Repair Study) Cohort. *J Am Coll Cardiol 2009;54:686–94*

Fennel WH. The responses of aged men to passive heating. *Am.J.Physiol 1969;67:118-119*

Fihn SD, Callahan CM, Martin DC, McDonell MB, Henikoff JG, White RH. The risk for and severity of bleeding complication in elderly patients treated with warfarin. *Ann Intern Med 1996;124(11):970-979*

Fong IW. New perspectives of infections in cardiovascular disease. *Curr Cardiol Rev 2009;5(2):87-104*

Formica D, Silvestri S. Biological effects of exposure to magnetic resonance imaging: an overview. *BioMedical Engineering Online 2004;3:11*

Fou AA. John Gibbon. The first 20 years of the heart-lung machine. *Tex Heart Inst J 1997;24(1):1-8*

Frank H, Buxbaum P, Huber L, Globits S, Glogar D, Wolner E, Mayr H, Imhof H. In vitro behaviour of mechanical heart valves in a 1.5 T superconducting magnet. *Eur Radiol 1992;2:555-558*

French DM, Sampson CC. Thrombosis of a Hufnagel valve. A case report. *J Nat Med Assoc 1961;53(2):144-147*

Fundarò P, Tartara PM, Villa E, Fratto P, Campisi S, Vitali EO. Mitral valve repair: Is there still a place for suture annuloplasty ? *Asian Cardiovasc Thorac Ann 2007;15:351-358*

Galli, C., Meucci, O., Scorziello, A., Werge, T. M., Calissano, P, and Schettini, G. Apoptosis in cerebellar granule cells is blocked by high KCl, forskolin, and IGF-1 through distinct mechanism of action: the involvement of intracellular calcium and RNA synthesis. J. *Neurosci. 1995;15, 1172–1179*

Gao G, Wu YX, Grunkemeier GL, Furnary AP, Starr A. Durability of pericardial versus porcine aortic valves. *JACC 2004;44(2):384-388*

Gatti G, Pugliese P. Preliminary experience in mitral valve repair using the Cosgrove–Edwards annuloplasty ring. *Interactive Cardiovasc Thorac Surg 2003;2:256-261*

Giannoglou GD, Antoniadis AP, Chatzizisis YS, Louridas GE. Adult Congenital Heart Disease Investigated with Cardiac Catheterization Over A 20-Year Period. *Open Cardiovasc Med J. 2009;3*:124–127

Gillinov AM, Cosgrove DM, Blackstone EH, Diaz R, Arnold JH, Lytle BW, Smedira NG, Sabik JF, McCarthy PM, Loop FD. Durability of mitral valve repair for degenerative disease. *J Thorac Cardiovasc Surg* 1998;*116:734-743*

Glover PM, Qian W, Cavin I, Bowtell R, Gowland PA. Magnetic-field-induced vertigo: A theoretical and experimental investigation. *Bioelectromagnetics 2007;28:349-361*

Gordon CJ. Normalising the thermal effects of radiofrequency radiation: body mass versus total body surface area. *Bioelectromagnetics 1987;8:111-118*

Gott VL. The second decade of biomaterials development and evaluation: a time to apply scientific method. *Bull N Y Acad Med 1972;48(2):216-224*

Braunwald-Cutter and Magovern-Cromie valves: Gott VL, Alejo DE, Cameron DE. Mechanical heart valves: 50 years of evolution. *Ann Thorac Surg 2003;76:S2230-2239*

Grissom CB. Magnetic-field effects in biology – a survey of possible mechanisms with emphasis on radical-pair recombination. *Chem.Rev.1995;95:3-24*

Grunkemeier GL, Wu YX. The silzone effect: how to reconcile contradictory reports? *Eur J Cardio-Thorac Surg 2004;25:371-375*

Gudbjartsson T, Absi T, Aranki S (2008). Mitral Valve Replacement In: *Cardiac Surgery in the Adult.* 3rd ed. New York: Cohn LH. McGraw-Hill. 1031-1068

Gudbjartsson T, Absi T, Aranki S. (2008). Mitral Valve Replacement. In: Cohn LH. McGraw-Hill *Cardiac Surgery in the Adult*. 3rd ed. New York: Cohn LH. McGraw-Hill. 1031-1068.

Habib G, Tribouilloy C, Thuny F, Giorgi R, Brahim A, Amazouz M et al. Prosthetic valve endocarditis: who needs surgery? A multicentre study of 104 cases. *Heart 2005;91:954–959*

Habib G. Management of infective endocarditis. *Heart 2006;92:124-130*

Haik J, Daniel S, Tessone A, Orenstein A, Winkler E. MRI induced fourth-degree burn in an extremity, leading to amputation. *Burns 2009;35:294-296*

Hall KV. The Medtronic-Hall valve: a design in 1977 to improve the results of valve replacement. *Eur J Cardio-Thorac Surg 1992;6[Suppl 1]:S64-S67*

Hall SC, Stevenson GW, Suresh S. Burn associated with temperature monitoring during magnetic resonance imaging. *Anesthesiology 1992;76:152*

Ham GLG, Engels JML, van de Wiel GT, Machielsen A. Peripheral nerve stimulation during MRI: effects of high gradient amplitudes and switching rates. *J.Magn.Reson.Imaging 1997;7:933-937*

Hamid MS, Sabbah HN, Stein PD. Influence of stent height upon stresses on the cusps of closed bioprosthetic valves. *J Biomec 1986;19(9):759-769*

Hammermeister K, Sethi GK, Henderson WG, Grover FL, Oprian C, Rahimtoola SH. Outcomes 15 years after valve replacement with a mechanical versus a bioprosthetic valve: Final report of the Veterans Affairs Randomized Trial. *J Am Coll Cardiol 2000;36:1152-1158*

Harken DE, Zoll PM. Foreign bodies in and in relation to the thoracic blood vessels and heart. *Am Heart J 1946;32(1):1-20*

Hartwell CG, Shellock FG. MRI of cervical fixation devices: sensation of heating caused by vibration of metallic components. *J.Magn.Reson.Imaging 1997;7(4):771*

Hashemi RH, Bradley WG Jr., Lisanti CJ (2004). Basic Principles of MRI. *In: MRI the Basics.* 2nd ed. Philadelphia. Lippincott Williams & Wilkins. 17-32

Hassoulas JA, Patrianakos AP, Parthenakis FI, Varda PE. Prosthetic aortic valve endocarditis complicated with annular abscess, sub-aortic obstruction and valve dehiscence. *Hellenic J Cardiol 2009;50:319-323*

Hebrank FX, Gebhardt M. SAFE-Model- a new method for predicting peripheral nerve stimulations in MRI. In: *Proceedings of the 8th Annual Meeting of ISMRM, Denver 2000. P2007*

Hilbert SL, Ferrans VJ, McAllister HA, Cooley DA. Ionescu-Shiley bovine pericardial bioprostheses. Histological and ultra structural studies. *Am J Pathol 1992;140:1195-1204*

Ho JC, Shellock FG. Magnetic properties in Ni-Co-Cr base Elgiloy. *J Mater Sci Mater Med 1999;10:555-560*

Hoen B, Alla F, Selton-Suty C, Béguinot I, Bouvet A, Briançon S et al. Changing profile of infective endocarditis. Results of a 1-year survey in France. *JAMA 2002;288(1):75-81*

Hoffman A, Faber SC, Werhahn KJ, Jäger L, Reiser M. Electromyography in MRI – First recordings of peripheral nerve activation caused by fast magnetic field gradients. *Magn Reson Med 2000;43:534-539*

Hoffman G, Lutter G, Cremer J. Durability of bioprosthetic cardiac valves. *Dtsch Arztebl Int 2008;105(8):143-148*

Hoffman JIE, Kaplan S. The incidence of congenital heart disease. *J Am Coll Cardiol 2002;39(12):1890-1900*

Hopkins PN, Polukoff GI. Risk of valvular heart disease associated with use of fenfluaramine. *BMC Cardiovasc Disord.* 2003;**3**:5

Hore PJ. Rapporteur's report: sources and interaction mechanisms. Progress in Biophysics and Molecular Biology 2005;87:205-212

Ikehata M, Koana T, Suzuki Y, Shimizu H, Nakagawa M. Mutagenicity and co-mutagenicity of static magnetic fields detected by bacterial mutation assay. *Mutat Res—Fundam Mol Mech Mutagen 1999;427:147–156*

Inoue K. Percutaneous transvenous mitral commissurotomy using the Inoue balloon. *Eur Heart J* 1991; 12(*Suppl B:* 99-108

Ionescu MI, Ross DN, Deac R, Grimshaw VA, Taylor SH, Whitaker W, Wooler GH. Autologous fascia lata for heart valve replacement. *Thorax 1970;25:46-56*

Ionescu A, Payne N, Fraser AG, Giddings J, Grunkemeier GL, Butchart EG. Incidence of embolism and paravalvular leak after St Jude silzone valve implantation: experience from the Cardiff Embolic Risk Factor Study. *Heart 2003;89:1055-1061*

Iyer RS, Jain R, Padmanabhan M, Chandra A, Agarwal S, Sekhar R, Dronamraju D. Closed mitral valvotomy versus balloon valvuloplasty: A comparison of 100 cases. *Asian Cardiovasc Thorac Ann 1998;6:285–28)*

Jauchem JR. Effects of drugs on thermal responses to microwaves. *Gen Pharmacol 1985;16:307-310*

Jindani A, Neville EM, Venn G, Williams BT. Paraprosthetic leak a complication of cardiac valve replacement. *J Cardiovasc Surg (Torino) 1991;32(4):503-508*

Johnston L, Conly JM. Intracardiac device and prosthetic infections: What do we know? *Can J Infect Dis Med Microbiol 2004;15(4):205-209*

Kagetsu NJ, Litt AW. Important considerations in measurement of attractive force on metallic implants in MR imagers. *Radiology 1991;179:505-508*

Kan JS, White RJ Jr, Mitchell SE, Gardner TJ. Percutaneous balloon valvuloplasty: A new method for treating congenital pulmonary valve stenosis. *N Engl J Med 1982;307:540-542*

Kanal E, Shellock FG, Lewin JS. Aneurysm clip testing for ferromagnetic properties: clip variability issues. *Radiology 1996;200:576-578*

Kanal E, Shellock FG, Talagala L. Safety considerations in MR imaging. *Radiology 1990;176:593-606*

Kandemir O, Tokmakoglu H, Yildiz U, Tezcaner T, Yorgancioglu AC, Gunay I, Suzer K, Zorlutuna Y. St Jude and CarboMedics mechanical heart valves in the aortic position. *Tex Heart Inst J 2006;33:154-9*

Kangarlu A, Shellock FG. Aneurysm clips: Evaluation of magnetic field interactions with an 8.0 T MR system. *J.Magn.Reson.Imaging 2000;12:107-111*

Karch AM. Don't get burnt by the MRI; transdermal patches can be a hazard to patients. *Am J Nursing 2004;104(8):31*

Kaufman J, Palmaz J, Weinshelbaum A, Woodruf D. The Hufnagel valve: a forgotten entity. *Am J Roentgenol 1982;139:1010-1012*

Kay JH, Magidson O, Meihaus JE. The surgical treatment of mitral insufficiency and combined mitral stenosis and insufficiency using the heart-lung machine. *Am J Cardiol 1962; 300-306*

Keens SJ. Burns caused by ECG monitoring during MRI imaging. *Anaesthesia 1996;51:1188-1189*

Keown KK. A brief history of anaesthesia and surgery of the heart and great vessels. *Can. Anaesth. Soc. 1982;29(4): 325-329*

Khan MN. The relief of mitral stenosis. *Tex Heart Inst J 1996;23:258-266*

Kidane AG, Burriesci G, Cornejo P, Dooley A, Sarkar S, Bonhoeffer P, Edirisnghe M, Seifalian AM. Current developments and future prospects for heart valve replacement therapy. *J Biomed Mater Res Part B: Appl Biomater 88B;2009:290-303*

Kim LH, Sonntag VK, Hott T, Nemeth JA, Klopfenstein JD, Tweardy L. Scalp burns from halo pins following magnetic resonance imaging. *J.Neurosurg 2003;99(1):186*

Kinouchi Y, Tanimoto S, Ushita T, Sato K, Yamaguchi H, Miyamoto H. Effects of static magnetic fields on diffusion in solutions. *Bioelectromagnetics 1988;9:159-166*

Kirlin JW, Donald DE, Harshbarger HG, Hetzel PS, Patrick RT, Swan HJC, Wood EH. Studies in Extracorporeal Circulation. I. Applicability of Gibbon-Type Pump-Oxygenator to Human Intracardiac Surgery: 40 Cases. *Ann Surg 1956;144(1):2–8*

Klucznik R, Carrier D, Pyka R, Haid R. Placement of a ferromagnetic intracerebral aneurysm clip in a magnetic field with a fatal outcome. *Radiology 1993;187:855-856*

Knopp M, Essig M, Debus J, Zabel HJ, van Kaick G. Unusual burns of the lower extremities caused by a closed conducting loop in a patient at MR imaging. *Radiology 1996;2000:572-575*

Kobayashi J, Sasako Y, Bandao K, Minatoya K, Niwaya K, Kitamura S. Ten-year experience of chordal replacement with expanded polytetrafluoroethylene in mitral valve repair. *Circulation 2000;102[19 suppl 3]:11130-11134*

Kouchoukos NT, Wareing TH, Murphy SF, Perrillo JB. Sixteen year experience with aortic root replacement. *Ann Surg 1991;214(3):308-318*

Krause I, Lev S, Fraser A, Blank M, Lorber M, Stojanovich L, Rovenskey J, Chapman J, Shoenfeld Y. Close association between valvular heart disease and central nervous system manifestations in the antiphospholipid syndrome. *Ann Rheum Dis 2005;64:1490-1493*

Kuntz RE, Tosteson ANA, Berman AD, Goldman L, Gordon PC, Leonard BM, McKay RG, Diver DJ, Safian RD. Predictors of event-free survival after balloon aortic valvuloplasty. *N Engl J Med 1991;325:17-23*

Lamas CC, Eykyn SJ. Bicuspid aortic valve – A silent danger: Analysis of 50 cases of infective endocarditis. *Clin Infect Dis 2000;30:336-341*

Lancet Editorial. Surgical operation for mitral stenosis. *Lancet 1902;i:461-462*

Laplace G, Lafitte S, Labèque JN, Perron JM, Baudet E, Deville C, Roques X, Roudaut R. Clinical significance of early thrombosis after prosthetic mitral valve replacement. *J Am Coll Cardiol 2004;43:1283-1290*

Lee JM, Haberer SA, Boughner DR. The bovine pericardial xenograft: I. Effect of fixation in aldehydes without constraint on the tensile viscoelastic properties of bovine pericardium. *J Biomed Mater Res 1989;23(5):457-475*

Leong SW, Soor GS, Butany J, Henry J, Thangaroopan M, Leask RL. Morphological findings in 192 surgically excised mitral valves. *Can J Cardiol 2006;22(12):1055-1061*

Levine GN, Gomes AS, Arai AE, Gluemke DA, Flamm SC, Kanal E, Manning WJ, Martin ET, Smith JM, Wilke N, Shellock FG. Safety of magnetic resonance imaging in patients with cardiovascular devices. *Circulation 2007;116:2878-2891*

Li M, Dumesnil JG, Mathieu P, Pibarot P. Impact of valve prosthesis-patient mismatch on pulmonary arterial pressure after mitral valve replacement. *J Am Coll Cardiolo 2005;45:1034-1040*

Lieberman EB, Bashore TM, Hermiller JB, Wilson JS, Pieper KS, Keeler GP, Pierce CH, Kisslo KB, Harrison JK, Davidson CJ. Balloon aortic valvuloplasty in adults: failure of procedure to improve long-term survival. *J Am Coll Cardiol, 1995;26:1522-1528*

Lillehei CW, Cohen M, Warden HE, Varco RI. The direct-vision intracardiac correction of tetralogy of Fallott, Pentalogy of Fallott, and pulmonary atresia defects. *Ann Surg 1955;142(3):418-442*

Lillehei CW, DeWall RA, Gott VL, Varco RL. The direct vision correction of calcific aortic stenosis by means of pump-oxygenator and retrograde coronary sinus perfusion. *Dis Chest 1956;30;123-132*

Lillehei CW, Gott VL, DeWall RA, Varco RL. The surgical treatment of stenotic or regurgitant lesions of the mitral and aortic valves by direct vision utilizing a pump-oxygenator. *J Thorac Surg 1958;35:154–90.*

Lim KO, Cheong KC. Effect of suturing on the mechanical properties of bovine pericardium – implications for valve bioprosthesis. *Med Eng Phys 1994;16:526-530*

Liu C-Y, Farahani K, Lu DSK, Duckwiler G, Oppelt A. Safety of MRI-guided endovascular guidewire applications. *J.Magn.Reson.Imaging 2000;12:75-78*

Loke YK, Derry S, Pritchard-Copley A. Appetite suppressants and valvular heart disease – a systematic review. *BMC Clinical Pharm 2002;2:6*

Loulmet DF, Carpentier A, Cho PW, Berrebi A, d'Atellis N, Austin CB, Couëtil JP, Lajos P. Less invasive techniques for mitral valve surgery. *J Thorac Cardiovasc Surg* 1998;*115:772-779*

lung B, Baron G, Butchart EG, Delahaye F, Gohlke-Bärwolf C, Levang OW, Tornos P, Vanoverschelde JL, Vermeer F, Boersma E, Revaud P, Vahanian A. A prospective survey of patients with valvular heart disease in Europe: The Euro Heart Survey on valvular heart disease. *Eur Heart J 2003;24:1231-1243*

Lytle BW, Pries BP, Taylor PC, Loop FD, Sapp SK, Stewart RW, McCarthy PM, Muehreke D, Cosgrove DM. Surgery for acquired heart disease. Surgical treatment of prosthetic valve endocarditis. *J Thorac Cardiovasc Surg 1996;11:198-210*

Mackay TJ, Wheatley DJ, Bernacca GM, Fisher AC, Hindlet CS. New polyurethane heart valve prosthesis: design, manufacture and evaluation. *Biomats 1996;17:1857-1863*

MacGregor JS, Cheitlin MD. Diagnosis and management of infective endocarditis. *Tex Heart Inst J. 1989;16(4):230–238*

Madden S, Kelly L. Update on acute rheumatic fever. *Can Fam Physician 2009;55(5):475-478*

Maisano F, Michev I, Rowe S, Addis A, Campagnol M, Guidotti A, Colombo A, Alfieri O. Transapical endovascular implantation of neochordae using a suction and suture device. *Eur J Cardiothorac Surg 2009;36:118-123*

Malott JC. Hazards of ferrous materials in MRI: a case report. *Radiol Technol 1987; 58(3):233-235*

Marelli AJ, Mackie AS, Ionescu-Ittu R, Rahme E, Pilote L. Congenital heart disease in the general population. Changing prevalence and age distribution. *Circulation 2007;115:163-172*

Markov M. Thermal vs. nonthermal mechanisms of interactions between electromagnetic fields and biological systems. *Bioelectromagnetics 2006:1-15*

Masri Z, Girardet R, Attum A, Barbie R, Yared I, Lansing A. Reoperation for prosthetic heart valve dysfunction. 19 years experience. *Tex Heart Inst J. 1990; 17(2):106-11*

Massel D, Little SH. Risks and benefits of adding anti-platelet therapy to warfarin among patients with prosthetic heart valves: A meta-analysis. *J Am Coll Cardiol 2001;37:569 –78*

Masters RG, Walley VM, Pipe AL, Keon WJ. Long-term experience with the Ionescu-Shiley pericardial valve. *Ann Thorac Surg 1995;60:S288-S291*

Mattei E, Triventi M, Calcagnini G, Censi F, Kainz W, Mendoza G, Basses HI, Bartolini P. Complexity of MRI induced heating on metallic leads: Experimental measurements of 374 configurations. *BioMedical Engineering Online 2008;7:11*

McConnell EM, Roberts C. Pathological findings in three cases of fungal endocarditis complicating open-heart surgery. *J.Clin.Path 1967;20:555-560*

Medicines Healthcare Regulatory Authority (MHRA). Device Bulletin. Safety guidelines for magnetic resonance imaging in clinical use. *United Kingdom Department of Health DB2007(3).*

Melville ID, Paul F, Roath S. High gradient magnetic separation of red cells from whole blood. *IEEE Trans.Magn. 1975; MAG-11:1701-1704*

Meredino KA, Thomas GI, Jesseph JE, Herron PW, Winterscheid LC, Vetto RR. The open correction of rheumatic mitral regurgitation and or stenosis. With Special Reference to Regurgitation Treated by Posteromedial Annuloplasty Utilizing a Pump-Oxygenator. *Ann Surg 1959 July;150(1):5–22.*

Miyakoshi J. Effects of static magnetic fields at the cellular level. *Prog Biophys Mol Biol 2005;87:213-223*

Mohr FW, Falk V, Diegeler A, Walther T, van Son JAM, Autschbach R, Borst HG. Minimally invasive port-access mitral valve surgery. *J Thorac Cardiovasc Surg 1998;115:567-571*

Moore FD. The advent of antibiotics: Episodes from the early days of the 'miracle drugs'. *Surgery 1999;126:83-84*

Moser E, Stadibauer A, Windischberger C, Quick HH, Ladd ME. Magnetic resonance imaging methodology. *Eur J Nucl Med Mol Imaging 2009;(Suppl 1):S30-S41*

Moss R, Munt B. Injection drug use and right sided endocarditis. *Heart 2003;89:577-581*

Muranaka H, Horigughi T, Usui S, Ueda Y, Nakamura O, Ideda F. Dependence of RF hearing on SAR and implant position in a 1.5T MR system. *Magn.Reson.Med.Sci 2007;6:199-209*

Mulder BJM. Ebstein's Anomaly in the adult patient. Neth Heart J. 2003;11(5)195-198

Mulder DG, Diesh G, Smith RT, McEachen JA, Adams FH, Maloney JV, Longmire WP. Repair of intracardiac defects. Operation under direct vision with the aid of hypothermia or a pump-oxygenator: Report of twelve cases. *Calif Med 1957;86(2):75-79*

Murray G, Roschlau W, Lougheed W. Homologous aortic-valve-segment transplants as surgical treatment for aortic and mitral insufficiency. *Angiology 1956;7:466-471*

Mylonakis E, Calderwood SB. Infective endocarditis in adults. *N Engl J Med 2001;345(18):1318-1330*

Nair K, Muraleedharan CV, Bhuvaneshwar GS. Developments of mechanical heart valves. *Sadhana 2003;28(Parts 3 & 4):575–587*

National Centre for Chronic Disease Prevention and Health Promotion. Chronic disease prevention: *The burden of heart disease, stroke, cancer, and diabetes, United States. National and State Perspectives 2002;*
http://www.cdc.gov/nccdphp/burdenbook2002/02_stroke.htm

Nesher G, Ilany J, Rosenmann D, Abraham AS. Valvular dysfunction in antiphospholipid syndrome: prevalence, clinical features and treatment. *Semin Arthritis Rheum 1997;27:27-35*

New PFJ, Rosen BR, Brady TJ et al. Potential hazards and artifacts of ferromagnetic and non-ferromagnetic surgical and dental devices in nuclear magnetic resonance imaging. *Radiology 1983;147:139-148*

Nicotera DJ, Hartzell P, Bellomo P, Wyllie G & A. H, Orrenius S. Glucocorticoids activate a suicide process in thymocytes through an elevation of cytosolic Ca2+ concentration. *Arch. Biochem. Biophys. 1989;269, 365–370*

Nitz WR, Oppelt W, Renz C, Make C, Lenhart M, Link J. On the heating of linear conductive structures such as guide wires and catheters in interventional MRI. *J.Magn.Reson.Imaging 2001;13:105-114*

Nyenhuis JA, Park S-M, Kamondetdacha R, Amjad A, Shellock FG, Rezai AR. MRI and implanted medical devices: Basic interactions with an emphasis on heating. *IEEE Transactions on Device and Materials Reliability 2005;5:467-480*

O'Brien MF, Gardner MA, Garlick B, Jalali H, Gordon JA, Whitehouse SL, Strugnell WE, Slaughter R. CryoLife-O'Brien stentless valve: 10-year results of 402 implants. *Ann Thorac Surg*. 2005;79:757–766

Oechslin E, Carrel T, Ritter M, Attenhofer Ch, von Segesser L, Kiowski W, Turina M, Jenni R. Pseudoaneurysm following aortic homograft: clinical implications ? *Br Heart J. 1995;74:645-649*

Office for National Statistics Online (ONS). Aging. Brief analysis – population change. *http://www.statistics.gov.uk accessed 24/06/2010*

Ohldag H, Tyliszczak T, Höhne R, Spemann D, Esquinazi P, Ungureanu M, Butz T. π-Electron ferromagnetism in metal-free carbon probed by soft X-ray dichroism. *Phy Rev Litt. 2007;98: 187204/1-187204/4*

Olsen EGJ, Al-Janabi N, Salamaó CS, Ross DN. Fascia lata valves; a clinicopathological study. *Thorax 1975;30:528-534*

Omar RZ, Morton LS, Beirne M, Blot WJ, Lawford PV, Hose R, Taylor KMT. Outlet strut fracture of Björk-Shiley convexo-concave valves: can valve-manufacturing characteristics explain the risk ? *J.Thorac Cardiovasc Surg 2001;121:1143-1149*

Otto CM, Lind BK, Kitzman DW, Gersh BJ, Siscovick DS. Association of aortic-valve sclerosis with cardiovascular mortality and morbidity in the elderly. *N Engl J Med 1999;341:142-147*

Oxenham H, Bloomfield P, Wheatley DJ, Lee RJ, Cunningham J, Prescott RJ, Miller HC. Twenty year comparison of a Bjork-Shiley mechanical heart valve with porcine bioprosthesis. *Heart 2003;89:715-721*

Oyer PE, Stinson EB, Miller DC, Jamieson SW, Mitchell RS, Shumway NE. Thromboembolic risk and durability of the Hancock bioprosthetic valve. *Eur Heart J 1984;5(suppl D):81-85*

Palacios IF. Farewell to surgical mitral commissurotomy for many patients. *Circulation 1998;97;223-226*

Paul F, Roath S, Melville D. Differential blood cell separation using a high gradient magnetic field. *Br.J.Haematolo. 1978;38:273-380*

Pavoni D, Badano LP, Ius F, Mazzaro E, Frassani R, Gelsomino S, Livi U. Limited long-term durability of the Cryolife O'Brien stentless porcine xenograft valve. *Circulation 2007;116[suppl I]:I.307-I.313*

Perlman BB, Freedman LR. Experimental endocarditis III: Natural history of catheter induced staphylococcal endocarditis following catheter removal. *Yale J Biol Med 1971;44:214-224*

Peterman MA, Donsky MS, Matter GJ, Robert WC. A Starr-Edwards model 6120 mechanical prosthesis in the mitral valve position for 38 years. *Am J Cardiol. 2006;97(5):756-758*

Pibarot P, Dumesnil JG. Prosthetic-patient mismatch: definition, clinical impact, and prevention. *Heart 2006;92:1022-1029*

Pictet J, Meuli R, Wicky S, van der Klink JJ. Radiofrequency heating effects around resonant lengths of wire in MRI. *Phys.Med.Biol 2002;47:2973-2985*

Prasad A, Mehra M, Park M, Scott R, Uber PA, McFadden PM. Cardiac allograft valvulopathy: a case of donor-anorexogenic-induced valvular disease. *Ann Thorac Surg 1999;68:1840-1841*

Prendergast BD. The changing face of infective endocarditis. *Heart 2006;92:879-885*

Pruefer D, Kalden P, Schreiber W, Dahm M, Buerke M, Thelen M, Oelert H. In vitro investigation of prosthetic heart valves in magnetic resonance imaging: evaluation of potential hazards. *J Heart Valve Dis 2001;10:410-414*

Raanani E, Spiegelstein D, Sternik L, Preisman S, Moshkovitza Y, Smolinksy AK, Shinfeld A. Quality of mitral valve repair: Median sternotomy versus port-access approach. *J Thorac Cardiovasc Surg 2010;140:86-90*

Radlick PH. Suspension of marketing Edwards Duromedics bileaflet valve models 3160 and 9120, all sizes. *Baxter, Important information, Santa Ana, CA, 1988:1-2*

Rahimtoola SH. Choice of Prosthetic Heart Valve for Adult Patients. *J Am Coll Cardiol 2003;41:893-904*

Rajamannan NM. Calcific Aortic Stenosis: Lessons Learned from experimental and Clinical Studies. *Arterioscler Thromb Vasc Biol. 2009; 29(2): 162–168*

Rallidis LS, Moyssakis IE. Nihoyannopoulos P. Natural history of early aortic paraprosthetic regurgitation: a five year follow-up. *Am Heart J. 1999;138(2; pt1): 351-357*

Ramsey G, Schmidt PJ. Transfusion medicine in Chicago, before and after the "blood bank". *Transfus Med Rev 2009;23(4):310-21*

Randall PA, Kohman LJ, Scalzetti EM, Szeverenyi NM, Panicek DM. Magnetic resonance imaging of prosthetic cardiac valves in vitro and in vivo. *Am J Cardiol 1988;1:973-976*

Rao S. Percutaneous balloon pulmonary valvuloplasty. State of the Art. *Cath Cardiovasc Interv 2007;69:747-763*

Rapaport E. Symposium on the effects of surgical treatment on the natural history of acquired heart disease. Part II. Aortic and mitral valve disease. Natural history of aortic and mitral valve disease. *Am J Cardiol 1975;35:221-227*

Ray DG, Subramanya R, Titus T, Tharakan J, Joy J, Venkitachalam CG, Kumar A, Balakrishnan KG. Balloon pulmonary valvolplasty: factors deterining short- and long-term results. *Int J Cardiol 1993;40:17-25*

Redfield M.M., Nicholson W.J., Edwards W.D., Tajik A.J. Valve disease associated with ergot alkaloid use: echocardiographic and pathologic correlations. *Ann Intern Med 1992;117:50-52*

Reichenspurner H, Boehm DH, Gulbins H, Schulze C, Wildhirt S, Welz A, Detter C, Reichart B. Three-dimensional video and robot-assited port-access mitral valve operation. *Ann Thorac Surg 2000;69:1176-1182*

Rekik S, Trabelsi I, Znazen A, Maaloul I, Hentati M, Frikha I, Ben Jemaa M, Hammami A, Kammoun S. Prosthetic valve endocarditis: management strategies and prognosis. *Neth Heart J 2009;17:56-60*

Reid KG. Design and construction of fascia lata aortic valve prostheses. *Thorax 1970;25:436-438*

Reilly JP. Magnetic field excitation of peripheral nerves and the heart: a comparison of thresholds. *Med Biol Eng Comput 1991;29:571-579*

Reilly JP (1992). Electrical stimulation and electropathology. *Cambridge: Cambridge University Press.504*

Richard G, Bevan A, Strzepa P. Cavitation threshold ranking and erosion characteristics of bileaflet heart valve prostheses. *J Heart Valve Dis 1994;3(suppl 1):S94-S101*

Ringel RE, Moulton AL, Burns JE, Brenner JI, Berman MA. Structural failure of a Starr-Edwards aortic track valve. *Tex Heart Inst J. 1983;10(1):81-83*

Rink TJ, Merritt JE. Calcium signalling. *Curr Opin Cell Biol 1990;2:198-205*

Roberts WC. The congenitally bicuspid aortic valve. A study of 85 autopsy cases. *Am J Cardiol 1970;26(1):72-83*

Roberts WC, Ko JM, Moore TR, Jones WH 3rd. Causes of pure aortic regurgitation in patients having isolated aortic valve replacement at a single US tertiary hospital (1993 – 2005). *Circulation 2006;114(5):422-429*

Roberts WC, Ko JM. Some observations on mitral and aortic valve disease. *Proc (Bayl Univ Med Cent) 2008;21(3):282-299*

Robertson NM, Diaz-Gomez M, Condon B. Estimation of torque on mechanical heart valves due to magnetic resonance imaging including an estimation of the significance of the Lenz effect using a computation model. *Phys.Med.Biol 2000;45:3798-3807*

Rodriguez-Artalejo F, Banegas Banegas JR, Guallar-Castillón P. Epidemiology of heart failure. *Rev Esp Cardiol 2004;57:163-170*

Rosen AD. Mechanism of action of moderate-intensity static magnetic fields on biological systems. *Cellular Biochemistry Biophysics 2003;39:163-173*

Rosengart TK, O'Hara M, Lang SJ, Ko W, Altorki N, Krieger KH, Isom OW. Outcome analysis of 245 CarboMedics and St. Jude valves implanted at the same institution. *Ann Thorac Surg 1998;66:1684-91*

Roudaut R, Serri K, Lafitte S. Thrombosis of prosthetic heart valves: diagnosis and therapeutic considerations. *Heart 2007;93:137-142*

Rowell LB. Cardiovascular aspects of human thermoregulation. *Circ.Res. 1983;52:367-379*

Sadee AS, Becker AE, Verheul HA, Bouma B, Hoedemaker G. Aortic valve regurgitation and the congenitally bicuspid aortic valve: a clinic-pathological correlation. *Br Heart J. 1992;67:439-441*

Sawyer-Glover AM, Shellock FG. Pre-MRI procedure screening: recommendations and safety considerations for biomedical implants and devices. *J.Magn.Reson.Imaging 2000;12:92-106*

Saxena P, Shehatha J, Downie S, Newman MAJ, Konstantinov IE. Translocation of prosthetic aortic valve in advanced prosthetic valve endocarditis. *Tex Heart Inst J 2009;3(6):604-606*

Schade R, Andersohn F, Suissa S, Haverkamp W, Garbe E. Dopamine agonists and the risk of cardiac-valve regurgitation. *N Eng J Med 2007;356:29-38*

Schaefer DJ, Bourland JD, Nyenhuis JA. Review of patient safety in time-varying gradient fields. *J.Magn.Reson.Imaging 2000;12:20-29*

Schaff HV, Carrel TP, Jamieson WRE, et al. Paravalvular leak and other events in Silzone-coated mechanical heart valves: a report from AVERT. *Ann Thorac Surg 2002;73:785-792*

Schenck JF. Health and physiological effects of human exposure to whole-body four-tesla magnetic fields during MRI. *Ann.N.Y.Acad.1992;649:285-301*

Schenck JF. Safety of strong, static magnetic fields. *J.Magn.Reson.Imaging 2000;12:2-19*

Schenck JF. Physical interactions of static magnetic fields with living tissues. *Progress in Biophysics and Molecular Biology 2005; 87:185-204*

Schmidt CE, Baier JM. Acellular vascular tissues: natural biomaterials for tissue repair and tissue engineering. *Biomats 2000;21:2215-2231*

Schueler BA, Parrish TB, Lin J-C, Hammer BE, Pangrle BJ, Ritenour ER, Kucharczyk J, Truwit CL. MRI compatibility and visibility assessment of implantable medical devices. *J Magn Reson Imaging 1999;9:596-603*

Schulz R, Werner GS, Fuchs JB, Andreas S, Prange H, Ruschewski W, Kreuzer H. Clinical outcome and echocardiographic findings of native and prosthetic valve endocarditis in the 1990s. *Eur Heart J 1996;17:281-288*

Select Committee on Health; www.parliament.uk; 21st September 2009 (accessed 29/09/09)

Sett SS, Hudon MPJ, Jamieson WRE, Chow AW. Prosthetic valve endocarditis. Experience with porcine bioprostheses. *J Thorac Cardiovasc Surg 1993;105:428-434*

Shaw TRD, Turnball CM, Currie P, Flapan AD, Pringle S, Lee BC. A comparison of cylindrical Inoue balloon techniques for mitral valvotomy in patients in the United Kingdom. *Br Heart J 1994;72:486-491*

Shellock FG. Radiofrequency energy-induced heating during MR procedures: A review. *J.Magn.Reson.Imaging 2000a;12:30-36*

Shellock FG. Prosthetic heart valves and annuloplasty rings: assessment of magnetic field interactions, heating and artifacts at 1.5 T. *J.Cardiovasc.Mag.Reson 2001;3(4):317-324*

Shellock FG. Biomedical implants and devices: Assessment of magnetic field interactions with a 3.0-Tesla MR system. *J.Magn.Reson.Imaging 2002;16:721-732*

Shellock FG, Crues JV. Corneal temperature changes induced by high-field-strength MR imaging with a head coil. *Radiology 1987;167:809-811*

Shellock FG, Crues JV. MR procedures: biological effects, safety and patient care. *Radiology 2004;232:635-652*

Shellock FG, Hatfield M, Simon BJ, Block S, Wambolt J, Starewicz PM, Punchard WFB. Implantable spinal fusion stimulator: assessment of MR safety and artifacts. *J Magn Reson Imaging 2000;12:214-223*

Shellock FG, Kanal E. Burns associated with the use of monitoring equipment during MR procedures. *J.Magn.Reson.Imaging 1996;4:271-272*

Shellock FG, Morisoli S. Evaluation of ferromagnetism, heating and artifacts produced by heart valve prostheses exposed to a 1.5 T MR system. *J.Magn.Reson.Imaging 1994;4:756-758*

Shellock FG, Morisoli S, Kanal E. MR procedures and biomedical implants, materials and devices: 1993 update. *Radiology. 1993;189:587-599*

Shellock FG, Nogueira M, Morisoli M. MRI and vascular access ports: ex vivo evaluation of ferromagnetism, heating and artifacts at 1.5 T. *J.Magn.Reson.Imaging 1995;4:481-484*

Shellock FG, Rothman B, Sarti D. Heating of the scrotum by high-field-strength MR imaging. *AJR 1990;154:1229-1232*

Shellock FG, Schaefer DJ, Gordon GJ. Effect of a 1.5T static magnetic field on body temperature of man. *Magn.Reson.Med 1986;3:644-647*

Shellock FG, Shellock VJ. Vascular access ports and catheters: ex vivo testing of ferromagnetism, heating and artifacts associated with MR imaging. *J.Magn.Reson.Imaging 1996;14:443-447*

Shellock FG, Shellock VJ. Cardiovascular catheters and accessories; ex vivo testing of ferromagnetism, heating and artifacts associated with MRI. *J.Magn.Reson.Imaging 1998;8(6):1338-1342*

Shellock FG, Shellock VJ. Metallic stents: evaluation of MR imaging safety. *AJR 1999;173:543-547*

Shellock FG, Tkach JE, Ruggieri PM, Masaryk TJ, Rasmussen PA. Aneurysm clips: evaluation of magnetic field interactions and translational attraction by use of "long-bore" and "shortbore" 3.0-T MR imaging systems. *Am J Neuroradiol 2003;24:463–471*

Shiono M, Sezai Y, Sezai A, Hata M, Iida M, Negishi N. Long-term results of the cloth-covered Starr-Edwards ball valve. *Ann Thorac Surg 2005;80:204-209*

Silva AKA, Silva E:. Egito EST, Carriço AS. Safety concerns related to magnetic field exposure. *Radiat Environ Biophys. 2006;45:245-252*

Simon P, Kasimir MT, Seebacher G, Weigel G, Ullrich R, Salzer-Muhar U, Rieder E, Wolner E. Early failure of the tissue engineered porcine heart valve SYNERGRAFT ™ in pediatric patients. *Eur J Cardio Thorac Surg 2003;23:1002-1006*

Smith CD, Nyenhuis A, Kildishev AV. Health effects of induced electric fields: Implications for metallic implants. In: *Magnetic Resonance Procedures: Health Effects and Safety. FG Shellock Ed. Boca Raton, Fl. CRC Press 2001, pp 393-414*

Smith-Bindman R, Miglloretti DL, Larson EB. Rising use of diagnostic medical imaging in a large integrated health system. *Health Aff (Millwood) 2008;27(6):1491-1502*

Soler-Soler J, Galve E. Valve disease. Worldwide perspective of valve disease. *Heart 2000;83:721-725*

Sommer T, Vahihaus C, Lauck G, v. Smekal A, Reinke M, Hofer U, Bock W, Träber F, Schneider C, Gieskek J, Jung W, Schild H. MR imaging and cardiac pacemakers: In vitro evaluation and in vivo studies in 51 patients at 0.5 T. *Radiology 2000;215:869-879*

Soulen RL, Budinger TF, Higgins CB. Magnetic resonance imaging of prosthetic heart valves. *Radiology 1985;154:705-707*

Stewart BF, Siscovick D, Lind BK, Gardin JM, Gottdiener JS, Smith VE, Kitzman DW, Otto CM, Cardiovascular Health Study. Clinical factors associated with calcific aortic valve disease. *J Am Coll Cardiol 1997;29:630-634*

St Goet FG, Fann JI, Komtebedde J, Foster E, O MC, Fogarty TJ, Feldman T, Block PC. Endovascular edge-to-edge mitral repair: short-term results in a porcine model. *Circulation 2003;108:1990-1993*

Svennevig JL, Abdelnoor M, Nitter-Hauge S. Twenty-five-year experience with the Medtronic-Hall valve prosthesis in the aortic position. A follow-up cohort study of 816 consecutive patients. *Circulation 2007;116:1795-1800*

Taghon TA, Bryan IF, Kurth CD. Pediatric radiology sedation and anesthesia. *Int Anesthesiol Clin 2006;44(1):65-79*

Talavilkar PH, Walbaum PR, Kitchin AH. Haemodynamic results of replacement of mitral and aortic valves with autologous fascia lata prostheses. *Thorax 1973;28:169-176*

Tavasoli Z, Abdolmaleki P, Mowla SJ, Ghanati F, Sarvestani AS. Investigation of the effects of static magnetic field on apoptosis in bone marrow stem cells of rat. *Environmentalist 2009; 29:220–224*

Teodori L, Albertini MC, Uguccioni F, et al Static magnetic fields affect cell size, shape, orientation and membrane surface of human glioblastoma cells, as demonstrated by electron, optic and atomic force microscopy. *Cytometry Part A 2005;69A:75-85*

Teodori L, Gohde W, Valente MG, Tagliaferri F, Coletti D, Perniconi B, Bergamaschi A, Cerella C, Ghibelli L. Static magnetic fields affect calcium fluxes and inhibit stress-induced apoptosis in human glioblastoma cells. *Cytometry 2002;49:143-149*

Tesler UF, Cerin G, Novelli E, Popa A, Diena M. Evolution of surgical techniques for mitral valve repair. *Tex Heart Inst J 2009;36(5):438-440*

Thiene G, Bortolotti U, Valente M, Valente M, Milano A, Calabrese F, Talenti E, Mazzucco A, Mazzucco V. Mode of failure of the Hancock pericardial valve xenograft. *Am J Cardiol 1989;63:129-133*

Trowbridge E, Croft CE. The standardisation of gauge length: Its influence on the relative extensibility of natural and chemically modified pericardium. *J Biomech 1986;19(12):1023-1033*

Tuladhar SM, Punjabi PP. Surgical reconstruction of the mitral valve. *Heart 2006;92:1373-1377*

Turbidy-Clark M, Carapetis JR. Subclinical carditis in rheumatic fever: A systemic review. *Int J Cardiol 2007;119:54-8*

Turpie A, Gent M, Laupacis A, Latour Y, Gunstensen J, Basile F, Klimek M, Hirsch J. A comparison of aspirin with placebo in patients treated with warfarin after heart valve replacement. *NEJM 1993;329:524-529*

Ulaner GA, Colletti PM. An unsuspected MR projectile: a "wooden" chair with metal bracing. *J.Magn.Reson.Imaging 2006;23:781-782*

United Kingdom Heart Valve Registry. The United Kingdom Heart Valve Registry Report 2005. *UK Heart Valve Registry 2007, London United Kingdom*

US Food & Drug Administration Centre for Devices and Radiological Health. A primer on medical device interactions with magnetic resonance imaging systems. Feb 7th, 1997 *www.fda.gov/edrh/ode/primerf6.html accessed 2nd December, 2009*

Valente M, Minarini M, Maizzi AF, Bortolotti U, Thiene G. Heart valve bioprosthesis durability: a challenge to the new generation of porcine valves. *Eur J Cardiothorac Surg 1992;6:82-90*

Smith CD, Nyenhuis A, Kildishev AV. Health effects of induced electric fields: Implications for metallic implants. In: *Magnetic Resonance Procedures: Health Effects and Safety. FG Shellock Ed. Boca Raton, Fl. CRC Press 2001, pp 393-414*

van der Graaf, de Waard F, van Herwerden LA, Defauw J. Risk of strut fracture of Björk-Shiley valves. *Lancet 1992;339:257-261*

van der Vorm ER, Dondorp AM, van Ketel RJ, Dankert J. Apparent culture-negative prosthetic valve endocarditis caused by peptostreptococcus magnus. *J Clin Microbiol 2000;38(12):4540-4642*

Vahanian A, Baumgartner H, Bax J, Butchart E, Dion R, Filippatos G, et al. Guidelines on the management of valvular heart disease The Task Force on the Management of Valvular Heart Disease of the European Society of Cardiology. *Eur Heart J. 2007;28:230–268*

Veinot JP. Pathology of inflammatory native valvular heart disease. *Cardiovasc Pathol 2006;15:243-251*

Verheugt CL, Uiterwaal CSPM, van der Velde ET, Meijboom FJ, Pieper PG, Vliegen HW, van Dijk PJ, Bouma BJ, Grobbee DE, Mulder BJM. Gender and outcome in adult congenital heart disease. *Circulation 2008;118:26-32*

Vesely I, Boughner D, Song T. Tissue buckling as a mechanism of bioproshetic valve failure. *Ann Thorac Surg 1988;46(3):302-308*

Vesely I. The evolution of bioprosthetic heart valve design and its impact on durability. *Cardiovasc Pathol 2003;12:277-286*

Vesely I. Heart valve tissue engineering. *Circ Res 2005;97:743-755*

Vilacosta I, Graupner C, San Román JA, Sarriá C, Ronderos R, Fernández C, Mancini L, Sanz O, Sanmartín JV, Stoermann W. Risk of embolization after institution of antibiotic therapy for infective endocarditis. *J Am Coll Cardiol 2002;39(9):1489-1495*

Vongpatanasin W, Hillis LD, Lange RA. Prosthetic Heart Valves. *Med Progress 1996;335(6):407-416*

Wahad S, Khan RA, Ullah E, Wahab A. Is MRI as safe as we think ? *South African Journal of Radiology 2008 (2). http://www.thefreelibrary.com*

Warnes CA. Bicuspid aortic valve and coarctation: two villains part of a diffuse problem. *Heart 2003;89:965-966*

Warnes CA. The adult with congenital heart disease. Born to be bad ? *J Am Coll Cardiol 2005;46(1):1-8*

Weale AE, Hutter J, Collins CMP. Rupture of a ventricular abscess after mitral valve replacement. *Br Heart J 1992;67:271-272*

Weersinghe A, Edwards MB, Taylor KM. First redo heart valve replacement. A 10 year analysis. *Circulation 1999;99:655-658*

Weintraub MI, Khoury A, Cole SP. Biological effects at 3 Tesla (T) MR imaging comparing traditional 1.5 T and 0.6 T in 1023 consecutive outpatients. *J. Neuroimaging 2007;17(3):241-5*

Weisse AB. The surgical treatment of mitral stenosis: The first heart operation. *Am J Cardiol 2009;103:143-147*

Welch W, Potvliege P, Primo G. Autologous fascia lata cardiac valve replacement. *Thorax 1971;26:271-276*

Wheatley DJ, Crawford FA, Kay PH, Chandler JG, Strong, 3rd MD, Strom JA, Shah PM, Keon WJ, Copeland, 3rd G, Lewis SS. A ten-year study of the Ionescu-Shiley low-profile bioprosthetic heart valve. *Eur J Cardiothorac Surg 1994;8:541-548*

Wheatley DJ, Fisher J, Reece IJ, Spyt T, Breeze P. Primary tissue failure in pericardial valves. *J Thorac Cardiovasc Surg 1987;94:367-374*

Wheatley DJ, Raco L, Bernaaca GM, Sim I, Belcher PR, Boyd JS. Polyurethane: material for the next generation of heart valve prostheses? *Eur J Cardio Thorac Surg 2000;17:440-448*

Wilke A, Hesse H, Hufnagel G, Maisch B. Mitral, aortic and tricuspid valvular heart disease associated with ergotamine therapy for migraine. *Eur Heart J 1997;18:701*

Winther FO, Fasmussen K, Tvete O, Halvorsen U, Haugsdal B. Static magnetic field and the inner ear. A functional study of hearing and vestibular function in man after exposure to a static magnetic field. *Scan Audiol 1999;25:57-59*

World Health Organization (WHO). The top ten causes of death. *Fact sheet no 310/November 2011;1-5.*
http://www.whoint/mediacentre/actsheets/fr310/en/index2.html accessed 23/09/2012

Yamada H. Mechanical properties of the circulatory organs and tissues. *In: Yamada H. ed.; Strength of biological materials. Baltimore, MD: The Williams & Wilkins Company, 1970, pp.106-137, 259-282*

Yener N, Oktar L, Erer D, Yardimci MM, Yener A. Bicuspid aortic valve. *Ann Thorac Cardiovasc Surg 2002;8(5):264-267*

Yuh WTC, Hanigan MT, Nerad JA, Ehrhardt JC, Carter KD, Kardon RH, Shellock FG. Extrusion of eye socket magnetic implant after MR imaging: Potential hazard to patient with eye prosthesis. *J.Magn.Reson.Imaging 1991;1:711-713*

Zhang G, Yen YF, Chronik BA, McKinnon GC, Schaefer DJ, Rutt BK. Peripheral nerve stimulation properties of head and body gradient coils of various sizes. *Magn Reson Med 2003;50:50-58*